DESIGN, SYNTHESIS AND BIOLOGICAL EVALUATION OF NOVEL SELECTIVE CANNABINOID RECEPTOR 2 (CB2) LIGANDS WITH THERAPEUTIC POTENTIALS

by

Abdulrahman A. Almehizia

B.Sc. in Pharmaceutical Sciences, King Saud University, 2007

Submitted to the Graduate Faculty of

The School of Pharmacy in partial fulfillment

of the requirements for the degree of

Doctor of Philosophy

University of Pittsburgh

2015

UNIVERSITY OF PITTSBURGH

SCHOOL OF PHARMACY

This dissertation was presented

by

Abdulrahman A. Almehizia

It was defended on

March 17th , 2015

and approved by

Dr. Paul Schiff, Professor, Pharmaceutical Sciences

Dr. Regis Vollmer, Professor, Pharmaceutical Sciences

Dr. Paul Floreancig, Professor, Chemistry

Dr. LiRong Wang, Research Assistant Professor, Pharmaceutical Sciences

Thesis /Dissertation Advisor: **Dr. Xiang-Qun (Sean) Xie**, Professor, Pharmaceutical Sciences

DESIGN, SYNTHESIS AND BIOLOGICAL EVALUATION OF NOVEL SELECTIVE CANNABINOID RECEPTOR 2 (CB2) LIGANDS WITH THERAPEUTIC POTENTIALS

Abdulrahman A. Almehizia, PhD

University of Pittsburgh, 2015

Cannabinoid receptors 1 and 2 (CB1 and CB2) belong to the rhodopsin-like family of the G-Protein Coupled Receptors (GPCRs). CB1 receptor is highly expressed in the central nervous system, while CB2 receptor is expressed mainly in the immune cells and the periphery. Targeting the CB2 receptor is believed to avoid the psychoactive side effects associated with CB1 receptor. CB2 receptor has been shown to be involved in several physiological functions as well as diseases, such as pain, multiple sclerosis, osteoporosis, and cancer, demonstrating the importance of the CB2 receptor as a therapeutic target. In the present study, we employed chemistry design and discovery to identify novel CB2 ligands, carried out *in-vitro* functional studies, and evaluated the therapeutic potentials.

Several chemical scaffolds were discovered and evaluated. The di-amide scaffold was discovered utilizing pharmacophore drug discovery and molecular docking studies. Several derivatives of the di-amide scaffold demonstrated potent and highly selective CB2 inverse agonists as well as potent osteoclast (OCL) inhibition capabilities. The di-amide derivatives suffered from weak anti-multiple myeloma (MM) properties and poor pharmacokinetic properties. A new scaffold was identified utilizing scaffold-hopping and molecular docking studies. However, the 2-(sulfonylamino)-2-phenylacetamide scaffold demonstrated weak CB2 binding affinity. Due to the

limitation of the two previous scaffolds, virtual screening and structure-based drug design were utilized for scaffold-hopping in order to identify highly potent CB2 specific ligands with new scaffolds. A new lead compound was identified and structure activity relationship (SAR) studies were conducted on the scaffold 4-(aminomethyl)-*N*,*N*-diethylaniline. Several novel compounds were discovered with high potency and selectivity towards the CB2 receptor. Cellular function assays were applied to characterize the functionality (agonist and inverse agonist) of these compounds. Overall, therapeutic studies showed that inverse agonism is essential for the OCL inhibition effects while anti-MM experiments showed that CB2 agonists are more effective than inverse agonists.

TABLE OF CONTENTS

LIST OF TABLES

LIST OF FIGURES

LIST OF SCHEMES

ACKNOWLEDGMENTS

Throughout my journey to complete my graduate study, I have met many people. These individuals have contributed to the successful completion of my Doctor of Philosophy degree. I would like to thank each and every one of them.

First and foremost, I would like to express my sincere thanks and appreciation to my research advisor Dr. Xiang Qun (Sean) Xie for considering me to join his laboratory. Dr. Xie gave me this huge opportunity to learn and develop my knowledge, guided me through all these years to grow into an independent scientist. Dr. Xie encouraged me into independent thinking, organizing my research work and guided me to stay focused which was successful inside the lab and outside the lab.

I would like to thank my thesis committee members: Dr. Paul Schiff, Dr. Regis Vollmer, Dr. Paul Floreancig and Dr. LiRong Wang for their continuous guidance, valuable input, and support throughout my dissertation work. I have great respect for them and would like to offer my most sincere gratitude to them for not only being great mentors but also supportive faculty members. Further, I would like to thank my previous committee member: Dr. Billy Day for his guidance and help.

I owe special thanks to Dr. Peng Yang for serving many roles of supportive team leader, helpful colleague and above all, a great friend and guide. I would also like to thank Qin Tong for being both a great guide to lab skills and also a fantastic lab manager. Special thanks to all the postdocs in the lab: Zhiwei Feng, and Shoucheng Du.

Special thanks to my fellow graduate student Mohammed Alqarni for all the support during my graduate studies and lab work. Thanks to all the senior students who had graduated recently Kyaw Myint, Chao Ma and Ananda Chowdhury for being the best senior graduate students and for the

positive guidance I received from them. Also thanks to new students Haizi Cheng, Nuozhou Wang, and Yan Zhang for giving me new motivations and supporting me. Thanks to Dr. Maggie Folan and Lori Schmotzer for being in charge of the graduate program and to all the faculty members, staff and graduate students in the Department of Pharmaceutical Sciences, School of Pharmacy, University of Pittsburgh.

I would like to send special thanks and regards to King Saud University, Saudi Arabia for their financial support throughout my PhD study and special thanks to Dr. Abdulaziz Aleisa, who was my academic advisor at the Saudi Arabian Cultural Mission, for his excellent support and work dedicated for many Saudi students in the United States.

I dedicate this work to my father, Abdulaziz Almehizia, and my mother, Muneerah Alshikh, and all my brothers back home for their support and love without them I could never be where I am today. Sincere thanks, appreciations and gratitude to my lovely wife, Lama Alaskar, for being with me throughout my PhD studies and throughout my life supporting me, standing by me, and encouraging me.

ABBREVIATIONS

2-AG	2-arachidonoylglycerol
3D	Three Dimensional
Å	Angstrom
AC	Adenylate cyclase
AEA	*N*-arachidonoylethanolamide (Anandamide)
AMP	Adenosine mono phosphate
Arg	Arginine
Asp	Aspartic acid
ATP	Adenosine tri phosphate
AUC	Area under the curve
B_{max}	Receptor density
BMD	Bone mineral density
BMME	Bone marrow microenvironment
BSA	Bovine Serum Albumin
C'	Carboxy terminal
cAMP	Cyclic adenosine mono phosphate
CB1/2	Cannabinoid receptor 1 or 2
CBD	Cannabidiol
CBN	Cannabinol
CDB	Compound Dilution Buffer
CHO	Chinese hamster ovaries
CHOP	C/EBP homologous protein
Cl	Clearance
cLogP	Calculated logarithm of octanol/water partition coefficient
cm	Centimeter
C_{max}	Maximum plasma concentration
CNS	Central Nervous System
CoMFA	Comparative molecular field analysis
CPM	Counts Per Minute
CREB	cAMP response element-binding
DAG	1,2-diacylglycerol
DCM	Dichloromethane
DMEM	Dulbecco's Modified Eagle's Medium
DMSO	Dimethyl sulfoxide
EC_{50}	Half maximal effective concentration
ECL	Extracellular loop
EDTA	Ethylene diamine tetraacetic acid
EGTA	Ethylene glycol tetraacetic acid
ERK	Extracellular signal-regulated kinase
FAAH	fatty acid amide hydrolase
FBS	Fetal bovine serum

FCS	Fetal calf serum
g	Gram
GC	Glucocorticoids
GDP	Guanosine 5'-diphosphate
GEF	GTP exchange factor
GIRKs	G-protein coupled inwardly rectifying potassium channels
Glu	Glutamic acid
GPCR	G protein coupled receptor
GPR55	G-protein coupled receptor-55
GTP	Guanosine 5'-triphosphate
Gα/βγ	G protein (Gα and Gβγ subunits)
Gαi	G alpha subunit inhibitory
Gαs	G alpha subunit stimulatory
h	Hours
hCB1/2	Human cannabinoid receptors 1 or 2
HPLC	High-performance liquid chromatography
HTS	High-throughput screening
Hz	Hertz
IC_{50}	Half maximal inhibitory concentration
ICL	Intracellular loop
Ig	Immunoglobulin
IGF-1,-2	Insulin-like growth factor 1 & 2
IL	Interleukin
Ile	Isoleucine
IMiDs	Immunomodulatory drugs
JNK	c-Jun N-terminal kinase
K_d	Dissociation constant
kDa	Kilo Dalton
K_i	Binding Affinity of the inhibitor
K_{ir}	Inwardly rectifying potassium currents
L	Liter
Leu	Leucine
Lys	Lysine
m/z	Mass-to-charge ratio
MAGL	monoacylglyceride lipase
MAPK	Mitogen-activated protein kinase
M-CSF	Macrophage colony-stimulating factor
MEK	MAP kinase kinase
MeOH	Methanol
Met	Methionine
MHz	Megahertz
mins	Minutes
mL	Milliliter
MM	Multiple Myeloma
mM	millimolar
mmol	Millimoles

mRNA	messenger RNA
MS	Mass spectrometry
N'	Amino terminal
NADA	N-arachidonoyl dopamine
NAPE	*N*-arachidonoyl-phosphatidylethanolamine
NAT	*N*-acyltransferase
NB	No binding
NFAT	Nuclear factor of activated T-cells
NF-κB	Nuclear factor kappa-light-chain-enhancer of activated B cells
nM	Nanomolar
NMR	Nuclear magnetic resonance
NT	Not tested
ºC	Degree Celsius
OD	Optical Density
OPG	Osteoprotegerin
PEA	*N*-palmitoylethanolamine
Phe	Phenylalanine
PI3K	phosphatidylinositol-3-kinas
PKA	Protein kinase A
PKB	Protein kinase B (Akt)
PLC	Phospholipase C
ppm	Parts per million
Pro	Proline
PTX	Pertussis toxin
QSAR	Quantitative structure activity relationship
RANKL	Receptor activator of nuclear factor kappa-B ligand
rpm	revolutions per minute
rt	room temperature
S.E.M	Standard Error of the Mean
SD	Standard deviation
Ser	Serine
SI	Selectivity index
$t_{1/2}$	Half-life
TGF-β	Transforming growth factor β
THC	Tetrahydrocannabinol
TLC	Thin layer chromatography
TM	Transmembrane
TNF	Tumor necrosis factor
TNF-α	Tumor necrosis factor-alpha
TRAP	Tartrate-resistant acid phosphate
Trp	Tryptophan
TRPV1	Transient receptor potential cation channel subfamily V member 1
TYR	tyrosine kinase receptors
Tyr	Tyrosine
UPS	Ubiquitin proteasome system
UV	Ultra-violet

Val	Valine
Vd	Volume of distribution
VEGF	Vascular endothelial growth factor
VOCCs	Voltage operated calcium channels
w/v	weight per volume
α-MEM	alpha-Minimum Essential Medium
µg	microgram
µL	microliter
µM	Micromolar

1.0 INTRODUCTION

1.1 THE ENDOCANNABINOID SYSTEM AND THE CANNABINOID RECEPTORS

1.1.1 THE G-PROTEIN COUPLED RECEPTORS SUPERFAMILY

The G-protein coupled receptors (GPCRs) represents the largest family of membrane proteins in the human genome with more than 800 different GPCRs. GPCRs can be classified based on the seven transmembrane (TM) segments into five different subfamilies: Class A – Rhodopsin-like family, Class B - Secretin family, Class C - Glutamate family, Class D - Adhesion family, and Class E - Frizzled/taste family [1]. All GPCRs share common structural features and can be divided into three parts: the extracellular region, the transmembrane region, and the intracellular region. The extracellular region consists of the amino terminus (N'), and extracellular loops (ECL1 – ECL3). The transmembrane region consists of seven hydrophobic transmembrane (TM1 – TM7) α-helices. And the intracellular region consists of three intracellular loops (ICL1 – ICL3) and a carboxyl terminus (C') (Figure 1.1) [2].

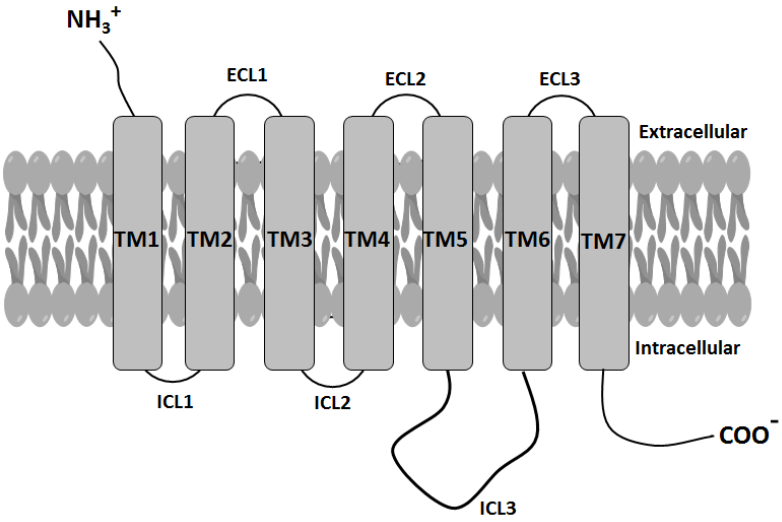

Figure 1.1. General GPCR structure

Common structural features of all GPCRs: seven hydrophobic transmembranes (TM1 – TM7), three extracellular loops (ECL1 – ECL 3), three intracellular loops (ICL1 – ICL3), extracellular amino (N′) terminal, and intracellular carbonyl (C′) terminal

GPCRs control several key physiological functions, such as neurotransmission, immune responses, cardiac and smooth muscle contraction and blood pressure regulation as well as hormone and enzyme regulations. Nevertheless, it has been shown that GPCRs have crucial roles in cancer progression and metastasis. Also, GPCRs represent 50 – 60% of all therapeutic agents in the market and it is expected to increase in the following years [3].

GPCR activation:

In most GPCRs, the receptor is present in the basal state and different ligand efficiencies alter this state. Ligand efficacy is the effect of the ligand on the function of the receptor. Agonists fully activate the receptor, partial agonists induce submaximal activation of the G-protein even when reaching saturable concentrations, inverse agonists inhibit the basal activity of the receptor, and antagonists block competitively the access of other ligands to the receptor. Upon GPCR activation, for example by its endogenous ligand, conformational changes occur within the TM region exposing intracellular sites involved in the interaction with the G-protein heterotrimer. G-protein heterotrimer contains α, β and γ subunits. Receptor and conformational changes catalyze the dissociation of guanosine diphosphate (GDP) bound to the Gα subunit and its replacement with guanosine triphosphate (GTP), leading to the dissociation of Gα from the Gβγ subunits. Both α•GTP subunits and Gβγ subunit complexes stimulate several downstream effectors, such as ion channels or enzymes. Signaling is terminated by the hydrolysis of GTP by the GTPase activity. The resulting GDP-bound α-subunit reassociates with the βγ- complex to enter a new cycle [4].

The nature of the functionality of GPCRs depends in the numerous subtypes of G-proteins. The α-subunit can be divided into four families: $G\alpha_s$, $G\alpha_i$/ $G\alpha_o$, $G\alpha_q$/ $G\alpha_{11}$, and $G\alpha_{12}$/ $G\alpha_{13}$. The α-subunit of the Gs protein couples many receptors to adenylate cyclase (AC) and mediates receptor-

dependent AC activation resulting in increases in the intracellular cyclic adenosine monophosphate (cAMP) concentration. The G proteins of the Gi/Go family are widely expressed and have been shown to mediate receptor-dependent inhibition of various types of (AC) resulting in decreases in the intracellular cAMP concentrations. The α-subunits of Gq and G11 regulate phospholipase C β-isoforms, including β1-, β3-, and β4-isoforms of phospholipase C (PLC). The G proteins G12 and G13 activate a variety of downstream effectors, such as phospholipase A_2, cadherin as well as radixin [5].

.

1.1.2 THE ENDOCANNABINOID SYSTEM

The endocannabinoid system is composed of cannabinoid receptors and their endogenous ligands. A few years after the first isolation and identification of the cannabinoid receptor 1, several endogenous ligands were discovered. In 1992, Devane and coworkers first reported the presence of a hydrophobic molecule in organic extracts of porcine brain (named anandamide, AEA). Mass spectrometry (MS) as well as nuclear magnetic resonance (NMR) studies determined the structure of the anandamide and identified it consisting of 20 carbon fatty acid, arachidonic acid, connected to ethanolamine through an amide linkage. Anandamide inhibited the specific binding of radio-labeled cannabinoid ligands in a competitive manner. In addition, anandamide produced a dose-dependent inhibition of electrically evoked twitch response of the mouse vas deference which demonstrates its psychotropic effects [6]. Later, 2-arachidonoylglycerol (2-AG) was discovered and characterized as the second endogenous cannabinoid [7].

AEA and 2-AG are derivatives of arachidonic acid and are synthesized on demand from phospholipids of cell membrane. Both ligands bind, with different affinities, CB1 and CB2 receptors. It has been shown that 2-AG exhibits high binding efficacy to cannabinoid receptors than AEA (Table 1.1) [8]. Several bioactive lipid mediators have been identified as endocannabinoids including *N*-palmitoylethanolamine (PEA), 2-arachidonoyl glycerol ether (noladin ether), oleamide, *N*-arachidonoyl dopamine (NADA), and virodhamine (Figure 1.2).

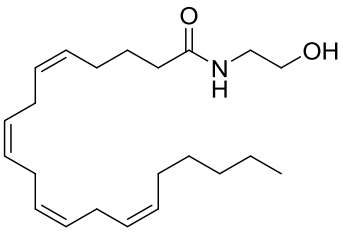

Anandamide
(AEA)

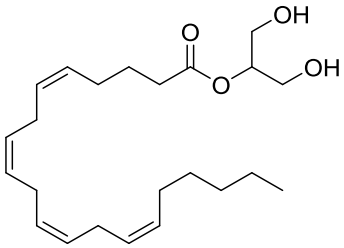

2-Arachidonyl glyceryl
(2-AG)

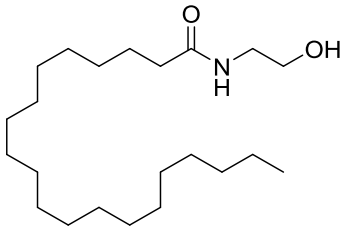

N-palmitoylethanolamine
(PEA)

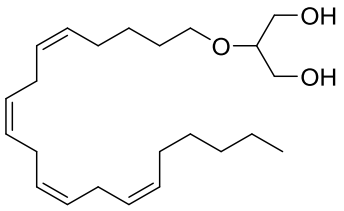

2-arachidonyl glyceryl ether
(noladin ether)

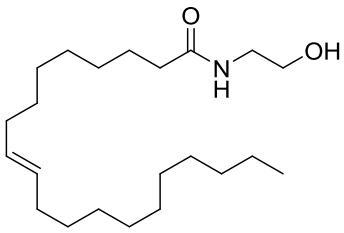

Oleamide

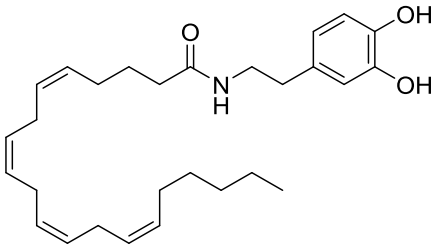

N-Arachidonoyl dopamine
(NADA)

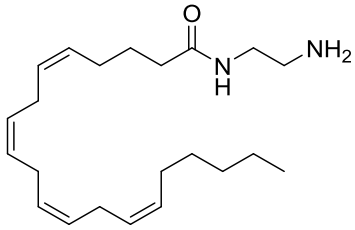

Virodhamine

Figure 1.2. Chemical structures of endocannabinoids

These endogenous ligands have been found in the brain, plasma and the periphery with varying concentrations. For example, anandamide concentration has been shown to be 200-fold lower than 2-AG. However, after receptor stimulation or depolarization, the anandamide concentration can rise up to 5-12 folds. Different enzymes and pathways are involved in the distinct synthesis of anandamide (and its derivatives, namely *N*-acylethanolamines) and 2-AG. Anandamide is formed by the cleavage of the phospholipid precursor *N*-arachidonoyl-phosphatidylethanolamine (NAPE) which is synthesized by the enzyme *N*-acyltransferase (NAT) from phosphatidylethanolamine. NAPE requires the presence of Ca^{2+} and the regulation by cAMP. Finally, phospholipase D (PLD) catalyzes the release of anandamide from NAPE (Figure 1.3) [9]. PLD activity is regulated by many receptors, stimuli or neurotransmitters, such as the activation of ionotropic glutamate *N*-methyl-*D*-Aspartate (NMDA) receptors, nicotinic α7 neuronal receptors, dopamine, glutamate, as well as acetylcholine.

The synthesis of 2-AG includes the cleavage of phosphatidylinositol (PI) to yield 1,2-diacylglycerol (DAG) which is catalyzed by a phospholipase enzyme, such as phospholipase C (PLC). DAG lipase subsequently catalyzes the conversion of DAG to 2-AG (Figure 1.3).

The degradation of endocannabinoids is mediated by two specific enzymatic systems: the fatty acid amide hydrolase (FAAH) for anandamide and related compounds and the monoacylglyceride lipase (MAGL) for 2-AG [10, 11].

Since the discovery and identification of the cannabis active molecule as well as the identification of cannabinoid receptors, endocannabinoid research gained a lot of attention to understand its physiological roles. It is now understood that endocannabinoids are involved in several physiological functions [12, 13]. Endocannabinoids have been shown to regulate cognitive functions and emotions in the cortex, hippocampus and amygdale [14].

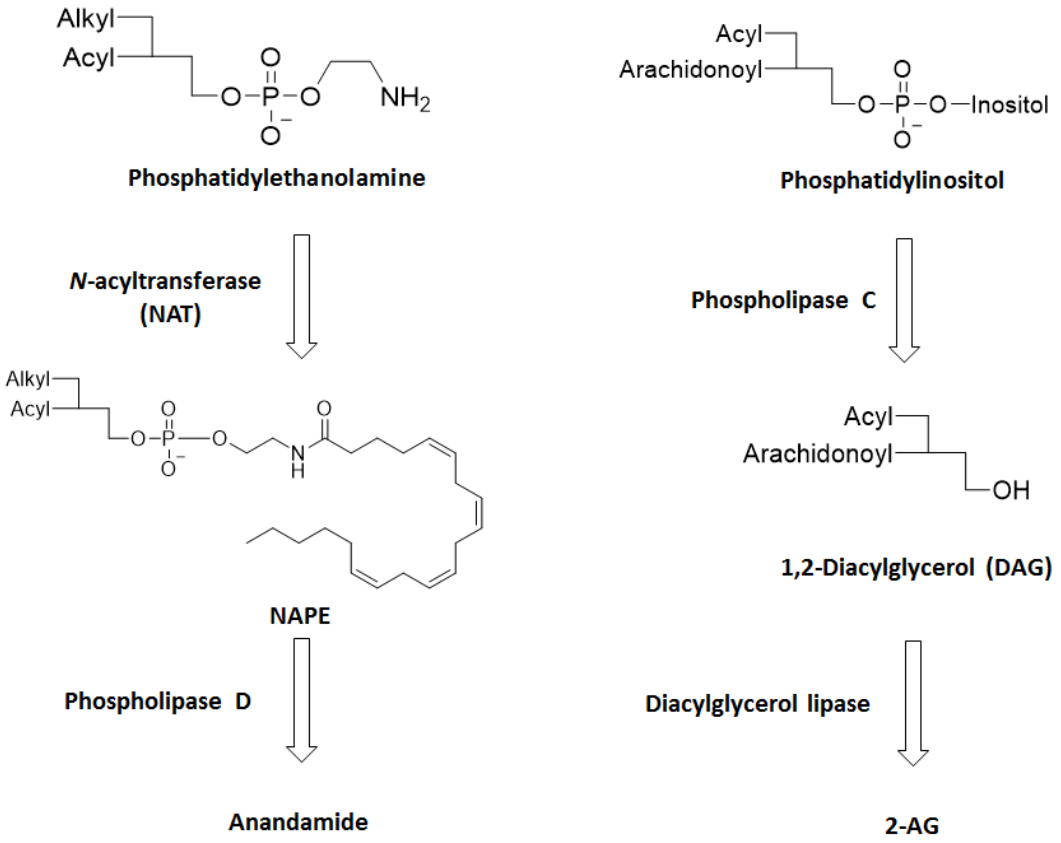

Figure 1.3. Mechanism of anandamide and 2-AG formation

N-acyltransferase (NAT) catalyzes the formation of *N*-arachidonoyl-phosphatidylethanolamine (NAPE). Subsequently, phospholipase D (PLD) catalyzes the release of anandamide from NAPE. Cleavage of phosphatidylinositol by phospholipase C (PLC) releases 1,2-diacylglycerol (DAG) in which DAG lipase converts DAG to 2-AG.

Endocannabinoids through modulations of the dopaminergic signaling modulate the control of movement and posture [15], involved in the regulation of pain perception [16], cardiovascular, gastrointestinal and respiratory functions [17, 18]. Endocannabinoids were also shown to modulate food intake, pituitary hypothalamus adrenal axis and reproduction [19].

Under pathological conditions, it has been shown that endocannabinoid levels changes within blood and tissues. For example, in neurodegenerative diseases (e.g. Alzheimer's and Parkinson's diseases), gastrointestinal disorders (e.g. colon inflammation), metabolic disorders (e.g. anorexia nervosa) and obesity, higher levels of endocannabinoids have been observed compared to normal tissues and states [20]. Importantly, elevated levels of endocannabinoids were observed in many tumors, such as colon carcinoma and colon polyps [21], glioblastoma, meningioma [22], prostate carcinoma [23], and pituitary adenoma [24]. Furthermore, strong evidence have demonstrated the anti-proliferative effects of endocannabinoids in different tumor cells and the involvement of AEA as well as 2-AG in the control of cell differentiation, proliferation, and death. Collectively, these data suggest critical roles of endocannabinoids as tumor growth modulators [25].

1.1.3 CANNABINOID RECEPTORS 1 (CB1)

Cannabinoid receptors are members of the Class – A Rhodopsin-like G-protein coupled receptors family. Cannabinoid receptor 1 (CB1) was first discovered and isolated in 1990 by Matsuda and colleagues from rat cerebral cortex [26]. Further cloning studies by Gerard and coworkers, aided the discovery of the CB1 receptors from human brain and testis [27]. The CB1 receptor is a 52.8 kDa, 472 amino acid polypeptide widely expressed throughout the whole body. It is believed to be highly expressed within the brain and the central nervous system (CNS). Specifically, CB1

receptor has been isolated from the hippocampus, basal ganglia (striatum, substantia nigra, and globus pallidus), cerebral cortex, amygdala, and the cerebellum. In addition, CB1 receptors have been found in the periphery, such as the spleen, tonsils, small intestine, and urinary bladder as well as low levels in uterus, ovaries, prostate, adrenal gland, and heart [28].

The field of cannabinoid research was reinforced with the first cannabinoid drug to reach the European market in 2006. SR141716 (commercially known as Rimonabant, developed by Sanofi-Aventis), a CB1 inverse agonist (Figure 1.9, Table 1.1), was granted an approval in Europe for the treatment of obesity by suppressing appetite with potential smoking cessation. However, the drug was withdrawn from the market in 2008 due to the serious side effects including depression and suicidal thoughts [29, 30].

1.1.4 CANNABINOID RECEPTORS 2 (CB2)

Cannabinoid receptor 2 (CB2) was cloned from the human promyelocytic leukemia cells (HL-60 cells) in 1993 by Munro and coworkers [31]. CB2 receptor is a 41 kDa, 360 amino acid polypeptide that shares 68% amino acid sequence homology with CB1 receptor within the transmembrane region and 44% for the whole protein [31]. Unlike CB1 receptor, CB2 receptors are mainly distributed in the periphery with no or limited distribution within the central nervous system. Importantly, the CB2 receptor has been found in the marginal zone of the spleen, tonsils, and on immune cells such as B-cells, monocytes, and T-cells [28, 31-33]. The high distribution of CB2 receptors in the periphery and limited distribution in the CNS implies that targeting CB2 receptors may avoid any central side effects that may arise from CB1 receptors. Nevertheless, the high expression of CB2 receptors on the immune system suggests the involvement of these receptors in many pathological and disease states and may serve as a powerful disease target.

1.1.5 ORPHAN RECEPTORS

Sawzdargo and coworkers first identified and cloned the G-protein coupled receptor-55 (GPR55) as an orphan receptor in 1999. GPR55 was reported to be highly expressed in the CNS especially the striatum [34]. It is also found in the gastrointestinal tract as well as in the adrenal glands [35]. In addition, Whyte *et al*. reported that GPR55 was highly expressed in osteoclasts and osteoblasts which played roles in bone regulation and function [36]. GPR55 is classified as a class-A rhodopsin-like GPCR with low sequence similarity to CB1 (13.5%) and CB2 (14.4%) receptors [1]. Upon activation, GPR55 couples to $G\alpha_{13}$ subunit which leads to stimulation of numerous GTPases including Ras Homology gene Family (member A: RhoA), Ras-related C3 botulinum toxin substrate 1 (rac1), cell division control protein 42 homolog (cdc42) [35, 37].

Stimulation of GPR55 induces F-actin formation under the control of $G\alpha_{13}$, RhoA and Rho-associated, coiled-coil containing protein kinase (ROCK). GPR55 activation also induces intracellular calcium release and activation of the transcription factors nuclear factor kappa-light-chain-enhancer of activated B cells (NF-κB), nuclear factor of activated T-cells (NFAT) and cAMP response element-binding (CREB) [38].

Ligand binding data showed that GPR55 binds to and is activated by the cannabinoid ligand CP55,940 (CB1 and CB2 receptor agonist). Furthermore, endocannabinoids including anandamide and virodhamine activate [^{35}S]GTPγS binding via GPR55 with nM potencies [35]. Nevertheless, there are conflicting data regarding ligands' binding to GPR55 which hesitated scientists to name GPR55 a cannabinoid receptor. Until today, GPR55 classification remains questionable and needs further studies [39].

1.1.6 CANNABINOID RECEPTORS SIGNALING

1.1.6.1 G-protein coupling

Both receptors couple with high affinity to the G-protein $G\alpha_{i/o}$ this was analyzed by utilizing the [^{35}S]GTPγS binding experiments in rat membrane proteins and in CHO cells expressing recombinant human CB2 receptors. Upon the activation of the $G\alpha_{i/o}$ with cannabinoid agonists, the subunit dissociates from the βγ dimer allowing the $G\alpha_{i/o}$ subunit to associates with its effector molecule (i.e. adenylate cyclase) (Figure 1.4).

It has been shown by Glass and coworker that unlike CB2 receptors, CB1 receptors were able to couple to G_s subunit in the absence of a functional $G\alpha_{i/o}$ protein and in the presence of pertussis toxin (PTX). PTX catalyzes ADP-ribosylation which uncouples the receptor from G_i proteins thus inactivating the G-protein resulting in high levels of cAMP [40].

1.1.6.2 Regulation of adenylate cyclase

Coupling of CB1 and CB2 receptors to $G\alpha_{i/o}$ subunit inhibit the production of adenylate cyclase (AC) in endogenous expression of these receptors in N18TG2 neuroblastoma cells leading to the inhibition of cAMP. As this response was blocked by PTX, it suggests the involvement of $G\alpha_{i/o}$ proteins. Similarly, for CHO transfected with CB1 and CB2 receptors, AC was inhibited leading to the inhibition of cAMP production in these cell-lines. AC inhibition or stimulation is critical in characterizing the functionality of cannabinoid ligands as the levels of cAMP can aid to distinguish between agonists and antagonists/inverse agonists (Figure 1.4). Cannabinoid agonists such as anandamide, WIN55212-2, and CP55,940 inhibited AC activity in rat cerebellum and in CHO cells transfected with CB1 and CB2 receptors highlighting that these ligands are cannabinoid agonists.

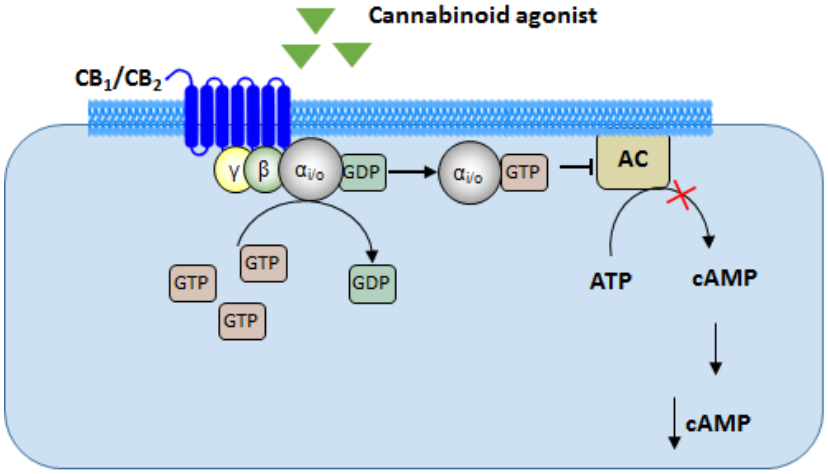

Figure 1.4. G-protein coupling and the regulation of adenylate cyclase.

Cannabinoid activation by agonists promotes the dissociation of GDP bound to the Gα subunit and replaces it with GTP. As a result, the Gα subunit dissociates from the Gγβ heterodimer subunit. The Gα then inhibits AC, thus inhibiting cAMP formation.

On the other hand, antagonist stimulation of CB1 and CB2 receptors inhibits the dissociation of the $G\alpha_{i/o}$ subunit from the $\beta\gamma$ dimer blocking the subunit to interact with its effector molecule AC and thus stimulating cAMP production.

1.1.6.3 Ceramide production through sphingomyelin hydrolysis and *de novo* synthesis

Ceramide is a lipid second messenger that has been shown to play important roles in the control of cell fate. CB1 receptor couple to the hydrolysis sphingomyelin by inducing sphingomyelinases in primary astrocytes and glioma cells which in turn increases the levels of ceramide. Increased ceramide levels has been shown to link the CB1 receptors to the activation of ERK 1/2 pathway through the mobilization of Raf-1. In primary astrocyte cultures, AEA, Δ^9–Tetrahydrocannabinol (Δ^9 –THC, phytocannabinoid), and HU-210 (CB1/CB2 non-selective agonist) induced rapid transient elevation of ceramide levels leading to increased glucose metabolism. This effect was inhibited by the selective CB1 inverse agonist (SR141716) suggesting a CB1 mechanism [40]. Sanchez *et al.* showed that the sphingomyelinases may be activated in G-protein-independent manner through an adaptor protein FAN (factor associated with neutral sphingomyelinase), which binds to the CB1 C-terminus leading to the coupling of CB1 receptor to stimulate sphingomyelinase activation, release of ceramide, and activation of the Raf-1/MAPK cascade [41]. It has been shown that chronic CB1 and CB2 activation in C6 glioma cells were also responsible in the *de novo* ceramide synthesis which activated ERK 1/2 via Raf-1 and subsequently activating MAPK leading to the initiation of apoptosis and cell death rather than glucose metabolism [42, 43].

1.1.6.4 Regulation of mitogen-activated protein kinase (MAPK)

Cellular functions such as cell growth, differentiation, proliferation, apoptosis as well as cell fate is controlled via complex signaling pathways. Among the important pathways is the MAPK pathway. Several researchers have investigated the relationship between cannabinoids and the MAPK signaling pathways. Normally the activation of this pathway is initiated by the activation of tyrosine kinase receptors (TYR) leading to the activation of the G protein Ras and thus activating MAP kinase kinase (MEK) leading to the phosphorylation and activation of MAPK cascade. *In-vitro* cell-culture studies on the signaling transduction pathways of cannabinoids utilizing WI-38 fibroblasts, U373MG astrocytic cells, C6 glioma cells, and primary astrocytes expressing recombinant CB1 receptors showed p42/p44 MAPK (known as extracellular protein kinase 1 and 2, ERK 1 and 2) activation which was inhibited by SR141716. As a result of the $G_{i/o}$ coupling of CB1 receptors, the $\beta\gamma$ dimer complex serves as a scaffold protein in the MAPK activation. This mechanism was blocked by the phosphatidylinositol-3-kinase (PI3K) inhibitors wortmannin and LY294002 suggesting the involvement of PI3K activation and the subsequent recruitment of protein kinase B (PKB), also known as Akt. The phosphorylation of PKB then phosphorylates and activates the three-kinase module of Raf-1, MAPK-ERK (MEK), and p42/p44 MAPK.

Experiments utilizing WIN55212-2 in N1E-115 neuroblastoma cells and hippocampal slice preparations suggested an alternative mechanism for the regulation of p42/p44 MAPK activity. The CB1 G_i-mediated inhibition of cAMP production and reduction of PKA would promote the dephosphorylation of c-Raf, thus permitting the Raf kinase to activate MEK in the p42/p44 MAPK kinase module [44, 45].

In cells expressing recombinant CB2 receptors (human promyelocytic-HL60 cells and CHO cells), phosphorylation of p42/p44 MAPK was observed, however, the PI3K pathway was

not involved. Studies on rat RTMGL1 microglial cells expressing CB2 receptors showed that 2-arachidonylglycerol (2-AG) activated the p42 MAPK activity and promoted cell proliferation [46]. In addition, stimulation of CB2 receptors in human prostate epithelial PC3 cells with Δ^9-THC or methanandamide activated the PI3K/PKB pathway and subsequently translocated Raf-1 to the membrane and phosphorylates p42/p44 MAPK. This effect was inhibited by SR144528 (CB2 inverse agonist) suggesting the involvement of CB2 receptors [47].

1.1.6.5 Immediate early genes: Krox 24 and Fos transcriptional factors

The activation of MAPK can induce the expression of immediate early genes such as Krox 24 (a zinc finger-binding transcription factor involved in growth, differentiation, and proliferation of cells), and Fos (able to regulate numerous transcriptional genes) in different regions of the brain following cannabinoid agonist stimulation. In U373MG human astrocytoma cells, Krox 20, Krox 24 and Jun B expression was mediated through the CB1 receptors [48], while the CB2 receptors mediated the expression of Krox 24 in HL 60 promyelocytes cells with downregulation of Fos [49, 50]. Cannabinoid agonists activated c-Jun N-terminal kinase (JNK1 and JNK2) in CHO cells expressing recombinant CB1 receptors. The mechanism of JNK activation is mediated through Gi/o coupling, PI3K, and Ras activation as explained by Rueda and coworkers [51].

1.1.6.6 Modulation of ion channels

CB1 signaling has been shown to inhibit Ca^{2+} influx by L-, N-, P/Q-, and R-type voltage operated calcium channels (VOCCs). The effect was PTX sensitive suggesting the involvement of $G_{i/o}$ protein coupling. As these effects were evident in the central neurons (presynaptic neurons), it suggests the involvement of CB1 receptors as these receptors are highly expressed compared to CB2 receptors.

Cannabinoid agonists WIN55212-2, CP55,940, and anandamide (endocannabinoid) inhibited N-type calcium channels via the CB1 receptor leading to a decrease in Ca^{2+} levels. Mackie and coworkers demonstrated that the decrease in Ca^{2+} levels was cAMP-independent since the response was not reversed by the addition of the synthetic cAMP (8-bromo-cAMP) [52]. Sugiura and colleagues measured the intracellular Ca^{2+} levels using fura-2 fluorescence studies in high K^{+} depolarized NG108-15 cells. 2-AG and anandamide inhibited the depolarization-evoked Ca^{2+} concentration and studies have shown that the N-type Ca^{2+} channel played a role in the depolarization since the N-type channel antagonist, ω-conotoxin, blocked this response [53, 54]. Utilizing neuronal expression systems, rat cervical ganglion transfected with CB1 receptors showed an inhibition in Ca^{2+} currents when treated with cannabinoid agonists such as WIN55212-2 and CP55,940. Further studies showed that these effects were PTX and ω-conotoxin sensitive confirming that these effects were on N-type Ca^{2+} channels. Furthermore, utilizing rat striatal neurons transfected with CB1 receptors, WIN55212-2 inhibited corticostriatal glutamatergic synaptic transmission which was also PTX and SR141716 sensitive and ω-conotoxin reversed this inhibition [55, 56].

Studies on AtT-20 pituitary tumor cells expressing recombinant CB1 receptors (not CB2 receptors) showed that anandamide and WIN55212-2 inhibited the Q-type Ca^{2+} currents which was PTX sensitive [57]. Utilizing fura-2 fluorescence studies in rat cortical and cerebellar brain slices showed that the P/Q-type Ca^{2+} fluxes were inhibited by anandamide and which was mediated through the $G_{i/o}$ protein-couples CB1 receptors as this effect was PTX and SR141716 sensitive [58].

CB1 receptors can also regulate the L-type Ca^{2+} currents. In rat brain arterial smooth muscle cells endogenously expressing CB1 receptors, anandamide and WIN55212-2 inhibited the L-type Ca^{2+} currents which was blocked by SR141716 and PTX [59].

1.1.6.7 Modulation of intracellular calcium concentration

Intracellular calcium concentration was increased by 2-AG and WIN55212-2 in NG108-15 neuroblastoma-glioma hybrid and N18TG2 neuroblastoma cells expressing CB1 receptors as determined by fura-2 fluorescence studies [53, 60]. Studies have shown the Ca^{2+} uptake by CB1 receptors couples to Gs protein, cAMP production, and protein kinase A (PKA) activation [61]. In addition, another mechanism highlights the coupling through Gi/o leading to tyrosine receptor kinase transactivation, PKC phosphorylation and the regulation of MAPK activity [62]. Interestingly, the phospholipase C (PLC) inhibitor U73122 blocked this response suggesting the involvement of an inositol 1,4,5-triphosphate (IP_3)-mediated release of Ca^{2+} [53, 60].

In calf pulmonary endothelial cells expressing CB2 receptors, anandamide increased calcium concentration and this effect was blocked by the CB2 inverse agonist SR144528 not the CB1 inverse agonist SR141716. The mechanism of the increase of Ca^{2+} levels resulted from the activation of phospholipase C [63].

1.1.6.8 Modulation of inwardly rectifying K^+ channels

CB1 is coupled to the activation of the inwardly rectifying potassium currents (K_{ir}). In AtT-20 pituitary tumor cells exogenously expressing CB1 receptors and HEK 293 cells endogenously expressing CB1 receptors, anandamide and WIN55212-2 activated the K_{ir} currents. The effect was PTX sensitive and was inhibited by AM251 (CB1 inverse agonist) implementing that $G_{i/o}$ involvement in these currents and this phenomena is known as the G-protein coupled inwardly

rectifying potassium channels (GIRKs). In addition, cAMP levels and PKA activity were not altered suggesting that a direct interaction exists between the G protein subunit and the ion channels [57, 64]. Studies in AtT-20 cells expressing CB2 receptors showed that these receptors has no effect on the GIRK or calcium channels [57].

1.2 CANNABINOID RECEPTOR LIGANDS

Cannabis sativa is one of the oldest plants to have been used as a medicine for a variety of diseases as well as for religious ceremonies and recreationally [65]. The therapeutic indications of *cannabis* stretches back for over 5000 years and many literature reported the use of the plant as an analgesic [66, 67], an anesthetic [68], an anti-inflammatory agent [69], for the treatment of hemorrhoids , and as an appetite stimulant [70]. Cannabinol (CBN) was the first phytocannabinoid to be isolated from *cannabis* and its structure was elucidated in the early 1930s by Cahn and coworkers (Figure 1.5). However, the first synthesis of CBN was achieved by two research groups Adam *et al.* in 1940 [71, 72] as well as by Todd and colleagues. Several derivatives of CBN were synthesized, such as $\Delta^{6a,10a}$-tetrahydrocannabinol ($\Delta^{6a,10a}$-THC) and its hexyl analog, synhexyl (also known as pyrahexyl or parahexyl) (Figure 1.5).

Two additional phytocannabinoids were isolated and identified, (-)-cannabidiol (CBD) and cannabidiolic acid by Adams and colleagues (Figure 1.5). Tetrahydrocannabinoids were extracted from *cannabis* and reported to exist as racemic mixtures of Δ^9-tetrahydrocannabinol (Δ^9-THC) and Δ^8-tetrahydrocannabinol by Loewe and coworkers. In 1964, Gaoni and Mechoulam isolated and characterized the main active constituent of the plant *Cannabis sativa*, Δ^9-THC (Figure 1.5) [70]. The activity Δ^9-THC was evaluated in a number of animal models including cataleptic reactions

in mice, motor activity and gross behavior in mice and rats as well as experiments on rhesus monkeys [8, 73, 74].

In the early 1970s, the cannabis use increased dramatically for recreational purposes in USA and UK as well as other Western countries. This potentiated the synthesis and pharmacological studies of Δ^9-THC. Consequently, experiments focused mainly on determining the active component related to the psychoactive properties of cannabis. Utilizing animal as well as human experiments on evaluating the effects of Δ^9-THC, showed that indeed Δ^9-THC is the main psychoactive component in cannabis. Following these studies and discoveries, several other constituents of cannabis such as cannabigerol, cannabichromene, and cannabicyclol were identified (Figure 1.5) [65].

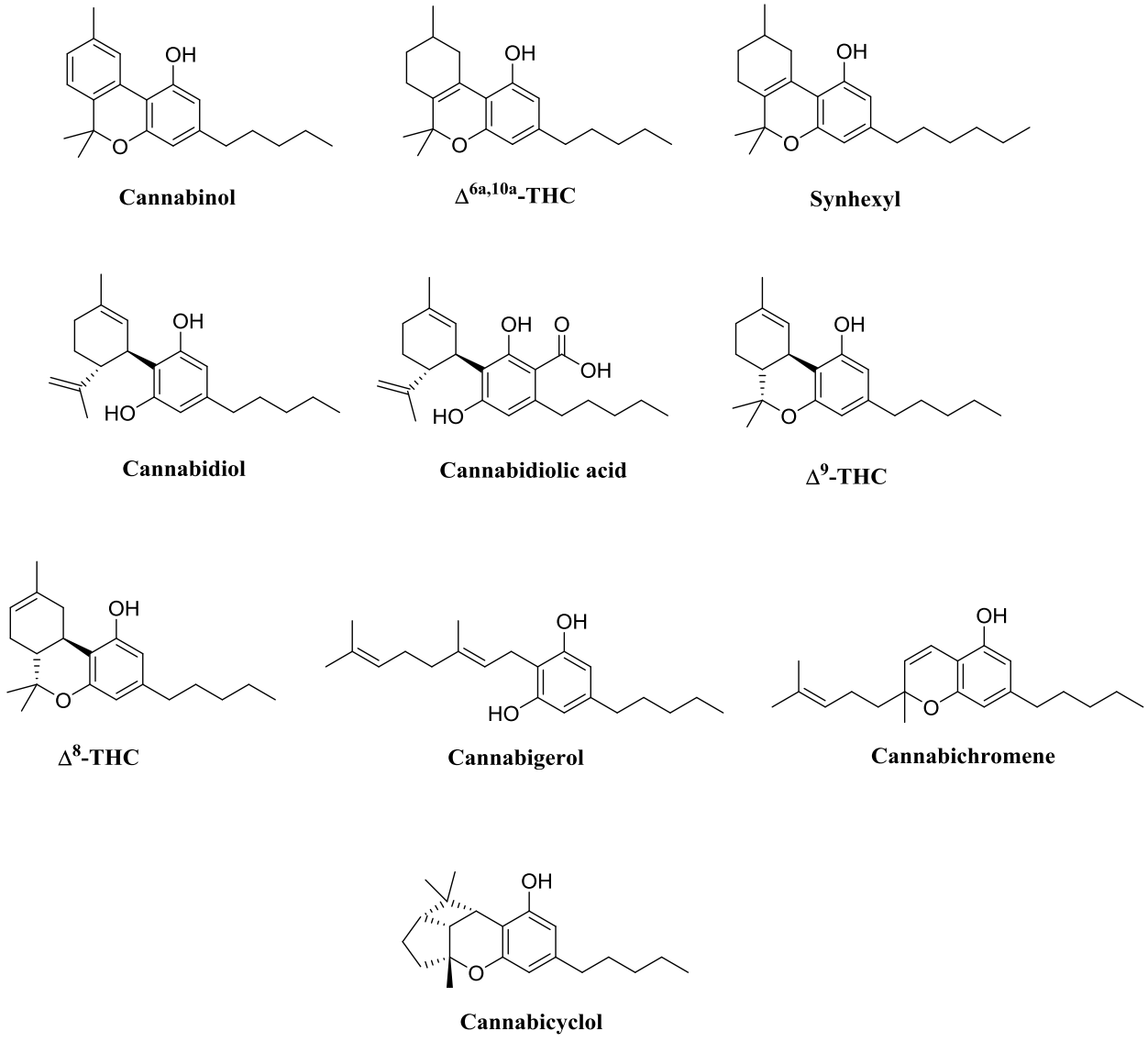

Figure 1.5. Chemical structures of plant cannabinoids (phytocannabinoids) and synthetic cannabinoids.

Chemical structures of phytocannabinoids: cannabinoid, cannabidiol, cannabidiolic acid, Δ^9-THC, Δ^8-THC, cannabigerol, cannabichromene, cannabicyclol as well as chemical structures of synthetic cannabinoids: $\Delta^{6a,10a}$-THC and synhexyl.

The structural characterization of Δ^9-THC paved the path toward cannabinoid research. Several research groups focused on cannabinoid research resulting in the design and synthesis of several structurally diverse classes of cannabinoid ligands. The cannabinoid receptor ligands can be classified into non-selective agonists, selective agonists, and selective antagonists/inverse agonists.

A. Non-selective agonists:

These ligands can bind and interact with both the CB1 and CB2 receptors with similar potency. Non-selective cannabinoid agonists can be classified according to their chemical structure to: classical, non-classical, aminoalkylindole, and eicosanoid (Figure 1.6).

1. Classical cannabinoids: classical cannabinoid ligands contain the dibenzopyran pharmacophore in their chemical structures. The classical cannabinoids include Δ^9-THC (Figure 1.5) and its synthetic analog (6a*R*)-*trans*-3-(1,1-dimethylheptyl)-6a,7,10,10a-tetrahydro-1-hydroxy-6,6-dimethyl-6*H*dibenzo[*b*,*d*]pyran-9-methanol (HU-210). HU-210 showed higher affinity to the CB1 and CB2 receptors than Δ^9-THC (Table 1.1).
2. Non-classical cannabinoids: these ligands are analogs of Δ^9-THC possessing bicyclic and tricyclic rings and lacking the pyran ring of Δ^9-THC. The most commonly used chemical probe in biochemical assay is (-)-*cis*-3-[2-hydroxy-4-(1,1-dimethylheptyl)phenyl]-*trans*-4-(3-hydroxypropyl)cyclohexanol (CP55,940). CP55,940 showed slight lower CB1 and CB2 affinity than HU-210 but higher than Δ^9-THC (Table 1.1).
3. Aminoalkylindole: these group of ligands differ significantly from classical and non-classical cannabinoids. The most common ligand in this group is *R*-(-)-[2,3-dihydro-5-methyl-3-(4-morpholinylmethyl)pyrrolo[1,2,3-*de*]-1,4-benzoxazin-6-yl]-1-naphthalenylmethanone mesylate (*R*-(+)-WIN55212-2). The (*R*)-(+)-isomer exhibits the

significant agonist activity while its (*S*)-(-)-isomer does not show any affinity to the cannabinoid receptors.

4. Eicosanoid: these cannabinoid differ significantly from other groups. Members of this group include the endocannabinoids AEA and 2-AG (Figure 1.2). AEA behaves as partial agonist with similar affinity to the CB1 receptor as Δ^9-THC. All eicosanoid cannabinoids showed lower affinity to the CB2 receptor than CB1 receptor (Table 1.1).

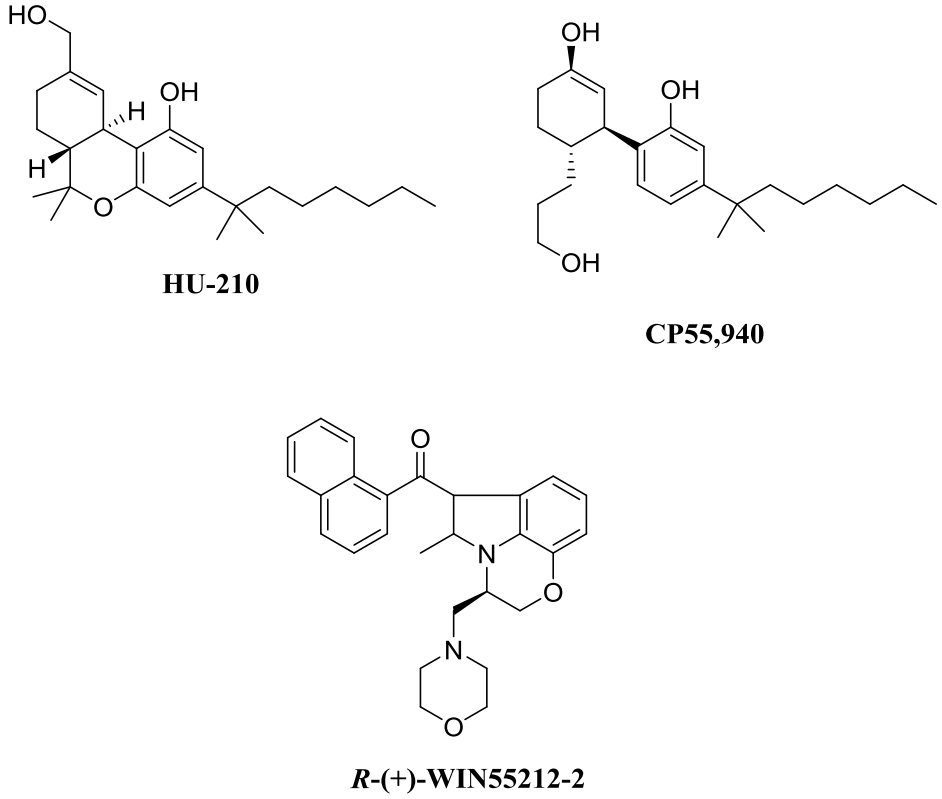

Figure 1.6. Non-selective CB1 and CB2 agonists.

Chemical structures of non-selective CB1 and CB2 agonists: HU-210, WIN55212-2 and CP55,940.

B. Selective CB1 and CB2 agonists:

1. Selective CB1 agonists: these include the synthetic analogs of AEA: *R*-(-)-methanandamide, arachidonyl-2'-chloroethylamide (ACEA), and arachidonylcyclopropylamide (ACPA), as well as 2-arachidonyl glyceryl ether (noladin ether) (Figure 1.7).

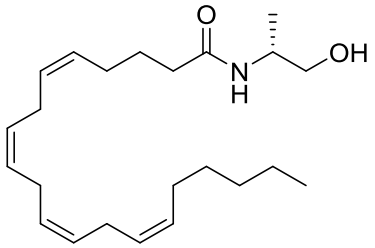

***R*-(-)-methanandamide**

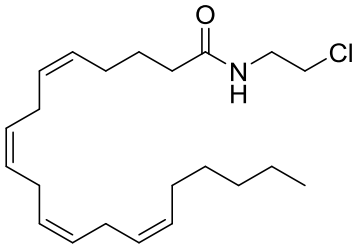

Arachidonyl-2'-chloroethylamide (ACEA)

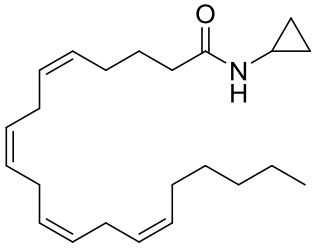

Arachidonylcyclopropylamide (ACPA)

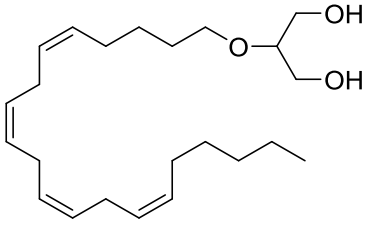

2-arachidonyl glyceryl ether (noladin ether)

Figure 1.7. Selective CB1 agonists

Chemical structures of CB1 selective agonists *R*-(-)-methanandamide, arachidonyl-2'-chloroethylamide (ACEA), and arachidonylcyclopropylamide (ACPA), as well as 2-arachidonyl glyceryl ether (noladin ether)

2. Selective CB2 agonists: can be classified according to their chemical structure into: classical, non-classical, and aminoalkylindole (Figure 1.8).
    a. Classical: includes the THC derivatives such as (6a*R*,10a*R*)-3-(1,1-dimethylbutyl)-6a,7,10,10a-tetrahydro-6,6,9 trimethyl-6*H*-dibenzo[*b*,*d*]pyran (JWH-133)
    b. Non-classical: {4-[4-(1,1-dimethylheptyl)-2,6-dimethoxy-phenyl]-6,6-dimethylbicyclo[3.1.1]hept-2-en-2-yl}times-methanol (HU-308)
    c. Aminoalkylindoles: includes (2-methyl-1-propyl-1*H*-indol-3-yl)-1-naphthalenylmethanone (JWH-015) and *R*-3-(2-iodo-5-nitrobenzoyl)-1-methyl-2-piperidinylmethyl)-1*H*-indole (AM1241)

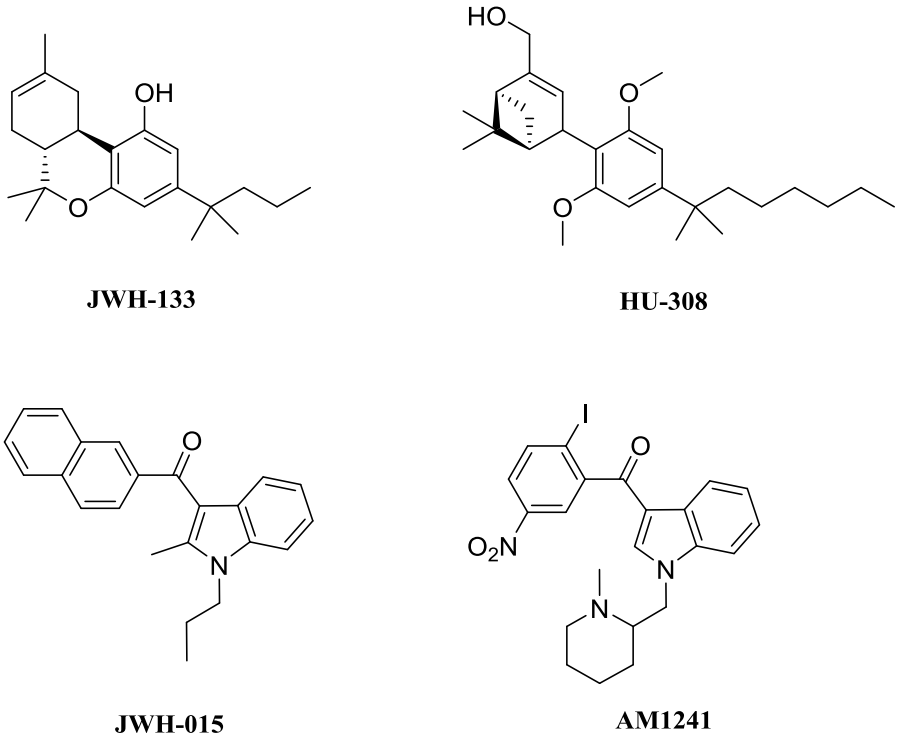

Figure 1.8. Selective CB2 agonists

Chemical structures of the CB2 selective agonists: JWH-133, HU-308, JWH-015, and AM1241

C. Selective CB1 and CB2 inverse agonists/antagonists:

1. Selective CB1 inverse agonists:

   Include ligands that can block the agonist-induced activation of CB1 receptors in a competitive manner and bind with significantly greater affinity to CB1 than CB2 receptors. These include the diarylpyrazole Rimonabant (SR141716), *N*-(piperidin-1-yl)-5-(4-iodophenyl)-1-(2,4-dichlorophenyl)-4-methyl-1*H*-pyrazole-3-carboxamide (AM251), 1-(2,4-dichlorophenyl)-5-(4-iodophenyl)-4-methyl-*N*-4-morpholinyl-1*H*-pyrazole-3-carboxamide (AM281), 4-[[6-methoxy-2-(4-methoxyphenyl)-3-benzofuranyl]carbonyl] benzonitrile (LY320135), and taranabant (MK-0364) (Figure 1.9).

2. Selective CB1 antagonists:

   These are ligands that are able to block the CB1 receptor without any reverse agonism effects. Examples of these ligands include: the structural analog of Rimonabant, *N*-piperidinyl-[8-chloro-1-(2,4-dichlorophenyl)-1,4,5,6-tetrahydrobenzo[6,7]cyclohepta[1,2-*c*]pyrazole-3-carboxamide] (NESS O327), and (6a*R*,10a*R*)-3-(1-methanesulfonylamino-4-hexyn-6-yl)-6a,7,10,10a-tetrahydro-6,6,9-trimethyl-6*H*-dibenzo[*b,d*]pyran (O-2050), which is the sulfonamide analog of Δ^8-THC with an acetylenic side chain (Figure 1.9).

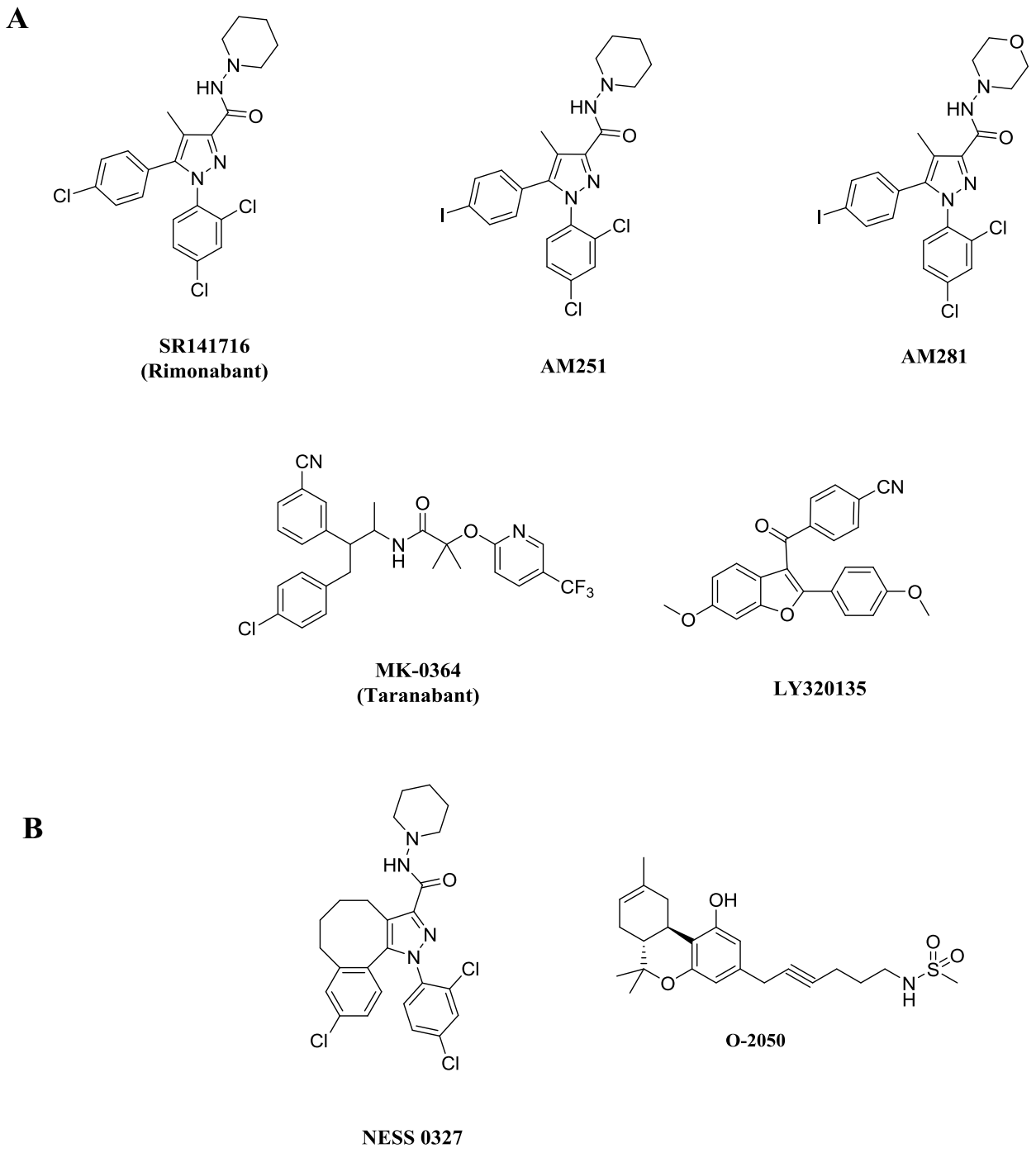

Figure 1.9. Selective CB1 inverse agonists/antagonists.

(**A**) Chemical structures of CB1 inverse agonists SR141716 (Rimonabant), AM251, AM281, MK-0364 (Taranabant), and LY320135. (**B**) Chemical structures of CB1 neutral antagonists NESS 0327, and O-2050.

3. Selective CB2 inverse agonists:

   These are ligands that block the agonist-induced CB2 receptor activation in a competitive manner, include [6-Iodo-2-methyl-1-[2-(4-morpholinyl)ethyl]-1*H*-indol-3-yl](4methoxyphenyl)methanone (6-iodopravadoline) (AM630), the diarylpyrazole *N*-[(1*S*)-endo-1,3,3-trimethyl bicyclo [2.2.1]heptan-2-yl]-5-(4-chloro-3-methylphenyl)-1-(4-methylbenzyl)-pyrazole-3-carboxamide (SR144528), and *N*-(1,3-benzodioxol-5-ylmethyl)-1,2- dihydro-7-methoxy-2-oxo-8-(pentyloxy)-3-quinolinecarboxamide (JTE-907) (Figure 1.10) [75].

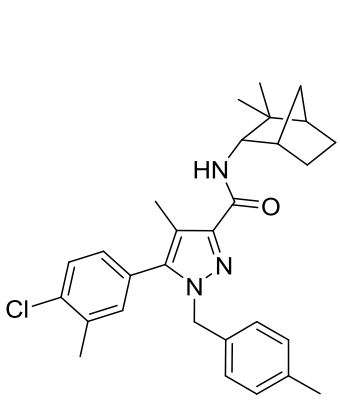

SR144528

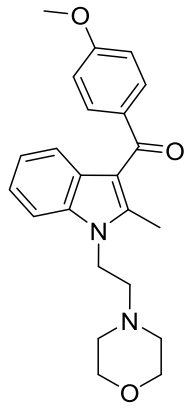

AM630

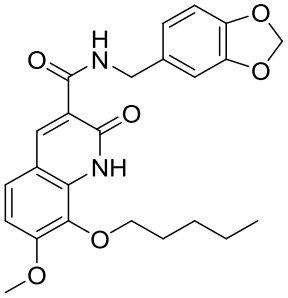

JTE-907

Figure 1.10. Selective CB2 inverse agonists.

Chemical structure of CB2 inverse agonists SR144528, AM630, and JTE-907

Table 1.1. Binding affinities (K_i) of CB1 and CB2 ligands

Cannabinoid Receptor Ligand	Binding Affinity (K_i) nM		Reference
	CB1	CB2	
Non-selective CB1 and CB2 agonists			
Δ^9-THC	41	36	[76]
HU-210	0.06	0.17	[39]
Anandamide (AEA)	61	279	[39]
2-AG	58	145	[77]
R-(+)-WIN55212	1.9	0.3	[76]
CP55,940	0.5	0.7	[78]
Selective CB1 agonists			
R-(-)-methanandamide	17.9	815	[39]
ACEA	1.4	195	[39]
ACPA	2.2	715	[39]
Noladin ether	9.1	480	[79, 80]
Selective CB2 agonists			
JWH-133	677	4.0	[81]
HU-308	> 10,000	22.7	[82]
JWH-015	383	14	[76]
AM1241	280	3.4	[83]
Selective CB1 inverse agonists			
SR141716	1.8	514	[84]
AM251	7.49	2290	[85]
AM281	12	4200	[86]
MK-0364	0.13	170	[87, 88]
Selective CB1 antagonists			
NESS 0327	0.00035	21	[89]
O-2050	6.8	250	[39]
Selective CB2 inverse agonists			
SR144528	437	0.6	[90]
AM630	5152	30	[91]
JTE-907	2370	35.9	[92, 93]

The binding affinities (*K*i) were measured by utilizing the radio-ligand displacement assay of labeled ligands (CP55940, SR144528, and/or SR141716). Binding affinities are expressed in nM.

1.3 THERAPEUTIC SIGNIFICANCE OF CANNABINOIDS

The endocannabinoid system (cannabinoids, cannabinoid receptors, and the proteins responsible for their synthesis, transports, and degradation) are highly expressed in different tissues of the body. It has been proven that the endocannabinoid system is involved in different regulatory functions such as the control of cardiovascular tone, energy metabolism, in the immune system, as well as in the reproductive system [94].

There are number of cannabinoid drugs that made it to the clinic in the past 30 years. The cannabis main active component, Δ^9-THC (dronabinol), itself reached the clinic as an anti-emetic drug for cancer patients and as an appetite stimulant for patients with AIDS in 1985 and 1992, respectively, and was marketed under the name Marinol® (Solvay Pharmaceuticals) [95, 96]. The synthetic analog of Δ^9-THC, known as nabilone, which is a non-selective CB1/CB2 receptor agonist was prescribed for the suppression of nausea and vomiting in chemotherapeutic patients and marketed under the name Cesamet® (Meda Pharmaceuticals) in 1981 [95]. Sativex® (GW Pharmaceuticals), which is a combination of Δ^9-THC and cannabidiol [97]. This drug was licensed in Canada in 2005 as an adjunctive treatment for the symptomatic relief of neuropathic pain in adults with multiple sclerosis [98, 99] and it is currently in phase III clinical trials for cancer pain patients [100].

As the high expression levels of CB1 receptors in the brain, especially in areas regulating appetite/satiety and the presence of these receptors in the gastrointestinal track as well as adipose tissues [101], research groups have focused on the potential weight loss mechanism when targeting the CB1 receptors [102]. As noted by several researchers, animals treated with cannabinoid agonists showed dramatic weight gain and obesity and this effect was not observed in CB1 receptor knockdown animals [103]. Based on these observations, possible blocking these receptors maybe

a new weight loss mechanism. Sanofi-Aventis Pharmaceuticals developed the first CB1 receptor inverse agonist for the purposes of appetite suppression and weight loss. The selective CB1 receptor inverse agonist SR141716, known as rimonabant (Acomplia®), reached the European market in 2006 [104, 105]. However, the US Food and Drug Administration (FDA) did not approve the marketing of the drug in the US due to some of the psychiatric side effects that were found in rimonabant's clinical trials [29, 30]. Eventually, the drug was withdrawn from the European market in 2008 when two patients on rimonabant committed suicide. Yet, CB1 blockade may still seem a valuable target in the field of weight regulation, and energy balance. Efforts should be focused on delivering such drugs without crossing the blood brain barrier in order to reduce psychoactive adverse effects. Furthermore, developing neutral antagonists lacking the CB1 inverse agonists' activities or developing periphery selective agents that do not target the CB1 receptors in the brain. The high expression of CB2 receptors in the periphery and immune tissues, however, accounts for its promising therapeutic uses without developing serious psychoactive side effects, albeit no approved CB2 selective drug has been approved, yet.

1.3.1 CANNABINOIDS AND TUMOR GROWTH

Cancer, the uncontrolled differentiation of cells, accounts for more than 14 million new cases and approximately 8.2 million deaths in 2012 worldwide, according to the World Health Organization. In the United States, there are more than 1.5 million new cases and more than 585 thousand deaths occurred due to cancer in 2014. Both sexes showed high mortality rates and new cases of lung cancer followed by prostate and breast cancers for men and women, respectively [106]. To date, cancer remains an invasive and incurable disease despite the continuous development of new treatments and methods.

Recently, cannabinoid receptors has been proven to be upregulated in tumor tissues compared to normal tissues. Specifically, cannabinoid receptors are highly expressed in different cancer tissues such as breast, prostate, and bone cancers suggesting these receptors are valuable targets for cancer cell attenuation [107]. Nomura and Thors showed aggressive tumor progression was observed associated with the upregulation of endocannabinoid-degrading enzymes in human tumor and cancer cell-lines. In mouse xenograft, reduction in the expression of monoacylglycerol lipase (the enzyme responsible for the degradation of endocannabinoid) reduced tumor growth and progression [108, 109]. Nevertheless, cannabinoids have been shown to play crucial roles as anti-tumor agents by reducing inflammation, cell proliferation, and cell survival. Munson and colleagues reported the first anti-tumor properties of cannabinoids in 1975. They reported the administration of Δ^9-THC inhibits lung adenocarcinoma growth *in-vitro* and *in-vivo* [110]. Since then the anti-cancer effects of cannabinoids have been studies extensively in order to understand the underlining mechanisms of these effects.

Anti-cancer signaling of cannabinoids:

The mechanism of the anti-tumor properties of cannabinoids is not fully illustrated. Cannabinoids exhibit anti-tumor activity through modulations of cell growth, cell migration, and apoptosis. These mechanisms differ with respect to cancer types and tissues. Figure 1.11 illustrates the anti-cancer signaling pathways of CB2 receptors. As previously explained, cannabinoids induce the *de novo* synthesis of ceramides. Ceramide activates the downstream signaling of ERK cascade resulting in cell-cycle arrest and apoptosis. Increasing ceramide levels due to cannabinoid stimulation, activates the p38-MAPK pathway. Activation of the p38-MAPK pathway leads to apoptosis through the activation of cysteine protease (caspases). Ceramide release may also activates the release of cytochrome c from the mitochondria to activate caspases leading to

apoptosis. Furthermore, increased ceramide levels co-recruits the activating transcription factor 4 (ATF4), tribbles homolog 3 (TRB3) and C/EBP homologous protein (CHOP) from the endoplasmic reticulum, all of which are involved in cellular response to stress stimuli leading to the downstream inhibition of protein kinase B (Akt) reducing the phosphorylation of I kappa B kinase (IKK) and thus inhibiting the nuclear factor kappa-light-chain-enhancer of activated B cells (NF-kB) activation and translocation [111]. Cannabinoid are coupled through the Gi/o proteins inhibiting adenylate cyclase production, thus reducing the cAMP levels. Reducing cAMP levels has been shown to inhibit the downstream protein kinase A (PKA) leading to apoptosis. Sustained activation of ERK induces the cyclin kinase inhibitor (p27/KIP1) resulting in cell-cycle arrest and apoptosis [107, 112]. CB2 receptor stimulation has been shown to inhibit the production of vascular endothelial growth factor (VEGF), thus inhibiting the migration, proliferation, and cell-survival of cancer cells through inhibiting angiogenesis [111].

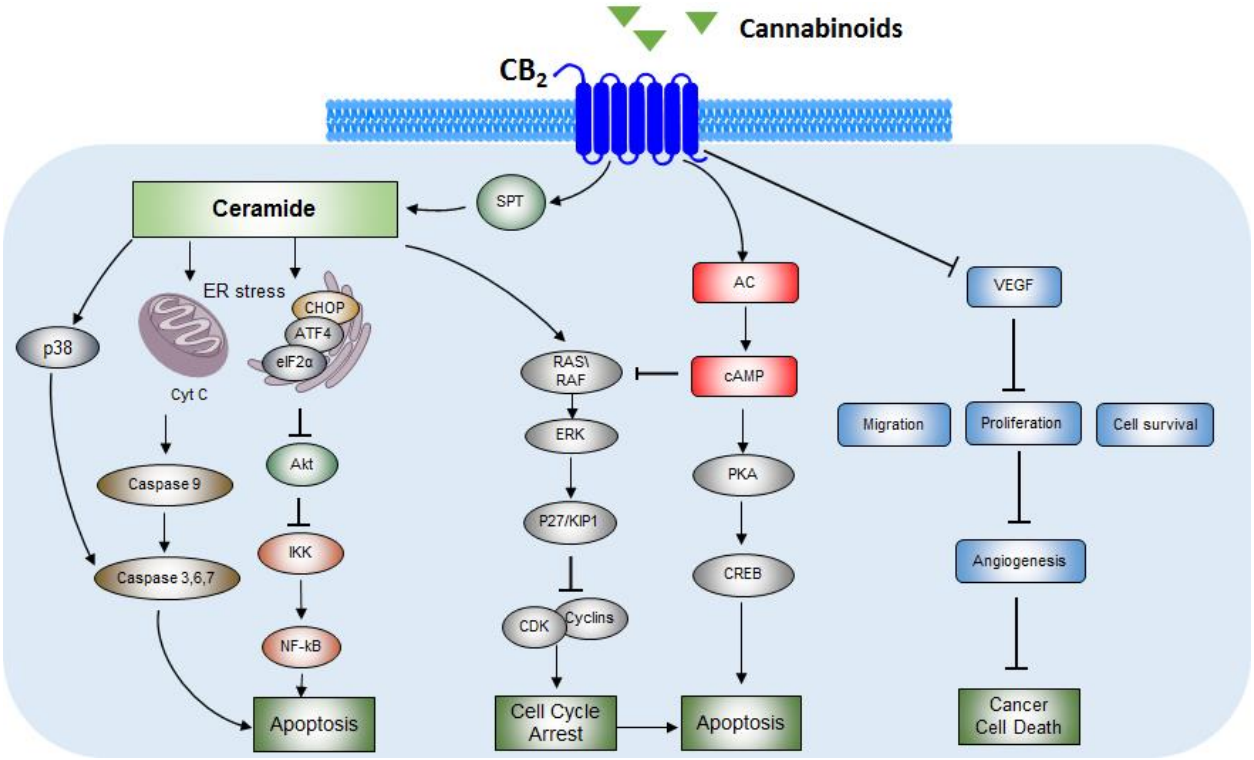

Figure 1.11. Anti-cancer signaling of CB2 receptors

Stimulation of CB2 receptor induces a *de novo* synthesis of ceramide leading to increase concentrations of ceramide levels. Ceramide activates ERK cascade leading to cell-cycle arrest and apoptosis. In addition, ceramide activates p38-MAPK leading to the activation of caspases and apoptosis. Ceramide also activates the release of cytochrome c thus activating caspases and apoptosis. Ceramide also induces ER stress activating ATF4, TRB3 and CHOP leading to the inhibition of Akt and NF-kB. Inhibition of AC reduces the levels of cAMP leading to the inhibition of PKA. CB2 receptor stimulation also inhibit VEGF thus inhibiting migration, survival and proliferation.

1.3.1.1 Breast cancer

Breast cancer accounts for 29% (~232 thousand) of new cancer cases and 15% (~72 thousand) of cancer deaths in the United States during 2014. Breast cancer is highly invasive and can metastasize to other organs such as lymph nodes, lungs, and bones. Studies show that there is high expression of CB2 receptors in breast cancer tissues and cell-lines compared to CB1 receptors. In addition, there is high correlation of the expression of CB2 receptors with known breast cancer markers such as estrogen and progesterone receptor levels, as well as the presence of the ERBB2/HER-2 oncogene [113]. Recently, the endocannabinoid system was shown to play important roles in tumor growth, apoptosis, and angiogenesis of breast cancer. Several breast cancer cell-lines were tested for the ability of cannabinoids to attenuate cancer growth. Δ^9-THC and cannabidiol (CBD) inhibited cell proliferation, induced apoptosis, and reduced migration in different breast cancer cell-lines. The mechanism was blocked by SR144528 (CB2 receptor inverse agonist) suggesting the roles of CB2 receptors. Qamri and co-workers investigated the effects of synthetic cannabinoids on different breast cancer cell-lines. Selective CB2 agonist JWH-133 at a dose of 10 μM was able to reduce breast cancer tumor growth, inhibit cancer migration, and induce apoptosis by caspase signaling cascade in MDA-MB231 and MDA-MB468 breast cancer cell-lines. In addition, JWH-133 was able to inhibit angiogenesis in different breast cancer cell-lines [114]. Endocannabinoids were also shown to have anti-tumor activity. Anandamide, 2-AG and methanandamide inhibited the proliferation, metastasis, and induced apoptosis of breast cancer cell-lines. Their underlining mechanism involved the utilization of CB1 and/or CB2 receptors [107].

In-vivo studies showed the ability of cannabinoids to attenuate tumor growth, migration, and angiogenesis. According to Caffarel *et al*., Δ^9-THC was able to inhibit cell proliferation and

angiogenesis in metastasis breast cancer animal model. This effect is mediated through the CB2 receptors, not the CB1 receptors. Further, the CB2 selective agonist JWH-133 was able to decrease size and number of tumors, reduces lung metastases, inhibit cell proliferation, and reduce angiogenesis in mice injected with different breast cancer cell-lines [114, 115]. In mice injected with the breast cancer cell-lines MDA-MB-231 and 4T1, cannabidiol reduced tumor size and decreased number of lung metastases [116]. Collectively, these data illustrates the importance of the endocannabinoid system in the cancer pathology and suggesting possible new target for future drugs targeting the cannabinoid receptors, particularly the CB2 receptors.

1.3.1.2 Prostate cancer

Prostate cancer is the tumor of the prostate gland in the male reproductive system. It is considered the second most frequently diagnosed tumor in men [117]. In 2014, over 233 thousand new cases were diagnosed and over 29 thousand of patients die from prostate cancer in the United States [106]. Prostate cancer can metastasize to other parts of the body, particularly the lymph nodes and the bones [118, 119].

Several studies have explored the involvement of the cannabinoid system in prostate cancer. The expression level of cannabinoid receptors in prostate cancer cell-lines were assessed and showed upregulated expression of CB1 and CB2 receptors in a wide range of cell-lines such as PC-3, DU-145, CWR22Rv1, LNCaP, and CA-HPV-10) as well as human prostate cancer tissues [47, 120-122]. *In-vitro* studies showed the ability of cannabinoids and endocannabinoids to attenuate prostate cancer growth and progression. Velasco and Ruiz demonstrated the anti-proliferative and pro-apoptotic effects of Δ^9-THC in different prostate cancer cell-lines [123, 124]. Furthermore, methanandamide exhibited nanomolar concentrations in the inhibition of prostate cancer proliferation and induced apoptosis. Olea-Herreo showed that these effects are mediate by CB2,

not CB1 receptors. In addition, the CB2 selective agonist, JWH-015, showed anti-proliferative, pro-apoptotic properties which were mediated by the CB2 receptors [125]. Sarfaraz and co-workers showed that WIN55212-2 inhibited cell growth and induced apoptosis in androgen-dependent and –independent prostate cancer cell-lines [122].

In-vivo data by Olea-Herreo and colleagues, showed JWH-015 was able to reduce tumor growth in athymic nude male mice injected with PC-3 cells and this effect was blocked by the CB2 selective inverse agonist SR144528 [125].

1.3.1.3 Bone cancer

There are two types of bone cancer: primary bone cancer, which originates from the bone, and metastatic bone cancer, which cancer is metastasized from other organs such as breast, lungs, or prostate. Primary bone cancer (sarcomas) can be divided into osteosarcoma (which develops in new tissues in growing bones) and chondrosarcoma (which develops in the cartilage). Osteosarcoma occurs frequently in young people (age 10 – 20) and chondrosarcoma occurs more frequently in adults [126]. There are more than 3,000 new cases of sarcoma diagnosed and more than 1,400 deaths occurred in the United States during 2014 [106].

The cannabinoid receptors have been shown to play roles in sarcomas. Khasabova *et al*., and Hald *et al.*, assessed the expression of cannabinoid receptors CB1 and CB2 in NCTC-2472 sarcoma cells [127, 128]. They showed upregulation of both receptors in these cells suggesting a possible role of the cannabinoid system in bone cancer. *In-vitro* studies examining the roles of cannabinoid ligands to attenuate sarcoma progression demonstrates the ability of WIN55212-2 to induce apoptosis in the NCTC-2472 sarcoma cell-lines. In addition, the CB2 selective agonist, AM-1241, reduced bone loss in mice injected with NCTC-2472 cell-line [129].

It is well-established that cannabinoids play critical roles in reducing bone-related pain. CP-55,940 produced anti-nociceptive effects in mice injected with different cells such as NCTC-2472 and B16-F10. It is believed that the anti-nociceptive properties of CP-55,940 is mediated by the CB1, but not CB2 receptors [130]. However, the selective CB2 agonist, AM-1241, produced similar anti-nociceptive effects that are mediated by the CB2 receptors [129, 131].

1.3.1.4 Blood cancer

According the American Cancer Society, there were over 35,000 deaths and more than 165,000 new cases of blood cancers during 2014 [106]. Several literature reported the involvement of the cannabinoid system in the attenuation of different types of blood cancers. McKallip and coworkers reported the expression of CB2 receptors in a number of human leukemia and lymphoma cell-lines, such as Jurkat, Molt-4, and Sup-T1. Furthermore, the reported the ability of THC, HU-210, anandamide, and JWH-015 to induce apoptosis in these cell-lines [132]. Gustafsson *et al.* reported the ability of *R*-(+)-methanandamide and WIN55212-2 to induce apoptosis via ceramide accumulation and p38 activation in mantle cell lymphoma [133]

Multiple myeloma (MM) is the malignant proliferation of plasma B cells in the bone marrow. It is associated with high levels of monoclonal proteins in the blood and/or urine, decreased immunoglobulin (Ig) levels and lytic bone diseases [134, 135].In 2013, nearly 22,000 new cases were diagnosed and more than 10,000 deaths occurred from the disease according to the American Cancer Society [136]. The incidence is higher with increasing age (between 60 and 70 years old) and only 3% of all patients are younger than 40 years old [137, 138].

The clinical manifestations of MM patients range from bone disease, hypercalcemia, hematological abnormalities, renal impairment and peripheral neuropathy. Bone diseases are presented in 60% of MM patients. These may include: lytic bone lesions, vertebral fractures and/or

osteoporosis. Hypercalcemia is considered the most common metabolic abnormality in MM (accounts for more than one-third of patients) [139]. Hypercalcemia results from osteolysis and bone resorption caused by secreted cytokines in the bone marrow microenvironment, such as receptor activator of nuclear factor-κB ligand (RANKL), macrophage inflammatory protein (MIP)-1α, and tumor necrosis factors (TNFs). Bone resorption leads to the efflux of calcium into the extracellular fluid [140]. The hematological abnormalities associated with MM include anemia, leukopenia and thrombocytopenia. Renal impairment affects more than 20% of MM patients. The mechanism of renal impairment in MM is related to the excess accumulation of light chains within the distal tubule leading to a condition known as myeloma kidney. Peripheral neuropathy represents a significant manifestation in MM patients during diagnosis and as a toxicity limitation of various agents used in the treatment of MM [139].

MM remains an incurable disease worldwide associated with complicated treatment regimens and modalities. Many complex molecular signaling pathways are involved in the MM pathogenesis, which accounts for the difficulty in managing the disease. The most important pathogenic contributor to the MM pathogenesis is the bone marrow microenvironment (BMME) in addition to other signaling pathways that have shown to be crucial in the MM pathogenesis. The advances in the understanding of the MM pathogenesis mechanisms aided the discovery of new chemical agents. Immunomodulatory drugs (IMiDs) such as thalidomide, lenalidomide and recently pomalidomide are used in the clinic to treat MM patients Figure 1.12 [141]. The Ubiquitin Proteasome System (UPS) plays a critical role in the MM disease progression. Many cell survival and cell growth proteins are regulated via the proteasome pathway. Bortezomib, Figure 1.12, is the first discovered proteasome inhibitor used in MM and is considered the first line treatment. Although the disease remains incurable, significant advances in the treatment and the development

of chemical agents have aided in the understanding of the disease pathogenesis with improved life expectancy of patients with median overall survival prolonged to 7 – 8 years [142].

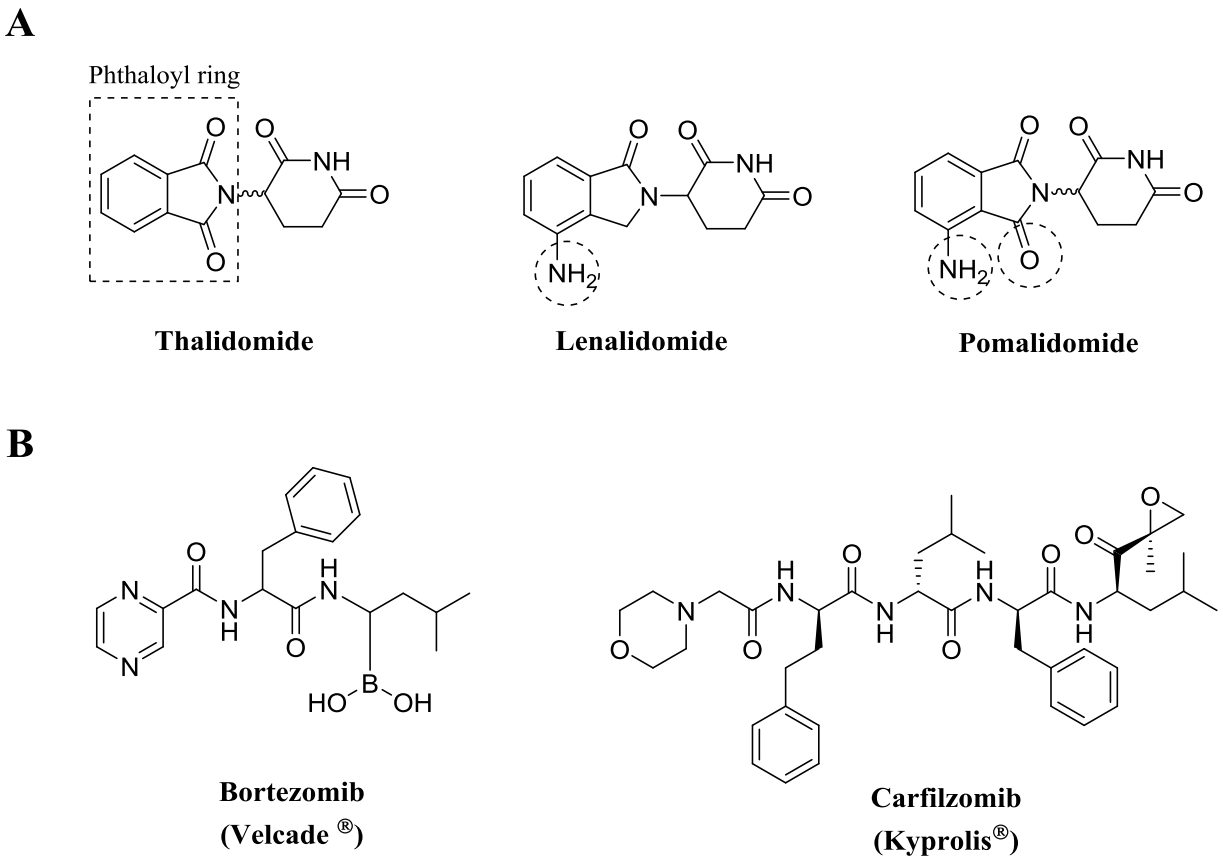

Figure 1.12. Chemical structures of anti-MM drugs in the market.

(A) Immunomodulatory drugs: Thalidomide (Thalomid®), Lenalidomide (Revlimid®, CC-5013) and Pomalidomide (Pomalyst®, CC-4047). Thalidomide was the first IMiD introduced in the market. Chemical modifications of the phthaloyl ring was performed by adding an amino group and removing one of the carbonyl groups to generate lenalidomide. Pomalidomide was derived from thalidomide with the addition of an amino group to thalidomide. **(B)** Proteasome inhibitors: Bortezomib, the first proteasome inhibitors approved for MM and carfilzomib the recently approved proteasome inhibitor for MM [143].

Although significant improvement of the life expectancy of the MM patient, the disease remains difficult to cure with current treatment modalities. The urge for discovering new mechanisms and targets to eradicate the disease remains a hot area of research. As the MM disease is a cancer of the plasma B cells, the cannabinoid receptors are known to be highly expressed in these cells, in particular the CB2 receptors. Recently, our lab carried out extensive studies to explore the CB2 receptors as novel target for MM disease. The expression of CB2 receptors in multiple myeloma cell lines were carried out by utilizing RT-PCR and western blot. Unlike CB1 receptors, western blot studies of multiple myeloma cell-lines (RPMI8226, U266, H929 and MM.1S) showed high expression levels of CB2 receptors Figure 1.13. This was confirmed by measuring the mRNA levels of CB2 using RT-PCR utilizing CB2 specific primers. These novel discoveries prompted us to carry on medicinal chemistry studies in order to identify novel CB2 ligands and explore the anti-cancer capabilities, particularly anti-MM properties.

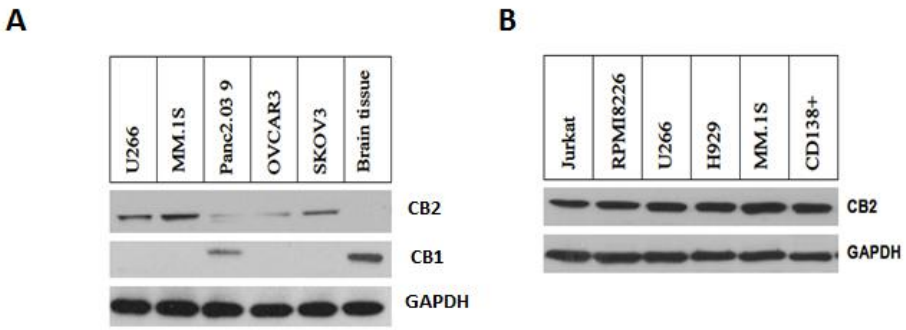

Figure 1.13. Cannabinoid receptors expression in different cell-lines.

(A) Comparison of the expression level of cannabinoid receptors 1 and 2 in different cancer cell-lines: MM cell-lines (U266, and MM.1S), pancreatic cancer cell-line (Panc2.039), ovarian cancer cell-line (OVCAR3, and SKOV3), as well as normal brain tissues. **(B)** CB2 receptor expression was measured in different MM cell-lines including Jurkat, RPMI8226, U266, H929, MM.1S as well as CD139+ [97].

1.3.2 CANNABINOIDS AND BONE HOMEOSTASIS

Bone remodeling process:

The bone structure, throughout the lifetime, undergoes substantial changes comprised of three phases: 1) rapid skeletal growth phase with increased bone peak; 2) steady state phase where the bone mass is constant; 3) age-related bone loss. These changes accounts for the continuous process of renewal and repair, known as the bone remodeling. Bone remodeling is highly regulated by various hormones, peptides, and cytokines which can be divided into four stages: bone resorption phase, reversal phase, bone formation phase, and the quiescence phase. Bone resorption is the process of the removal of old bone by osteoclasts (large multinucleated, motile, and highly specialized cell derived from monocytes [144]). Several growth factors and cytokines are involved in the formation and activity of osteoclasts including the receptor activator of nuclear factor kappa-B ligand (RANKL), osteoprotegerin (OPG), and macrophage colony forming factor (M-CSF) [145-147]. Rapid apoptosis and removal of the osteoclasts by phagocytosis occurs which activates the reversal phase. During this phase, the old bone is coated by a thin layer of a matrix rich in glycosaminoglycans, glycoproteins, and acid phosphatases [148]. Osteoblasts (multinucleated cells originating from mesenchymal osteoprogenitor cells in the bone marrow [149]) attach to the resorbed site by several proteins and growth factors such as the transforming growth factor β (TGF-β), and type-1 collagen. Parathyroid hormone, estrogen, and vitamin D3 are also known to stimulate osteoblast differentiation [150]. Following the bone formation phase is the quiescence phase where mature osteoblasts are either buried within the newly matrix as osteocytes or converted to lining cells covering the new bone [151].

Impairment of the bone resorption and bone formation due to local and systemic factors accounts for the major causes of bone diseases. Osteoporosis is a common degenerative disease

characterized by reduced bone mineral density (BMD) and increased bone fragility and fractures [152]. Osteoporosis causes more than 8.9 million fractures every year and it is estimated to affect 200 million women worldwide. Bone fractures is the main cause of morbidity among osteoporotic patients in the elderly. In 2000, there were about 9 million new osteoporotic fractures: 1.6 million in the hip, 1.7 million in forearm, and 1.4 million were in the vertebrae [153]. Worldwide incidence of hip fractures is projected to increase by 310% and 240% in men and women, respectively, by the year 2050 [154]. Primary osteoporosis occurs in women at their postmenopausal period where levels of estrogen naturally declines. Decreasing levels of estrogen causes a rapid increase in the secretion of several cytokines and growth factors such as interleukin-1 (IL-1), interleukin-6 (IL-6) and tumor necrosis factor-alpha (TNF-α) as well as decreases secretions of TGF-β in the bone. Elevated levels of these cytokines and growth factors results in increased osteoclast activity (osteoclastogenesis) as well as osteoblast activity [155]. In addition, lower levels of estrogen is associated with increased levels of RANKL and M-CSF (both stimulate osteoclastogenesis) and decreased levels of OPG [156].

Secondary osteoporosis is caused by the long-term treatment with glucocorticoids (GCs). Glucocorticoids are class of steroid hormones that has many uses as immunosuppressive agent with a common bone loss side effect. Long-term GC treatment is associated with decreased bone formation and osteonecrosis (collapse of large joints). GCs regulate osteoblast production and promote the apoptosis of osteoblasts (inhibit osteoblastogenesis) and regulate osteoclasts by inhibiting osteoclast formation. GCs inhibit the synthesis of osteoclastogenesis promoters such as IL-1 and TNFs. In addition, GSs play important roles in reducing the metabolic and proliferative activity of osteoblasts. For example, GCs have been shown to inhibit the synthesis of collagenase-

3, reduce the expression of insulin-like growth factor 1 and 2 (IGF-1, -2), and decreased TGF-β1 activity [157].

Roles of Cannabinoids in the bone remodeling process:

Endocannabinoids and their metabolizing enzymes have been reported, recently, in the skeleton. The endogenous cannabinoids AEA and 2-AG were found in high concentration in the bone marrow. In addition, osteoclasts and osteoblasts are able to produce AEA and 2-AG. Osteoclasts, osteoblasts, stromal cells, osteocytes, and adipocytes are capable to express the endocannabinoid metabolizing enzymes, such as NAPE-phospholipase D, FAAH, and DAGLs α and β. Furthermore, several studies demonstrated the expression of the cannabinoid receptors 1 and as well as GPR55 and TRPV1 in the skeleton. Specifically, CB1 receptors are expressed in low levels in osteoblasts and the mouse bone marrow-derived stromal cells. In contrast, CB2 receptors are highly expressed in osteoclasts, osteoblasts, and osteocytes.

Following estrogen-deficiency in mice, CB1 and CB2 expression were highly upregulated in osteoclasts and osteoclasts bone-marrow precursor cells. CB1 selective inverse agonist, AM251, and CB2 selective inverse agonist, AM630, inhibited osteoclast formation, fusion, polarization, and activity [158]. However, there are conflicting data on the effect cannabinoid agonists of osteoclasts and osteoblasts. Endocannabinoids (AEA, 2-AG), synthetic cannabinoids CP55940, JWH133 and HU308 increased osteoclast number, size, and stimulated bone resorption. Other research groups demonstrated that the CB2 selective agonist HU308 inhibited osteoclast formation [158-160]. These data suggest the importance of the cannabinoid system in the regulation of bone mass and that the development of CB2 selective inverse agonist show a promising new class in the treatment of osteoporosis.

The bone marrow microenvironment (BMME) plays a critical role in the progression of MM. In fact, MM cells stimulate osteoclastogenesis by the increasing levels of RANKL and decreasing OPG levels. In addition, MM cells block the differentiation and activity of osteoblasts. Adhesion molecules, such as the vascular cell adhesion molecule 1 (VCAM-1) is highly expressed and produced from MM and BM cells. Adhesion molecules have been demonstrated to upregulate RANKL expression and downregulate OPG levels. Furthermore, the interaction of MM cells to the bone marrow has been reported to produce several cytokines and growth factors that are anti-apoptotic and promote osteoclastogenesis. Examples of these cytokines are IL-6, IGF-1, stromal cell-derived factor 1 (SDF-1α), and VEGF.

Osteoclasts produced from the BM interaction with MM cells enhance the MM growth and survival. In addition, osteoclasts protect the MM cell from apoptosis and play roles in the resistant mechanisms of MM to anti-cancer drugs [161].

2.0 RECENT DEVELOPMENT OF CANNABINOID RECEPTOR 2 LIGANDS

Since the isolation and discovery of the main active constituent of *Cannabis sativa*, Δ^9-THC, cannabinoid research gained a lot of attention. This was reinforced by the discovery and isolation of the two main cannabinoid receptors 1 and 2. Several chemotype compounds were developed with different potency and selectivity properties. As we have shown in Chapter 1 the critical roles of the cannabinoid system in several physiological and disease state, the development of cannabinoid ligands has gained a lot of attention. Specifically, CB2 selective ligand discovery is of highest demands as the expression of this receptor is higher in the periphery and the immune system. Furthermore, the recent withdrawal of the CB1 selective inverse agonist, Rimonabant, from the European market highlighted the complex signaling pathways involved in the cannabinoid system.

In the past decade, over 400 CB2 chemical patents, and over 1500 new chemical ligands have been developed. Due to the lack of a high-resolution X-ray crystal structure of the CB2 receptor, several chemical discovery and development methods were employed, such as pharmacophore drug discovery, high-throughput screening methods (computational and biochemical), molecular docking studies, and fragment-based drug discovery. This chapter will highlight the recent advances in the development of selective CB2 ligands and demonstrating the different scaffold and strategies employed in the development of these ligands.

2.1 TETRAHYDROCANNABIOID DERIVATIVES

Since the discovery of the Δ^9-THC, several tetrahydrocannabinol derivatives have been developed with high potency and selectivity. Huffman and coworkers explored the different modifications on the classical THC chemical scaffold. As have been shown previously, the removal of the phenolic hydroxyl group from Δ^8-THC led to the discovery of JWH-133 (section 1.2) which was evaluated in several disease states, such as inflammatory pain, hepatic injury, and colitis as well as anti-tumor properties. Recently, Huffman developed new bromo-Δ^8-THC by replacing the phenolic hydroxyl to aryl bromide which resulted in the discovery of novel ligands with high CB2 potency and selectivity (Compound **2.1**, CB2 K_i = 28 nM, Figure 2.1).

Burdick and coworkers reported the synthesis of novel Δ^9-THC derivatives as selective CB2 ligands. The chemistry focused on the conversion of the phenol of Δ^9-THC to other functionality through palladium catalyzed reactions. Two analogs with sub 100 nM affinity for the CB1 and CB2 receptors were discovered (compounds **2.2** and **2.3**, Figure 2.1) [162].

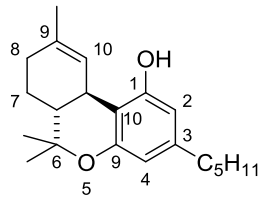

Δ^9-THC

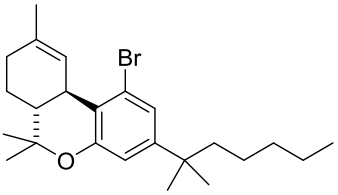

2.1
CB2 K_i = 28 nM

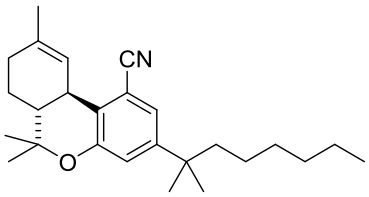

2.2
CB2 K_i = 5.3 nM
CB1 K_i = 67.8 nM
SI = 13

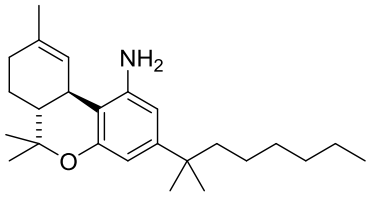

2.3
CB2 K_i = 2.9 nM
CB1 K_i = 11.7 nM
SI = 4

Figure 2.1. Chemical structures of THC derivatives

2.2 PURINE DERIVATIVES

Hollinshead *et al*. at Eli Lilly performed medium throughput screening of a GPCR focused library of 130 K compounds utilizing competition-binding assay for hCB2 and hCB1 receptors. Subsequently the hit compounds were tested for their functionality by utilizing the [^{35}S]-GTPγS hCB2 assay in CHO cells. The lead compound **2.4**, a thienopyrimidine derivative, was identified which possessed moderate CB2 selectivity (hCB2 K_i = 16 nM) and behaved as a full agonist (CB2 EC_{50} = 24.8 nM) (Figure 2.2). Compound **2.4** also suffered from poor metabolic stability *in-vitro* as well as rapid *in-vivo* clearance. Subsequently, it was subjected to chemical modification to improve its potency, selectivity and physicochemical properties. The replacement of the thienopyrimidine core with a purine core, moderately improved the potency as well as physicochemical properties (compound **2.5**). With further optimizations and modification, compound **2.6** was discovered with high potency, selectivity as well as improved metabolic and physicochemical properties (Figure 2.2) [163].

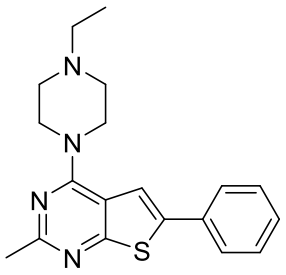

2.4
CB2 K_i = 16 nM

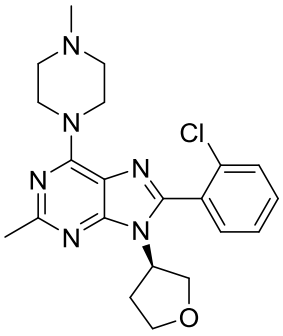

2.5
CB2 EC_{50} = 8.8 nM
CB1 EC_{50} > 100,000 nM

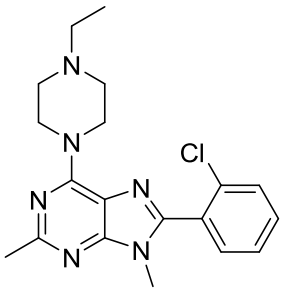

2.6
CB2 EC50 = 4.6 nM
CB1 EC50 = 948 nM

Figure 2.2. Chemical structures of purine derivatives

2.3 PYRIDINE DERIVATIVES

Scientists at GlaxoSmithKline carried out a research to discover novel CB2 selective agonist with the aim at improving *in-vitro* metabolic stability as well as CB2 selectivity. High-throughput screening identified aminopyridine, compound **2.7** (Figure 2.3), which was subjected to chemical modifications to overcome the metabolic instability. The SAR studies included: 1) to replace the lipophilic azepane ring, 2) to reduce the electron density of the aminopyridine core by introducing ring substitutions, and 3) to replace the dichlorophenyl with less lipophilic heterocycles. Initial SAR study led to the identification of **2.8** by replacing the azepane ring with a morpholine. Compound **2.8** showed good CB2 potency but relatively high *in vitro* clearance. Keeping the morpholine group as the amine substituent, SAR studies were carried out to investigate the replacement of the dichlorophenyl with different groups and fragments, to introduce electron withdrawing substituents into the core, and to lower the lipophilicity by introducing another pyridyl ring to the core. As a result several analogs were synthesized and biologically evaluated yielding varying potencies and metabolic stabilities, for example compound **2.9** [164]. Further SAR studies were carried out on the three positions of the lead compound led to the discovery of **2.10** which showed high CB2 potency and good pharmacokinetic profile as well as its ability as an anti-inflammatory agent after oral administration (Figure 2.3) [165].

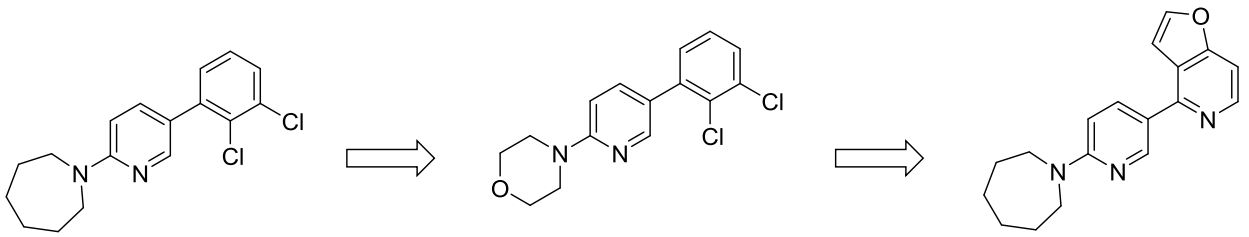

2.7
CB2 EC_{50} = 40 nM

2.8
CB2 EC_{50} = 79 nM

2.9
CB2 EC_{50} = 63 nM

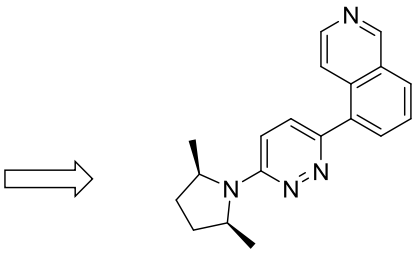

2.10
CB2 EC_{50} = 10 nM
SI = 794

Figure 2.3. Chemical structures of aminopyridines

A research group led by Bartolozzi *et al.* patented over 150 pyridine derivatives. Among those derivatives, 126 compounds exhibited high CB2 affinity. Importantly, compound **2.11**, showed the highest CB2 affinity with CB2 EC_{50} of 0.093 nM. *In-vitro* studies demonstrated the ability of these pyridine derivatives to reduce inflammatory pain (Figure 2.4) [166].

Chu *et al.* aimed on the discovery of pyridine derivatives by chemical modifications of a series of (morpholinomethyl)aniline carboxamides (exemplified by compound **2.12**). The replacement of a phenyl ring with a pyridine led to the discovery of a novel chemical series of CB2 ligands. Compound **2.14** demonstrated the highest CB2 affinity and selectivity among those new series (CB2 K_i = 24 nM, CB1 K_i = 3800 nM, Figure 2.4). Moreover, this compound showed good efficacy *in-vivo* after oral administration in a neuropathic pain rat model [167].

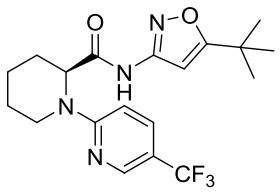

2.11
CB2 EC_{50} = 530 nM

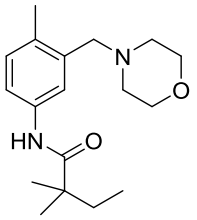

2.12
CB2 K_i = 120 nM
CB1 K_i = 4% inhibition at 10 μM

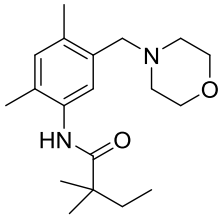

2.13
CB2 EC_{50} = 530 nM
CB1 K_i = 18% inhibition at 10 μM

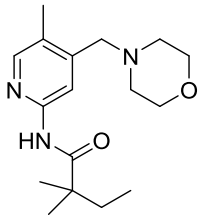

2.14
CB2 K_i = 24 nM
CB1 K_i = 3800 nM

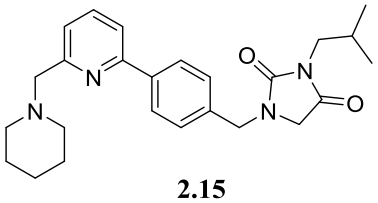

2.15
CB2 EC_{50} = 2.5 nM
SI > 1000
hERG pK_i = 5.5
F% (po) = 4%

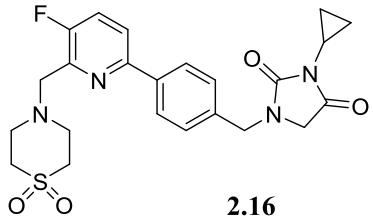

2.16
CB2 EC_{50} = 10 nM
SI > 1000
hERG pK_i < 4
F% (po) = 100%

Figure 2.4. Chemical structures of pyridine derivatives

Merck scientist performed compound screening followed by small optimization campaign that resulted in the identification a series of 1-(4-(pyridin-2-yl)benzyl)imidazolidine-2,4-dione derivatives. The initial hit compound **2.15**, possessed high CB2 affinity (CB2 EC_{50} = 2.5 nM) with more than 1000-fold selectivity over CB1 receptors. The hit compound however showed low oral bioavailability with some affinity for the hERG ion channel. Chemical modification of the hit compound led to the discovery of compound **2.16**, which demonstrated high CB2 affinity (CB2 EC_{50} = 10 nM) and selectivity (SI >1000) and behaved as an agonist with high bioavailability (Figure 2.4) [168].

2.4 PYRIMIDINE CARBOXAMIDES DERIVATIVES

A group of scientists at GlaxoSmithKline initiated a program to discover selective CB2 agonists with the aim to treat chronic pain, since CB2 agonists were shown to reduce inflammatory pain in the carrageenan model [169]. Pharmacophore drug discovery approach was utilized by collecting the structures of known cannabinoid ligands to generate the pharmacophore model. Subsequently, about 1000 compounds were selected and tested for their CB2 and CB1 affinity by utilizing the [^{35}S]-GTPγS assay. The hit compound **2.17**, a trifluoromethyl substituted pyrimidine ester showed high CB2 affinity with no affinity towards the CB1 (CB2 EC_{50} = 630 nM, CB1 EC_{50} > 10,000 nM). Lead optimization and chemical modifications were carried out and compound **2.18** was identified. Compound **2.18** showed high CB2 affinity (CB2 EC_{50} = 63 nM) and selectivity with an oral ED_{50} of 0.1 mg/kg in the rat FCA model of inflammatory pain. Currently, this compound is known as GW 842166X and is in clinical trial for the treatment of inflammatory pain (Figure 2.5) [170].

GW 833972A was also identified at GlaxoSmithKline (data unpublished) as a selective CB2 full agonist (CB2 EC_{50} = 50 nM). In addition, GW 833972A was tested on human and on guinea-pig sensory nerves in the airways and showed its ability in the treatment of chronic cough (Figure 2.5) [171].

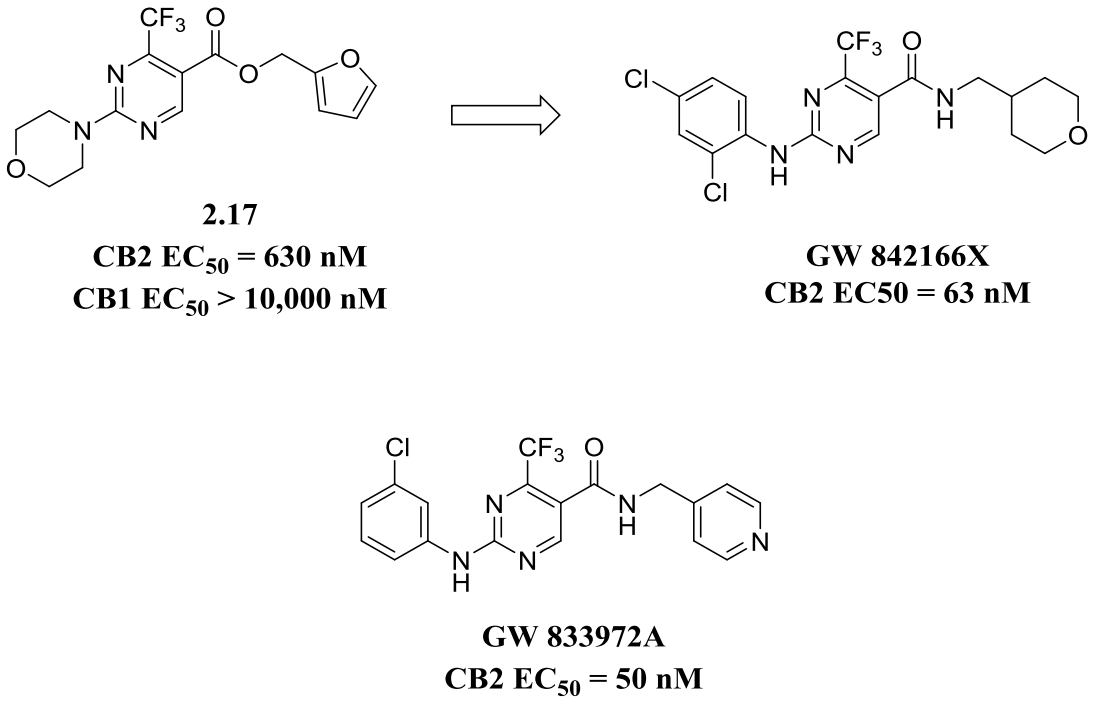

2.17
CB2 EC_{50} = 630 nM
CB1 EC_{50} > 10,000 nM

GW 842166X
CB2 EC50 = 63 nM

GW 833972A
CB2 EC_{50} = 50 nM

Figure 2.5. Pyrimidine carboxamides derivatives

2.5 DIHYDROQUINOLINE-3-CARBOXAMIDES AND 1,8-NAPHTHYRIDINONE

Researchers at the University of Lille first reported the discovery and identification of 4-oxo-1,4-dihydroquinoline-3-carboxamide derivatives as a novel class of CB2 receptor agonists. Their design and synthesis approach was based on other known cannabinoid pharmacophores by modifying two positions on the 4-oxo-1,4-dihydroquinoline-3-carboxamide scaffold. At the R1, they introduced different alkyl or benzyl groups, while at position 3 they tested different aliphatic or aromatic carboxamide groups. Four derivatives exhibited high CB2 affinity and selectivity based on competition-binding experiments utilizing [^{3}H]-CP-55940 on CB1 and CB2 receptors (CB2 K_i < 38 nM, SI > 150). Moreover, in the [^{35}S]-GTPγS binding assay, these derivatives were shown to behave as CB2 agonists. Particularly, compound **2.19** bearing a 1-(3,5-dimethyl)adamantyl at the R1 position, hydrogen on the R2 position, and *n*-pentyl at the R3 position displayed the highest CB2 potency with a CB2 K_i of 15.8 nM (Figure 2.6) [172, 173]. Manera *et al*. explored different substitution on the 4-oxo-1,4-dihydroquinoline core at the R4 position and reported a series of substituted 4-oxo-1,4-dihydroquinoline-3-carboxamide derivatives. Two compounds demonstrated high CB2 affinity and selectivity with CB2 K_i = 4.8 and 3.3 nM for compounds **2.20** and **2.21**, respectively, and both compounds behaved as CB2 agonists (Figure 2.6) [174].

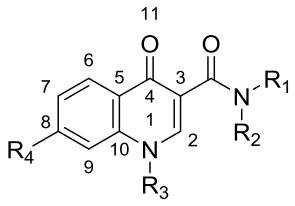

4-oxo-1,4-dihydroquinoline-3-carboxamide Scaffold

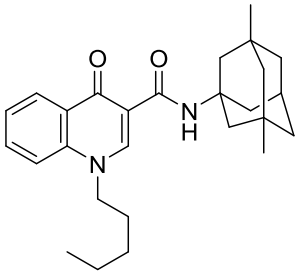

2.19
CB2 K_i = 15.8 nM

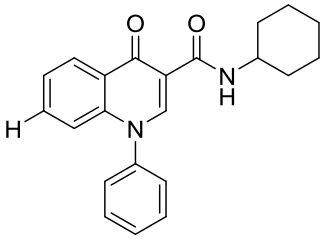

2.20
CB2 K_i = 4.8 nM

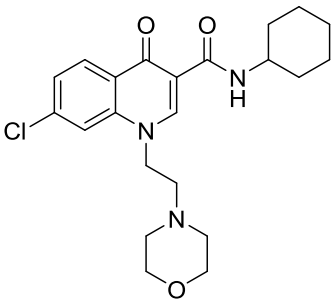

2.21
CB2 K_i = 3.3 nM

Figure 2.6. 4-oxo-1,4-dihydroquinoline-3-carboxamide derivatives

In addition, Manera *et al*. reported new 4-oxo-1,4-dihydroquinoline-3-carboxamide derivatives with substitutions on the 4-oxo-1,4-dihydroquinoline core, namely the 1,8-naphthyridin-4(1*H*)-on-3-carboxamide scaffold. Molecular docking studies were carried out on the designed derivatives to illustrate the interactions of the ligands with the constructed CB1 and CB2 homology models. Compound **2.22** (also known as CB13), showed a CB2 K_i of 50 nM with a selectivity of over 50 and behaved as a CB2 agonist (Figure 2.7) [174]. Cinachi *et al.* reported that CB13 induced apoptosis in 2 human cancer cell-lines by increasing ceramide levels. In addition CB13 demonstrated the ability to slow the growth of a mouse model of colon cancer [175].

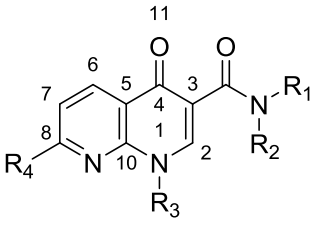

1,8-naphthyridin-4(1*H*)-on-3-carboxamide scaffold

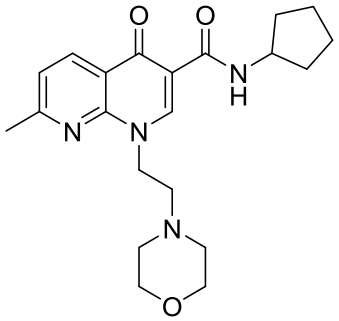

2.22 (CB13)
CB2 K_i = 50 nM
SI > 50

Figure 2.7. 1,8-naphthyridin-4(1*H*)-on-3-carboxamide derivatives

Following the discovery and identification of the 1,8-naphthyridin-4(1*H*)-on-3-carboxamide, Manera *et al*. investigated another modification on the 1,8-naphthyridin-4(1*H*)-on-3-carboxamide central core and synthesized a series of 1,8-naphthyridin-2(1*H*)-on-3-carboxamide. Compounds **2.23** and **2.24** showed the highest CB2 binding affinity of 0.9 and 5.8 nM with selectivity indices of 286 and 262, respectively. Interestingly, these two compounds were 13-fold and 7-fold more potent than the corresponding *trans*-isoforms for compounds **2.23** and **2.24**, respectively (Figure 2.8) [176].

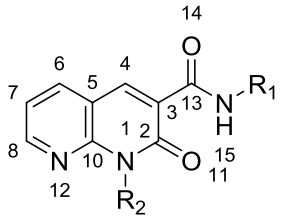

1,8-naphthyridin-2(1*H*)-on-3-carboxamide scaffold

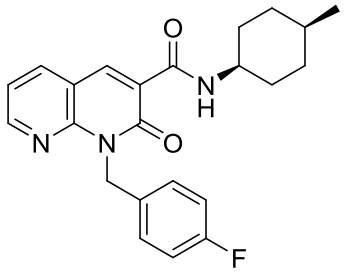

2.23
CB2 K_i = 0.9 nM
SI = 286

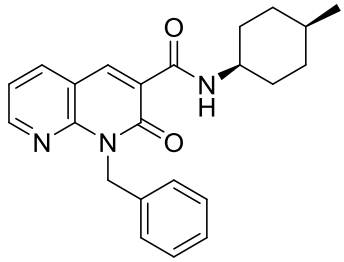

2.24
CB2 K_i = 5.8 nM
SI = 262

Figure 2.8. 1,8-naphthyridin-2(1*H*)-on-3-carboxamide derivatives

Research group at the University of Siena explored different substitutions on the quinolone core of the 4-oxo-1,4-dihydroquinoline-3- carboxamide scaffold. They tested various substitutions such as halides, aryl, alkyl, alkoxy, and aryloxy groups differing steric/electrostatic properties. Moreover, The N-1 pentyl chain and adamantyl group were either retained or replaced with other lipophilic groups, such as prop-1-en-3-yl, but-1-en-4-yl, pent-1-en-5-yl, or (*R*)-1-phenylethyl. Several ligands were shown to possess high CB2 affinity and selectivity. Specifically, compounds **2.25** and **2.26** exhibited CB2 binding affinity of 6.3 and 3.8 nM with a selectivity index of 194 and > 2666, respectively (Figure 2.9). Importantly, compound **2.25** showed analgesic activity in the formalin test of acute peripheral and inflammatory pain in mice [177]. Moreover, compound **2.26** exhibited anti-nociceptive properties. These two compounds differed in their cellular functionality as demonstrated by the [^{35}S]-GTPγS binding assay which showed compound **2.25** behaved as an agonist while compound **2.26** is an inverse agonist and that both CB2 agonists and inverse agonists show anti-inflammatory properties. It is believed that the aliphatic substitutions at the R2 position influenced the agonism property while aryl substitution influenced the inverse agonism property [178].

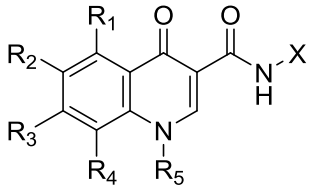

4-oxo-1,4-dihydroquinoline-3-carboxamide scaffold

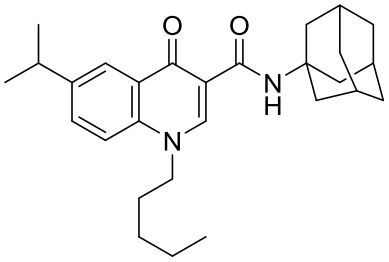

2.25
CB2 K_i = 6.3 nM
SI = 194

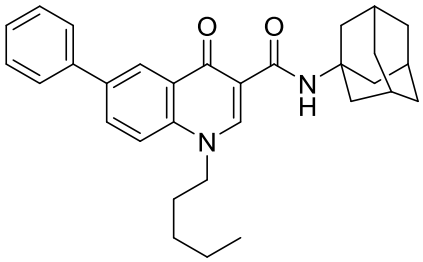

2.26
CB2 K_i = 3.8 nM
SI > 2666

Figure 2.9. Recent 4-oxo-1,4-dihydroquinoline-3- carboxamide derivatives

El Bakali *et al.* investigated the replacement of the 1,4-dihydroquinoline moiety with 1,4-dihydropyridine moiety. In addition, replacement of the 4-oxo- moiety with 4-thioxo- was studied. Several selective CB2 ligands were reported and compound **2.27** exhibited the highest affinity (CB2 K_i = 4 nM, SI > 148, Figure 2.10). Importantly, they reported that the functionality of this series is controlled by its C-6 substituent (R3) where agonists bear a methyl or a *tert*-butyl group and inverse agonists bear a phenyl or 4-chlorophenyl group [179].

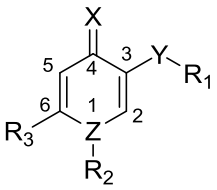

4-oxo-1,4-dihydropyridine-3-carboxamide scaffold

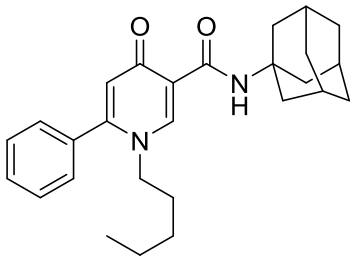

2.27
CB2 K_i = 4 nM
SI > 148

Figure 2.10. 4-oxo-1,4-dihydropyridine-3-carboxamide derivatives

By the utilization of the three-dimensional quantitative structure activity relationship (3D-QSAR) studies, Brogi *et al.* generated a three-dimensional computational model by using the Phase software which was utilized for the design and synthesis of new CB2 selective ligands. As a result, this computational model aided in the discovery and identification of compound **2.28** which is a structural derivative from 4-quinolone-3-carbaxamide with the insertion of a methyl group at the 8-position which potentiated the CB2 affinity dramatically (Figure 2.11) [180]. Structural modification carried out on the compound **2.28** lead by Pasquini and coworkers, they replaced the 8-methyl with 8-methoxy, compound **2.29** which showed high affinity and selectivity towards the CB2 receptor (CB2 K_i = 0.6 nM, CB1 K_i > 10000, SI > 16666, Figure 2.11). Functional studies demonstrated that this compound behaved as an inverse agonist with anti-nociceptive effects in the formalin test [181].

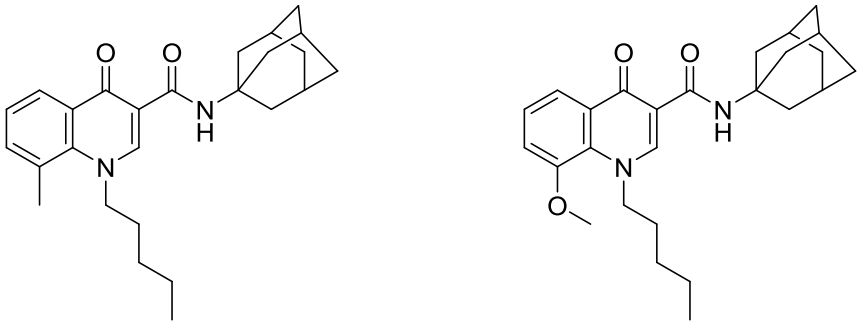

2.28
CB2 K_i = 4.9 nM
SI > 10000 nM

2.29
CB2 K_i = 0.6 nM
CB1 K_i > 10000 nM
SI > 16666

Figure 2.11. Chemical structures of *N*-(adamantan-1-yl)-4-oxo-8-methyl-1-pentyl-1,4-dihydroquinoline-3-carboxamide and *N*-(adamantan-1-yl)-4-oxo-8-methoxy-1-pentyl-1,4-dihydroquinoline-3-carboxamide

Due to the low solubility profile of the dihydroquinoline-3-carboxamide derivatives, bioisosteric replacement of the amide by heterocyclic moieties was utilized to improve the physicochemical and pharmacodynamic properties in a series developed by Mugnaini and colleagues. They reported a new series of 1,6-disubstituted-4-quinolone-3-carboxamide derivatives with high CB2 potency and selectivity. Among the series of derivatives, the triazole derivative, compound **2.30**, displayed highest affinity with improved physicochemical and pharmacodynamic properties (CB2 K_i = 1.2 nM, CB1 K_i > 10000, SI > 8620). Furthermore, compound **2.30**, was shown to behave as an inverse agonist and demonstrated its ability as an anti-nociceptive agent (Figure 2.11) [182]. In another attempt to explore different substitutions on the 4-quinolone-3-carboxamide, Pasquini *et al*. reported the synthesis and pharmacology of 7-substituted quinolone-3-carboxamides. Varying affinities for both CB1 and CB2 receptors were observed. The *N*-(3,4-dichlorobenzyl) amide derivatives, compounds **2.31** and **2.32**, displayed high affinity toward the CB1 receptor. While the *N*-fencylamide derivative, compound **2.33**, displayed high CB2 affinity (Figure 2.12). All three ligands demonstrated as partial agonists with very low permeability in blood brain barrier (BBB) model. Due to their low penetration to the BBB, these ligands may serve as a starting point to develop cannabinoid ligands with low CNS distribution [183].

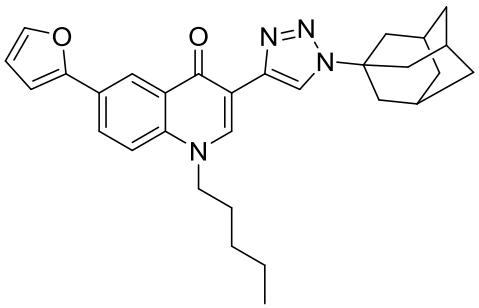

2.30
CB2 K_i = 1.2 nM
SI > 8620

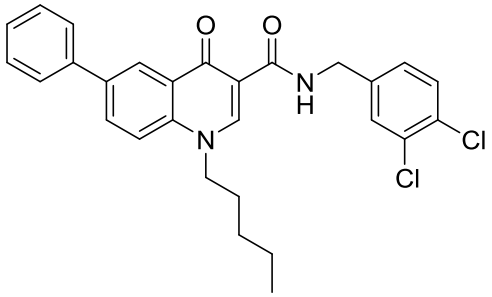

2.31
CB2 K_i > 10000 nM
CB1 K_i = 390 nM

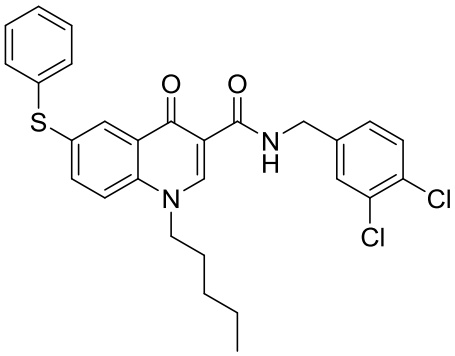

2.32
CB2 K_i > 10000 nM
CB1 K_i = 420 nM

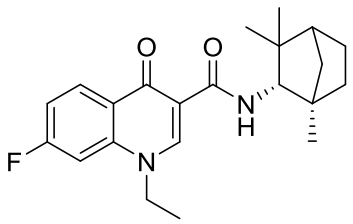

2.33
CB2 K_i = 7.3 nM
CB1 K_i = 959.7 nM
SI = 131

Figure 2.12. Chemical structures of 1,6-disubstituted-4-quinolone-3-carboxamide and 7-substituted quinolone-3-carboxamides derivatives

Recently, several nitrogen heterocyclic derivatives were synthesized and tested for their affinity on human CB1 and CB2 receptors. Replacement of the 1,8-naphthyridinone core with 2-pyridine, as in compound **2.34**, reduced the CB2 affinity albeit its improved solubility. On the other hand, the 1,8-naphthrydinone-3-carboxamide compound **2.35**, showed high affinity and selectivity properties. Furthermore, these two compounds were evaluated for their anti-proliferative properties by utilizing different cancer cell-lines. They both inhibited the proliferation of the cancer cells, in particular, the DU-145 prostate cancer cell-line [184].

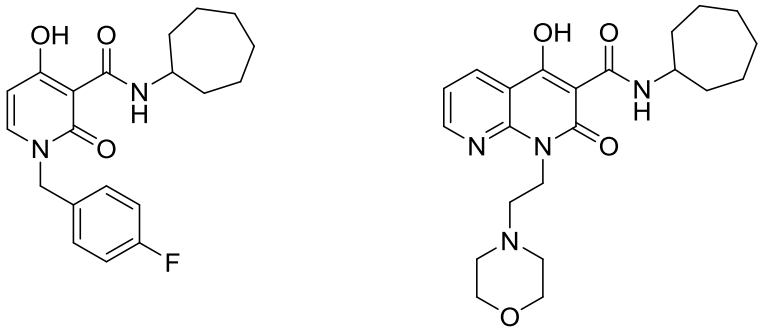

2.34
CB2 K_i = 7.8nM
CB1 K_i = 43 nM
SI = 5.5

2.35
CB2 K_i = 1.8 nM
CB1 K_i = 234 nM
SI = 130

Figure 2.13. Chemical structures of 2.34 and 2.35

Baraldi *et al.* at the University of Ferrara reported a series of 7-oxo-[1,4]oxazole[2,3,4-*ij*]quinoline-6-carboxamides derivatives as selective CB2 ligands [185]. Their design was based on hybrid ligand design which incorporates structural features of known cannabinoid ligands. The design of compound **2.37** was based on the quinolone compound **2.36** and the known cannabinoid ligand WIN55212-2. Further exploration led to the identification of compounds **2.38** and **2.39**, which displayed high affinity and selectivity (Figure 2.14).

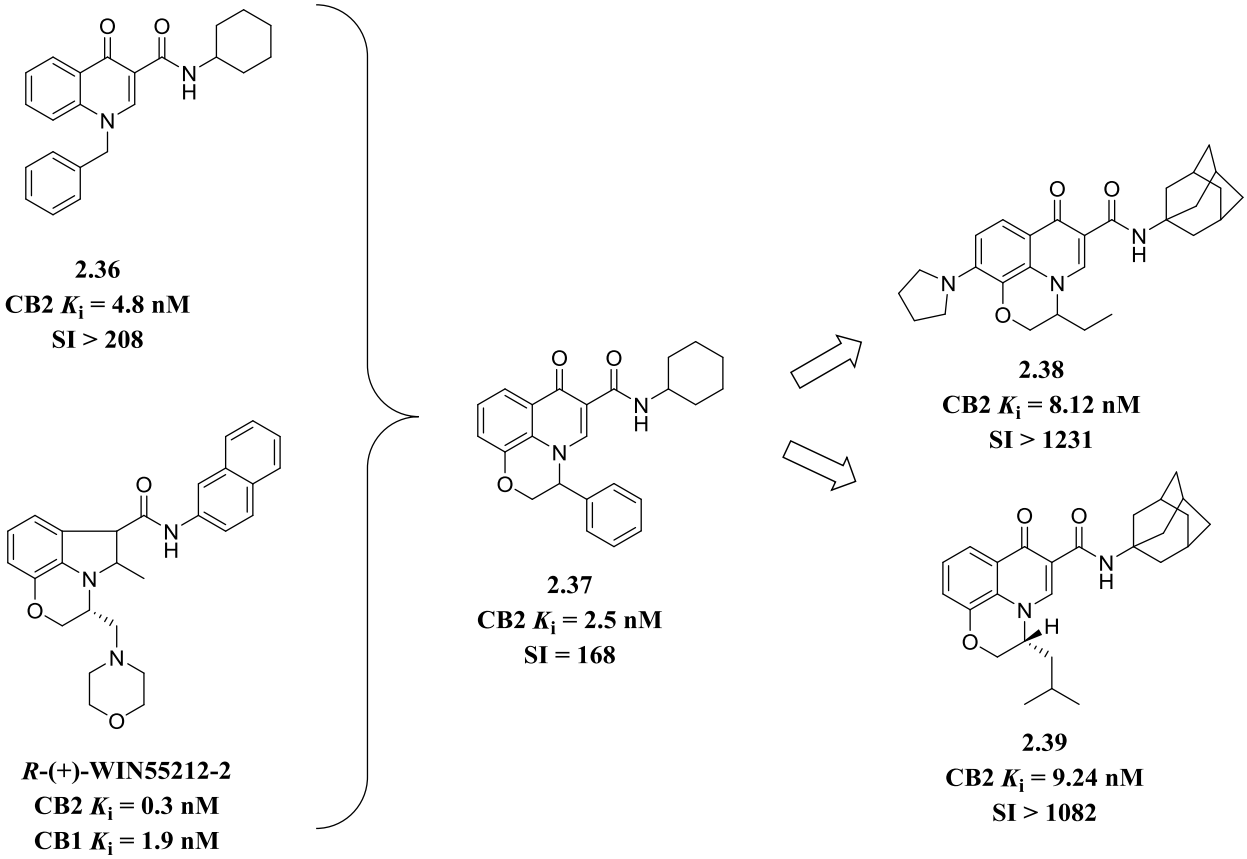

Figure 2.14. Development of 7-oxo-[1,4]oxazole[2,3,4-*ij*]quinoline-6-carboxamides

Tabrizi and co-workers [186] demonstrated the discovery of a new class of selective CB2 derivatives, heteroaryl-4-oxopyridine / 7-oxopyrimidine series, by pharmacophore analysis and structural modifications based on previously discovered CB2 selective ligands and the known CB2 agonists (HU-210, JWH-133, CP55940, HU-308, *R*-(+)-WIN55212, JWH-015, AM1241, AM630, as well as SR144528). They depicted several pharmacophoric properties into their chemistry designs in order to discover novel CB2 selective agonists. As a result, four scaffolds were designed and several substitution at different positions were evaluated. Subsequently, four compounds showed the highest CB2 affinity and selectivity and exhibited varying functionalities, Table 2.1.

Table 2.1. Chemical structures of selective CB2 ligands developed by Tabrizi *et al*.

Entry	Chemical Structure	hCB2 K_i (nM)	Functional Class
1.40	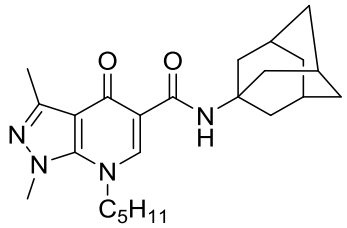	9.51	Partial agonist
1.41	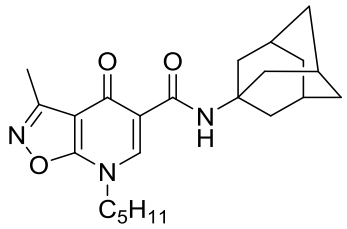	21	Full agonist
1.42	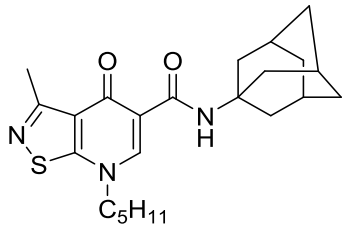	1.12	Inverse agonist
1.43	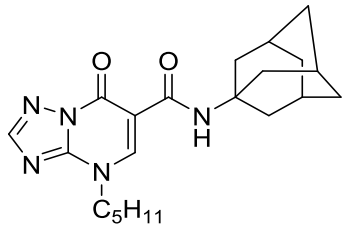	20	Partial agonist

CB2 affinity was calculated by using [^{3}H]CP-55,940 as radioligand calculated on human CB2 CHO membranes.

2.6 INDOLE-BASED DERIVATIVES

The indole moiety is present in many known cannabinoid ligands, as shown previously, such as WIN55212-2, JWH-015, and AM1241. Researchers at Merck Laboratories extended the development of indole derivatives based on GW405833 (CB2 K_i = 10 nM, CB1 K_i = 2000 nM) by replacing the indole moiety with imidazopyridine core giving three varying scaffolds (Figure **2.15**) [187]. The imidazopyridines were shown to be potent CB2 agonists with adjustable CNS penetration properties. SAR studies performed on the three imidazopyridine scaffold led to the production of several CB2 selective agonists with analgesic effects. Compounds **2.44**, **2.45**, **2.46**, **2.47**, and **2.48** are reported to exhibit the highest CB2 affinity and selectivity with hCB2 cAMP IC_{50} of 5, 0.7, 7, 33, and 36 nM, respectively (Figure **2.15**).

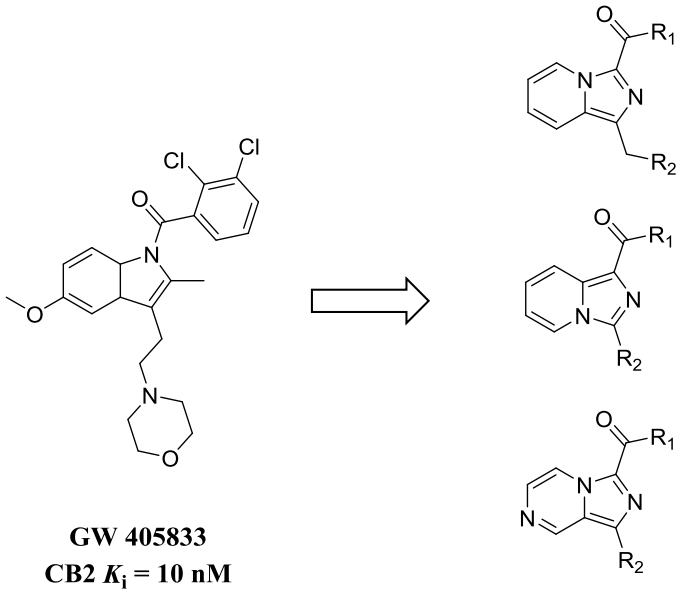

GW 405833
CB2 K_i = 10 nM
CB1 K_i = 2000 nM

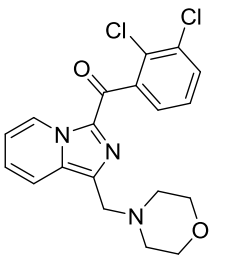

2.44
CB2 EC_{50} = 5 nM
CB1 EC_{50} = 2229 nM

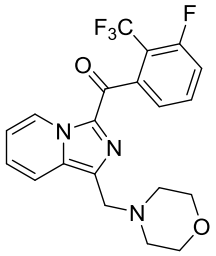

2.45
CB2 EC_{50} = 0.7 nM
CB1 EC_{50} = 2229 nM

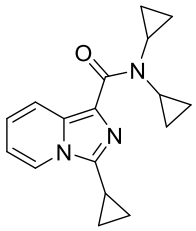

2.46
CB2 EC_{50} = 7 nM
CB1 EC_{50} > 17000 nM

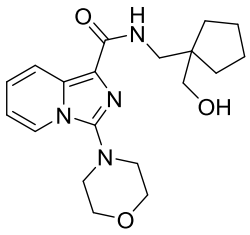

2.47
CB2 EC_{50} = 33 nM
CB1 EC_{50} > 17000 nM

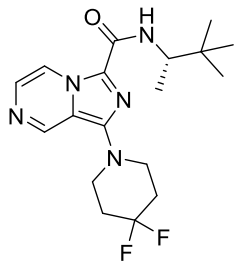

2.48
CB2 EC_{50} = 36 nM
CB1 EC_{50} > 17000 nM

Figure 2.15. Chemical structures of imidazopyridine

2.7 BENZIMIDAZOLE DERIVATIVES

Johnson and Johnson developed 5-sulfonyl-benzimidazoles as potent and selective CB2 agonists. Their studies was initiated by a high-throughput screening and identified compound **2.49** with a CB2 EC_{50} of 25 nM and SI = 354. Initial SAR studies aided in the discovery and synthesis of compound **2.50** which is an ortho-substituted pyridylsulfone analog with high selectivity with acceptable drug-like properties. However, compound **2.50** suffered from low solubility and inhibited CYP-450 isoforms which limited its *in-vivo* activity [188]. Further SAR studies identified compounds **2.51** and **2.52** displaying high CB2 affinity and selectivity with CB2 EC_{50} of 8.2 and 7.7 nM and CB1 EC_{50} of > 10000 and 3428 nM, respectively (Figure 2.16). Although both compounds show comparable CB2 affinity and selectivity, only compound **2.51** displayed good, sustained activity in a chronic model of neuropathic pain. This may be attributed of the good solubility observed in compound **2.51** but not **2.52**. Furthermore, both compounds, **2.51** and **2.52**, delayed the onset of clinical symptoms in an experimental model for multiple sclerosis which is attributed for their agonism properties [189].

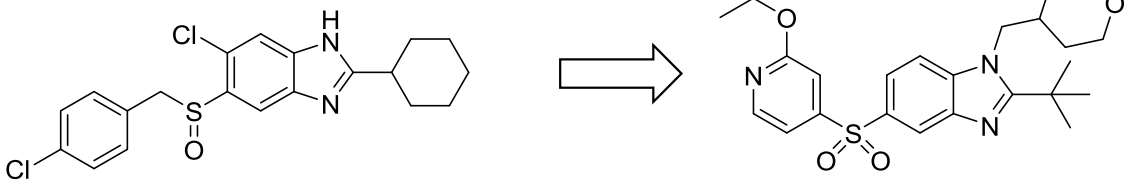

2.49
CB2 EC_{50} = 25 nM
SI = 354

2.50
CB2 EC_{50} = 0.3 nM
SI = 4266

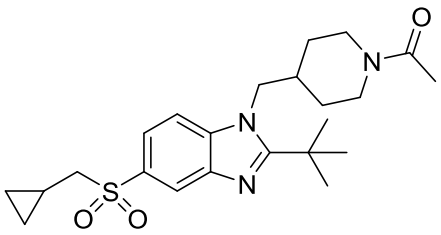

2.51
CB2 EC_{50} = 8.2 nM
CB1 EC_{50} > 10000

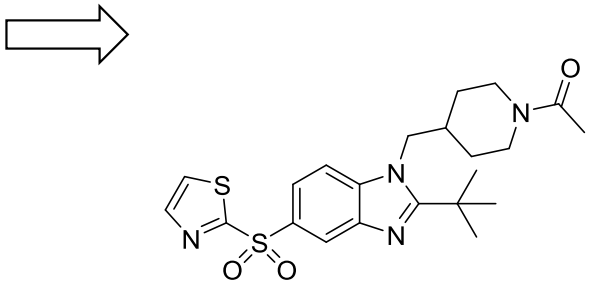

2.52
CB2 EC_{50} = 7.7 nM
CB1 EC_{50} = 3428

Figure 2.16. Chemical structures of the benzimidazoles 2.49 - 2.52

Yu *et al.* at AstraZeneca produced a peripherally restricted cannabinoid receptor agonist on the CB1 receptor and a partial agonist of the CB2 receptor, compound **2.53** (also known as AZ11713908) (Figure 2.17). This compound exhibited poor BBB penetration which potentiated its peripheral analgesic properties in inflammatory and neuropathic pain animal models [190]. A research group in Pfizer led by Watson and coworkers reported a series of benzimidazoles as analgesics based on their previously reported benzimidazole CB2 agonist (compound **2.54** CB2 EC_{50} = 12 nM, CB1 EC_{50} > 19400 nM). Due to its high *in-vivo* clearance (Cl 75 mL/min/kg) and the modest oral bioavailability, SAR studies were carried out based on molecular docking simulation studies. Compound **2.55** was synthesized and reported to have high CB2 affinity (CB2 EC_{50} = 3.2 nM) and selectivity (CB1 K_i > 10000 nM) with improved CNS penetrative properties. Further optimization led to the discovery of compound **2.56** with high CB2 affinity and selectivity, the highest CNS penetration properties as well as reduced hERG activity (Figure 2.17) [191].

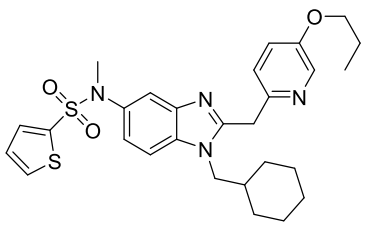

2.53 (AZ11713908)
CB2 EC_{50} = 6 nM
SI = 8

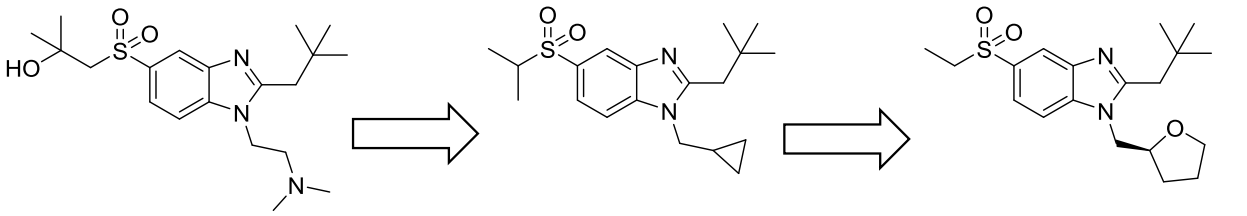

2.54
CB2 EC_{50} = 12nM
CB1 K_i > 19400 nM

2.55
CB2 EC_{50} = 3.2 nM
CB1 K_i > 10000 nM

2.56
CB2 EC_{50} = 11 nM
CB1 EC_{50} = 15000 nM

Figure 2.17. Chemical structures of the benzimidazoles 2.53 – 2.56

2.8 IMIDAZOLES

Cara Therapeutics, Inc. reported the identification of more than 600 substituted imidazoheterocyclic compounds with different CB2 and CB1 receptors affinities. The magnitude of binding ranged from 0.1 nM to 10000 nM. Among the 600 compounds, compound **2.57** showed high affinity and selectivity with CB2 EC_{50} < 0.1 – 10 nM and CB1 EC_{50} > 10000 nM (Figure 2.18) [192].

Lang and coworkers at Solvay Pharmaceuticals reported the synthesis and SAR study of novel imidazole derivatives with varying affinities and functionalities. Their strategy was to design CB2 inverse agonist based on the CB1 receptor inverse agonist SR141716 (Rimonabant) pharmacophore properties. Compound **2.58** exhibited the highest CB2 receptor affinity (K_i = 1.03 nM) and the highest selectivity (SI > 9708) (Figure 2.18) [193].

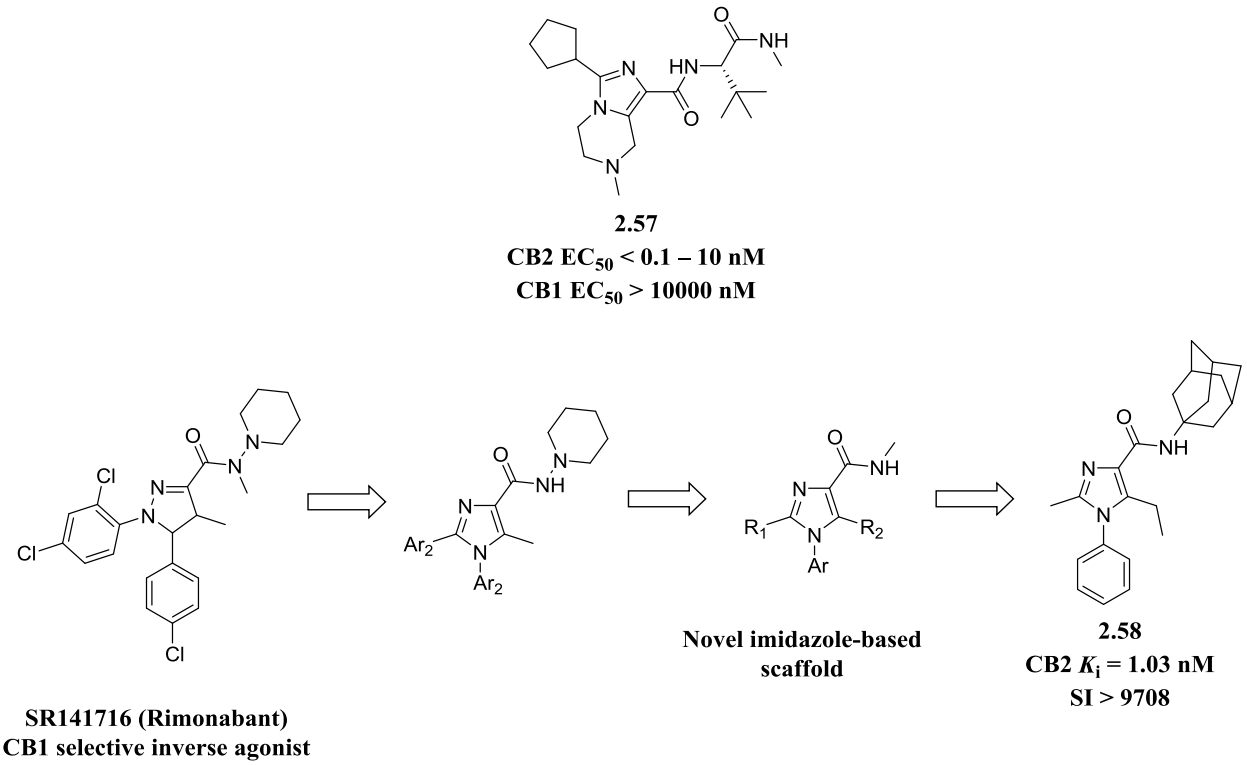

Figure 2.18. Chemical structures imidazole derivatives

Merck laboratories performed high-throughput screening to identify novel CB2 chemotype. Compound **2.59** was identified and exhibited high CB2 affinity (CB2 K_i = 42 nM) with moderate selectivity. Moreover, compound **2.59** was shown to behave as an agonist as demonstrated by the cAMP assay. Subsequently, a series of 2,4-diphenyl-1*H*-imidazole scaffold were synthesized and SAR as well as pharmacokinetic data were studied. Compounds **2.60** and **2.61** displayed the highest CB2 affinity, CB2 EC_{50} = 5 nM and 10 nM, respectively. In addition the selectivity indices were 510 and 245 for compound **2.60** and **2.61**, respectively (Figure 2.19) [194].

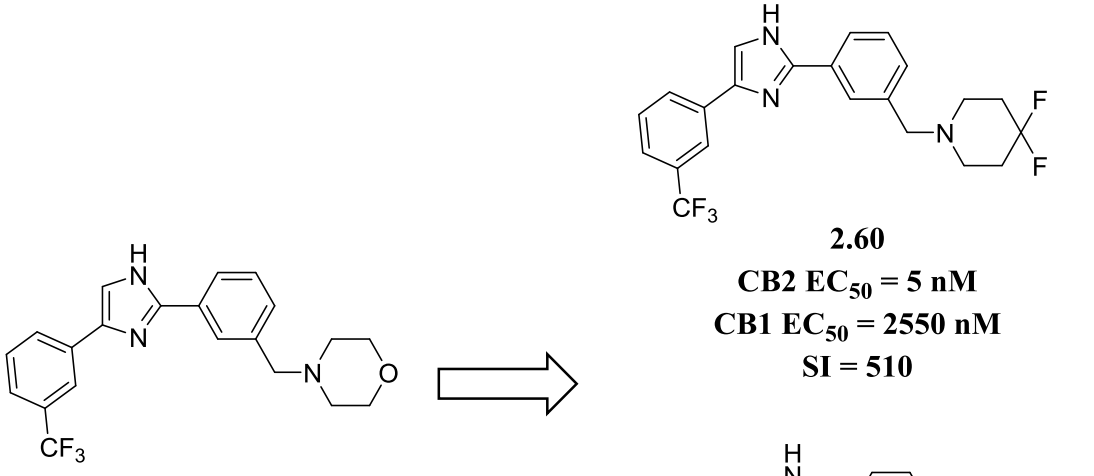

2.59
CB2 K_i = 42 nM
CB1 K_i > 1000 nM

2.60
CB2 EC_{50} = 5 nM
CB1 EC_{50} = 2550 nM
SI = 510

2.61
CB2 EC_{50} = 10 nM
CB1 EC_{50} = 2450 nM
SI = 245

Figure 2.19. Chemical structures of 2,4-diphenyl-1*H*-imidazole

2.9 THIOPHENE AMIDE DERIVATIVES

Nelson and coworkers at Abbott identified several thiophene bisamide compounds utilizing high-throughput screening of the Abbott compound collection. SAR studies of the thiophene bisamide scaffold produced several CB2 selective agonists. Importantly, compounds **2.62**, **2.63**, and **2.64** showed the highest CB2 affinity and selectivity and behaved as agonists (Figure **2.20**). Compound **2.62**, effectively produced analgesia in behavioral models of neuropathic, inflammatory, and postsurgical pain as well as demonstrating excellent bioavailability properties [195]. Nycomed Pharma performed high-throughput screening of ~300,000 compounds and identified the hit compound **2.65** with CB2 EC_{50} = 10 nM and CB1 EC_{50} = 251 nM. Extensive SAR studies on the hit compound aided in the synthesis of compounds **2.66** and **2.67** with high affinity and selectivity (Figure **2.20**). Compound **2.66** produced analgesia after oral administration in inflammatory pain models of writhing and carrageenan-induced allodynia [196].

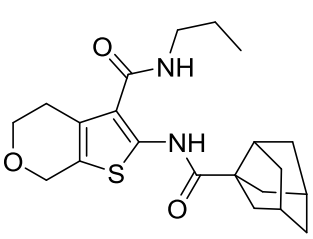

2.62
CB2 K_i =21 nM
CB1 K_i = 1549 nM

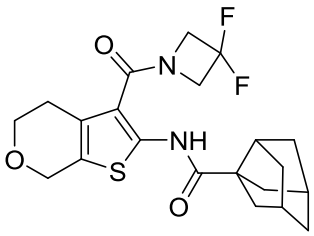

2.63
CB2 K_i =5.6 nM
CB1 K_i = 3388 nM

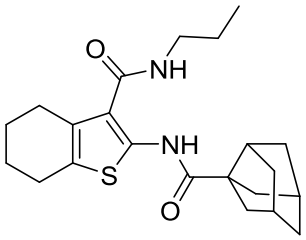

2.64
CB2 K_i =2 nM
CB1 K_i = 1905 nM

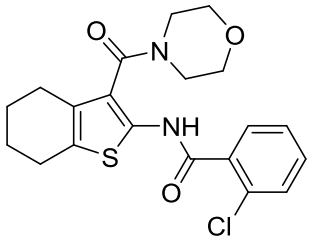

2.65
CB2 EC_{50} = 10 nM
CB1 EC_{50} = 251 nM

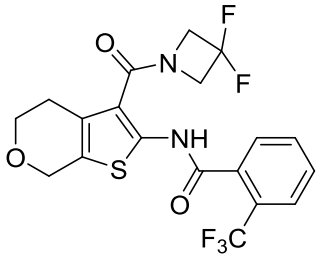

2.66
CB2 EC_{50} = 6.5 nM
CB1 EC_{50} = 798 nM

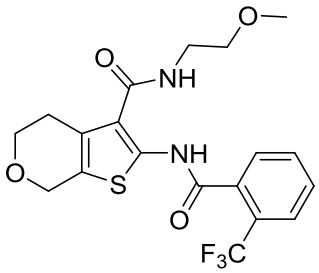

2.67
CB2 EC_{50} = 17 nM
CB1 EC_{50} = 8710 nM

Figure 2.20. Thiophene amide derivatives

2.10 SULFONAMIDE DERIVATIVES

Scientists at Boehringer Ingelheim Pharma led by Berry and coworkers identified 192 sulfonyl carboxamide compounds exhibiting CB2 modulatory activity [197]. About 80 compounds demonstrated CB2 agonism and were evaluated for their pharmaceutical uses. Among those 80 compounds, compound **2.68** which showed high CB2 affinity (CB2 EC_{50} = 0.04 nM) and as an anti-inflammatory agent (Figure 2.21). Two years later, another series of compounds was patented by Boehringer Ingelheim Pharma and reported the identification of a series of heterocyclic sulfone compounds with CB2 agonism properties. The new series of heterocyclic sulfone scaffold demonstrated anti-inflammatory as well as analgesic properties [198]. Compound **2.69** demonstrated the highest CB2 affinity among those series with CB2 K_i of 25 nM and behaved as an agonist (Figure 2.21).

Since the first identification of the triaryl bis-sulfones scaffold and the discovery of compound **2.70** (also known as Sch.225336, Figure 2.21) as selective CB2 inverse agonist by the Schering-Plough Research Institute in 2003, several SAR studies were carried out to optimize affinity, selectivity as well pharmacokinetic/pharmacodynamic properties. Shankar *et al*. studied the variations of the substitution pattern on the aromatic rings and the linkers (L_1 and L_2) of the aromatic rings (Figure 2.21). Changes at L_2 were not tolerated, and sulfone was determined to be the best overall for L_1 and L_2. Substitution on the phenyl rings showed a preference for a small group at the 2-position of the C-ring and a small alkyl or halogen at the 4-position of the B-ring as in compound **2.71** (known as Sch.356036, Figure 2.21) [199]. Gilbrt *et al*. modified compound **2.71** by converting the aryl A-ring to a piperidine ring. The piperidine ring was further replaced to a spirocyclopropyl piperidine moiety. Such modification led to the identification of compound **2.72** with improved CB2 potency and selectivity (CB2 K_i = 0.9 nM, SI > 1000, Figure 2.21) [200].

Another SAR study of compound **2.71** was carried out by Lavey and coworkers. The changes to compound **2.71** include the addition of polar groups to the 2-fluorophenyl ring, replacement of the fluorophenyl ring with heterocycles and other groups, and changing the $NHSO_2CH_3$ group into a $NHSO_2CF_3$ to allow the formation of salts to improve solubility. Compound **2.73** (also known as Sch.414319, Figure 2.21) was identified with high CB2 affinity and selectivity (CB2 K_i = 2 nM, SI = 3393) as well as improved pharmacokinetic properties [201].

Merck laboratories led by Tong *et al*. expanded the SAR of **2.73** identified another highly potent and selective CB2 inverse agonist, compound **2.74**, with CB2 K_i of 0.4 nM and SI of 3500, Figure 2.21) [202].

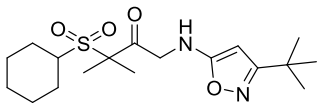

2.68
CB2 EC_{50} = 0.04 nM

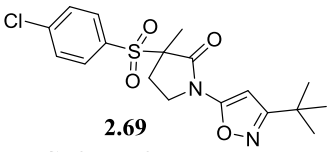

2.69
CB2 K_i = 25 nM

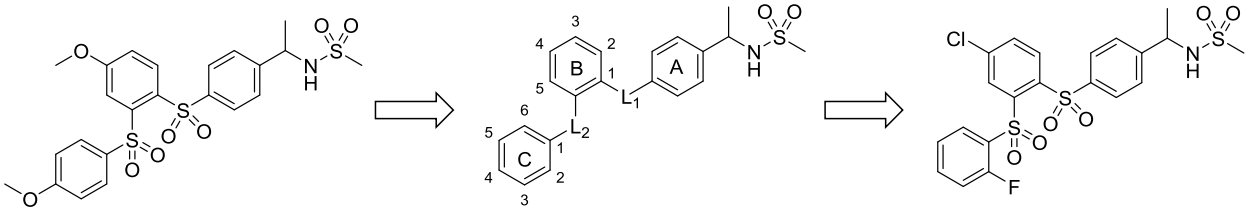

2.70 (Sch.225336)
CB2 K_i = 0.4 nM
CB1 K_i = 905 nM
SI = 2263

2.71 (Sch.356036)
CB2 K_i = 1 nM
SI = 4387

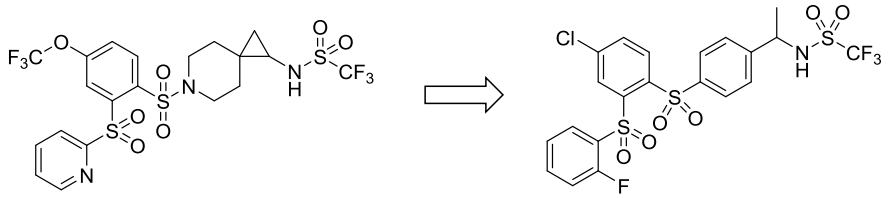

2.72
CB2 K_i = 0.9 nM
SI > 1000

2.73 (Sch.414319)
CB2 K_i = 2 nM
SI = 3393

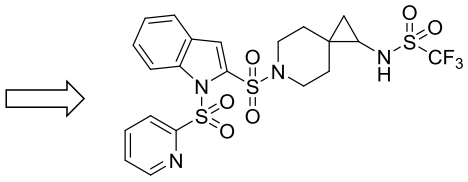

2.74
CB2 K_i = 0.4 nM
SI = 3500

Figure 2.21. Sulfonamide derivatives

2.11 CONCLUSION

The involvement of the cannabinoid system in different physiological and disease states potentiated the high demand for developing cannabinoid ligands. It is now well appreciated that with CNS limitations accompanied with CB1 targeting, developing selective CB2 ligands is more promising. In fact, several CB2 selective ligands have undergone or are currently in clinical trials for different diseases. For example, cannabinor (PRS-211375, compound **2.75**, Figure 2.22) was evaluated by Pharmos Corporation in Phase II clinical trials as an anti-nociceptive agent. Furthermore, Glenmark Pharmaceuticals conducted a Phase I clinical trial to evaluate the selective CB2 agonist tedalinab (GRC-10693, compound **2.76**, Figure 2.22) for the treatment of osteoarthritis and neuropathic pain. Clinical studies demonstrated the ability of tedalinab to reduce bone pain in osteoarthritis and neuropathic patients [203]. In addition, Kyowa Hakko Kirin reported the testing of the CB2 agonist KHK-6188 (no structural data reported) in clinical trials for pain in Phase II clinical study for postherpetic neuralgia [204]. Shinogi Pharmaceuticals reported the discovery of 3-carbamoyl-2-pyridone based CB2 agonist, namely S-7774698 (compound **2.77**, Figure 2.22) with promising antipruritic effects [205]. S-7774698 was evaluated in a Phase II randomized and double-blind clinical study to evaluate its efficacy in patients with atopic dermatitis with no published data yet [206].

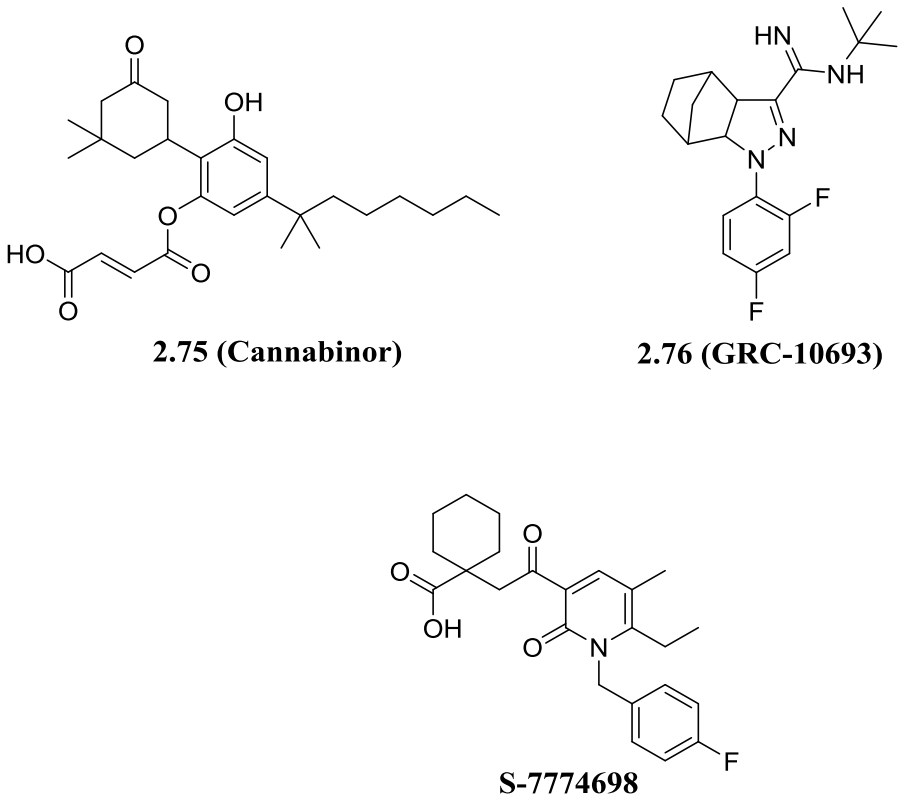

2.75 (Cannabinor) **2.76 (GRC-10693)**

S-7774698

Figure 2.22. Chemical structures of selective CB2 ligands in clinical trials

To date, the 3D X-ray crystal structure of CB2 receptor has not been resolved demanding different methods of ligand discovery. As demonstrated in this chapter, many ligand discovery tools were employed such as computer-aided drug discovery (molecular docking, QSAR/CoMFA, and pharmacophore modeling), high-throughput screening as well as mutational studies. Also, many selective CB2 ligands have been discovered and yet a lot of ligands will be discovered due to the different functions of the cannabinoid system and the therapeutic potentials CB2 ligands hold. Several novel CB2 chemotype were reported suggesting the variety of the CB2 ligands and the potential of different other chemical moieties to be developed. More structural modifications to improve efficacy, physicochemical properties, and pharmacokinetic properties will advance the use of CB2 ligands into the clinic.

3.0 GENERAL METHODS AND MATERIAL

3.1 COMPUTER MODELING

All molecular docking studies, pharmacophore modeling, Quantitative Structure Activity Relationship (QSAR)/Comparative Molecular Field Analysis (CoMFA) and virtual screening procedures were performed using SYBYL X 1.3 (Tripos, Inc.). Molecular docking studies were performed using the Surflex-Dock GemX^{TM} module in the SYBYL software. The docking interactions were analyzed based on the FlexX-Pharm Docking/CScore [207]. Pharmacophore studies were performed using the GALAHAD^{TM} module (Tripos, Inc.) to generate pharmacophore models. QSAR/CoMFA was performed using the QSAR module (Tripos, Inc.). Our CB2 homology model [208] was utilized for the docking and virtual screening procedures. Refined figures and contours were obtained using PyMol 1.7 (Schrödinger®, LCC) platform.

3.2 CHEMISTRY

All reagents were purchased from commercial suppliers and used without further purification. Analytical thin-layer chromatography (TLC) was performed on SiO_2 plates 250 µm on Alumina from Whatman. Visualization was accomplished by ultra-violet (UV) irradiation at 254 nm. The purification experiments were conducted using Preparative Silica gel TLC plates (1000 µm. 20 cm × 20 cm) or Flash chromatography (Biotage, Isolera Inc.), where indicated. Flash column chromatography was performed using the Biotage Isolera flash purification system with SiO_2 60

(particle size 0.040−0.055 mm, 230−400 mesh). Proton and carbon NMR were determined on Bruker 400 MHz or Bruker 600 MHz NMR spectrometer, where indicated. Chemical shifts are reported as delta (δ) values in parts per million (ppm) as referenced to residual solvent. ^{1}H NMR spectra are reported as follows: chemical shift, number of protons, multiplicity (s = singlet, d = doublet, t = triplet, q = quartet, m = multiplet, br = broad peak), and coupling constant. Chemical shifts are reported relative to that of tetramethylsilane at 0.00 ppm. Compound purity of at least 95% was confirmed by HPLC. LC-MS analysis was recorded on a Shimadzu HPLC instrument with a Hamilton reversed phase column (HxSil, C18, 3 μm, 2.1 mm × 50 mm (H2)); eluent A consisting of 5% CH_3CN in H_2O; eluent B consisting of 90% CH_3CN in H_2O; flow rate of 0.2 mL/ min; UV detection, 254 and 214 nm. HPLC coupled to electrospray ionization-mass spectrometry (ESI-MS) Quadrupole-time-of-flight (QTOF) tandem mass spectrometry QSTAR Elite (Applied Biosystems).

3.3 CANNABINOID RECEPTORS MEMBRANE PROTEIN PREPARATIONS

Membranes are isolated from Chinese Hamster Ovary (CHO) cells stably expressing both CB1 and CB2 receptors. These cells were cultured in 50:50 mixtures of DMEM and Ham's F-12 with the supplementation with antibiotics. The cells were harvested in phosphate-buffered saline containing 0.4% EDTA. The membrane proteins were prepared by homogenization of cells in 50 mM Tris buffer with 10% sucrose. Centrifugation was performed and the supernatant was collected. The supernatant was ultra-centrifuged at 50,000 x g for 45 minutes at 4°C and the membranes were stored at -80 °C.

3.4 RADIO-LIGAND COMPETITION BINDING ASSAYS

3.4.1 Saturation Binding Assay

Saturation binding experiment is initially performed in order to characterize the membrane receptor preparation. The experiment is carried out as previously described [209]. It measures the total and non-specific binding at various concentrations of the radioligand. Two values are measured; K_d (equilibrium dissociation constant) and B_{max} (receptor density). Briefly, the membrane fractions (20 μg) were incubated with increasing concentrations of [^{3}H] H](−)-cis-3-[2-hydroxy-4-(1,1-dimethylheptyl)phenyl]-trans-4-(3-hydroxypropyl) cyclohexanol (CP55,940) (0.01–5nM) in 96-well plates at 30 °C with slow shaking for 1 h. The incubation buffer was composed of 50 mM Tris–HCl (pH 7.4), 5 mM $MgCl_2$, 2.5 mM EGTA and 0.1% (w/v) fatty acid free BSA. Hot ligand was diluted in incubation buffer supplemented with 10% dimethyl sulfoxide and 0.4% methylcellulose. Non-specific binding was determined in the presence of 1:1000 unlabeled CP-55,940 (5000 nM) in excess. The reaction was terminated by rapid filtration through Unifilter GF/C filter plates using a Unifilter Cell Harvester (PerkinElmer). After the plate was allowed to dry overnight, 30 μL MicroScint-20 cocktail (PerkinElmer) was added to each well and the radioactivity was counted using a PerkinElmer TopCounter.

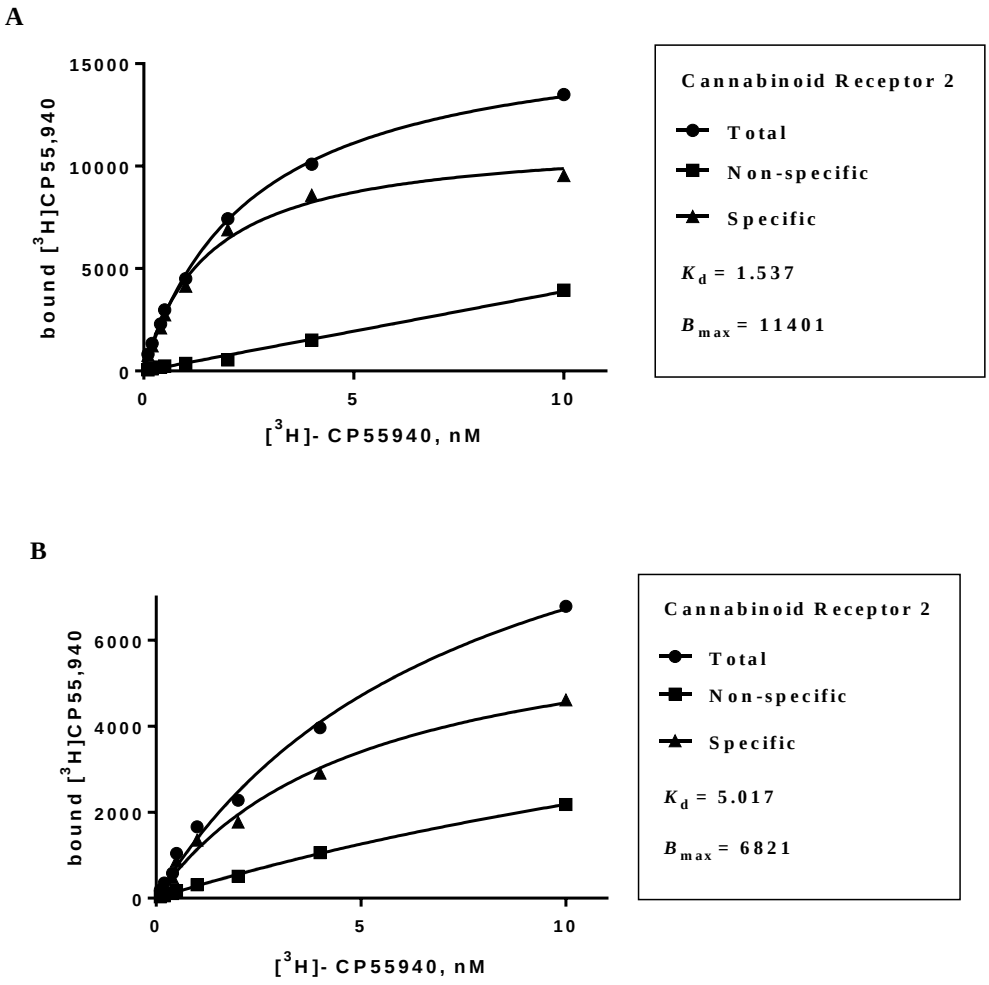

Figure 3.1. Saturation binding assay of CB2 and CB1 membrane preparations.

Saturation binding assay was performed with membrane proteins preparations harvested from CHO cells stably expressing either CB1 or CB2 receptors by increasing the concentration of hot ligand, [^{3}H]-CP55,940, using a fixed amount of target protein. A 1:1000 excess of cold CP55,940 was added in the reaction mixture to account for non-specific binding. Total (●) and non-specific (■) binding was measured and the deduced specific binding saturation isotherm (▲) was obtained as the difference between total and nonspecific binding. **(A)** Cannabinoid receptor 2 saturation binding curve (CB2); **(B)** Cannabinoid receptor 1 saturation binding curve (CB1). Assay was performed in triplicate. Data presented as mean ± SEM.

The assay provides the K_d (equilibrium dissociation constant) and B_{max} (receptor density) that provides information on the membrane preparation. Total binding (receptor + radioligand), non-specific binding (receptor + radioligand + excess cold ligand) and specific binding of the radioligand (total minus non-specific) were plotted versus the free concentration of the radioligand. The K_d is determined using non-linear regression analysis using GraphPad Prism as: Bound = B_{max} * [L] / ([L] + K_d), where [L] is the hot ligand concentration (Figure 3.1).

3.4.2 Radio-Ligand Competition Binding Assay

The competitive radio-ligand binding assays for CB1 and CB2 receptors were performed as described previously using a Perkin Elmer 96-well Top Counter to determine the cannabinoid receptor binding affinity (K_i) for CB1 or CB2 ligands by displacing [^{3}H]-CP55,940. [209]. Briefly, the compounds to be tested are diluted in binding buffer (50 mM Tris-HCl (pH 7.4), 5 mM $MgCl_2$, 2.5 mM EGTA, and 0.1% (w/v) fatty acid free BSA), supplemented with 10% dimethyl sulfoxide and 0.4% methylcellulose. Each assay plate well contains a total of 200 µL of reaction mixture comprising 5 µg of CB1 (or CB2) membrane protein, labeled [^{3}H]-CP55,940 at a final concentration of 3 nM, and the unlabeled ligand at its varying dilutions. Plates were incubated at 30 °C for 1 h with gentle shaking. The reaction was terminated by rapid filtration through Unifilter GF/B filter plates using a UniFilter cell harvester (PerkinElmer). After the plate was allowed to dry overnight, 30 µL MicroScint-0 cocktail (PerkinElmer) was added to each well and the radioactivity was counted by using a PerkinElmer TopCount. All assays were performed in triplicate and data points represented as mean ± S.E.M. The K_i was calculated by using nonlinear regression analysis (Prism 5, GraphPad) utilizing the Cheng-Prusoff equation: K_i = IC_{50} / 1 + ([L]/K_d), with the K_d values determined from saturation binding experiments (Figure 3.2).

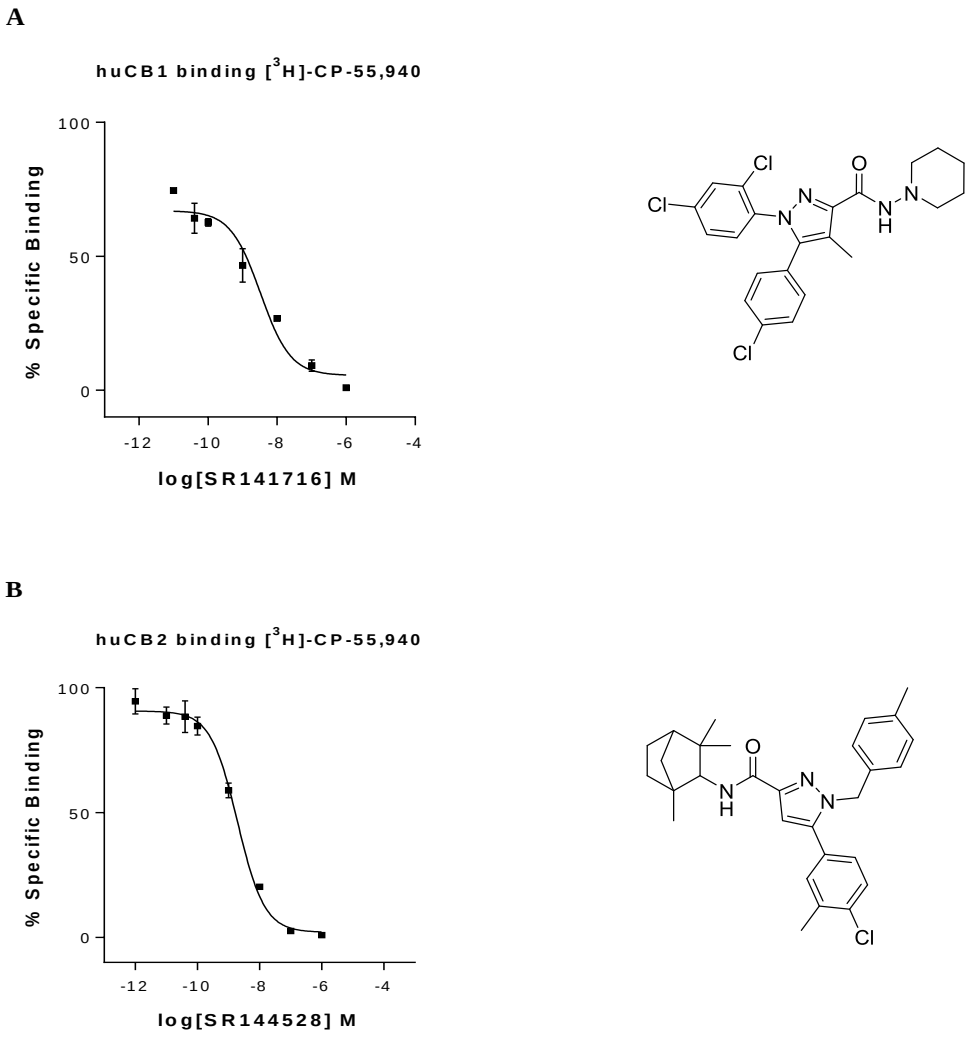

Figure 3.2. Competition binding profiles for SR141716 and SR144528.

Competition binding experiments were performed on membrane proteins harvested from CHO cells stably expressing CB1 or CB2 receptors. Competitive displacement of the [^{3}H]-CP55,940 was obtained by using an increased amount of cold ligands **(A)** Competition binding profile of cannabinoid receptor 1 selective ligand, SR141716, K_i = 3.12 nM. **(B)** Competition binding profile of cannabinoid receptor 2 selective ligand, SR144528, K_i = 1.55 nM. Assay was performed in triplicate. Data represented as mean ± SEM.

3.5 CYCLIC ADENOSINE MONOPHOSPHATE (CAMP) ASSAY

Cellular cyclic adenosine monophosphate (cAMP) levels were measured according to the reported method using LANCE cAMP 384 kits (PerkinElmer) [210]. This assay determines the functionality of the synthesized derivatives (agonist, antagonist/inverse agonist) by measuring the cAMP accumulation. The assay is a time-resolved fluorescence resonance energy transfer (TR-FRET) immunoassay designed to measure cAMP produced upon modulation of adenyl cyclase (AC) activity by GPCRs. The assay is based on the competition between the europium-labeled cAMP tracer complex and total cAMP for binding sites on cAMP-specific antibodies. The anti-bodies are labeled with Alexa Fluor dye that is sensitive to energy emissions. The fluorescence intensity decreases in the presence cAMP from the tested samples.

CB2 receptor transfected CHO cells were seeded in a 384-well white ProxiPlates with a density of 2000 cells per well in 5 μL of RPMI-1640 medium containing 1% dialyzed FBS, 25 mM HEPES, 100 μg/mL penicillin, 100 U/mL streptomycin and 200 μg/mL of G-418. After culture overnight at 37 $^{\circ}$C and 5% CO_2, 2.5 μL of cAMP antibody and RO20-1724 (final concentration 50 μM) in stimulation buffer (DPBS 1x, containing 0.1% BSA) were added to each well, followed by the addition of 2.5 μL compound with forskolin (final 5 μM) for agonist-inhibited adenylate cyclase (AC) activity assay. After incubation at room temperature for 45 min, 10 μL of detection reagent was added into each well. The plate was then incubated for 1 h at room temperature and measured in Synergy H1 hybrid reader (BioTek) with excitation at 340 nm and emission at 665 nm. Each cAMP determination was made via at least two independent experiments, each in triplicate. EC_{50} values were determined by nonlinear regression, dose–response curves (GraphPad Prism 5).

Figure **3.3** illustrates the cAMP assay of two known CB2 ligands; HU-308 (CB2 agonist), and SR144528 (CB2 inverse agonist).

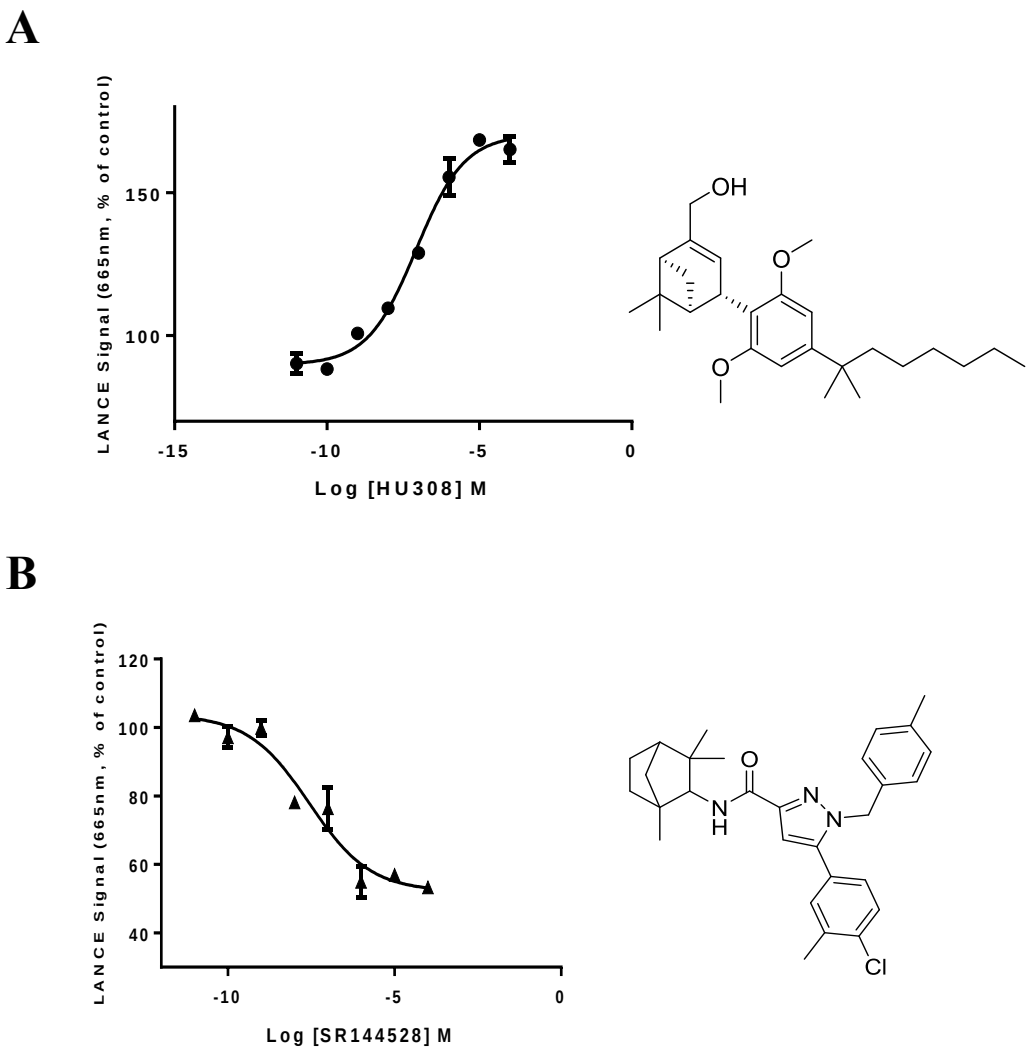

Figure 3.3. LANCE cAMP signal profiles for reference CB2 ligands HU-308 and SR144528

Comparisons of the LANCE signal of two CB2 receptor ligands in stably transfected CHO cells expressing human CB2 receptors in a concentration-dependent manner. **(A)** LANCE signal profile of a cannabinoid receptor 2 agonist, HU-308. **(B)** LANCE signal profile of a cannabinoid receptor 2 inverse agonist, SR144528. Assay was performed in triplicate. Data represented as mean ± SEM.

3.6 CELL-VIABILITY ASSAY

The purpose of the cell-viability assay can be divided to: A) to test the anti-proliferation properties of our synthesized derivatives on MM cell-lines, and B) to test the cytotoxicity effects of the derivatives. The synthesized CB2 ligands are tested for anti-cancer (anti-proliferation) activity and cytotoxicity effects using MTT 3-(4,5-dimethylthiazol-2-yl)-2,5-diphenyltetrazolium bromide colorimetric cell viability assay as described in the literature [211]. The anti-MM properties were examined on two MM cell-line: RPMI8226 and MM1.S. For the cytotoxicity assay, two cell-lines were utilized: the osteoclast precursor RAW 267.7 cell-lines and bone marrow macrophages (BMM) derived cell-lines. The principle of the MTT assay is that the mitochondrial activity for most viable cells is constant. Thus, an increase or decrease in the number of viable cells is linearly related to mitochondrial activity. The mitochondrial activity of the cells is reflected by the conversion of the tetrazolium salt MTT into insoluble formazan crystals (dark purple) by cellular reductase, which can be solubilized for measurement. Thus, measuring the formazan concentration by optical density (OD) will reflect any increase or decrease in cell viability. A plate spectrophotometer reader was used to measure the OD at 570 nm. Briefly, MTT stock was prepared by dissolving 500 mg MTT (Sigma, St. Louis, USA) in 10 mL PBS. Continuous stirring for 1 hour in the dark, filtered and stored at – 20 ºC. Cells were seeded in a 96-well at a cell number of $1.5 \times 10^3 – 3 \times 10^3$ cells per well in RPMI-1640 medium containing 5% FCS to a volume of 100 μL. Divide the well into: blank, control and treatment groups in triplicates. The blank wells contains only the assay media, while the control wells contain only the assay media plus ≤ 0.1% DMSO with no drug. Add the synthesized derivatives into the wells after dilution with DMSO and incubate for 48 hours at 37 °C 5% CO_2. MTT (20 μL) solution is added to each well, shaking 150 rpm for 5 minutes, and then incubated for 2-5 hours at 37 °C 5% CO_2. The metabolism product

(formazan) was dissolved in 200 μL DMSO and the plate was shaken at 150 rpm for 5 minutes. Optical density was then read at 540 nm and subtracted from the background at 720 nm.

In order to generate BMM, first the L-929 (murine fibroblast cell-line that secrets M-CSF) supplemented media is generated according to the following: L-929 cell-lines are seeded at a density of 7×10^6 cells/plate in α-MEM media supplemented with 10% FBS, 100 U/mL penicillin, and 100 μg/mL streptomycin. The plates were incubated for 3 – 5 days at 37 ºC and 5% CO_2, then the L-929 supernatant were collected. α-MEM media was mixed with 10% FBS, 10 – 30% L-929 supernatant, 2-5% β-mercaptoethanol and penicillin/streptomycin (L-929 conditioned media, stored at -20 ºC). Bone marrow cells harvested from the femur and tibia of 4- to 6-week-old C57/BL6 mice were plated at density of 7×10^6 cells/plate in 10 mL L-929 conditioned media and incubated at 37 ºC and 5% CO_2 for 7 – 10 days, changing media every 3 days. After incubation, the BMM were harvested and ready to use. For the cell-viability assay, the same procedure of MTT assay described above is used.

3.7 OSTEOCLAST FORMATION ASSAY

Mouse osteoclast formation assay was performed as previously described [212, 213]. Bone marrow cells were harvested from the femur and tibia of 4- to 6-week-old C57/BL6 mice washed with α-MEM filtered through a 70 mm cell strainer, and seeded in a 96-well plate at a density of 2×10^5 cells per well (50 μL). To examine the effect of our synthesized CB2 ligands on the formation of osteoclast cells, ligands were diluted to the desired concentrations in DMSO and added to each well in the presence of 30 ng/mL receptor activator of nuclear factor kappa-B ligand (RANKL) (ProSpec, NJ) and 15 ng/mL macrophage colony-stimulating factor (M-CSF) (R&D Systems) to

a total volume of 50 μL. Plates were incubated at 37 °C 5% CO_2 changing half media every 3 days with or without treatment. After 7 – 10 days, cells were fixed and stained for tartrate-resistant acid phosphate (TRAP) (Sigma) activity according to the recommendation of the manufacturer. TRAP+ multinucleated cells with more than three nuclei were counted as osteoclasts.

3.8 STATISTICAL ANALYSIS

Radioligand binding assays as well as the CB2 functional assays (cAMP) were performed in triplicates and expressed as the mean ± SEM. Cell viability assay and the osteoclast formation assay were performed in triplicates and the data are expressed as the mean ± SD. Comparisons between the groups were made with unpaired Student's *t* test. Statistical differences were as follows: no significance (NS) $P>0.05$, $*P<0.05$, $**P<0.01$, $***P<0.001$, and $****P<0.0001$ compared with the control groups.

4.0 DESIGN, SYNTHESIS, AND BIOLOGICAL EVALUATIONS OF DI-AMIDE DERIVATIVES AS SELECTIVE CB 2 INVERSE AGONISTS

4.1 INTRODUCTION

4.1.1 Discovery of Cannabinoid Receptor 2 (CB2) Ligands

To develop potent and selective cannabinoid receptor 2 ligands, 3D pharmacophore modeling and *in-silico* virtual screening studies were carried out. The 3D-QSAR studies of CB2 bioactive antagonists were utilized using the genetic algorithm based pharmacophore alignment method (GALAHAD, Tripos, Inc.). The training set consisted of 20 known active CB2 ligands and 980 random compounds to ensure the liability of the generated pharmacophore models. The resulted pharmacophore and virtual screening studies lead to the discovery of a novel CB2 scaffold, **XIE-35** (Figure 4.1) [214]. The hit compound was subjected to radio-ligand competition binding assay in order to validate its potency and selectivity towards the CB2 receptor (Figure 4.2). **XIE-35** showed high potency and selectivity towards the CB2 receptor (CB2 K_i = 31.7 nM, CB1 K_i = 4185 nM, SI = 132).

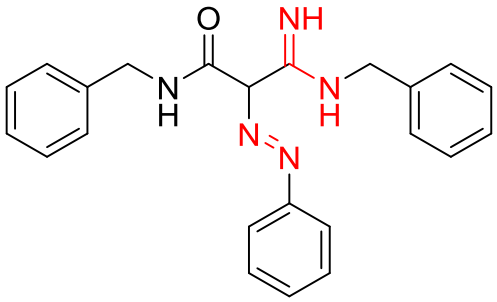

Figure 4.1. Chemical structure of XIE-35

The hit compound, **XIE-35**, showed a novel CB2 chemical structure consisting of a carbon center, an amidine group, an azo- group (R-N=N-R) and three benzyl rings.

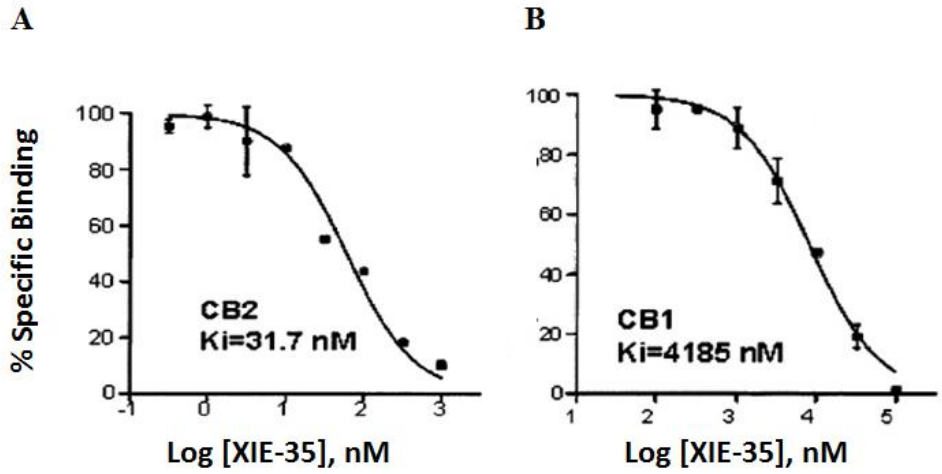

Figure 4.2. Competition binding profile for XIE-35

Competition binding experiments were performed on membrane proteins harvested from CHO cells stably expressing CB1 or CB2 receptors. Competitive displacement of the [^{3}H]-CP55,940 was obtained by using an increased amount of cold ligands. **(A)** Competition binding profile of XIE-35 utilizing CB2 membrane proteins, K_i = 31.7 nM. **(B)** Competition binding profile of XIE-35 utilizing CB1 membrane proteins, K_i = 4185 nM.

To further test the hit compound, **XIE-35**, for functionality, LANCE cyclic adenosine monophosphate (cAMP) assay was carried out to determine its agonism, antagonism or inverse agonism profile. cAMP is a secondary messenger that can be measured using cell-based assay in GPCR's to determine the ligand's functionality. The assay was carried out as described in Chapter 3. CB2 receptors are $G\alpha_{i/o}$-Protein Coupled Receptors which an agonist will inhibit the forskolin-induced cAMP production, resulting in an increase of the LANCE signal. An antagonist or an inverse agonist, on the other hand, decreases the LANCE signal toward forskolin-induced cAMP accumulation. As shown in Figure 4.3, increasing concentrations of compounds SR144528 and **XIE-35** caused reductions of the LANCE signal indicating that these compounds are inverse agonist. However, increasing concentrations of compound CP-55,940 caused an increase in the LANCE signal which is exhibited by CB2 agonists. These results indicate that **XIE-35** is a selective CB2 receptor inverse agonist.

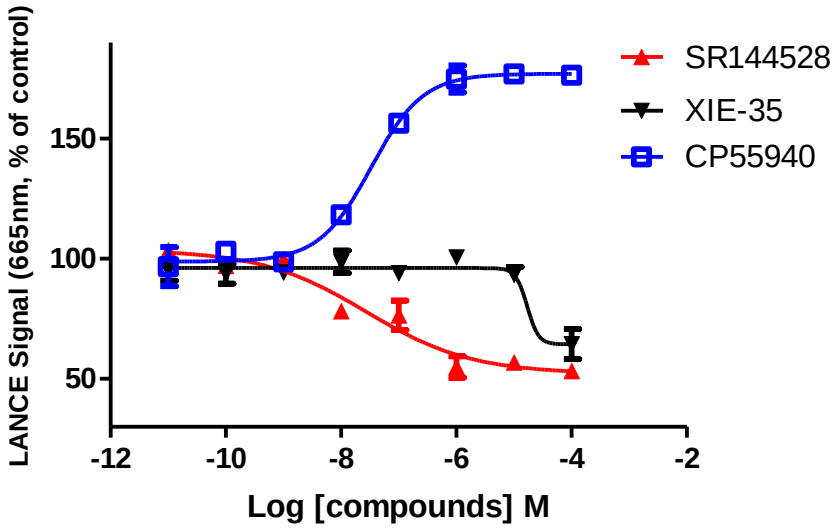

Figure 4.3. LANCE cAMP signal of XIE-35 and known CB2 ligands

Stably transfected CHO cells expressing human CB2 receptors was utilized in LANCE cAMP assay. CP-55,940 is a known CB2 agonist, while SR 144528 is a known CB2 inverse agonist. Assay was performed in triplicate. Data represented as mean ± SEM

4.1.2 Scaffold Hopping and Lead Optimization

Although **XIE-35** showed high potency and selectivity towards the CB2 receptor, the chemical structure has limitations that require chemical modifications. The amidine scaffold is an unfavorable drug moiety as it will cause poor solubility and bioavailability. In addition the azo-group is known to be a toxic moiety that requires modifications to replace it. As a result, scaffold hopping was performed utilizing pharmacophore and molecular docking studies. The pharmacophore alignment studies were performed using GALAHAD module (Tripos, Inc.) utilizing four known CB2 inverse agonists (SR144528, AM630, JTE-907, and Sch.225336) as well as **XIE-35**, and the molecular docking was performed using Surflex-Dock module (Tripos, Inc.). The 3D pharmacophore model suggested four hydrophobic (light blue), one hydrogen bond acceptor (green), and one hydrogen bond donor (pink) features (Figure 4.4). Utilizing the pharmacophore model, we carried out a 3D database screening via the UNITY pharmacophore search program (SYBYL X1.3). As a result, compound **4.1** (*N*,*N*′-((4-(dimethylamino)phenyl)methylene)-bis(2-phenylacetamide)) was discovered and identified with novel chemotype (Figure 4.5). Structural analysis of **4.1** shows the replacement of the amidine group with an amide moiety which retains the hydrogen bonding feature. Furthermore, the azo-group was removed, yet retaining the hydrophobic property of ring B. Finally, molecular docking was performed using Surflex-Sim module (Tripos, Inc.), which suggested that adding bulky groups on ring B may help in improving the binding affinity.

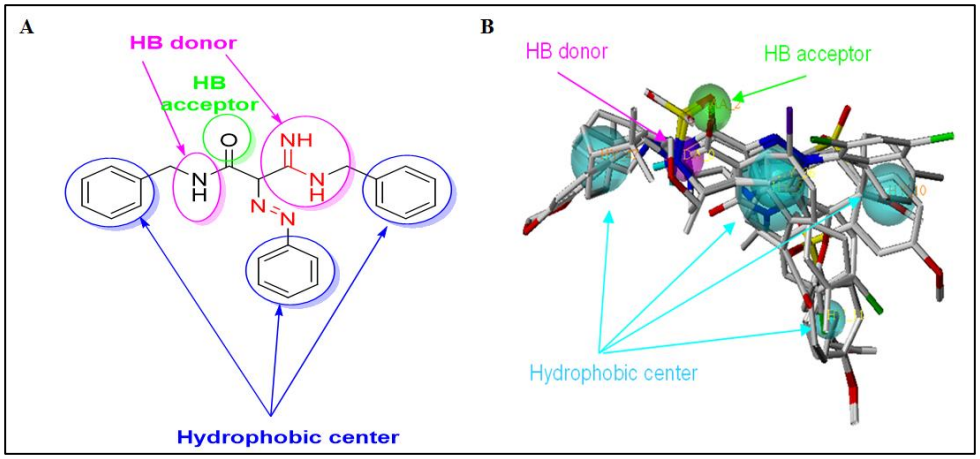

Figure 4.4. Pharmacophore model

The pharmacophore alignment model was generated using GALAHAD module (Tripos, Inc.). **(A)** Pharmacophore properties of **XIE-35**. **(B)** Pharmacophore model utilizing four known CB2 inverse agonists (SR144528, AM630, JTE-907, and Sch.225336) as well as **XIE-35**.

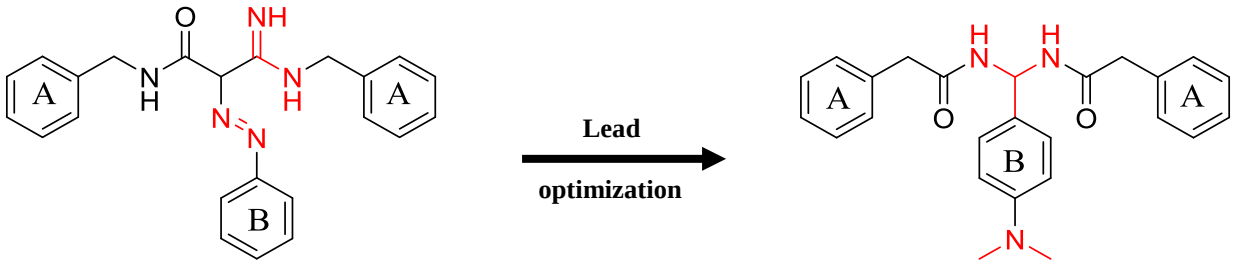

XIE-35 **Compound 4.1**

Figure 4.5. Scaffold hopping and lead optimization of XIE-35.

The hit compound, **XIE-35**, was subjected to chemical modifications and optimizations based of pharmacophore alignment and docking studies to identify **4.1**. The amidine group and the adjacent amide moiety was replaced with a di-amide backbone. The azo- group was replaced and the distance between ring B and the di-amide backbone was reduced.

The modified hit compound, **4.1**, represents a novel CB2 structure. The important features of **4.1** are: (i) di-amide scaffold; (ii) two un-substituted benzyl rings (ring A); (iii) a *p*-substituted benzyl ring (ring B) attached with dimethyl amine. The binding affinities of **4.1** towards the CB2 and CB1 are illustrated in Figure 4.6.

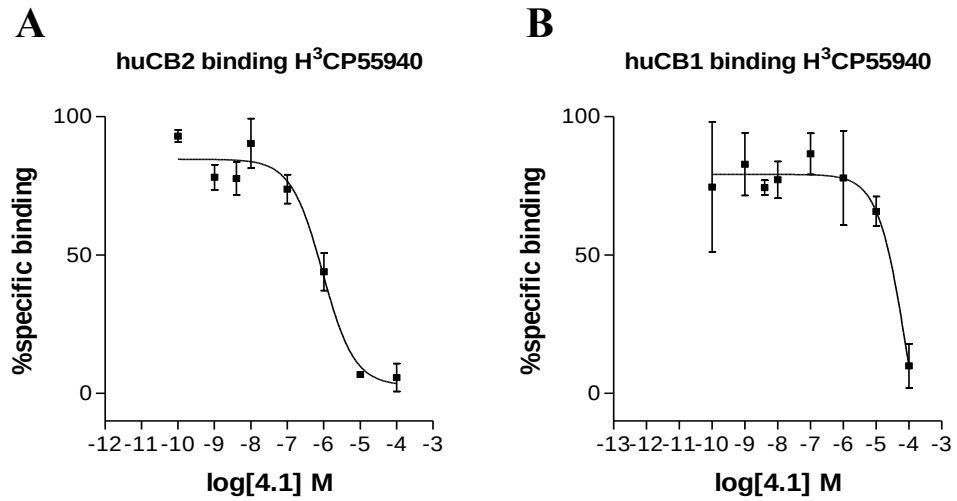

Figure 4.6. Competition binding profile for compound 4.1.

Competition binding experiments were performed on membrane proteins harvested from CHO cells stably expressing CB1 or CB2 receptors. Competitive displacement of the [^{3}H]-CP55,940 was obtained by using an increased amount of cold ligands. **(A)** Competition binding profile of **4.1** utilizing CB2 membrane proteins, K_i = 777 nM. **(B)** Competition binding profile of **4.1** utilizing CB1 membrane proteins, K_i > 20,000 nM.

The goal of the lead optimization is to obtain highly potent and selective CB2 ligands that will be further tested for OCL formation experiments as well as anti-MM activity. Thus, the lead modification strategy was to perform a structure activity relationship (SAR) studies in order to develop selective ligands. The SAR plan included: preserving the aromatic moiety of ring A and to add small substitutions on the ring, such as Cl, CF_3, etc. Also, to introduce bulky groups on ring B in order to preserve the hydrophobic hollow in the CB2 binding pocket.

4.2 RESULTS AND DISCUSSION

4.2.1 Chemistry Synthesis

The chemistry synthesis routes for the di-amide derivatives are illustrated in Scheme 1. The commercially available 2-phenylacetonitrile was treated with concentrated H_2SO_4 to give 2-phenylacetamide. 2-Phenylacetamide was reacted with substituted aldehyde in the presence of either trimethylsilyl chloride (TMSCI) or trimethylsilyl trifluoromethanesulfonate ($F_3CSO_3SiMe_3$) (compounds **4.1** – **4.22** and **4.42** – **4.43**). Similarly, when the building block 2-(4-Chlorophenyl)acetamide and (4-(trifluoromethyl)phenyl)acetamide were reacted with substituted aldehyde in the presence of TMSCl yielded the corresponding compounds **4.23 – 4.31** and **4.32 – 4.38**. Furthermore, when the commercially available amide building blocks benzamide, 3-phenylpropanamide, cinnamamide, isobutyramide, pivalamide, pentanamide, hexanamide, octanamide, and decanamide reacted with substituted aldehyde yielded the corresponding compounds **4.39**, **4.40**, **4.41**, **4.44**, **4.45**, **4.46**, **4.47**, **4.48**, and **4.49**. For compound **4.20**, *N*, *N'*-((4-nitrophenyl)methylene)bis(2-phenylacetamide) was subjected to nitro reduction when treated with palladium and hydrazine. The intermediate was then subjected alkylation utilizing benzyl bromide. The target compounds were purified by flash chromatography or preparative TLC where indicated and confirmed by NMR as well as LC-MS.

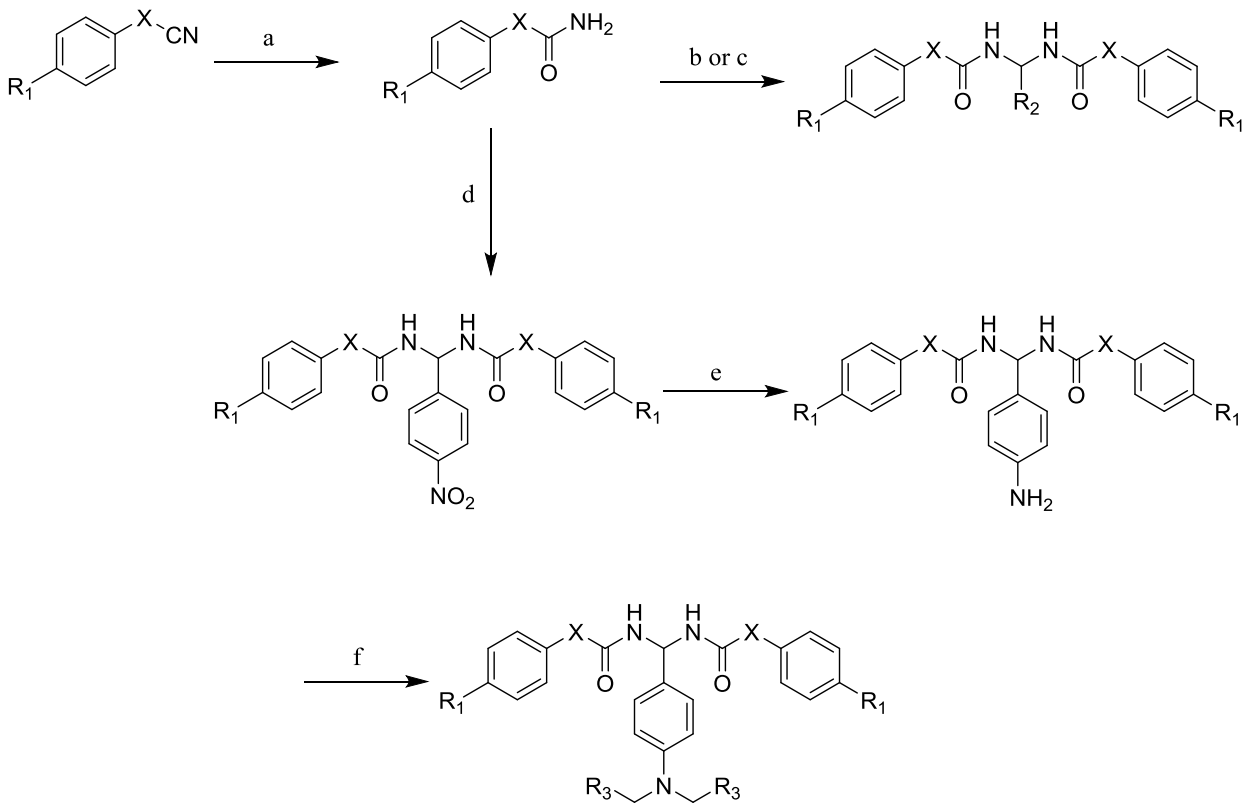

Scheme 1. Synthesis routes of di-amide derivatives.

R_1: H, -Cl, -CF_3, R_2: substituted aldehydes, and R_3: phenyl. Reagents and conditions: (a) concentrated H_2SO_4, 0 °C, 12 h. (b) Method 1: substituted aldehyde, anhydrous dichloroethane, TMSCl, 70 °C, 3 – 12 h. (c) Method 2: substituted aldehyde, anhydrous dichloroethane, $F_3CSO_3SiMe_3$, rt, 12 h. (d) 4-nitrobenzaldehyde, anhydrous dichloroethane, TMSCl, 70 °C, 3 – 12 h. (e) ethanol, palladium (10%), hydrazine, 70 °C, 3 h. (f) substituted bromide, DMF, K_2CO_3, rt, 12 h.

4.2.2 Structure Activity Relationship Analysis

In light of the lead optimization strategy, medicinal chemistry modifications were carried out and synthesized 49 di-amide derivatives. The SAR study was carried out on the basis of CB1 and CB2 binding affinities and selectivities. The radio-ligand binding affinities were carried by performing [^{3}H]-CP55,940 radio-ligand displacement assay utilizing membrane protein preparations of CHO cells stably expressing human CB1 and CB2 receptors. CB1 selective ligand (SR141716) was used as a positive control along with the tested compounds. CB2 selective ligand (SR144528) was used as a positive control with the tested compounds. The chemical structures, physicochemical properties, binding affinities, and selectivity indices are tabulated in Table 4.1 - Table 4.4.

The first SAR study was focused on the different substitutions on ring B while keeping ring A without substitutions. Ring B was modified with substitutions varying in size, electron character and position. Twenty-one compounds were synthesized (**4.2** – **4.22**, Table 4.1). Compared to compound **4.1**, the removal of the *p*-dimethylamino group significantly decreased the CB2 binding activity (compound **4.2**, CB2 K_i = 9930 nM). The CB2 binding affinity was reduced upon introducing fluorine atoms to different positions of ring B (ortho, meta, and para positions) (compounds **4.3**, **4.4**, and **4.5**, CB2 K_i 35330, 12670, and 10900, respectively). The binding affinities of the F-substituted compounds towards the CB2 receptor was in the order of *p*-F > *m*-F > *o*-F. Similarly, introducing *p*-trifluoromethyl to ring B showed improved CB2 binding affinity (compound **4.14**, CB2 K_i = 596 nM) while *o*-trifluoromethyl substitution on ring B showed significant binding activity reduction (compound **4.13**, CB2 K_i = 11780 nM). Furthermore, replacing the *p*-fluorine with chlorine (compound **4.6**) or bromine (compound **4.7**) showed weak

binding affinities. We concluded from these results that substitution at the para position of ring B may play an essential role in the CB2 binding affinity. In addition, introducing *p*-methyl to ring B (compound **4.8**) improved the CB2 binding affinity, however compound **4.8** showed high CB1 affinity (compound **4.8**, CB2 K_i = 494 nM, CB1 K_i = 109 nM). Introducing bioisostere isopropyl (compound **4.9**) instead of the *p*-diethylamino significantly improved the binding affinity as well as selectivity (CB2 K_i = 85 nM, CB1 K_i > 20,000 nM, selectivity index > 235).

Next, we further investigated para substitutions on ring B by introducing different alkoxy groups. Three alkoxy groups were tested varying in size, methoxy (**4.10**), ethoxy (**4.11**), and isopropoxy (**4.12**). Compound **4.10** with methoxy group showed similar activity and selectivity compared to the parent compound (**4.10**, CB2 K_i = 783 nM, CB1 K_i > 20000 nM, selectivity index > 235). Compound **4.11** with ethoxy group showed slight decrease in binding activity (**4.11**, CB2 K_i = 1500 nM). Compound **4.12** with the isopropoxy group showed slight increase in the binding activity (**4.12**, CB2 K_i = 313 nM, CB1 K_i > 20000, selectivity index > 64). These results indicate that the size of the alkoxy group influence the binding affinity and selectivity.

In order to explore the electronic and steric effects on the binding affinity and selectivity, we introduced a *p*-NO_2 group to ring B (compound **4.15**). However, **4.15** completely lost the CB2 binding affinity. When reducing the nitro group to the corresponding amine (compound **4.16**), the CB2 binding activity was restored but remained weak (**4.16**, CB2 K_i = 12550 nM). When replacing the *p*-amino with *p*-diethylamine group, the CB2 binding affinity and selectivity was significantly improved (compound **4.17**, CB2 K_i = 64 nM, CB1 K_i > 20000, selectivity index >313). Compound **4.17** was identified to be more potent and selective that the lead compound **4.1**. As the introduction of the *p*-diethylamine to ring B resulted in a potent and selective compound, we tested different substituted amino groups on ring B. As a result, a number of potent compounds were identified

bearing *p*-dipropylamino, *p*-dibutylamino, *p*-dibenzylamino. *p*-pyrrolidinyl, and *p*-piperidyl (compounds **4.18**, **4.19**, **4.20**, **4.21**, and **4.22**, respectively). These five amino substituted compounds showed high potency and selectivity compared to the lead compound **4.1**. Comparing to compound **4.17** with the *p*-diethylamino on ring B, compound **4.18** with a *p*-dipropylamino group showed the highest activity and selectivity (CB2 K_i = 22 nM, selectivity index > 909). Increasing the size of the para substituted amine on ring B more than three carbons (compound **4.19** bearing *p*-dibutylamino) slightly reduced the binding affinity compared to compound **4.17** (**4.19**, CB2 K_i = 221 nM, selectivity index > 90). To further confirm the importance of the size of para substituted amine on ring B, compound **4.21** bearing a pyrrolidinyl group on ring B showed a similar activity (CB2 K_i = 71 nM, selectivity index > 281). While compound **4.20** with *p*-dibenzylamino on ring B and compound **4.22** with a *p*-piperidylamino showed reduced CB2 activities. Thus, these results showed that the size of the para substituted amine at the para position on ring B play crucial roles in the binding activity.

Table 4.1. Radioligand competition binding affinity and physicochemical properties of di-amide derivatives on ring B

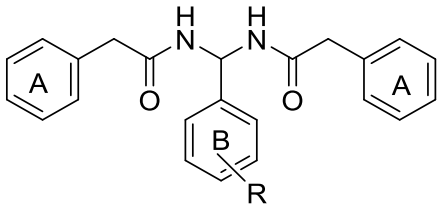

Entry	R	MW	cLogP	K_i (CB2), nM	K_i (CB1), nM	SI
4.1	*p*-$(CH_3)_2N$-	401.50	4.04	777	> 20,000	> 26
4.2	H	358.43	3.93	9930	NT	-
4.3	*o*-F-	376.42	4.08	35330	NT	-
4.4	*m*-F-	376.42	4.08	12670	NT	-
4.5	*p*-F-	376.42	4.08	10900	NT	-
4.6	*p*-Cl-	392.88	4.54	3081	NT	-
4.7	*p*-Br-	437.33	4.70	2226	NT	-
4.8	*p*-CH_3-	372.46	4.45	494	109	-
4.9	*p*-*i*-C_3H_7-	400.51	5.18	85	> 20,000	> 235
4.10	*p*-CH_3O-	388.46	3.78	783	> 20,000	> 26
4.11	*p*-C_2H_5O-	402.49	4.13	1500	NT	-
4.12	*p*-*i*-C_3H_7O-	416.51	4.55	313	> 20,000	> 64
4.13	*o*-CF_3-	426.43	4.81	11780	NT	-
4.14	*p*-CF_3-	426.43	4.81	596	> 20,000	> 34
4.15	*p*-NO_2-	403.43	3.87	NB	NT	-
4.16	*p*-H_2N-	373.45	2.51	12550	NT	-
4.17	*p*-$(C_2H_5)_2N$-	429.55	4.76	64	> 20,000	> 313
4.18	*p*-$(C_3H_7)_2N$-	457.61	5.80	22	> 20,000	> 909
4.19	*p*-$(C_4H_9)_2N$-	485.66	6.69	221	> 20,000	> 90
4.20	*p*-(benzyl)$_2$N-	553.69	7.33	203	> 20,000	> 99
4.21	*p*-pyrrolidinyl-	427.53	4.45	71	> 20,000	> 281

4.22	*p*-piperidyl-	441.56	4.89	595	> 20,000	> 34
SR144528				2.1	NT	-
SR141716				NT	10.6	-

Binding affinities of compounds for CB1 and CB2 receptor were evaluated using [^{3}H]CP-55,940 radioligand competition binding assay. NB: no binding, *K*i > 20000 nM. NT: not tested. SI: selectivity index for CB2, calculated as K_i(CB1)/K_i(CB2) ratio. The binding affinities of reference compounds were evaluated in parallel with tested compounds. CB2 reference compound SR144528 and CB1 reference compound SR141716.

Further, we explored the effect of variations on ring A by introducing Cl or CF_3. Two series of compounds were synthesized: **4.23** – **4.31** (Table 4.2) and **4.32** – **4.38** (Table 4.3). The first series included compounds with *p*-Cl substitution on ring A and the substitutions on ring B were tested. Among the nine compounds, five compounds (**4.26** – **4.30**) showed improved binding activity to CB2. Comparing compound **4.26** with *p*-Cl on ring B and ring A (CB2 K_i = 154, selectivity index >130) with compound **4.6** with un-substituted rings A and *p*-Cl on ring B (CB2 K_i = 3081 nM), the chlorine substitutions on rings A improved the binding affinity and selectivity. Same results were observed when comparing compounds **4.27** with **4.8**, **4.28** with **4.10**, **4.29** with **4.22** and **4.30** with **4.14**. The second series of compounds (**4.32** – **4.38**) with $–CF_3$ substitution on rings A showed completely no binding to the CB2 receptors. These results indicated that the *p*-Cl substitution on rings A is better than $–CF_3$ and H.

Table 4.2. Radioligand competition binding affinity and physicochemical properties of di-amide derivatives with substituted chloride on ring A

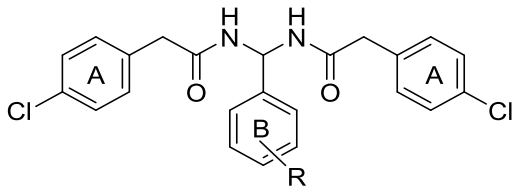

Entry	R	MW	cLogP	K_i (CB2), nM	K_i (CB1), nM	SI
4.23	H	427.32	5.14	NB	NT	-
4.24	*o*-F-	445.31	5.29	10850	NT	-
4.25	*p*-F-	445.31	5.29	NB	NT	-
4.26	*p*-Cl-	461.77	5.75	154	> 20,000	> 130
4.27	*p*-CH_3-	441.35	5.66	462	> 20,000	> 43
4.28	*p*-CH_3O-	457.35	4.98	310	> 20,000	> 65
4.29	*o*-CF_3-	495.32	6.02	158	> 20,000	> 127
4.30	*p*-CF_3-	495.32	6.02	101	> 20,000	> 198
4.31	*p*-NO_2-	472.32	5.08	NB	NT	-
SR144528				2.1	NT	-
SR141716				NT	10.6	-

Binding affinities of compounds for CB1 and CB2 receptor were evaluated using [^{3}H]CP-55,940 radioligand competition binding assay. NB: no binding, Ki > 20000 nM. NT: not tested. SI: selectivity index for CB2, calculated as K_i(CB1)/K_i(CB2) ratio. The binding affinities of reference compounds were evaluated in parallel with tested compounds. CB2 reference compound SR144528 and CB1 reference compound SR141716.

Table 4.3. Radioligand competition binding affinity and physicochemical properties of di-amide derivatives with substituted trifluoromethyl (-CF_3) on ring A

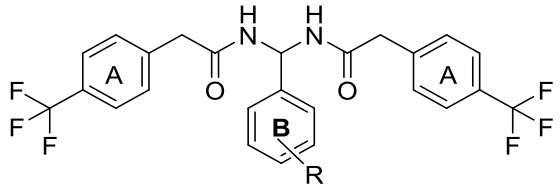

Entry	R	MW	cLogP	K_i (CB2), nM	K_i (CB1), nM	SI
4.32	H	494.43	5.69	NB	NT	-
4.33	*o*-F-	512.42	5.83	NB	NT	-
4.34	*p*-F-	512.42	5.83	NB	NT	-
4.35	*p*-Cl-	528.87	6.29	NB	NT	-
4.36	*p*-CH_3-	508.46	6.20	NB	NT	-
4.37	*p*-CH_3O-	524.45	5.53	NB	NT	-
4.38	*o*-CF_3-	562.43	6.57	NB	NT	-
SR144528				2.1	NT	-
SR141716				NT	10.6	-

Binding affinities of compounds for CB1 and CB2 receptor were evaluated using [^{3}H]CP-55,940 radioligand competition binding assay. NB: no binding, *K*i > 20000 nM. NT: not tested. SI: selectivity index for CB2, calculated as K_i(CB1)/K_i(CB2) ratio. The binding affinities of reference compounds were evaluated in parallel with tested compounds. CB2 reference compound SR144528 and CB1 reference compound SR141716.

Next, we studied the importance of the distance from ring A to the amide group (compounds **4.39** – **4.41**, Table 4.4). Reducing or increasing the distance between ring A and the amide group of compound **4.17** by removing CH_2 (compound **4.39**), inserting -CH_2CH_2- (compound **4.40**), or inserting –CH=CH- (compound **4.41**) retained the CB2 binding affinity and selectivity with minimal decrease.

To explore the importance of the aromatic property of ring B on the CB2 binding affinity and selectivity, we explored the effects of removing the aromatic ring B of compound **4.17** and replacing it with various alkyl chains varying in length (compounds **4.42** and **4.43**, Table 4.4). Replacing ring B with butyl alky chain (**4.42**) or pentyl (**4.43**) resulted in complete loss of binding activity. These results indicate that aromatic property of ring B plays crucial roles in the CB2 binding affinity.

We further studied the importance of ring A by replacing the aromatic rings with different alkyl chains while retaining ring B with *p*-diethylamino group (compounds **4.44** – **4.49**, Table 4.4). Replacing the benzyl groups with a branched chain isopropyl (compound **4.44**) or *tert*-butyl group (compound **4.45**) significantly decreased the CB2 binding affinity. However, replacing the benzyl group with a butyl alkyl chain (compound **4.46**) showed a slight decrease in binding activity. Importantly, replacing the benzyl group with a pentyl alkyl chain showed a remarkable CB2 binding affinity and selectivity (compound **4.47**, CB2 K_i = 25 nM, CB1 K_i > 20000, selectivity index > 800). Compared to compound **4.47**, increasing the length of the alkyl chain with *n*-C_7H_{15} (compound **4.48**) or *n*-C_9H_{19} (compound **4.49**) showed a slight decrease in binding activity with CB2 K_i of 146 nM, selectivity index > 136 and CB2 K_i = 160 nM, selectivity index > 125, respectively. From these results, we conclude that distance between the ring A and the amide group play a slight role and the –CH_2 is optimal. Also, ring B is important for retaining the CB2 binding

activity. Finally, aromatic rings A may be replaced with alkyl chains and the pentyl group in optimal for binding activity.

Table 4.4. Radioligand competition binding affinity and physicochemical properties of di-amide derivatives with varying substitutions

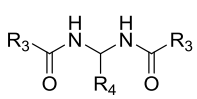

Compounds 4.39 - 4.41

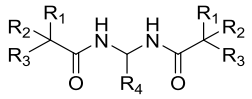

Compounds 4.42 - 4.49

Entry	R_1	R_2	R_3	R_4	MW	cLogP	K_i (CB2), nM	K_i (CB1), nM	SI
4.39	-	-		*N*,*N*-diethylaniline	401.50	4.80	688	> 20,000	> 29
4.40	-	-	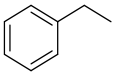	*N*,*N*-diethylaniline	457.61	5.64	213	> 20,000	> 93
4.41	-	-	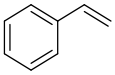	*N*,*N*-diethylaniline	453.58	5.80	167	> 20,000	>119
4.42	H	H		-C_4H_9	338.44	3.75	35970	NT	-
4.43	H	H		-C_5H_{11}	352.47	4.19	18200	> 20,000	-
4.44	H	-CH_3	-CH_3	*N*,*N*-diethylaniline	333.46	3.57	2636	NB	-
4.45	-CH_3	-CH_3	-CH_3	*N*,*N*-diethylaniline	361.52	4.69	3553	NB	-
4.46	H	H	-C_3H_7	*N*,*N*-diethylaniline	361.52	4.27	182	> 20,000	>109
4.47	H	H	-C_4H_9	*N*,*N*-diethylaniline	389.57	5.16	25	> 20,000	>800
4.48	H	H	-C_6H_{13}	*N*,*N*-diethylaniline	445.68	7.9	146	> 20,000	>136
4.49	H	H	-C_8H_{17}	*N*,*N*-diethylaniline	501.79	10.0	160	> 20,000	>125
SR144528							2.1	NT	--
SR141716							NT	10.6	--

Binding affinities of compounds for CB1 and CB2 receptor were evaluated using [^{3}H]CP-55,940 radioligand competition binding assay. NB: no binding, *K*i > 20000 nM. NT: not tested. SI: selectivity index for CB2, calculated as K_i(CB1)/K_i(CB2) ratio. The binding affinities of reference compounds were evaluated in parallel with tested compounds. CB2 reference compound SR144528 and CB1 reference compound SR141716.

4.2.3 *In-Vitro* Functional Assay

To determine the functionality (agonist or antagonist functions) of the synthesized CB2 ligands, ligands that exhibited high potency and selectivity were subjected to LANCE cAMP assay. The assay was carried out as stated in Chapter 3. Six compounds (**4.1**, **4.9**, **4.17**, **4.18**, **4.21**, and **4.47**) were chosen for the assay utilizing CB2 cells harvested from CHO cells stably expressing CB2 receptors. CB2 receptors are $G_{\alpha i}$-coupled receptors in which an agonist will inhibit the forskolin-induced cAMP production resulting in an increase of the LANCE signal. An antagonist or an inverse agonist will induce the cAMP formation resulting in a decrease of the LANCE signal. Thus, LANCE signal is inversely proportional to cAMP level. As illustrated in Figure 4.7, increasing concentrations of compounds **4.1**, **4.9**, **4.17**, **4.18**, **4.21**, **4.47** as well as SR144528 (CB2 inverse agonist) led to reductions of the LANCE cAMP signal. These results indicate that these ligands are inverse agonists. This behavior was not seen with CB2 agonists CP-55,940 and HU-308 as they inhibited cAMP production.

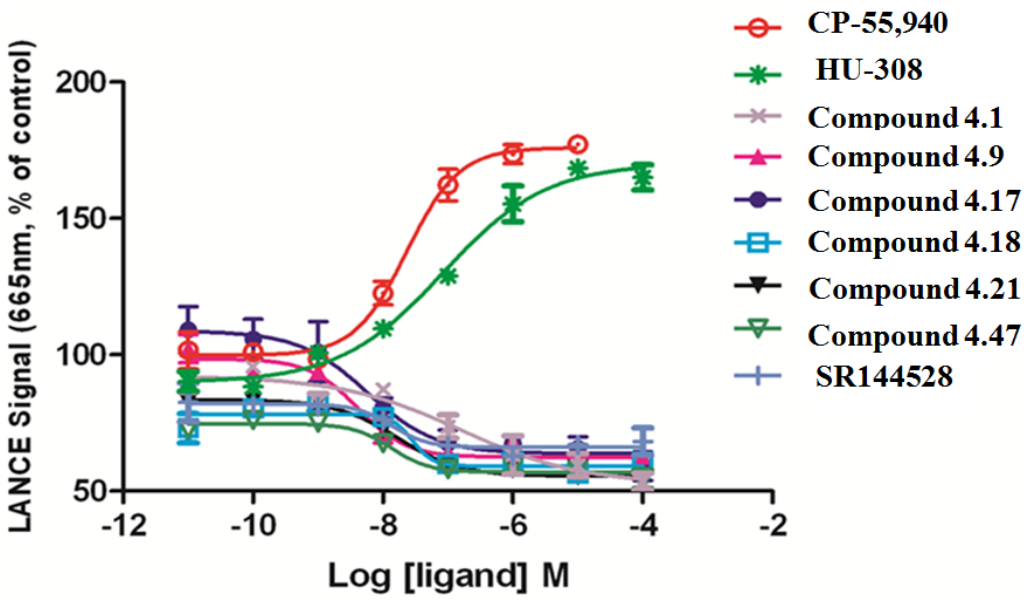

Figure 4.7. LANCE cAMP signal of the di-amide derivatives

Stably transfected CHO cells expressing human CB2 receptors were utilized in LANCE cAMP assay. HU-308 and CP-55,940 are known CB2 agonist, while SR 144528 is a known CB2 inverse agonist. Compounds **4.1**, **4.9**, **4.17**, **4.18**, **4.21**, and **4.47** as well as SR144528 inhibited the cAMP production with an EC_{50} value of 159 ± 8.68, 4.11 ± 3.66, 5.73 ± 6.37, 28.33 ± 2.54, 17.08 ± 2.11, 13.42 ± 2.07, and 13.7 ± 2.81 nM, respectively. Data represented as the mean ± SEM of one representative experiment of three experiments carried out in triplicates.

4.2.4 CB2 Inverse Agonist as Osteoclast Inhibitors

As the cannabinoid receptors and the endocannabinoid systems have been proven to have roles in bone remodeling and homeostasis, we tested several synthesized ligands for their anti-osteoclastogenesis activities. The assay is based on the OCL formation after receptor activator of nuclear factor kappa-B ligand (RANKL) induction. Non-adherent mononuclear bone marrow cells were seeded at a density of 2×10^5 cells/well in a 96- well plate. Test wells were treated with the highly potent and selective CB2 derivatives (**4.9**, **4.12**, and **4.17**). In addition, the known CB2 inverse agonist, SR144528, was used as a positive control and compound **4.1** was also tested for comparison reasons. Plates were incubated for 3 weeks in the presence of RANKL (50 ng/mL) and M-CSF (10 ng/mL). The detailed experimental protocol was outlined in Chapter 3. All compounds were tested in concentrations of 10 μM, 1 μM, and 0.1 μM. Control groups included wells treated with RANKL, wells without RANKL, and wells treated with SR144528.

All tested ligands exhibited a concentration-dependent inhibition of osteoclastogenesis. The synthesized ligands exhibited even more inhibition activity than the known CB2 inverse agonist (SR144528). As illustrated in Figure 4.8, compound **4.17** showed the strongest inhibition activity with inhibition rates of 72%, 79% and 84% at 0.1, 1 and 10 μM, respectively. In addition, compound **4.17** was more potent in inhibiting the OCL than the lead compound **4.1**, as it showed and inhibition rate of 75%, 77% and 82% at 0.1, 1 and 10 μM, respectively. Overall, these data suggest that our medicinal chemistry design and synthesis were successful in improving CB2 binding level as well as the therapeutic level.

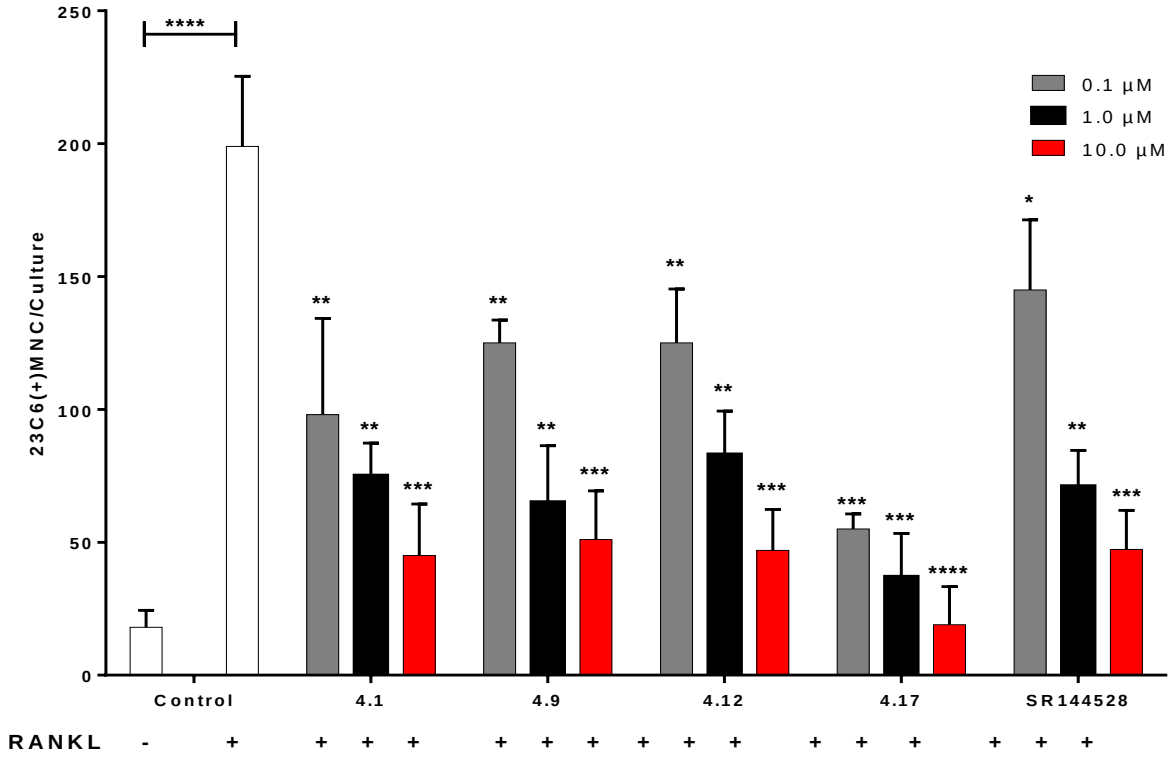

Figure 4.8. Osteoclast inhibition activity by di-amide derivatives.

Inhibition of human osteoclastogenesis by the di-amide derivatives. Human-bone-marrow-derived mononuclear cells (2×10^5 cells/well) were seeded in a 96- well plate for 3 weeks in the presence of RANKL (50 ng/mL) and M-CSF (10 ng/mL). Control group were divided into RANKL positive and RANKL negative. Cultures were stained with TRAP staining kit (Sigma). TRAP positive OCLs containing three or more nuclei were counted as OCL. Results represented as the mean ± SD of three experiments carried out in triplicates. Statistical differences are as follows: **P*<0.05, ***P*<0.01, ****P*<0.001, and *****P*<0.0001 compared with the control (RANKL +).

4.2.5 Multiple Myeloma Anti-Proliferation Studies

To test whether our newly synthesized compounds possesses anti-proliferation effects on MM cell-lines, we first analyzed the proliferation activity of the known selective CB2 ligands including, SR144825 and CP-55,940. As illustrated in Figure 4.9, the CB2 inverse agonist, SR144528, exhibited low anti-proliferative effects on MM cell-lines with IC_{50} of 19.4 µM and 25 µM for RPMI8226 and MM1.S cell-lines, respectively. On the other hand, the CB2 agonist, CP55940, showed good anti-proliferative effects on MM cell-lines with an IC_{50} of 2.76 µM and 2.17 µM for RPMI8226 and MM1.S, respectively. These data suggest that CB2 agonist may play crucial roles as anti-MM.

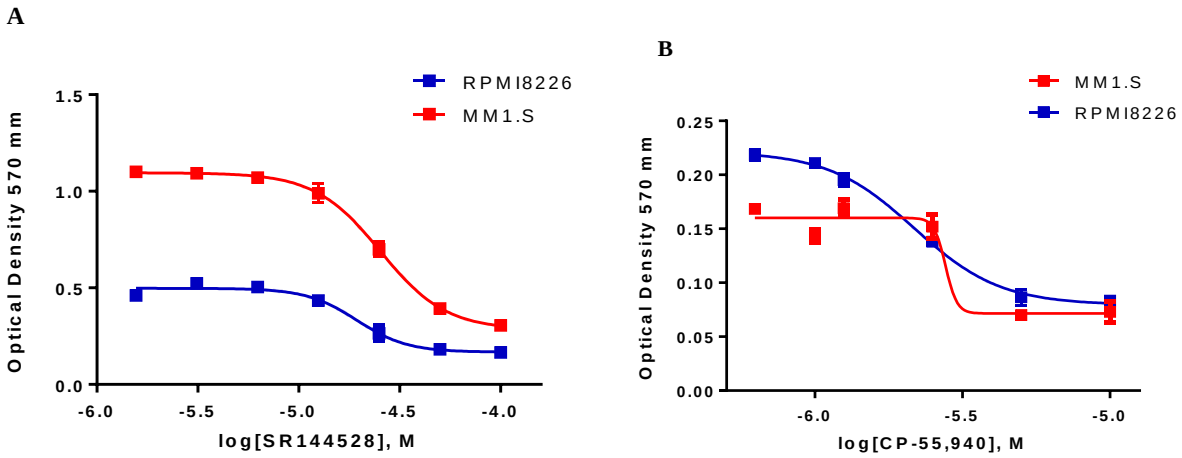

Figure 4.9. IC_{50} of known CB2 ligands on MM cell-lines

IC_{50} was measured by utilizing the MTT-colorimetric assay. MM cell-lines RPMI8226 and MM1.S were seeded at a density of 3×10^3 / well and treated with varying concentrations of the compounds. (**A)** IC_{50} of **SR144528** = 19.4 µM and 25 µM for RPMI8226 and MM1.S cell-lines, respectively. **(B)** IC_{50} of **CP55,940** = 2.76 µM and 2.17 µM for RPMI8226 and MM1.S cell-lines, respectively. Data is the mean ± SD of three experiments carried out in triplicates.

For our newly synthesized CB2 ligands, we utilized the MTT assay to screen our compounds for their anti-MM activity using 10 µM concentration of the compounds. Four compounds with high CB2 affinity and selectivity were utilized in the MTT screening studies. As shown in Figure 4.10, nearly all the derivatives exhibited low inhibition rates on the MM cell-lines RPMI8226 and MM1.S. As expected, these results indicates that developing selective CB2 agonists is more promising as anti-MM agents.

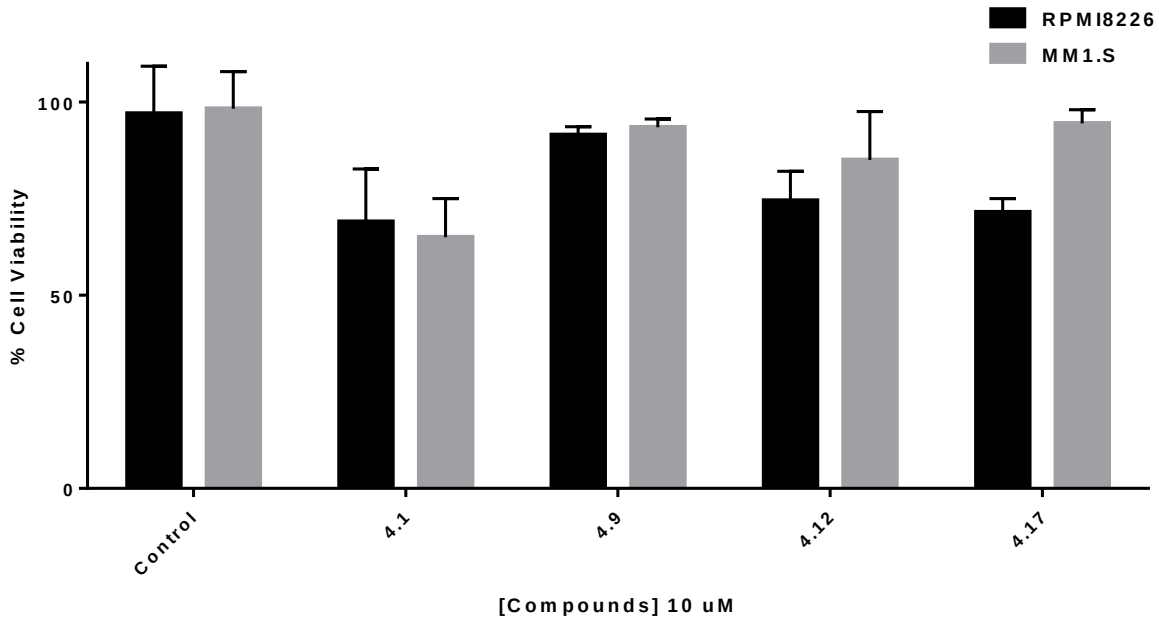

Figure 4.10. Cell viability screening of the di-amide derivatives on MM cell-lines

Two multiple myeloma cell-lines (MM1.S and RPMI8226) were utilized to study the anti-proliferation effects of the synthesized derivatives. Cells were plated at density of 3×10^3/well in 96-well plates. Cells were incubated with 10 µM concentration of the tested derivatives for 3 days. The cell viability was determined with the MTT assay. All of the compounds demonstrated no significant (NS) inhibition rates (NS = P >0.05 compared with the control which was defined as 100%). Data is the mean ± SD of three experiments carried out in triplicates.

4.2.6 Stability and Pharmacokinetic Studies

As the excellent *in-vitro* activity profiles of several of the newly discovered novel CB2 ligands, we utilized compound **4.17** as a representative compounds of the di-amide CB2 scaffold to carry out *in-vivo* pharmacokinetic (PK) studies and to establish PK profile in rats. After oral administration of compound **4.17**, the maximal plasma concentration was 8 µg/L (C_{max}), plasma exposure of 23.46 µg/L*h ($AUC_{0-\infty}$), an elimination half-life ($t_{1/2}$) of 2.69 hours, and a clearance of 1649.1 L/h/kg.

Table 4.5. Oral pharmacokinetic properties of 4.17

Parameter	Unit	No.1	No.2	No.3	Mean
$AUC_{(0-t)}$	µg/L*h	14.20	28.08	28.10	23.46
$AUC_{(0-\infty)}$	µg/L*h	16.47	28.10	28.19	24.25
λ	1/h	0.23	0.32	0.24	0.26
C	µg/L	0.52	0.01	0.02	0.18
$t_{1/2}$	h	3.04	2.20	2.84	2.69
T_{max}	h	0.17	0.17	1.00	0.44
Vd	L/kg	5326	2260	2908	3498
CL	L/h/kg	1214	712	709	879
C_{max}	µg/L	8	11	4	8

AUC, area under the concentration−time curve; C_{max}, peak plasma concentration of a drug after administration; CL, clearance; T_{max}, time to reach C_{max}; $t_{1/2}$, elimination half-life; Vd, volume of distribution.

The poor PK profile of **4.17** (and other di-amide derivatives) may be attributed to the di-amide scaffold as in acidic conditions, the di-amide is subjected hydrolysis in which the ligand will break down into 2-phenylacetamide and (*Z*)-*N*-(4-(diethylamino)benzylidene)-2-phenylacetamide. Figure 4.11 illustrates the possible instability mechanism due to the di-amide scaffold. Nevertheless, intravenous (IV) PK studies were not conducted due to the instability and poor water solubility of the di-amide scaffold.

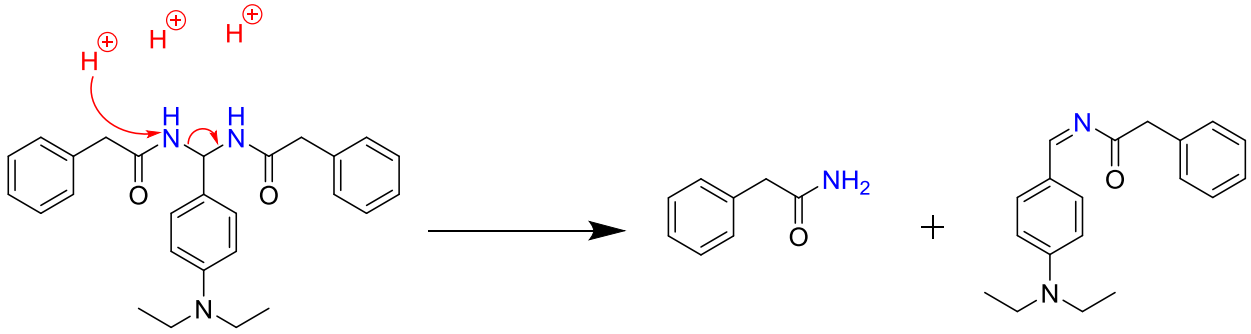

Compound 4.17

Figure 4.11. Compound 4.17 acidic instability.

In acidic conditions (i.e. gastric acid), the di-amide scaffold of compound **4.17** is subjected to hydrolysis resulting in the breakdown of the compound. The possible byproducts are 2-phenylacetamide and (*Z*)-*N*-(4-(diethylamino)benzylidene)-2-phenylacetamide. As a result, poor pharmacokinetic properties were observed.

4.3 CONCLUSION

In this chapter, we utilized ligand discovery tools in order to discover and identify novel CB2 chemotype including pharmacophore modeling as well as high-throughput screening methodologies. 3D-QSAR studies were carried out to identify **XIE-35** as a new CB2 selective inverse agonist with CB2 K_i = 31.7 nM, CB1 K_i = 4185, and SI of > 132. Due to the structural limitations of **XIE-35**, lead optimization was carried out by utilizing pharmacophore model generation followed by virtual screening to identify compound **4.1**. Compound **4.1** was identified as a novel CB2 chemotype with the di-amide scaffold and was subjected to SAR studies to identify and explore different structural modifications on the di-amide scaffold.

In the SAR studies, we designed and synthesized 49 di-amide derivatives with variations on the aromatic rings A and B. The SAR studies revealed: (1) the para-substituted amino group on ring B plays crucial roles in the CB2 receptor binding affinity and selectivity, different functional groups were tolerated and the *p*-dipropylamino group is optimal, (2) small group substitutions on ring A showed that *p*-Cl is better substituent than $-CF_3$ and H, (3) the aromatic ring B is essential to retain potency toward the CB2 receptor. Our results and findings are consistent with the pharmacophore findings where aromatic ring B is necessary for CB2 affinity. Among the 49 di-amide derivatives, five compounds **4.9**, **4.17 4.18**, **4.21**, and **4.47** exhibited high potency and selectivity toward the CB2 receptor (CB2 K_i < 90 nM, CB1 K_i > 20000 nM). Furthermore, functional assay (cAMP assay) confirmed that these five compounds are selective CB2 inverse agonists.

Importantly, osteoclast formation assay utilizing human bone marrow cells confirmed that the top novel di-amide CB2 inverse agonists inhibited the osteoclast formation at low doses. Compound **4.17** demonstrated the highest inhibition rate of 72% at low concentration (0.1 μM)

suggesting important roles for selective CB2 inverse agonists as anti-osteoclastogenesis and ultimately for treating osteoporosis. On the other hand, anti-proliferation studies on MM cell-lines showed low inhibitory effects of our newly discovered compounds and that developing CB2 agonists rather than inverse agonists may play key roles as anti-MM agents as demonstrated by the inhibition abilities of CP-55,940 on MM cell-lines. In addition, pharmacokinetic studies of the di-amide scaffold were conducted and demonstrated moderate elimination half-life, plasma exposure as well as clearance properties. Furthermore, i.v. PK studies were not conducted due to the limited stability and solubility of the compounds. Albeit the limitations of the di-amide scaffold, our novel selective CB2 inverse agonists represent a novel class of CB2 ligands that can be further optimized as anti-osteoclastogenesis agents with improved pharmacokinetic properties. Nevertheless, the newly discovered selective ligands represent a new chemotype that can be utilized as chemical probes in different biochemical assays.

4.4 EXPERIMENTAL

4.4.1 Pharmacophore Modeling and Virtual Screening

Genetic algorithm-based pharmacophore alignment (GALAHAD™, Tripos Inc.) approach was used to derive a 3D pharmacophore model based on known CB2 inverse agonists including SR144528, AM630, JTE-907, Sch.225336 and **XIE-35**. The derived pharmacophore model was then examined and refined using our in-house training database which contained a mixture of random molecules and known CB2 ligands. The derived pharmacophore model was subsequently used as a query in the UNITY (Tripos Inc.) program to perform virtual screening on a structurally diverse representative compound database [132]. Top ranked screened compounds from the pharmacophore search were obtained commercially or via material transfer agreement (MTA) to be experimentally validated for CB2 binding activity and selectivity.

4.4.2 Chemistry

4.4.2.1 General synthesis procedure of 2-Phenylacetamide building blocks

2-Phenylacetamide.

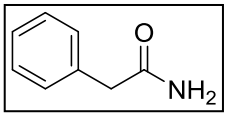

Benzyl cyanide (5 g, 42.7 mmol) was added slowly to concentrated sulfuric acid (20 mL) cooled by a water-ice bath. The solution was stirred overnight. The reaction mixture was poured into ice-water and neutralized with 20% NaOH. The aqueous phase was extracted by ethyl acetate (3 × 15 mL). The combined organic layer was washed with water (3 × 10 mL) and brine (3 × 10 mL), dried over anhydrous $MgSO_4$, filtered, concentrated under reduced pressure, and the residue was recrystallized from ethyl acetate and hexane to give

the desired compound. (4.5 g, yield: 78%). ^{1}H NMR (400 MHz, DMSO-d_6) δ7.54 (s, 1H), 7.20−7.32 (m, 5H), 6.87 (s, 1H), 3.38 (s, 2H).

2-(4-Chlorophenyl)acetamide.

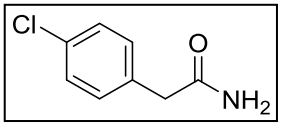

Yield: 65%. ^{1}H NMR (400 MHz, DMSO-d_6) δ 7.49 (s, 1H), 7.34−7.35 (m, 2H), 7.26−7.27 (m, 2H), 6.92 (s, 1H), 3.34−3.37 (m, 2H).

(4-(Trifluoromethyl)phenyl)acetamide.

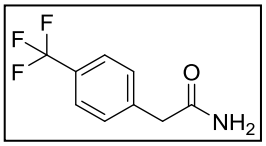

Yield: 80%. ^{1}H NMR (400 MHz, DMSO-d_6) δ 7.65 (d, J = 8.0 Hz, 2H), 7.58 (s, 1H), 7.49 (d, J = 8.0 Hz, 2H), 7.00 (s, 1H), 3.51 (s, 2H).

4.4.2.2 General synthesis procedure for the coupling reaction between amide and aldehyde

General Method 1 [215]:

***N,N′*-((4- (dimethylamino)phenyl)methylene)bis(2-phenylacetamide) (4.1)**. To a suspension of

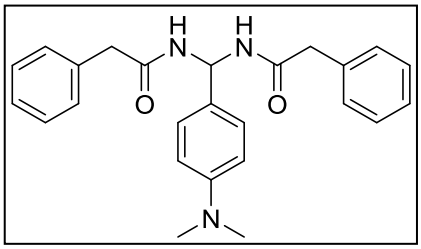

4-(dimethylamino)benzaldehyde (149 mg, 1 mmol) and 2-phenylacetamide (270 mg, 2 mmol) in anhydrous dichloroethane (2 mL) was added TMSCl (216 mg, 2 mmol) . The mixture was heated at 70 °C for 12 h, then cooled to room temperature and the crude product precipitated from the solution. The crude product was recrystallized with methanol and hexane to give the final product. Off-white solid (140 mg, yield: 35%).^{1}H NMR (400 MHz, DMSO-d_6) δ 8.89 (d, J = 8.0 Hz, 2H), 7.59 (s, 2H), 7.41 (d, J = 8.8 Hz, 2H), 7.21−7.32 (m, 10H), 6.54 (t, J = 8.0 Hz, 1H), 3.52 (dd, J = 14.0, 15.6 Hz, 4H), 3.06 (s, 6H). LC−MS (ESI): m/z 402.1 $(M + H)^+$.

***N,N′*-(phenylmethylene)bis(2-phenylacetamide) (4.2)**. Compound **4.2** was prepared from 2-phenylacetamide and benzaldehyde using method 1. White solid (240 mg, yield: 67%).[1]H NMR (400 MHz, DMSO-d_6) δ 8.78 (d, J = 7.2Hz, 2H), 7.21−7.35 (m, 15H), 6.55 (t, J = 7.8 Hz, 1H), 3.50 (dd, J = 13.8, 20.4 Hz, 4H). LC−MS (ESI): *m/z* 359.3 $(M + H)^+$.

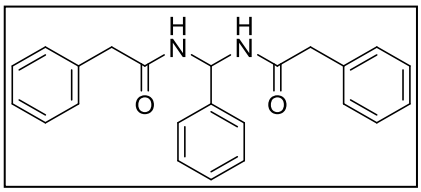

***N,N′*-((2-fluorophenyl)methylene)bis(2-phenylacetamide) (4.3)**. Compound **4.3** was prepared from 2-phenylacetamide and 2-fluorobenzaldehyde using method 1. White sold (240 mg, yield: 64%). [1]H NMR (400 MHz, DMSO-d_6) δ 8.87 (d, J = 7.8 Hz, 2H), 7.44 (t, J = 7.8 Hz, 1H), 7.36 (q, J = 6.6 Hz, 1H), 7.17−7.29 (m, 12H), 6.74 (t, J = 7.8 Hz, 1H), 3.48 (dd, J = 14.4, 24.0 Hz, 4H). LC−MS (ESI): *m/z* 377.2 $(M + H)^+$.

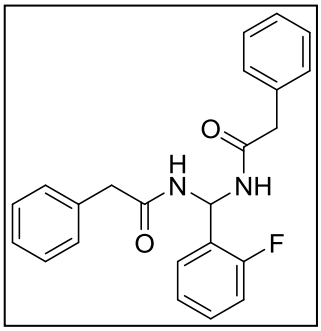

***N,N′*-((4-fluorophenyl)methylene)bis(2-phenylacetamide) (4.5)**. Compound **4.5** was prepared from 2-phenylacetamide and 4-fluorobenzaldehyde using method 1. White solid (271 mg, yield: 72%). [1]H NMR (400 MHz, DMSO-d_6) δ 8.79 (d, J = 8.0 Hz, 2H), 7.16−7.36 (m, 14H), 6.54 (t, J = 8.0 Hz, 1H), 3.52 (dd, J = 14.4, 15.6 Hz, 4H). LC−MS (ESI): *m/z* 377.2 (M + H)+.

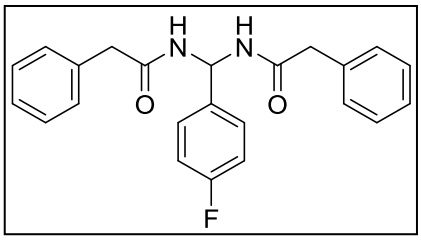

***N,N′*-((4-chlorophenyl)methylene)bis(2-phenylacetamide) (4.6).** Compound **4.6** was prepared from 2-phenylacetamide and 4-chlorobenzaldehyde using method 1. White solid (279 mg, yield: 71%). [1]H NMR (400 MHz, DMSO-d_6) δ 8.83 (d, J = 7.8 Hz, 2H), 7.41 (d, J = 7.8 Hz, 2H), 7.21−7.32 (m, 12H), 6.51 (t, J = 7.8 Hz, 1H), 3.50 (dd, J = 14.4, 17.4 Hz, 4H). LC−MS (ESI): *m/z* 393.2 $(M + H)^+$.

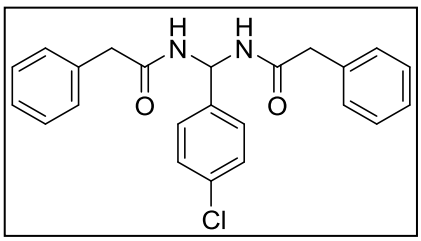

***N,N′*-(*p*-tolylmethylene)bis(2-phenylacetamide) (4.8)**. Compound **4.8** was prepared from 2-phenylacetamide and 4-methylbenzaldehyde using method 1. White solid (260 mg, yield: 70%). ^{1}H NMR (400 MHz, DMSO-d_6) δ 8.71 (d, J = 8.0 Hz, 2H), 7.13−7.32 (m, 14H), 6.52 (t, J = 8.0 Hz, 1H), 3.51 (dd, J = 14.4, 15.6 Hz, 4H), 2.29 (s, 3H). LC−MS (ESI): *m/z* 373.1 $(M+H)^+$.

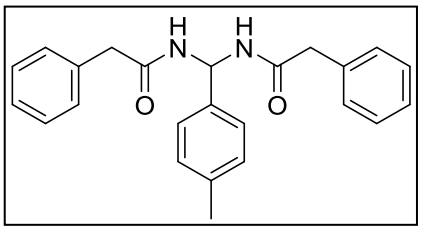

***N,N′*-((4-methoxyphenyl)methylene)bis(2-phenylacetamide) (4.10)**. Compound **4.10** was prepared from 2-phenylacetamide and 4-methoxybenzaldehyde using method 1. White solid (240 mg, yield: 62%). ^{1}H NMR (400 MHz, DMSO-d_6) δ 8.70 (d, J = 7.6 Hz, 2H), 7.21−7.31 (m, 12H), 6.89 (d, J = 8.8 Hz, 2H), 6.51 (t, J = 8.0 Hz, 1H), 3.74 (s, 3H), 3.50 (dd, J = 14.0, 17.2 Hz, 4H). LC−MS (ESI): *m/z* 389.1 $(M+H)^+$.

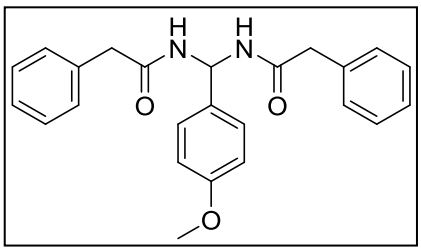

***N,N′*-((2-(trifluoromethyl)phenyl)methylene)bis(2-phenylacetamide) (4.13)**. Compound **4.13** was prepared from 2-phenylacetamide and 2-(trifluoromethyl)benzaldehyde using method 1. White solid (299 mg, yield: 70%). ^{1}H NMR (400 MHz, DMSO-d_6) δ 8.87 (d, J = 7.2 Hz, 2H), 7.78 (d, J = 7.6 Hz, 1H), 7.68−7.73 (m, 2H), 7.54 (t, J = 7.6 Hz, 1H), 7.19−7.30 (m, 10H), 6.83 (t, J = 6.8 Hz, 1H), 3.46 (dd, J = 14.0, 17.6 Hz, 4H). LC−MS (ESI): *m/z* 427.0 $(M+H)^+$.

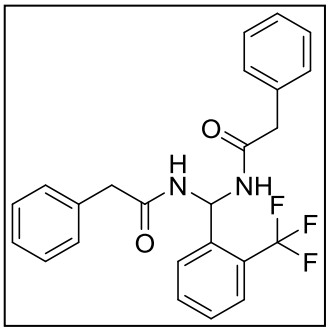

***N,N′*-((4-(trifluoromethyl)phenyl)methylene)bis(2-phenylacetamide) (4.14)**. Compound **4.14**

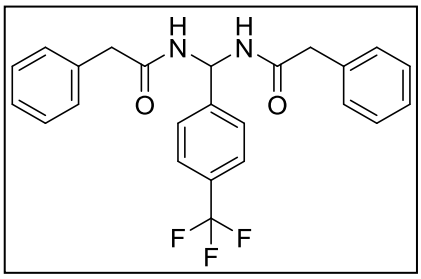

was prepared from 2-phenylacetamide and 4-(trifluoromethyl)benzaldehyde using method 1. White solid (320 mg, yield: 75%). ^{1}H NMR (400 MHz, DMSO-d_6) δ 8.89 (d, J = 7.6 Hz, 2H), 7.72 (d, J = 7.6 Hz, 2H), 7.51 (d, J = 7.6 Hz, 2H), 7.25−7.30 (m, 10H), 6.58 (t, J = 7.2 Hz, 1H), 3.53 (s, 4H). LC−MS (ESI): *m/z* 427.2 $(M + H)^+$.

***N,N′*-((4-nitrophenyl)methylene)bis(2-phenylacetamide) (4.15)**. Compound **4.15** was prepared

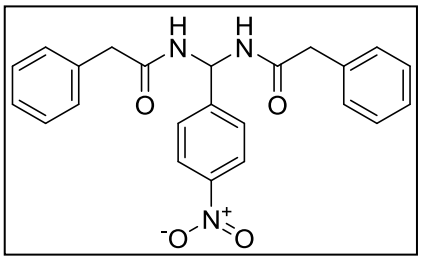

from 2-phenylacetamide and 4-nitrobenzaldehyde using method 1. White solid (339 mg, yield: 84%). ^{1}H NMR (400 MHz, DMSO-d_6) δ 8.98 (d, J = 7.6 Hz, 2H), 8.20−8.23 (m, 2H), 7.56 (d, J = 8.4 Hz, 2H), 7.23−7.32 (m, 10H), 6.58 (t, J = 7.6 Hz, 1H), 3.53 (s, 4H). LC−MS (ESI): *m/z* 404.1 $(M + H)^+$.

***N,N′*-((4-(dipropylamino)phenyl)methylene)bis(2-phenylacetamide) (4.18)**. Compound **4.18**

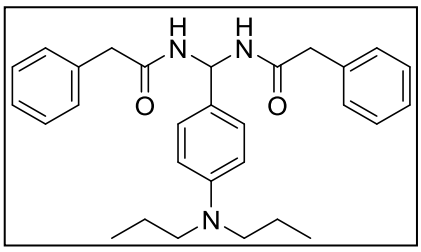

was prepared from 2-phenylacetamide and 4-(dipropylamino)benzaldehyde using method 1. White solid (70 mg, yield: 15%). ^{1}H NMR (400 MHz, CD_3OD) δ 7.25−7.30 (m, 10H), 7.10 (d, J = 8.8 Hz, 2H), 6.62 (d, J = 8.8 Hz, 2H), 6.57 (s, 1H), 3.56 (s, 4H), 3.24−3.26 (m, 4H), 1.54−1.64 (m, 4H), 0.93 (t, J = 7.6 Hz, 6H). LC−MS (ESI): *m/z* 458.2 $(M + H)^+$.

***N,N′*-((4-(pyrrolidin-1-yl)phenyl)methylene)bis(2-phenylacetamide) (4.21)**. Compound **4.21**

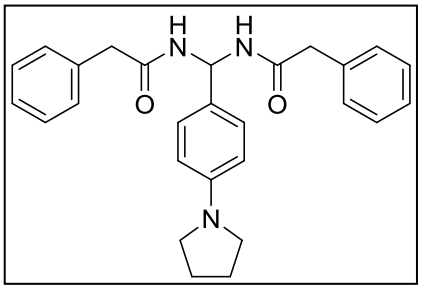

was prepared from 2-phenylacetamide and 4-(pyrrolidin-1-yl)benzaldehyde using method 1. White solid (52 mg, yield: 12%). ^{1}H NMR (400 MHz, DMSO-d_6) δ 8.58 (d, J = 8.0 Hz, 2H), 7.20−7.31 (m, 10H), 7.08 (d, J = 8.4 Hz, 2H), 6.42−6.49 (m, 3H), 3.44−3.45 (m, 4H), 3.18− 3.20 (m, 4H), 1.93−1.96 (m, 4H). LC−MS (ESI): *m/z* 428.2 (M +H)$^+$.

***N,N′*-(phenylmethylene)bis(2-(4-chlorophenyl)acetamide) (4.23).** Compound **4.23** was

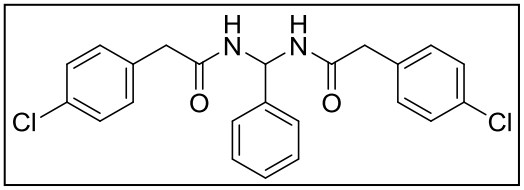

prepared from 2-(4-chlorophenyl)acetamide and benzaldehyde using method 1. White solid (222 mg, yield: 52%). ^{1}H NMR (400 MHz, DMSO-d_6) δ 8.88 (d, J = 7.8 Hz, 2H), 7.25−7.41 (m, 13H), 6.52 (t, J = 7.8 Hz, 1H), 3.50 (s, 4H). LC−MS (ESI): *m/z* 427.1 (M + H)$^+$.

***N,N′*-((2-fluorophenyl)methylene)bis(2-(4-chlorophenyl)-acetamide) (4.24).** Compound **4.24**

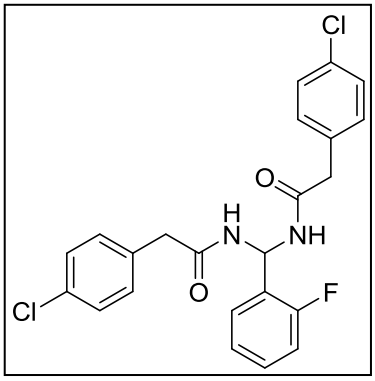

was prepared from 2-(4-chlorophenyl)acetamide and 2-fluorobenzaldehyde using method 1. White solid (280 mg, yield: 63%). ^{1}H NMR (400 MHz, DMSO-d_6) δ 8.93 (d, J = 7.2 Hz, 2H), 7.45 (t, J = 7.2 Hz, 1H), 7.33−7.37 (m, 5H), 7.25−7.26 (m, 4H), 7.18− 7.21 (m, 2H), 6.73 (t, J = 7.2 Hz, 1H), 3.48 (s, 4H). LC−MS (ESI): *m/z* 445.0 (M + H)$^+$.

***N,N′*-((4-fluorophenyl)methylene)bis(2-(4-chlorophenyl)-acetamide) (4.25)**. Compound **4.25**

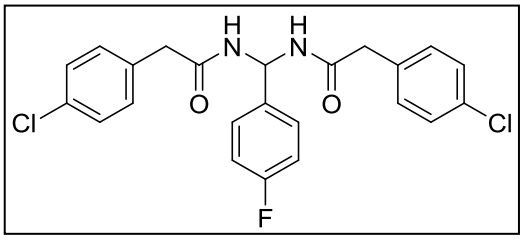

was prepared from 2-(4-chlorophenyl)acetamide and 4-fluorobenzaldehyde using method 1. White solid (300 mg, yield: 67%). ^{1}H NMR (400 MHz, DMSO-*d6*) δ 8.82 (d, J = 7.6 Hz, 2H), 7.34−7.37 (m, 6H), 7.27 (d, J = 8.4 Hz, 4H), 7.19 (t, J = 8.8 Hz, 2H), 6.51 (t, J = 8.0 Hz, 1H), 3.51 (s, 4H). LC−MS (ESI): *m/z* 444.9 $(M+H)^+$.

***N,N′*-((4-chlorophenyl)methylene)bis(2-(4-chlorophenyl)-acetamide) (4.26)**. Compound **4.26**

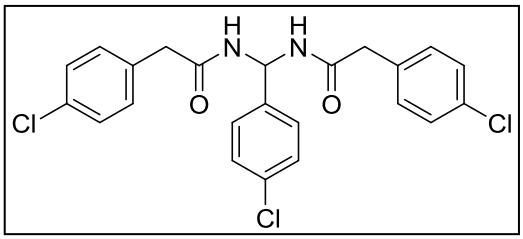

was prepared from 2-(4chlorophenyl)acetamide and 4-chlorobenzaldehyde using method 1. White solid (323 mg, yield: 70%). ^{1}H NMR (400 MHz, DMSO-d_6) δ 8.88 (d, J = 7.8 Hz, 2H), 7.42 (d, J = 8.4 Hz, 2H), 7.31−7.35 (m, 6H), 7.26 (d, J = 8.4 Hz, 4H), 6.47 (t, J = 7.8 Hz, 1H), 3.50 (s, 4H). LC−MS (ESI): *m/z* 460.8 $(M+H)^+$.

***N,N′*-(*p*-tolylmethylene)bis(2-(4-chlorophenyl)acetamide) (4.27)**. Compound **4.27** was

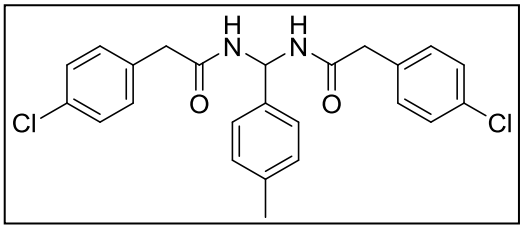

prepared from 2-(4-chlorophenyl)acetamide and 4-methylbenzaldehyde using method 1. White solid (388 mg, yield: 88%). ^{1}H NMR (400 MHz, DMSO-d_6) δ 8.76 (d, J = 8.0 Hz, 2H), 7.34 (d, J = 8.4 Hz, 4H), 7.28 (d, J = 8.4 Hz, 4H), 7.17 (q, J = 8.0 Hz, 4H), 6.50 (t, J = 7.6 Hz, 1H), 3.51 (s, 4H), 2.29 (s, 3H). LC−MS (ESI): *m/z* 441.3 $(M+H)^+$.

***N,N′*-((4-methoxyphenyl)methylene)bis(2-(4-chlorophenyl)-acetamide) (4.28)**. Compound

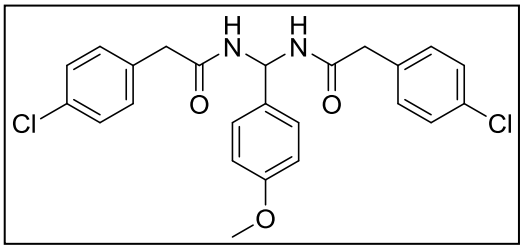

4.28 was prepared from 2-(4-chlorophenyl)acetamide and 4-methoxybenzaldehyde using method 1. White solid (416 mg, yield: 91%). ^{1}H NMR (400 MHz,

DMSO-d_6) δ 8.73 (d, J = 7.6 Hz, 2H), 7.34 (d, J = 8.8 Hz, 4H), 7.26 (d, J = 8.4 Hz, 4H), 7.21 (d, J = 8.8 Hz,2H), 6.90 (d, J = 8.8 Hz, 2H), 6.46 (t, J = 8.0 Hz, 1H), 3.74 (s, 3H), 3.49 (s, 4H). LC−MS (ESI): *m/z* 457.2 (M + H)+.

***N,N′*-((2-(trifluoromethyl)phenyl)methylene)bis(2-(4-chlorophenyl)acetamide) (4.29).**

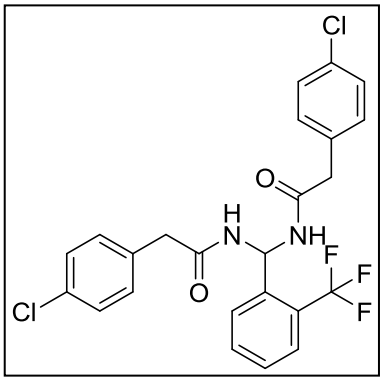

Compound **4.29** was prepared from 2-(4-chlorophenyl)acetamide and 2-(trifluoromethyl)benzaldehyde using method 1. White solid (406 mg, yield: 82%). ^{1}H NMR (400 MHz, DMSO-d_6) δ 8.04 (d, J = 6.0 Hz, 2H), 7.81 (d, J = 7.8 Hz, 1H), 7.72 (d, J = 7.8 Hz, 1H), 7.62 (t, J = 7.8 Hz, 1H), 7.52 (t, J = 7.8 Hz, 1H), 7.27−7.30 (m, 8H), 7.06 (t, J = 7.2 Hz, 1H), 3.52 (s, 4H). LC−MS (ESI): *m/z* 495.0 $(M + H)^+$.

***N,N′*-((4-(trifluoromethyl)phenyl)methylene)bis(2-(4-chlorophenyl)acetamide) (4.30).**

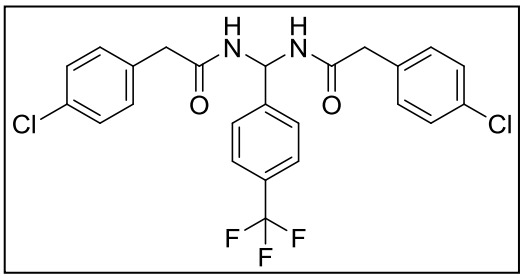

Compound **4.30** was prepared from 2-(4-chlorophenyl)acetamide and 4-(trifluoromethyl)benzaldehyde using method 1. White solid (421 mg, yield: 85%). ^{1}H NMR(400 MHz, DMSO-d_6) δ 8.96 (d, J = 7.6 Hz, 2H), 7.73 (d, J = 8.4 Hz, 2H), 7.54 (d, J = 8.4 Hz, 2H), 7.35 (d, J = 8.4 Hz, 4H), 7.28 (d, J = 8.4 Hz, 4H), 6.57 (t, J = 7.6 Hz, 1H), 3.54 (s, 4H). LC−MS (ESI): *m/z* 495.2 $(M + H)^+$.

***N,N′*-((4-nitrophenyl)methylene)bis(2-(4-chlorophenyl)-acetamide) (4.31)**. Compound **4.31** was prepared from 2-(4-chlorophenyl)acetamide and 4-nitrobenzaldehyde using method 1. Off-white solid (425 mg, yield: 90%). ^{1}H NMR (400 MHz, DMSO-d_6) δ 9.02 (d, J = 8.0 Hz, 2H), 8.24−8.25 (m, 2H),

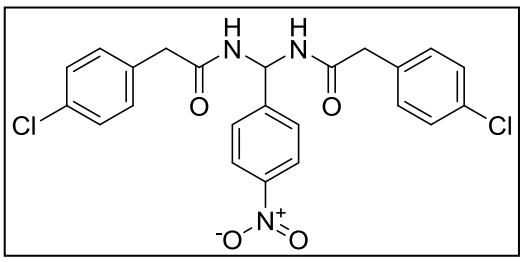

7.56−7.58 (m, 2H), 7.34−7.37 (m, 4H), 7.26−7.29 (m, 4H), 6.55 (t, *J* = 8.0 Hz, 1H), 3.53 (s, 4H). LC−MS (ESI): *m/z* 472.0 $(M + H)^+$.

***N,N′*-(phenylmethylene)bis(2-(4-(trifluoromethyl)phenyl)- acetamide) (4.32).** Compound **4.32**

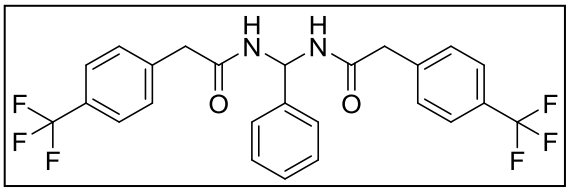

was prepared from 2-(4-(trifluoromethyl)phenyl)acetamide and benzaldehyde using method 1. White solid (410 mg, yield: 83%). ^{1}H NMR (400 MHz, DMSO-d_6) δ 8.94 (d, *J* = 7.8 Hz, 2H), 7.63 (d, *J* = 7.8 Hz, 4H), 7.48 (d, *J* = 8.4 Hz, 4H), 7.29−7.37 (m, 5H), 6.55 (t, *J* = 7.8 Hz, 1H), 3.63 (s, 4H). LC−MS (ESI): *m/z* 495.1 $(M + H)^+$.

***N,N′*-((2-fluorophenyl)methylene)bis(2-(4-(trifluoromethyl)-phenyl)acetamide) (4.33)**.

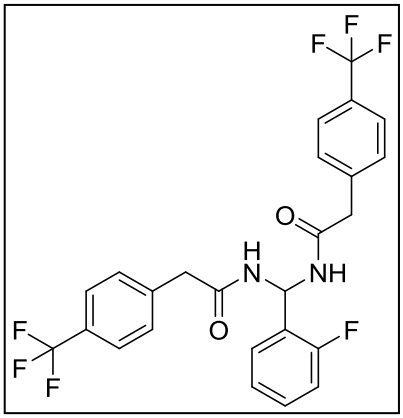

Compound **4.33** was prepared from 2-(4-(trifluoromethyl)phenyl)acetamide and 2-fluorobenzaldehyde using method 1. White solid (440 mg, yield: 86%). ^{1}H NMR (400 MHz, DMSO-d_6) δ 8.99 (d, *J* = 7.2 Hz, 2H), 7.63 (d, *J* = 7.8 Hz, 4H), 7.46 (d, *J* = 7.8 Hz, 5H), 7.36−7.40 (m, 1H), 7.21 (t, *J* = 7.8 Hz, 2H), 6.74 (t, *J* = 7.8 Hz, 1H), 3.60 (s, 4H). LC−MS (ESI): *m/z* 513.0 $(M + H)^+$.

***N,N′*-((4-fluorophenyl)methylene)bis(2-(4-(trifluoromethyl)-phenyl)acetamide) (4.34).**

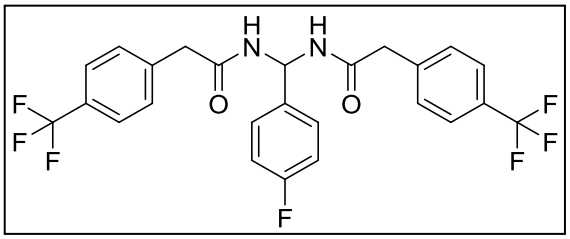

Compound **4.34** was prepared from 2-(4-(trifluoromethyl)phenyl)acetamide and 4-fluorobenzaldehyde using method 1. White solid (460mg, yield: 90%). ^{1}H NMR (400 MHz, DMSO-d_6) δ 8.95 (d, *J* = 8.4 Hz, 2H), 7.63 (d, *J* = 8.4 Hz, 4H), 7.47 d, *J* = 8.4 Hz, 4H), 7.37 (dd, *J* = 5.4,

8.4 Hz, 2H), 7.19 (t, *J* = 8.4 Hz, 2H), 6.51 (t, *J* = 7.8 Hz, 1H), 3.62 (s, 4H). LC−MS (ESI): *m/z* 513.2 $(M + H)^+$.

***N,N′*-((4-chlorophenyl)methylene)bis(2-(4-(trifluoromethyl)-phenyl)acetamide) (4.35).**

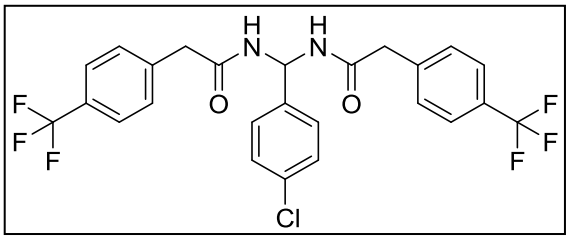

Compound **4.35** was prepared from 2-(4-(trifluoromethyl)phenyl)acetamide and 4-chlorobenzaldehyde using method 1. White solid (450 mg, yield: 85%). ^{1}H NMR(400 MHz, DMSO-d_6) δ 8.96 (d, *J* = 7.8 Hz, 2H), 7.63 (d, *J* = 7.2 Hz, 4H), 7.46 (d, *J* = 7.8 Hz, 4H), 7.43 (dd, *J* = 1.8, 8.4 Hz, 2H), 7.34−7.35 (m, 2H), 6.50 (t, *J* = 7.2 Hz, 1H), 3.62 (s, 4H). LC−MS (ESI): *m/z* 529.0 $(M + H)^+$.

***N,N′*-(*p*-tolylmethylene)bis(2-(4-(trifluoromethyl)phenyl)-acetamide) (4.36).** Compound **4.36**

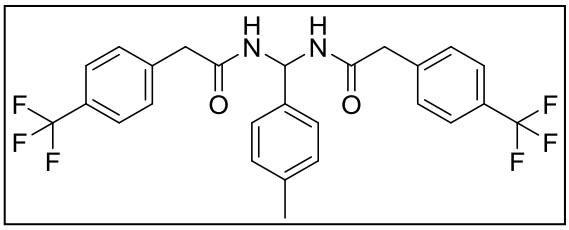

was prepared from 2-(4-(trifluoromethyl)phenyl)acetamide and 4-methylbenzaldehyde using method 1. White solid (412 mg, yield: 81%). ^{1}HNMR(400 MHz, DMSO-d_6) δ 8.87 (d, *J* = 8.4 Hz, 2H), 7.63 (d, *J* = 7.8 Hz, 4H), 7.47 (d, *J* = 8.4 Hz, 4H), 7.20 (d, *J* = 8.4 Hz, 2H), 7.15 (d, *J* = 7.8 Hz, 2H), 6.49 (t, *J* = 7.8 Hz, 1H), 3.61 (s, 4H), 2.28 (s, 3H). LC−MS (ESI): *m/z* 509.1 $(M + H)^+$.

***N,N′*-((4-methoxyphenyl)methylene)bis(2-(4-(trifluoromethyl)-phenyl)acetamide) (4.37).**

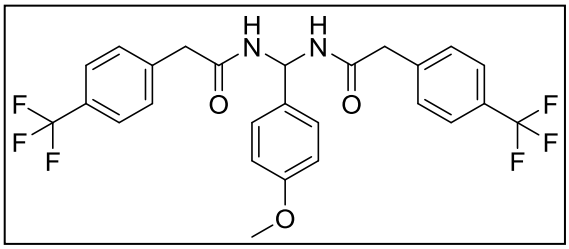

Compound **4.37** was prepared from 2-(4-(trifluoromethyl)phenyl)acetamide and 4-methoxybenzaldehyde using method 1. White solid (450 mg, yield: 86%). ^{1}H NMR(400 MHz, DMSO-d_6) δ 8.85 (d, *J* = 7.8 Hz, 2H), 7.63 (d, *J* = 7.8 Hz, 4H), 7.47 (d, *J* = 7.8 Hz, 4H),7.24 (d, *J* = 9.0

Hz, 2H), 6.91 (d, *J* = 8.4 Hz, 2H), 6.48 (t, *J* = 7.8 Hz, 1H), 3.74 (s, 3H), 3.61(s, 4H). LC−MS (ESI): *m/z* 525.1 $(M + H)^+$.

***N,N′*-((4-(trifluoromethyl)phenyl)methylene)bis(2-(4-(trifluoromethyl)phenyl)acetamide)**

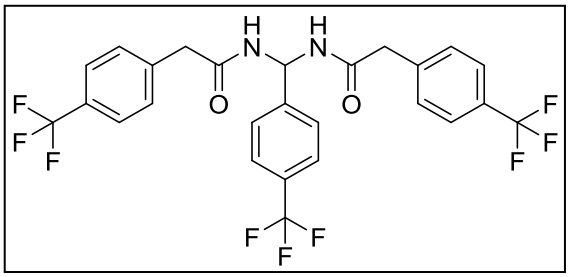

(4.38). Compound **4.38** was prepared from 2-(4-(trifluoromethyl)phenyl)acetamide and 4-(trifluoromethyl)-benzaldehyde using method 1. White solid (415 mg, yield: 74%). ^{1}H NMR (400 MHz, DMSO-d_6) δ 9.08 (d, *J* = 7.2 Hz, 2H), 7.73 (d, *J* = 7.8 Hz, 2H), 7.63 (d, *J* = 7.8 Hz, 4H), 7.56 (d, *J* = 7.8 Hz, 2H), 7.48 (d, *J* = 7.8 Hz, 4H), 6.60 (t, *J* = 7.8 Hz, 1H), 3.35−3.43 (m, 4H). LC−MS (ESI): *m/z* 562.9 $(M + H)^+$.

***N,N′*-((4-(diethylamino)phenyl)methylene)dibenzamide (4.39)**. Compound **4.39** was prepared

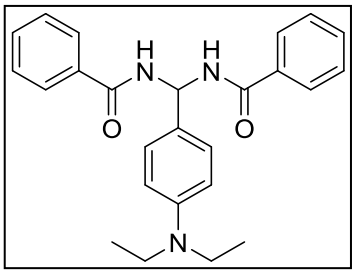

from benzamide and 4-(diethylamino)-benzaldehyde using method 1. White solid (293 mg, yield: 73%). ^{1}H NMR (400 MHz, CD_3OD) δ 9.24 (d, *J* = 7.6 Hz, 1H), 7.88−7.93 (m, 4H), 7.81 (d, *J* = 8.8 Hz, 2H), 7.46−7.65 (m, 9H), 7.20 (m, 1H), 3.70−3.81 (m, 4H), 1.17 (t, *J* = 7.2 Hz, 6H). LC−MS (ESI): *m/z* 402.2 $(M + H)^+$.

***N,N′*-((4-(diethylamino)phenyl)methylene)bis(3-phenylpropanamide) (4.40).** Compound **4.40**

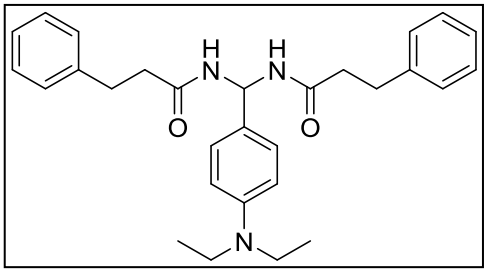

was prepared from 3-phenylpropanamide and 4-(diethylamino)benzaldehyde using method 1. White solid (302 mg, yield: 66%). ^{1}H NMR (400 MHz, CD_3OD) δ 8.29−8.30 (m, 2H), 7.17−7.29 (m, 10H), 6.92 (d, *J* = 8.4 Hz, 2H), 6.56 (d, *J* = 8.4 Hz, 2H), 6.46 (t, *J* = 8.0 Hz, 1H), 2.82 (t, *J* = 7.6 Hz, 4H), 2.42−2.47 (m, 4H), 1.07 (t, *J* = 6.8 Hz, 6H). LC−MS (ESI): *m/z* 458.2 $(M + H)^+$.

***N,N′*-((4-(diethylamino)phenyl)methylene)bis(3-phenylacrylamide) (4.41).** Compound **4.41**

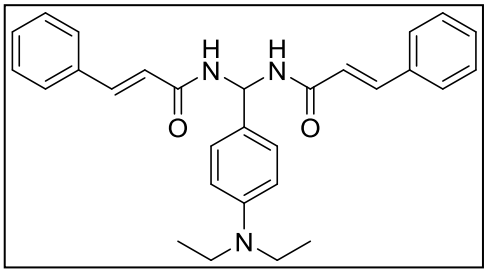

was prepared from cinnamamide and 4-(diethylamino)benzaldehyde using method 1. Off-white solid (309 mg, yield: 68%). ^{1}H NMR (400 MHz, CD_3OD) δ 8.68−8.70 (m, 2H), 7.38−7.58 (m, 12H), 7.19 (d, J = 8.8 Hz, 2H), 6.79 (d, J = 16.0 Hz, 2H), 6.66−6.68 (m, 3H), 3.29−3.35 (m, 4H), 1.08 (t, J = 7.2 Hz, 6H). LC−MS (ESI): *m/z* 454.2 $(M + H)^+$.

***N,N′*-((4-(diethylamino)phenyl)methylene)bis(2-methylpropanamide) (4.44).** Compound **4.44**

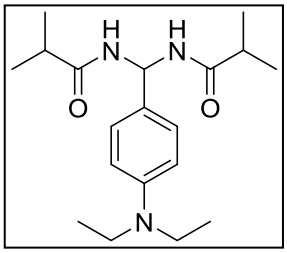

was prepared from isobutyramide and 4-(diethylamino)benzaldehyde using method 1. White solid (267 mg, yield: 80%). ^{1}H NMR (400 MHz, CD_3OD) δ 7.18 (d, J = 8.4 Hz, 2H), 6.70−6.73 (m, 2H), 6.56 (s, 1H), 3.35−3.50 (m, 2H), 2.47−2.54 (m, 4H), 1.13−1.16 (m, 12H). LC−MS (ESI): *m/z* 334.2 $(M + H)^+$.

***N,N′*-((4-(diethylamino)phenyl)methylene)bis(2,2-dimethylpropanamide) (4.45).** Compound

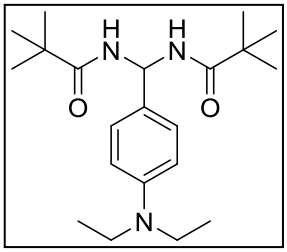

4.45 was prepared from pivalamide and 4-(diethylamino)benzaldehyde using method 1. White solid (278 mg, yield: 77%). ^{1}H NMR (400 MHz, DMSO-d_6) δ 7.70 (d, J = 8.8 Hz, 2H), 7.03 (d, J = 8.8 Hz, 2H), 6.62 (d, J = 8.8 Hz, 2H), 6.52 (t, J = 8.4 Hz, 1H), 3.30−3.33 (m, 4H), 1.12 (s, 18H), 1.05−1.08 (m, 6H). LC−MS (ESI): *m/z* 362.2 $(M + H)^+$.

***N,N′*-((4-(diethylamino)phenyl)methylene)dipentanamide (4.46).** Compound **4.46** was prepared from pentanamide and 4-(diethylamino)-benzaldehyde using method 1. White solid (250 mg, yield: 69%). ^{1}H NMR (400 MHz, CD_3OD) δ 7.18 (d, J = 8.8 Hz, 2H), 6.71 (d, J = 8.8 Hz, 2H), 6.58 (t, J = 8.4 Hz, 1H), 3.33−3.41 (m, 4H), 2.25 (t, J = 7.2 Hz, 4H), 1.58−1.66 (m, 4H), 1.33−1.43 (m, 4H), 1.14 (t, J = 7.2 Hz, 6H), 0.95 (t, J = 2.8 Hz, 6H). LC−MS (ESI): *m/z* 362.2 $(M + H)^+$.

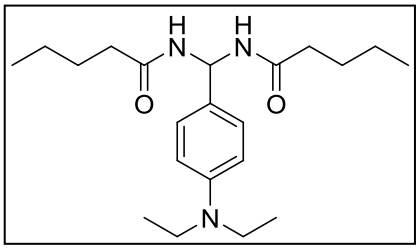

***N,N′*-((4-(diethylamino)phenyl)methylene)dihexanamide (4.47).** Compound **4.47** was prepared from hexanamide and 4-(diethylamino)-benzaldehyde using method 1. White solid (297 mg, yield: 76%). ^{1}H NMR (400 MHz, CD_3OD) δ 7.19 (d, J = 8.8 Hz, 2H), 6.71 (d, J = 8.8 Hz, 2H), 6.58 (t, J = 8.4 Hz, 1H), 3.35−3.41 (m, 4H), 2.19−2.26 (m, 4H), 1.61−1.68 (m, 4H), 1.32−1.35 (m, 8H), 1.14 (t, J = 6.8 Hz, 6H), 0.94 (t, J = 2.8 Hz, 6H). LC−MS (ESI): *m/z* 390.3 $(M + H)^+$.

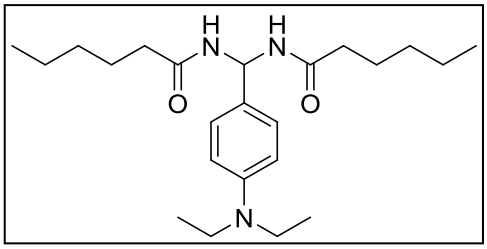

***N,N′*-((4-(diethylamino)phenyl)methylene)dioctanamide (4.48).** Compound **4.48** was prepared from octanamide and 4-(diethylamino)-benzaldehyde using method 1. White solid (308 mg, yield: 68%). ^{1}H NMR (400 MHz, DMSO-d_6) δ 8.21 (d, J = 8.0 Hz, 2H), 7.07 (d, J = 8.8 Hz, 2H), 6.61 (d, J = 8.8 Hz, 2H), 6.42 (t, J = 8.0 Hz, 1H), 3.29−3.31 (m, 4H), 2.06−2.14 (m, 4H), 1.47−1.50 (m, 4H), 1.08−1.24 (m, 16H), 1.06 (t, J = 7.2 Hz, 6H), 0.94 (t, J = 7.2 Hz, 6H). LC−MS (ESI): *m/z* 446.3 $(M + H)^+$.

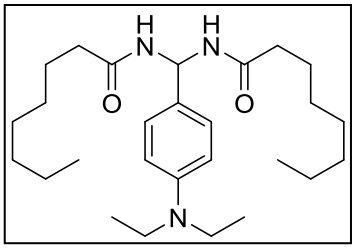

***N,N′*-((4-(diethylamino)phenyl)methylene)bis(decanamide) (4.49).** Compound **4.49** was

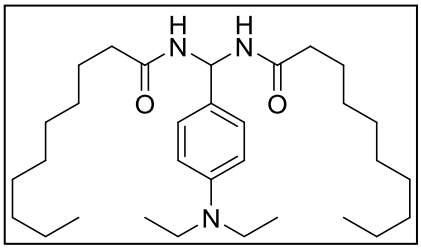

prepared from decanamide and 4-(diethylamino)-benzaldehyde using method 1. White solid (281 mg, yield: 56%). ^{1}H NMR (400 MHz, DMSO-d_6) δ 8.99 (d, J = 9.6 Hz, 1H), 8.38 (d, J = 8.8 Hz, 1H), 6.99 (d, J = 8.8 Hz, 2H), 6.58 (d, J = 8.4 Hz, 2H), 5.84 (d, J = 8.4 Hz, 1H), 3.27−3.30 (m, 4H), 2.33 (t, J = 7.2 Hz, 4H), 2.14 (t, J = 7.2 Hz, 4H), 1.50−1.55 (m, 4H), 1.24−1.28 (m, 24H), 1.06 (t, J = 7.2 Hz, 6H), 0.87 (t, J = 7.2 Hz, 6H). LC−MS (ESI): m/z 502.4 $(M + H)^+$.

General Method 2 [216]:

***N,N′*-((3-fluorophenyl)methylene)bis(2-phenylacetamide) (4.4).** To a suspension of 2-

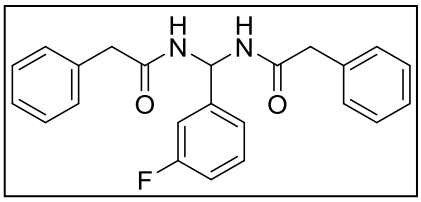

phenylacetamide (540 mg, 4 mmol) in dry dichloromethane (2 mL) was added 3-fluorobenzaldehyde (250 mg, 2 mmol) and trimethylsilyltrifluoromethane sulfonate (22 mg, 0.1 mmol). The mixture was vigorously stirred for 12 h at room temperature, diluted with toluene (4 mL), and filtered. The precipitate was washed several times with toluene which was recrystallized with methanol and hexane to give the final product as white solid (290 mg, yield: 77%). ^{1}H NMR (400 MHz, DMSO-d_6) δ 8.83 (d, J = 8.0 Hz, 2H), 7.06−7.42 (m, 14H), 6.53 (t, J = 7.6 Hz, 1H), 3.47−3.55 (m, 4H). LC−MS (ESI): m/z 377.2 $(M + H)^+$.

***N,N′*-((4-bromophenyl)methylene)bis(2-phenylacetamide) (4.7).** Compound **4.7** was prepared

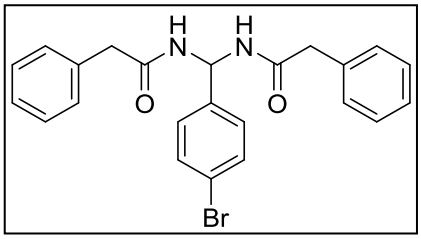

from 2-phenylacetamide and 4-bromobenzaldehyde using method 2. White solid (390 mg, yield: 89%). ^{1}H NMR (400 MHz, DMSO-d_6) δ 8.82 (d, J = 7.6 Hz, 2H), 7.53−7.56 (m, 2H),

7.21−7.33 (m, 12H), 6.48 (t, *J* = 7.6 Hz, 1H), 3.46−3.54 (m, 4H). LC−MS (ESI): *m/z* 437.0 $(M + H)^+$.

***N,N′*-((4-isopropylphenyl)methylene)bis(2-phenylacetamide) (4.9).** Compound **4.9** was

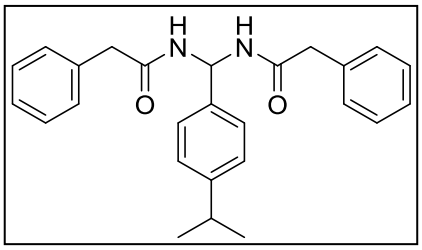

prepared from 2-phenylacetamide and 4-isopropylbenzaldehyde using method 2. Off-white solid (260 mg, yield: 65%). ^{1}H NMR (400 MHz, DMSO-d_6) δ 8.73 (d, *J* = 8.0 Hz, 2H), 7.20−7.32 (m, 14H), 6.51 (t, *J* = 8.0 Hz, 1H), 3.46−3.54 (m, 4H), 2.85−2.89 (m, 1H), 1.19 (d, *J* = 6.8 Hz, 6H). LC−MS (ESI): *m/z* 401.2 $(M + H)^+$.

***N,N′*-((4-ethoxyphenyl)methylene)bis(2-phenylacetamide) (4.11).** Compound **4.11** was

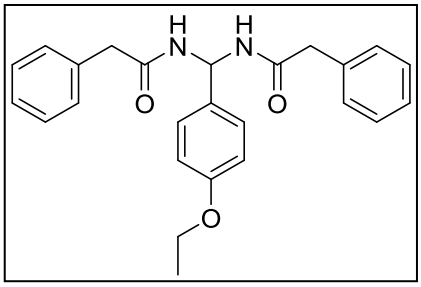

prepared from 2-phenylacetamide and 4-ethoxybenzaldehyde using method 2. White solid (280 mg, yield: 70%). ^{1}H NMR (400 MHz, DMSO-d_6) δ 8.69 (d, *J* = 8.0 Hz, 2H), 7.18−7.31 (m, 10H), 6.88 (d, *J* = 6.4 Hz, 2H), 6.48 (t, *J* = 8.0 Hz, 1H), 3.98−4.03 (m, 2H), 3.45− 3.52 (m, 4H), 1.31 (t, *J* = 6.8 Hz, 3H). LC−MS (ESI): *m/z* 403.1 $(M + H)^+$.

***N,N′*-((4-isopropoxyphenyl)methylene)bis(2-phenylacetamide) (4.12).** Compound **4.12** was

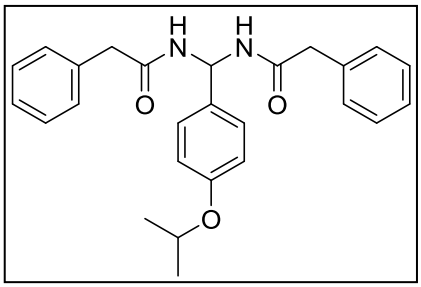

prepared from 2-phenylacetamide and 4-isopropoxybenzaldehyde using method 2. White solid (335 mg, yield: 81%). ^{1}H NMR (400 MHz, DMSO-d_6) δ 8.69 (d, *J* = 7.6 Hz, 2H), 7.18−7.13 (m, 12H), 6.87 (d, *J* = 6.8 Hz, 2H), 6.48 (t, *J* = 8.0 Hz, 1H), 4.58−4.61 (m, 1H), 3.45− 3.53 (m, 4H), 1.25 (d, *J* = 6.0 Hz, 6H). LC−MS (ESI): *m/z* 417.2 $(M + H)^+$.

***N,N′*-((4-(diethylamino)phenyl)methylene)bis(2-phenylacetamide) (4.17).** Compound **4.17**

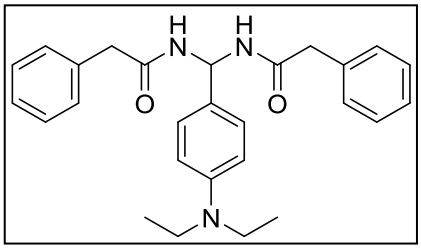

was prepared from 2-phenylacetamide and 4-(diethylamino)benzaldehyde using method 2. White solid (335 mg, yield: 78%). ^{1}H NMR (400 MHz, DMSO-d_6) δ 8.60 (d, J = 8.0 Hz, 2H), 7.21−7.31 (m, 10H), 7.07 (d, J = 8.4 Hz, 2H), 6.60 (d, J = 8.8 Hz, 2H), 6.43 (t, J = 8.0 Hz, 1H), 3,44−3.52 (m, 4H), 3.29−3.34 (m, 4H), 1.06 (t, J = 7.6 Hz, 6H). LC−MS (ESI): *m/z* 430.3 $(M + H)^+$.

***N,N′*-((4-(dibutylamino)phenyl)methylene)bis(2-phenylacetamide) (4.19).** Compound **4.19**

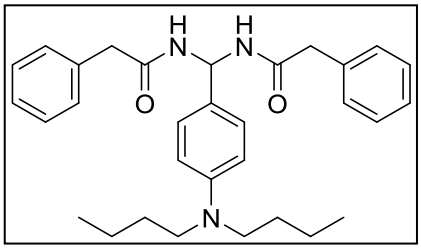

was prepared from 2-phenylacetamide and 4-(dibutylamino)benzaldehyde using method 2. Yellow solid (410 mg, yield: 85%). ^{1}H NMR (400 MHz, DMSO-d_6) δ 8.58 (d, J = 8.0 Hz, 2H), 7.20−7.31 (m, 10H), 7.06 (d, J = 8.8 Hz, 2H), 6.57 (d, J = 8.8 Hz, 2H), 6.41 (t, J = 8.0 Hz, 1H), 3.47−3.48 (m, 4H), 3.22−3.26 (m, 4H), 1.43−1.50 (m, 4H), 1.26−1.35 (m, 4H), 0.91 (t, J = 7.6 Hz, 6H). LC−MS (ESI): *m/z* 486.2 $(M + H)^+$.

***N,N′*-((4-(piperidin-1-yl)phenyl)methylene)bis(2-phenylacetamide) (4.22).** Compound **4.22**

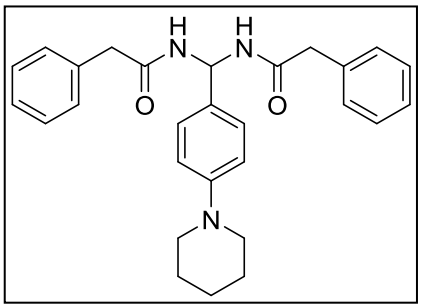

was prepared from 2-phenylacetamide and 4- (piperidin-1-yl)benzaldehyde using method 2. Red solid (375 mg, yield: 85%). ^{1}H NMR (400 MHz, DMSO-d_6) δ 8.80 (d, J = 8.0 Hz, 2H), 7.15−7.32 (m, 14H), 6.51 (t, J = 8.0 Hz, 1H), 3.37−3.52 (m, 8H), 1.61−1.83 (m, 6H). LC− MS (ESI): *m/z* 442.3 $(M + H)^+$.

***N,N′*-(pentane-1,1-diyl)bis(2-phenylacetamide) (4.42).** Compound **4.42** was prepared from 2-

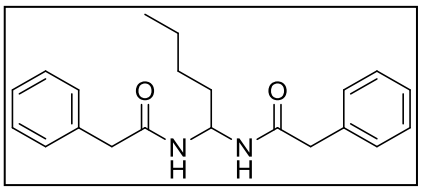

phenylacetamide and pentanal using method 2. White solid (280 mg, yield: 83%). ^{1}H NMR (400 MHz, DMSO-d_6) δ 8.25 (d, J = 8.0 Hz, 2H), 7.19−7.30 (m, 8H), 5.30 (t, J = 7.6 Hz, 1H), 3.36−3.44 (m, 4H), 1.56−1.62 (m, 2H), 1.14−1.26 (m, 4H), 0.81 (t, J = 7.2 Hz, 3H). LC−MS (ESI): m/z 339.1 $(M + H)^+$.

***N,N′*-(hexane-1,1-diyl)bis(2-phenylacetamide) (4.43).** Compound **4.43** was prepared from 2-

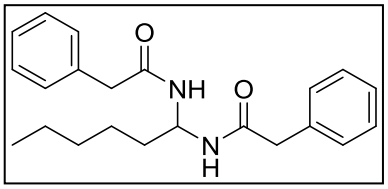

phenylacetamide and hexanal using method 2. White solid (327 mg, yield: 93%). ^{1}H NMR (400 MHz, DMSO-*d6*) δ 8.25 (d, J = 8.0 Hz, 2H), 7.19−7.30 (m, 8H), 5.29 (t, J = 7.6 Hz, 1H), 3.39−3.44 (m, 4H), 1.57−1.59 (m, 2H), 1.18−1.23 (m, 6H), 0.82 (t, J = 6.8 Hz, 3H). LC− MS (ESI): m/z 353.3 $(M + H)^+$.

4.4.2.3 General Method of Reduction

***N,N′*-((4-aminophenyl)-methylene)bis(2-phenylacetamide) (4.16)**. To a suspension of *N,N′*-

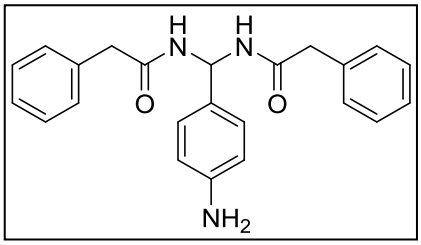

((4-nitrophenyl)methylene)bis(2-phenylacetamide) **(4.15)** (403 mg, 1 mmol) in ethanol (2 mL) was added the palladium (10%, 3.0 mg) and hydrazine (0.05 mL, 1.5 mmol). The mixture was stirred for 3 h at 70 °C. After filtration, the filtrate was evaporated to dryness on a rotary evaporator. The crude compound was further purified by recrystallization from ethanol. After the sample was dried in a vacuum at room temperature, **4.16** was obtained as a yellow solid (370 mg, yield: 99%). ^{1}H NMR (400 MHz, DMSO-d_6) δ 8.54 (d, J = 8.0 Hz, 2H), 7.20−7.31 (m, 10H), 6.92 (d, J = 8.4 Hz, 2H), 6.49 (d, J = 8.4 Hz, 2H), 6.39 (t, J = 8.0 Hz, 1H), 5.04 (bs, 2H), 3.43−3.53 (m, 4H). LC−MS (ESI): m/z 374.1 $(M + H)^+$.

4.4.2.4 General Method of Alkylation

***N,N′*-((4-(dibenzylamino)-phenyl)methylene)bis(2-phenylacetamide) (4.20).** Compound **4.16**

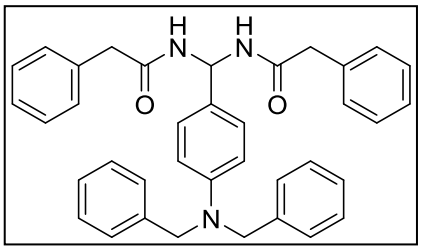

(373 mg, 1 mmol), K_2CO_3 (0.27 g, 1.95 mmol), and DMF (10 mL) were placed in a flask equipped with a condenser and a magnetic stirrer. Benzyl bromide (376 mg, 2.2 mmol) was added, and the mixture was stirred at room temperature for 12 h. The reaction solution was poured into water and extracted with EA. The combined organic layers were washed with water and brine and then dried over Na_2SO_4. The mixture was filtered, and the solvent was evaporated in vacuum. The residue was purified by flash chromatography on silica gel to obtain **4.20** as an off-white solid (282 mg, yield: 51%). ^{1}H NMR (400 MHz, DMSO-d_6) δ 8.50 (s, 2H), 7.18−7.35 (m, 20H), 7.01 (d, J = 8.8 Hz, 2H), 6.62 (d, J = 8.8 Hz, 2H), 6.39 (t, J = 8.0 Hz, 1H), 4.70 (s, 4H), 3.44−3.45 (m, 4H). LC−MS (ESI): *m/z* 554.2$(M + H)^+$.

5.0 DESIGN, SYNTHESIS, AND BIOLOGICAL EVALUATION OF SUBSTITUTED 2-(SULFONYLAMINO)-2-PHENYLACETAMIDE DERIVATIVES

5.1 INTRODUCTION

Although the di-amide scaffold yielded novel, highly potent, and selective CB2 chemotype ligands, the scaffold suffered some limitations that require chemical modifications. As highlighted in Chapter 4, compound **4.17** showed several pharmacokinetic limitations including low elimination half-life after oral administration. This limitation is mainly due to the di-amide backbone. The di-amide backbone had to be modified in order to overcome these issues. Scaffold hopping was carried out based on molecular docking interactions and structural features. As highlighted in Figure 5.1, the di-amide backbone was replaced with an amide and sulfonamide backbone with three varying positions (R1, R2, and R3). Based on the previous pharmacophore model in Chapter 4, three hydrophobic groups were utilized on the R groups with different substitutions, length and size as well as charge. Hydrogen bond acceptors and donors were preserved in the new scaffold (two hydrogen bond donors and three hydrogen bond acceptors). We hypothesized that these modifications will yield ligands with good CB2 affinity and selectivity as well as overcoming PK limitations associated with the di-amide scaffold derivatives.

The new scaffold, 2-(sulfonylamino)-2-phenylacetamide, holds three R positions, R1: connect with different substituted phenyl amines, R2: connect with different substituted sulfonamides and R3: connect with either aliphatic or aromatic groups (Figure 5.1).

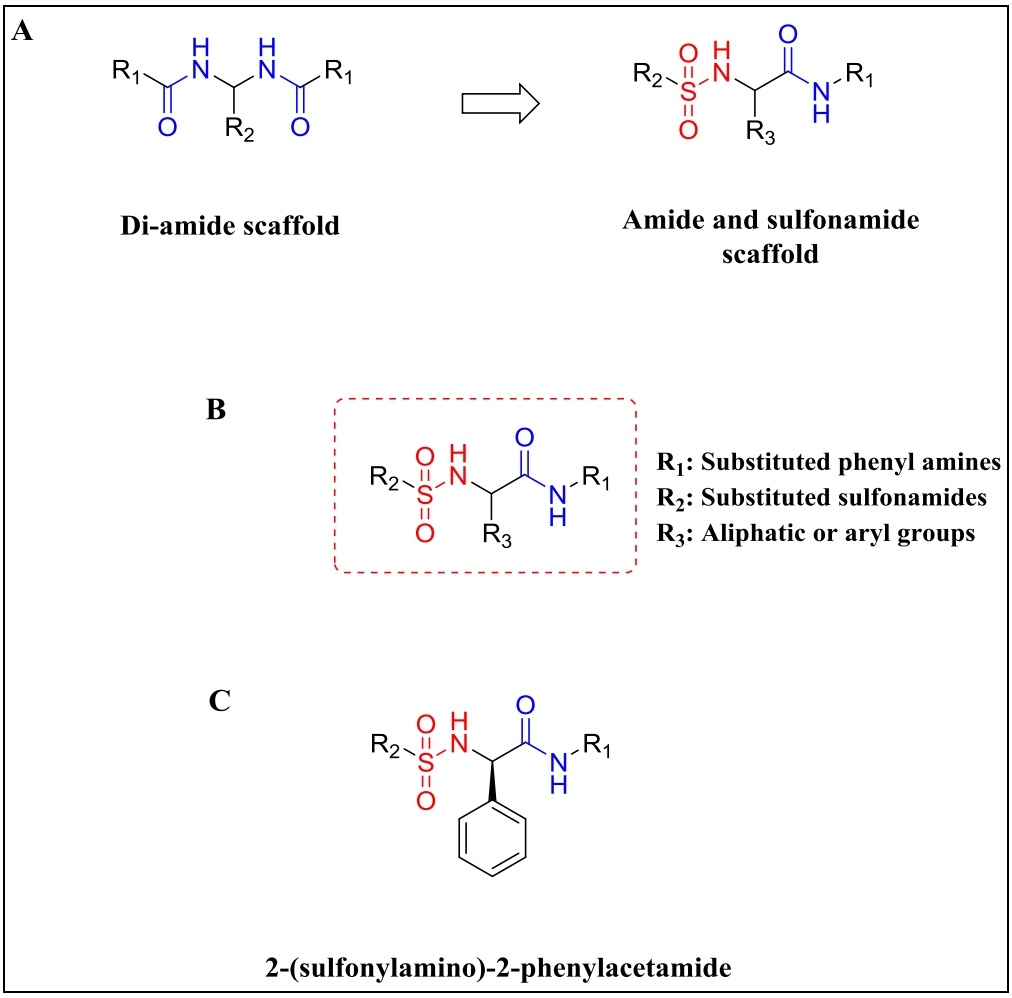

Figure 5.1. 2-(sulfonylamino)-2-phenylacetamide scaffold hopping and chemistry optimization strategy

The di-amide scaffold was subjected to scaffold hopping and modification based on molecular docking and chemical features studies. **(A)** di-amide scaffold and the amide-sulfonamide scaffold. **(B)** The chemistry optimizations strategies. **(C)** The final structure of the 2-(sulfonylamino)-2-phenylacetamide scaffold

5.2 RESULTS AND DISCUSSION

5.2.1 Chemistry Synthesis

The chemistry synthesis routes of 2-(sulfonylamino)-2-phenylacetamide derivatives are illustrated in Scheme 2. The commercially available methyl (*R*)-2-amino-2-phenylacetate was reacted with different substituted sulfonyl chloride to give the intermediate methyl (*R*)-2-(sulfonamido)-2-phenylacetate (intermediate-1). When methyl (*R*)-2-amino-2-phenylacetate was reacted with 4-methoxybenzenesulfonyl chloride**,** 4-isopropoxybenzenesulfonyl chloride**,** benzenesulfonyl chloride**,** [1,1'-biphenyl]-4-sulfonyl chloride**,** naphthalene-2-sulfonyl chloride**,** and pentane-1-sulfonyl chloride, compounds **5.1 – 5.6** were obtained, respectively. Intermediate-1 was then treated with different reaction conditions to yield the final products. Intermediate-1 was reacted with different substituted amines to yield compounds **5.8**, **5.9**, **5.11**, and **5.25** (method 1). When intermediate-1 was reacted with substituted amines in the presence of toluene, the corresponding compounds were obtained **5.10**, **5.12 – 5.14**, **5.16**, **5.23**, **5.26**, and **5.27** (Method 2). In another method, intermediate-1 was subjected to ester hydrolysis in order to obtain the corresponding carboxylic acid. This was achieved by treating intermediate-1 with lithium hydroxide to yield intermediate-2 (compounds **5.7**, and **5.32**). Intermediate-2 was subjected to acylation in order to achieve acyl chlorides. Acylation was achieved by treating intermediate-2 with thionyl chloride. Acyl chloride derivatives were then reacted with substituted amines to yield compounds **5.15**, **5.24**, and **5.29** (method 3). In method 4, intermediate-2 was subjected to amine coupling utilizing coupling reagents (HOBt/EDCI) to yield the target compounds **5.18 – 5.22**, **5.28**, **5.30**, and **5.31**. All final products were purified by flash chromatography or preparative TLC where indicated and confirmed with NMR and LC-MS.

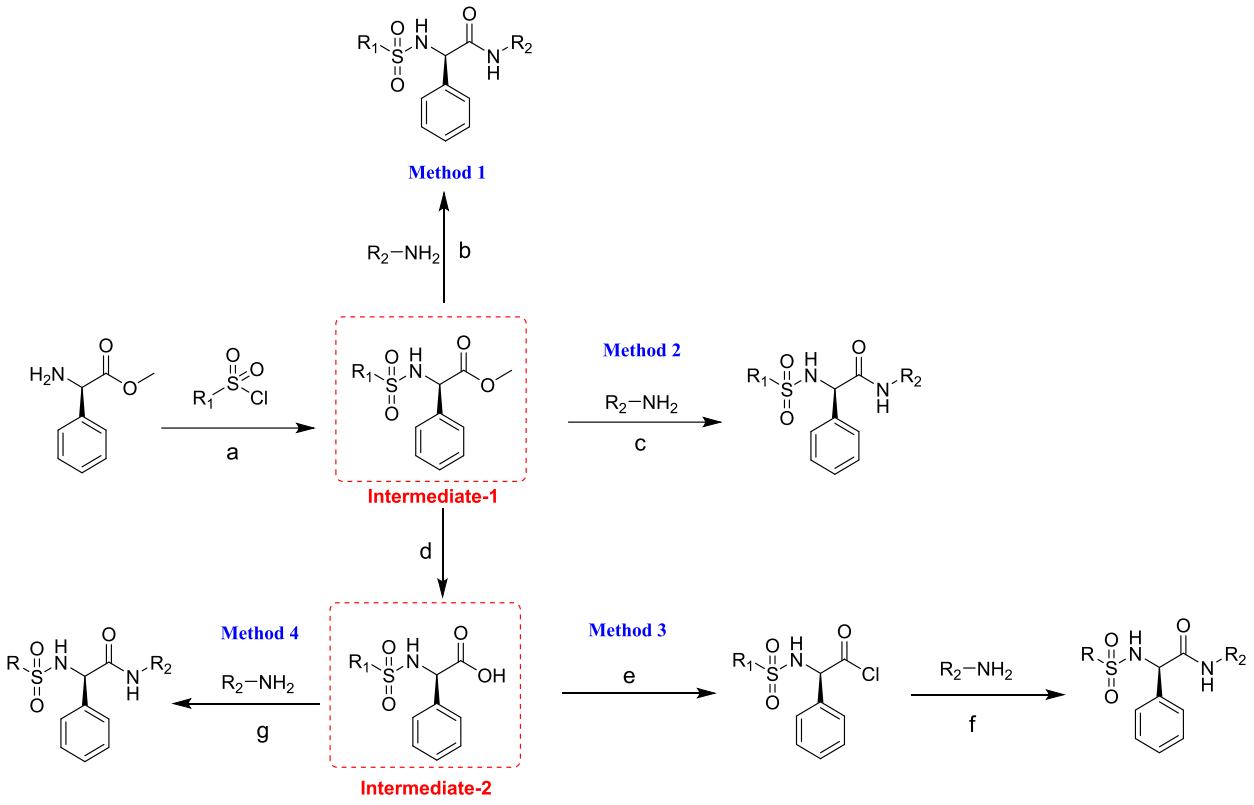

Scheme 2. Synthesis routes of 2-(sulfonylamino)-2-phenylacetamide derivatives.

Reagents and conditions: (a) substituted sulfonyl chloride (R_1), TEA, DCM, rt, 12 hr. (b) substituted amine (R_2), MeOH, 70 °C, 12 h. (c) substituted amine (R_2), toluene, 125 °C, 12 h. (d) LiOH, THF:H_2O, 4 °C, 12 h. (e) Thionyl chloride, EA, 80 °C, 2 h. (f) substituted amine (R_2), TEA, EA, rt, 12 h. (g) substituted amine (R_2), HOBt/EDCI, rt, TEA, THF, 12 h.

5.2.2 Structure Activity Relationship Analysis

Radioligand-competition binding experiments were carried out as described in Chapter 3 (materials and method) utilizing membrane protein preparations stably expressing human CB2 and CB1 receptors. CB2 selective ligand SR144528 was used as positive control in binding experiments. Similarly, the CB1 selective ligand SR141728 was utilized as a positive control in binding experiments. Different sulfonyl amide intermediates were explored for the CB2 receptor binding affinity. Compounds with different substituted sulfonyl amide groups yielded varying CB2 receptor affinity. Compound **5.1** with *p*-methoxyphenyl group displayed a CB2 K_i of 1050 nM. Compound **5.2** with isopropoxybenzene showed a CB2 K_i of 7640 nM. Compound **5.3** with a phenyl group showed no CB2 affinity (CB2 K_i > 20000 nM). Compound **5.4** bearing a bi-phenyl group showed a CB2 K_i = 2650 nM. Compound **5.5** with a naphthalene group displayed a CB2 K_i of 1080 nM. Finally, compound **5.6** with an aliphatic chain (pentane) showed no CB2 receptor binding affinity (CB2 K_i > 20000 nM). The highly-to-moderately potent intermediates were chosen for further SAR studies. CB2 binding affinities of the phenylacetamide intermediates are shown in Table **5.1**. Intermediates **5.1** and **5.5** were chosen for further SAR studies (CB2 K_i < 1100 nM). Other intermediates (**5.2** – **5.4**, and **5.6**) were ignored due to their low CB2 receptor binding affinity (CB2 K_i > 2000 nM).

Table 5.1. Chemical structures, physicochemical properties and radioligand competition binding affinity for 2-(sulfonylamino)-2-phenylacetamide scaffold intermediates

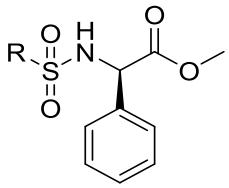

Entry	R	MW	cLogP	K_i (CB2), µM
5.1	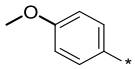	335.37	2.71	1.05
5.2	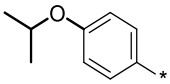	363.43	3.55	7.64
5.3		305.35	2.44	NB
5.4	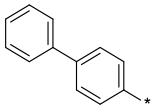	381.44	4.32	2.65
5.5	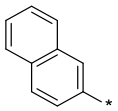	355.41	3.61	1.08
5.6	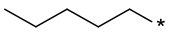	299.39	2.94	NB

Binding affinity for CB2 receptor were evaluated using [^{3}H]CP-55,940 radioligand competition binding assay. NB: no binding, K_i > 20000 nM. CB2 reference compound SR144528.

The first SAR study was carried out on the intermediate bearing *p*-methoxyphenyl fragment connected to the sulfone group. This intermediate showed moderate CB2 binding affinity (compound **5.1**, CB2 K_i = 1.05 μM, Table 5.1). By keeping the *p*-methoxyphenyl connecting to the sulfone group we introduced several fragments connected to the amide groups varying in size, property, and charge and synthesized 18 derivatives (Table 5.2).

Compared to compound **5.1**, converting the methoxy group adjacent to the amide group to hydroxide by ester hydrolysis resulted in complete loss of the CB2 receptor binding affinity (compound **5.7**). By the aim of having three phenyl (hydrophobic) rings, we introduced several substituted phenyls to compound **5.1**. Un-substituted phenyl ring showed loss of the CB2 binding affinity (compound **5.15**, CB2 K_i = 13700 nM). Increasing the distance between the phenyl ring and the amide group showed minimal effects of the CB2 binding affinity (compound **5.9**, CB2 K_i = 15000 nM) compared to **5.15**. We then tested different substitutions on the phenyl ring varying in size and position. Introducing *p*-Cl on the phenyl ring showed weak CB2 binding affinity (compound **5.11**, CB2 K_i = 9500 nM). However, introducing 1,2-dichlorophenyl showed improved CB2 binding affinity compared to *p*-Cl (compound **5.12**, CB2 K_i = 3490 nM). Further, introducing *p*-diethylamine on the phenyl ring showed improved CB2 receptor binding affinity and selectivity (CB2 K_i = 586 nM, CB1 K_i > 20000 nM, SI, 34). Reducing the size of the diethylamine with dimethylamine showed weak CB2 binding affinity (compound **5.23**, K_i = 4260 nM). This shows that the diethylamine moiety is important in CB2 binding affinity. Replacing the diethylamine with a hydroxyl group abolished the CB2 binding affinity and selectivity (compound **5.22**, CB2 K_i = 6920 nM). Also, when the aromatic property was replaced with cyclohexylmethanamine or cycloheptylmethanamine, the CB2 binding affinity was reduced (compounds **5.10**, and **5.24**, CB2 K_i = 5200 nM, and 7020 nM, respectively).

Next we wanted to explore the effects of replacing the phenyl group connected with the amide with different heterocyclic groups. Introducing 2-methylthiophene (compound **5.18**), 2-methylfuran (compound **5.19**), and a morpholine group (compound **5.21**) abolished the CB2 receptor binding affinity (CB2 K_i > 14000 nM). In addition, we explored introducing bulky groups such as adamantine and bicyclo[2.2.1]heptane. Compound **5.17** bearing adamantine showed moderate CB2 binding affinity (compound **5.17**, CB2 K_i = 1860 nM, CB1 K_i = 8000 nM). However, compound **5.20** bearing the bicyclo[2.2.1]heptane group showed weaker binding affinity (CB2 K_i = 9400 nM).

By keeping two phenyl rings, we tested the effects introducing aliphatic chain instead of the phenyl group. Long aliphatic chain (C_7H_{15}) lost the CB2 binding affinity (compound **5.8**, CB2 K_i 15000 nM). However, shorter aliphatic chain (C_4H_9, compound **5.16**) showed improved CB2 binding affinity (CB2 K_i = 1500 nM) compared to compound **5.8**. Finally, reducing the fragment size connected to the amide group showed moderate CB2 as well as CB1 binding affinity (compound **5.14**, CB2 K_i = 2900 nM, CB1 K_i = 5600 nM).

Collectively, these data demonstrated that this intermediate, methyl (*R*)-2-((4-methoxyphenyl)sulfonamido)-2-phenylacetate, may not be a suitable scaffold for developing CB2 selective ligands and different intermediate scaffold should be explored.

Table 5.2. Intermediate I radioligand competition binding affinity and physicochemical properties

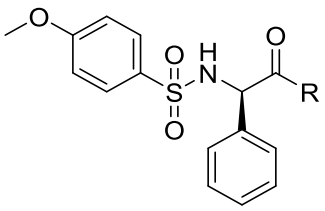

Entry	R	MW	cLogP	K_i (CB2), µM	K_i (CB1), µM
5.7	-OH	321.35	2.45	NB	NT
5.8	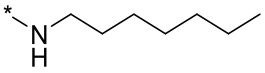	418.55	5.12	15	NT
5.9	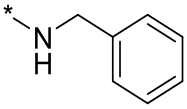	410.49	3.83	15	NT
5.10	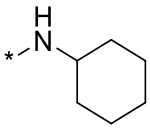	416.53	4.59	5.2	NT
5.11	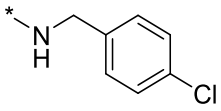	444.93	4.54	9.5	NT
5.12	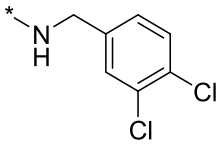	479.38	5.13	3.49	10.6
5.13	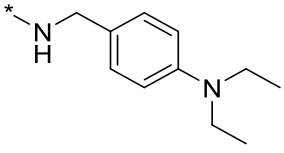	481.61	5.05	0.586	> 2000
5.14	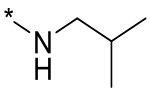	376.47	3.40	2.90	5.6
5.15	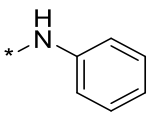	396.46	3.64	13.7	NT

5.16	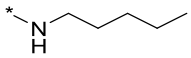	390.50	4.06	1.5	NT
5.17	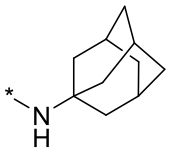	454.58	4.60	1.86	8
5.18	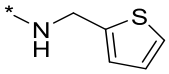	416.51	3.47	14.5	NT
5.19	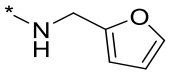	400.45	3.00	NB	NT
5.20	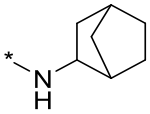	414.52	4.25	9.4	NT
5.21	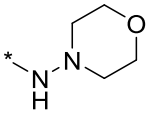	405.47	2.69	NB	NT
5.22	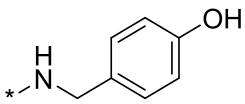	440.51	3.37	6.92	NT
5.23	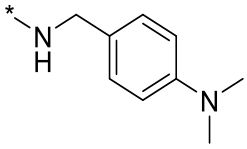	439.53	3.81	4.26	NT
5.24	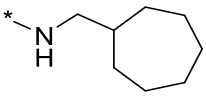	416.54	4.53	7.02	NT
SR144528				0.002	-
SR141716				-	0.0018

Binding affinities for CB1 and CB2 receptor were evaluated using [^{3}H]CP-55,940 radioligand competition binding assay utilizing SR141716 for CB1 and SR144528 for CB2 as reference compounds. NB: no binding, K_i > 20000 nM. NT: not tested.

Next, we replaced the *p*-methoxyphenyl with a naphthalene fragment as this intermediate showed relatively better CB2 binding affinity compared to other intermediates (compound **5.5**, CB2 K_i = 1080 nM, Table 5.1) and synthesized 8 derivatives (Table 5.3). Comparing compound **5.27** bearing 1,2-dichlorobenzene group with compound **5.12**, both compounds showed comparable CB2 binding affinity with a slight improvement in compound **5.27** (CB2 K_i = 2840 nM) but weaker when compared to compound **5.5**. Introducing an un-substituted phenyl ring showed weak CB2 binding affinity (compound **5.29**, CB2 K_i = 4960 nM) but better than compound **5.15** (CB2 K_i = 13700 nM). In addition, increasing the distance between the phenyl ring and the amide group showed no effect on the CB2 affinity (compound **5.25**, CB2 K_i = 4720 nM) but better than compound **5.9** (CB2 K_i = 15000 nM). Introducing adamantine group improved the CB2 binding affinity (CB2 K_i = 618 nM, CB1 K_i = 4640 nM, SI = 7.5). In addition, compound **5.28** bearing bicyclo[2.2.1]heptane group exhibited low CB2 binding affinity (CB2 K_i = 976 nM). Introducing 5-methy-1,2,3-trimethoxybenzene and methylcyclohexane showed weak-to-no binding (compounds **5.26**, and **5.30** with CB2 K_i of 7140 nM and 4880 nM, respectively). Introducing adamantine group showed weak CB2 binding (compound **5.31**, CB2 K_i = 6180 nM). As a result, we conclude that the scaffold 2-(sulfonylamino)-2-phenylacetamide is not optimal for the design and synthesis of selective CB2 ligands.

Table 5.3. Intermediate II radioligand competition binding affinity and physicochemical properties

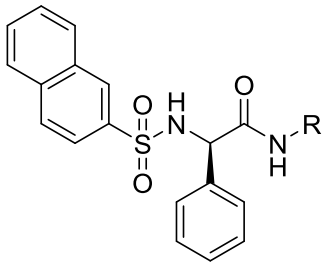

Entry	R	MW	cLogP	K_i (CB2), μM	K_i (CB1), μM
5.25	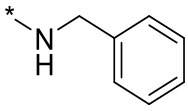	430.52	4.72	4.97	2.6
5.26	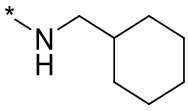	436.57	5.49	7.14	NT
5.27	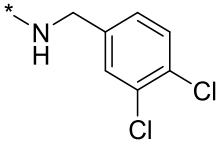	499.41	6.03	2.84	NT
5.28	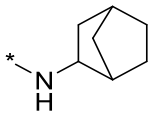	434.55	5.15	0.976	1.2
5.29	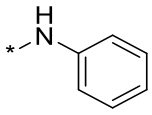	416.50	4.54	4.96	NT
5.30	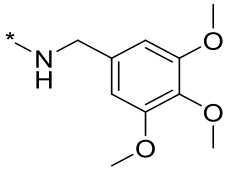	520.60	4.02	4.88	NT
5.31	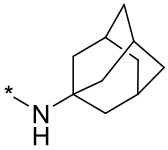	474.62	5.50	6.18	4.64
5.32	-OH	341.4	3.34	NB	NT

SR144528	0.002	-
SR141716	-	0.0018

Binding affinities for CB1 and CB2 receptor were evaluated using [^{3}H]CP-55,940 radioligand competition binding assay utilizing SR141716 for CB1 and SR144528 for CB2 as reference compounds. NB: no binding, K_i > 20000 nM. NT: not tested.

5.2.3 Multiple Myeloma Anti-Proliferation Studies

Despite the weak to moderate binding affinity and selectivity toward the CB2, we carried out anti-proliferation screening studies utilizing two MM cell-lines RPMI8226 and MM1.S. As detailed in the experimental section, Chapter 3.0 cell-lines were seeded at a density of 3×10^3 cells/well in a 96-well plate and treated with 5.0 μM of the tested derivatives for 3 days. MTT assay was carried out as previously described to measure the inhibition rates of the different derivatives in comparison to the control wells. As illustrated in Figure 5.2, two 2-(sulfonylamino)-2-phenylacetamide derivatives, compounds **5.12** and **5.31**, exhibited inhibition rates of 58% and 92% in the RPMI8226 cell-lines, respectively, as well as 42% and 68% in the MM1.S cell-line respectively. However, these two compounds exhibited distinct CB2 binding profile, thus suggesting that these two compounds may have different targets.

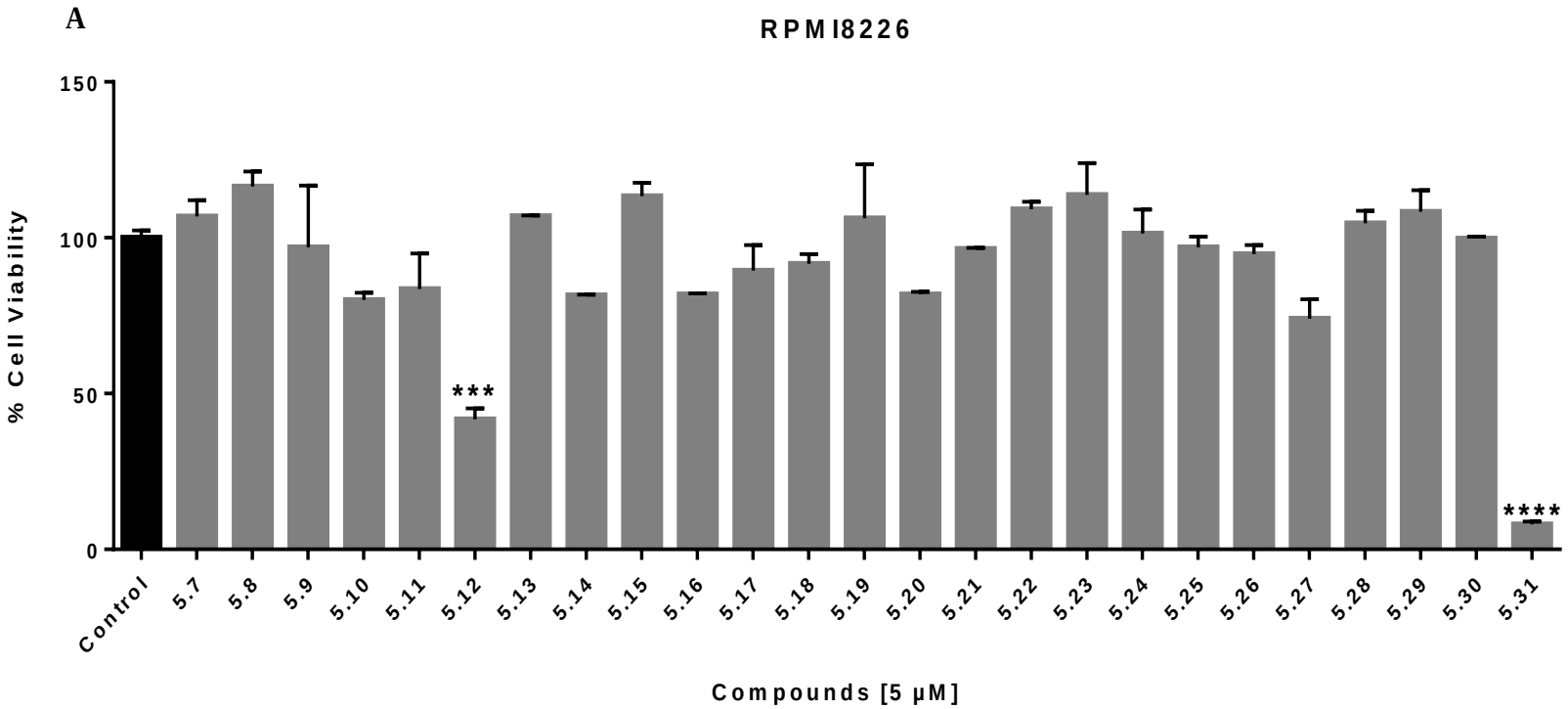
A
RPMI8226
% Cell Viability
150
100
50
0
***
****
Control
5.7
5.8
5.9
5.10
5.11
5.12
5.13
5.14
5.15
5.16
5.17
5.18
5.19
5.20
5.21
5.22
5.23
5.24
5.25
5.26
5.27
5.28
5.29
5.30
5.31
Compounds [5 μM]

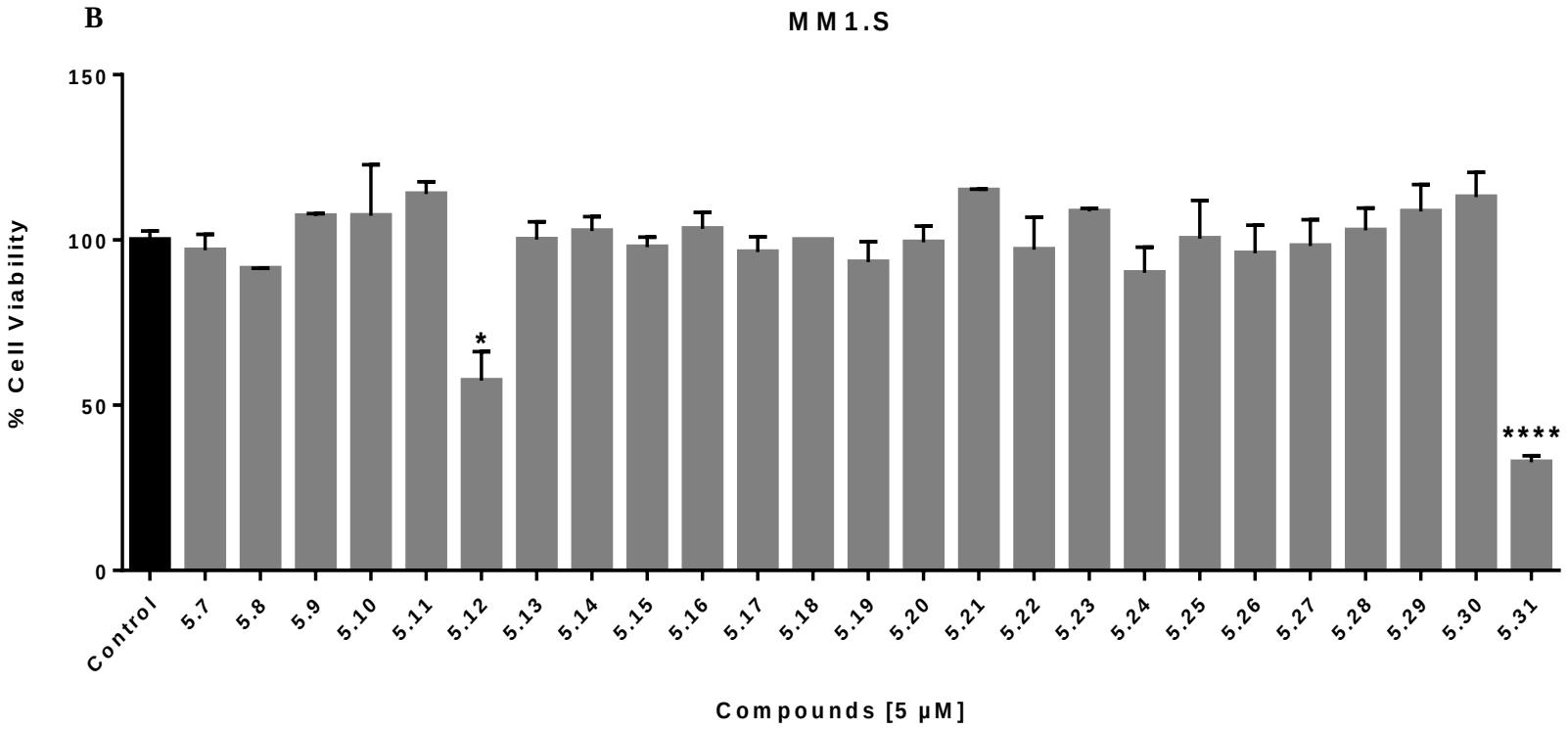

Figure 5.2. Cell viability screening of the 2-(sulfonylamino)-2-phenylacetamide derivatives on MM cell-lines

MM cell-lines, **(A)** RPMI8226, and **(B)** MM1.S were utilized to study the anti-proliferation effects of the synthesized derivatives. Cells were plated at density of 3×10^3/well in 96-well plates. Cells were incubated with 5 µM concentration of the tested derivatives for 3 days. The cell viability was determined by the MTT assay. Data are represented as the mean ± SD of three experiments carried out in triplicates. Statistical differences are as follows: *P<0.05, and ****P<0.0001 compared with control incubations which were defined as 100%.

5.2.4 Target Exploration for Compounds 5.12 and 5.31

The two compounds **5.12** and **5.31** exhibited potent anti-MM on two MM cell-lines with moderate CB2 receptor binding affinity. As a result, we attempted to explore the possible target of these two compounds by utilizing the High-Throughput Docking (HTD, https://www.cbligand.org/MM) tool developed in our lab [133]. The HTD tool is a webpage interface that allows the user to enter the chemical structure(s) and perform docking screenings on different known MM protein targets to identify possible targets for a chemical structure. A tabulated results including protein abbreviations (as identified in the Protein Data Bank, i.e., PDB name), full protein name, and the docking score as well as hyperlinks to the published co-crystal structures or published NMR protein structures.

We carried out HT-Docking on MM targets utilizing the two compounds. As shown in Figure 5.3, the two compounds exhibited high docking scores on three important MM protein targets, MAPK 14, CDK-2, and JAK-2. The docking scores were the highest with the two compounds targeting MAPK-14 (docking scores for **5.12** and **5.31** were 8.60 and 8.47, respectively).

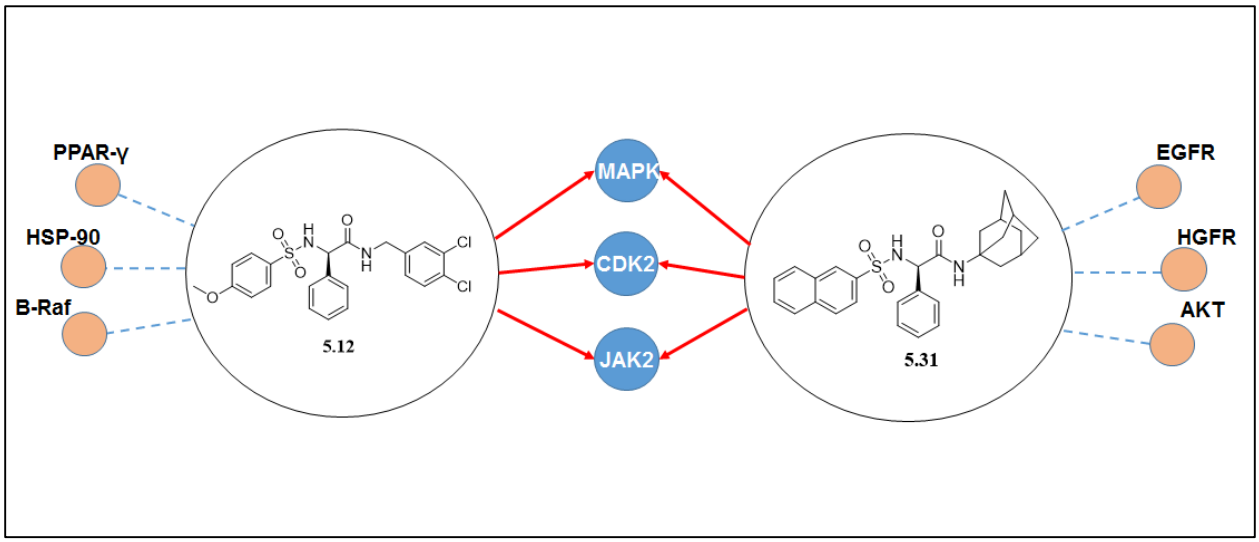

Figure 5.3. Illustration of the HT-Docking of compounds 5.12 and 5.31

High-throughput docking was carried out using our web-based HTD tool. MAPK: Mitogen-activated protein kinase-14, CDK2: cyclin-dependent kinase-2, JAK2: Tyrosine-protein kinase-2, PPAR-γ: Peroxisome proliferator-activated receptor gamma. HSP-90: Heat-shock protein-90, EGFR: Epidermal growth factor receptor, HGFR: Hepatocyte growth factor receptor, AKT: protein kinase B.

As the highest docking score was achieved with MAPK-14, we performed specific molecular docking studies utilizing MAPK-14 co-crystal structure (PDB: 3NEW) to analyze the detailed molecular interactions between compounds **5.12** and **5.31** with important amino acids in the binding pocket of MAPK-14. Comess and coworkers reported the X-ray crystal structure of MAPK in complex with their in-house ligand. They reported the following important amino acids in the binding pocket of MAPK-14: Pro191, Trp197, Leu246, Ile250, Ser252, and Leu291 (Figure 5.4).

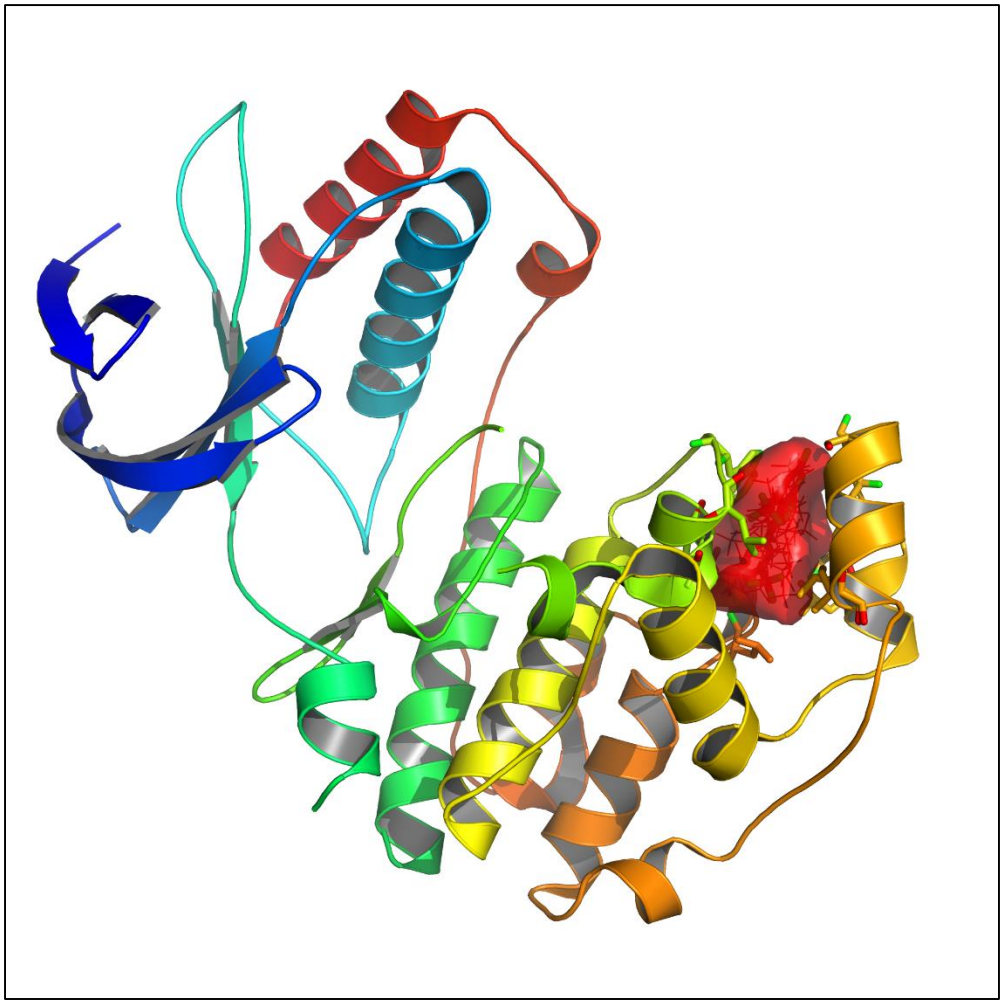

Figure 5.4. Co-crystal structure of MAPK-14 complex with MAPK-14 inhibitor

Reported important amino acids are Pro191, Trp197, Leu246, Ile250, Ser252, and Leu291. Protein structure was retrieved from the Protein Data Bank using PDB ID: 3NEW. Protein preparation and binding pocket illustration was carried out by the SYBYL X1.3 software and refined using PyMol.

Docking studies was carried out by the Surflex-Dock (SYBYL X1.3) software on the MAPK-14 co-crystal structure (PDB: 3NEW). Docking results of compounds **5.12** and **5.31** demonstrated an excellent fit of these two compounds in the binding pocket as well as interactions with surrounding amino acids. Furthermore, these two compounds superimposed perfectly over the reported MAPK-14 lignad reported in the co-crystal structure (Figure 5.5). This suggests that these two compounds are promising MAPK-14 modulators that may play essentials roles in the MAPK signaling cascades.

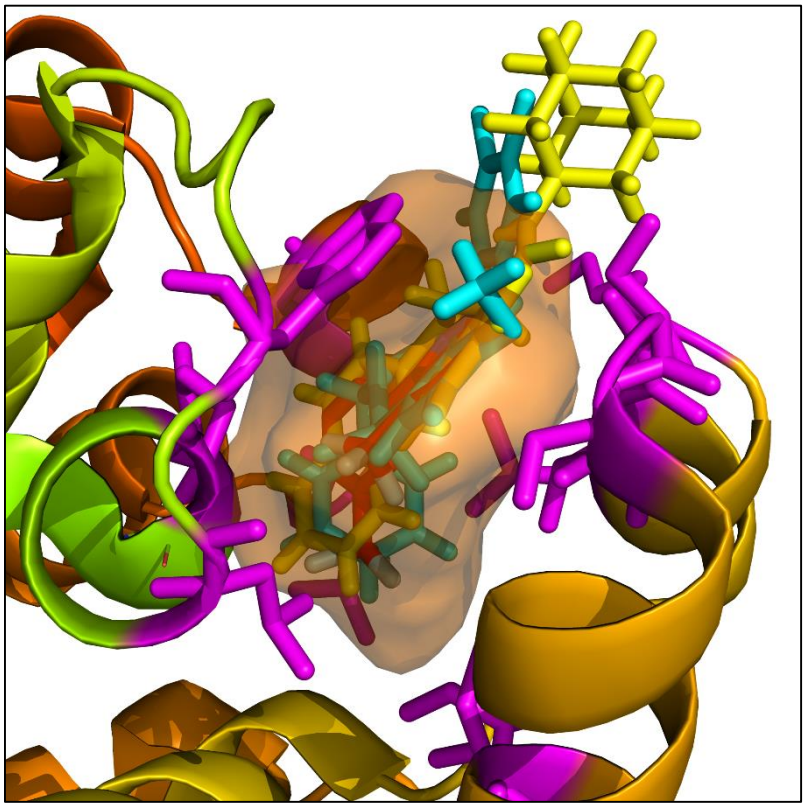

Figure 5.5. Binding pocket analysis

Compound **5.12** and **5.31** interaction with MAPK-14 defined binding pocket in complex with the reported inhibitor. Compound **5.12** is color coded in cyan, compound **5.31** is color coded in yellow and the reported inhibitor is color coded in red. Important amino acids are color coded in magenta.

5.3 CONCLUSION

Scaffold hopping was performed on the di-amide scaffold to overcome the limitations associated with it. As described earlier, the di-amide backbone rendered the synthesized ligands instability in acidic medium, which resulted in poor PK profile. A new scaffold, the 2-(sulfonylamino)-2-phenylacetamide, was introduced bearing an amide and a sulfonamide groups. SAR studies were carried out to explore the different fragments connected with the scaffold with the aim of achieving high affinity and selectivity for the CB2 receptor. A library of 32 derivatives were synthesized and analyzed for SAR based on CB2 binding profile. Nearly, all the derivatives exhibited moderate-to-weak CB2 receptor binding profile except for compound **5.13** with CB2 K_i = 586 nM.

The anti-proliferation on MM cell-lines were carried out in order to study the inhibition profile of the 2-(sulfonylamino)-2-phenylacetamide derivatives. MTT assay was carried out to perform high-throughput anti-proliferation studies utilizing compound concentrations at 5 µM on two MM cell-lines (RPMI8226 and MM1.S). Among the synthesized analogs, two compounds, **5.12** and **5.31**, exhibited strong inhibition rates on the MM cell-lines. However, as shown in their CB2 binding profile, these two compounds showed different binding profiles suggesting that the MM inhibition may arise from the two compounds targeting other MM proteins.

In order to explore different protein target that the two compounds are targeting, we carried out high-throughput docking studies utilizing our generated HTD-Anti-MM web-based tool. Interestingly, the results of the HTD of the two compounds were almost identical. Both compounds exhibited high docking scores on MAPK-14, JAK-2, and CDK-2, in which all are known MM proteins. As a result, we carried out extensive docking studies utilizing MAPK-14 co-crystal structure to identify the binding pocket and the possible binding pose of our two analogs. Interestingly, the two compounds exhibited similar binding pose as the reported MAPK-14 ligand

as well as several interactions of the analogs with important amino acids within the binding pocket. These data suggests that these two analogs target the MAPK-14 protein with high affinity and these two compounds may be further studies for *in-vitro* experiments to verify their ability as MAPK-14 modulators and ultimately anti-MM agents.

Collectively, to serve the purpose of designing and developing highly potent and selective CB2 ligands, this scaffold was terminated as a CB2 scaffold. As a result, we had to look further for the development of CB2 ligands with optimized therapeutic activities, drug-like properties, as well as improved PK profile. However, with the interesting HTD data, the two compounds **5.13** and **5.31** represent a novel chemical structure with potential anti-MM properties.

5.4 EXPERIMENTAL

5.4.1 Chemistry

General Synthesis of Sulfonamide Building Blocks [217]:

Methyl (*R*)-2-((4-methoxyphenyl)sulfonamido)-2-phenylacetate (5.1).

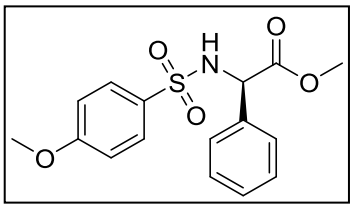

Methyl (*R*)-2-amino-2-phenylacetate (165 mg, 1.0 mmol) in dichloromethane (DCM, 10 mL) was chilled in ice bath with the exclusion of moisture, and then triethylamine (TEA, 121 mg, 1.2 mmol) was added to it. The resulting solution was treated drop wise under stirring with 4-methoxybenzenesulfonyl chloride (206 mg, 1.0 mmol), then left overnight at room temperature. The reaction solution was poured into water and extracted with EA. The combined organic layers were washed with water and brine and then dried over Na_2SO_4. The mixture was filtered and the solvent was evaporated in vacuum. The residue was purified by flash chromatography (ethyl acetate/ petroleum ether, 1:2) on silica gel to obtain methyl (*R*)-2-((4-methoxyphenyl)sulfonamido)-2-phenylacetate. White solid (250 mg, yield: 74%). ^{1}H NMR (400 MHz, DMSO-d_6) δ8.74 (d, J = 9.6 Hz, 1H), 7.68–7.64 (m, 2H), 7.29–7.27 (m, 5H), 7.03–7.00 (m, 2H), 4.98 (d, J = 9.20 Hz, 1H), 3.81 (s, 3H), 3.46 (s, 3H). LC-MS (ESI): *m/z* 335.9 $(M + H)^+$.

Methyl (*R*)-2-((4-isopropoxyphenyl)sulfonamido)-2-phenylacetate (5.2).

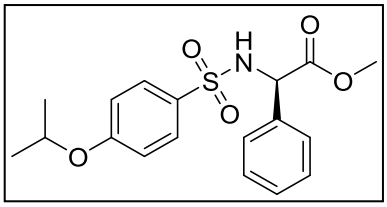

Off-white solid (60 mg, yield: 17%). ^{1}H NMR (400 MHz, DMSO-d_6) δ8.71 (s, 1H), 7.63–7.60 (m, 2H), 7.35 (s, 5H), 6.99–6.95 (m, 2H), 4.98 (d, J = 13.20 Hz, 1H), 4.73–4.67 (m, 1H), 3.61 (s, 3H), 1.31 (d, J = 6.0 Hz, 6H). LC-MS (ESI): *m/z* 364.1 $(M + H)^+$.

Methyl (*R*)-2-phenyl-2-(phenylsulfonamido)acetate (5.3).

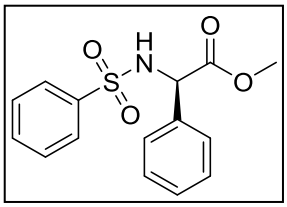

White solid (30 mg, yield: 10%). ^{1}H NMR (400 MHz, DMSO-d_6) δ8.92 (s, 1H), 7.74–7.72 (m, 2H), 7.58–7.48 (m, 3H), 7.28 (s, 5H), 5.04 (s, 1H), 3.45 (s, 3H). LC-MS (ESI): *m/z* 306.1 $(M + H)^+$.

Methyl (*R*)-2-([1,1'-biphenyl]-4-sulfonamido)-2-phenylacetate (5.4).

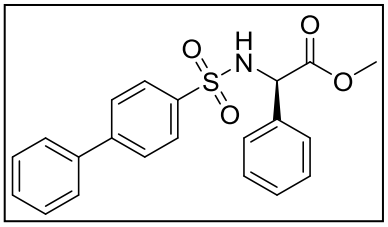

Yellow solid (150 mg, yield: 40%). ^{1}H NMR (400 MHz, DMSO-d_6) δ8.97 (s, 1H), 7.88 (s, 4H), 7.81–7.61 (m, 2H), 7.53–7.37 (m, 3H), 7.36–7.20 (m, 5H), 5.08 (d, *J* = 9.20 Hz, 1H), 3.47 (s, 3H). LC-MS (ESI): *m/z* 382.0 $(M + H)^+$.

Methyl (*R*)-2-(naphthalene-2-sulfonamido)-2-phenylacetate (5.5).

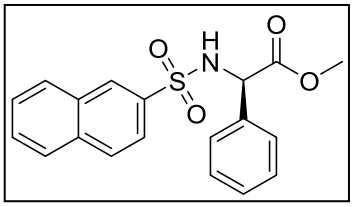

White solid (37 mg, yield: 11%). ^{1}H NMR (400 MHz, DMSO-d_6) δ8.36 (s, 1H), 8.10 (d, *J* = 7.60 Hz, 1H), 8.02 (t, *J* = 10.0 Hz, 2H), 7.76–7.75 (m, 1H), 7.72–7.64 (m, 2H), 7.29–7.19 (m, 5H), 5.23 (s, 1H), 3.25–3.17 (m, 3H). LC-MS (ESI): *m/z* 356.1 $(M + H)^+$.

Methyl (*R*)-2-(pentylsulfonamido)-2-phenylacetate (5.6).

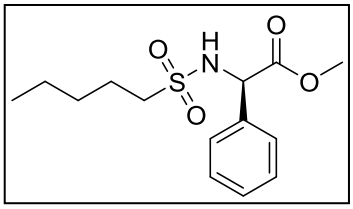

Yellow oil (10 mg, yield: 5%). ^{1}H NMR (400 MHz, DMSO-d_6) δ7.56-7.27(m, 6H), 4.74 (s, 1H), 3.66 (s, 3H), 3.48 (s, 3H), 3.38 (t. *J* = 7.0 Hz, 2H), 1.65-1.60 (m, 4H). LC-MS (ESI): *m/z* 300.1 $(M + H)^+$.

Ester hydrolysis:

(*R*)-2-((4-methoxyphenyl)sulfonamido)-2-phenylacetic acid (5.7) [218].

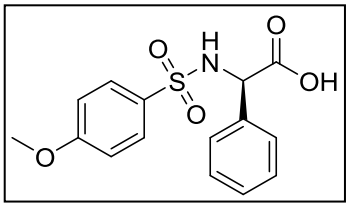

Methyl (*R*)-2-((4-methoxyphenyl)sulfonamido)-2-phenylacetate (**5.1**) (335 mg, 1 mmol) was dissolved in THF (10 mL), and a solution of $LiOH \cdot H_2O$ (3 mmol) in an equal volume of water was added. When hydrolysis was completed (24 h), the reaction solution was poured into water and extracted with EA. The combined organic layers were washed with water and brine and then dried over Na_2SO_4. The mixture was filtered and the solvent was evaporated in vacuum without further purification needed to obtain (*R*)-2-((4-methoxyphenyl)sulfonamido)-2-phenylacetic acid (**5.7**). Yellow solid (300 mg, yield: 94%). ^{1}H NMR (400 MHz, DMSO-d_6) δ12.92 (s, 1H), 8.52 (d, J = 8.8 Hz, 1H), 7.68–7.64 (m, 2H), 7.28–7.24 (m, 5H), 7.00–6.88 (m, 2H), 4.83 (d, J = 9.2 Hz, 1H), 3.80 (s, 3H). LC-MS (ESI): *m/z* 322.1 $(M + H)^+$.

(*R*)-2-(naphthalene-2-sulfonamido)-2-phenylacetic acid (5.32).

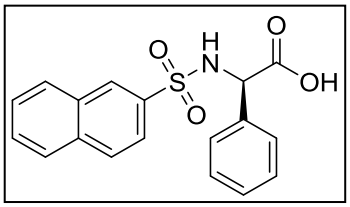

White solid (65 mg, yield: 19%). ^{1}H NMR (400 MHz, DMSO-d_6) δ12.90 (s, 1H), 8.35 (s, 1H), 8.09–7.99 (m, 3H), 7.79–7.63 (m, 4H), 7.29–7.14 (m, 5H), 4.92 (s, 1H). LC-MS (ESI): *m/z* 342.1 $(M + H)^+$.

General methods for amide preparations:

Method 1 [219]:

(*R*)-*N*-heptyl-2-((4-methoxyphenyl)sulfonamido)-2-phenylacetamide (5.8).

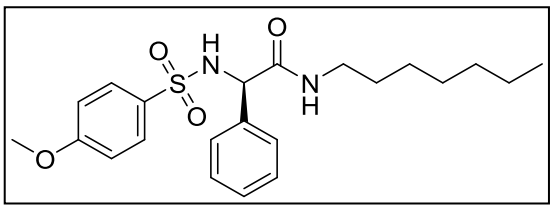

The ester Methyl (*R*)-2-((4-methoxyphenyl)sulfonamido)-2-phenylacetate (**5.1**) (335 mg, 1 mmol) was dissolved in methanol (10 mL) and then heptyl amine (138 mg, 0.2 mL, 4 mmol) was added drop wise. The solution was heated

to reflux for 24 h, and then cooled to room temperature. The resulting mixture was concentrated in vacuum which was purified by flash chromatography (ethyl acetate/petroleum ether, 1:2) to give the desired product (*R*)-N-heptyl-2-((4-methoxyphenyl)sulfonamido)-2-phenylacetamide. Yellow solid (15 mg, yield: 4%). ^{1}H NMR (400 MHz, DMSO-d_6) δ8.90 (s, 1H), 7.96 (t, J = 1.6 Hz, 2H), 7.74–7.57 (m, 5H), 7.45 (d, J = 7.6 Hz, 2H), 3.96 (s, 1H), 3.91 (s, 2H), 3.29–3.23 (m, 3H), 1.30–1.56 (m, 10H), 0.88–0.81 (m, 3H). LC-MS (ESI): *m/z* 419.0 $(M + H)^+$.

(*R*)-*N*-benzyl-2-((4-methoxyphenyl)sulfonamido)-2-phenylacetamide (5.9).

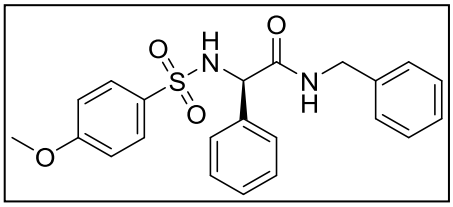

White solid (170 mg, yield: 41%). ^{1}H NMR (400 MHz, DMSO-d_6) δ8.64 (t, J = 6.0 Hz, 1H), 8.42 (s, 1H), 7.66 (d, J = 8.8 Hz, 2H), 7.34–7.31 (m, 2H), 7.26–7.21 (m, 5H), 7.03–6.98 (m, 2H), 6.96 (d, J = 10.8 Hz, 2H), 4.98 (s, 1H), 4.19–4.04 (m, 2H), 3.80 (s, 3H). LC-MS (ESI): *m/z* 411.2 $(M + H)^+$.

(*R*)-*N*-(4-chlorobenzyl)-2-((4-methoxyphenyl)sulfonamido)-2-phenylacetamide (5.11).

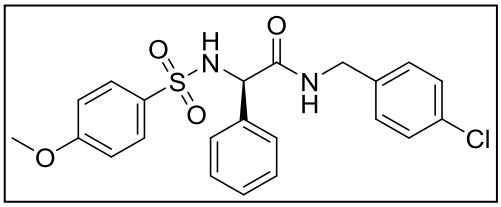

Yellow solid (30 mg, yield: 7%). ^{1}H NMR (400 MHz, DMSO-d_6) δ8.80 (t, J = 7.0 Hz, 1H), 7.70-7.66 (m, 3H), 7.38-7.25 (m, 9H), 7.09-7.0 (m, 2H), 4.82 (s, 1H), 4.04-4.00 (m, 2H), 3.79 (s, 3H). LC-MS (ESI): *m/z* 446.0 $(M + H)^+$.

(*R*)-*N*-benzyl-2-(naphthalene-2-sulfonamido)-2-phenylacetamide (5.25).

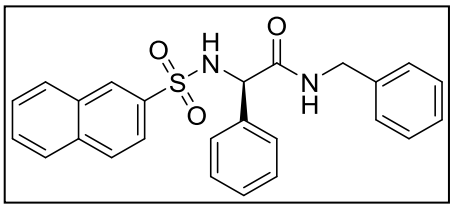

Yellow solid (90 mg, yield: 21%). ^{1}H NMR (400 MHz, DMSO-d_6) δ8.62–8.8.55 (m, 2H), 8.01-7.99 (m, 5H), 7.80–7.78 (m, 3H), 7.71-7.68 (m, 4H), 7.48-7.46 (m, 3H), 6.85-5.09 (m, 2H), 4.79 (s, 1H), 4.76 (s, 2H). LC-MS (ESI): *m/z* 430.8 $(M + H)^+$.

Method 2:

(*R*)-*N*-(cyclohexylmethyl)-2-((4-methoxyphenyl)sulfonamido)-2-phenylacetamide (5.10).

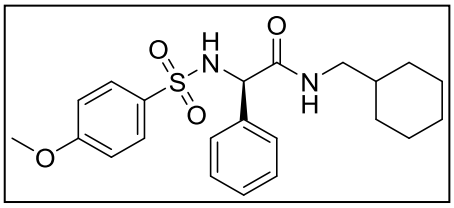

Methyl (*R*)-2-((4-methoxyphenyl)sulfonamido)-2-phenylacetate (**5.1**) (335 mg, 1 mmol) was dissolved in toluene. Cyclohexylmethanamine (226 mg, 2 mmol) was added to the mixture. The mixture was allowed to reflux for 1 h at 125 °C. The reaction was cooled at room temperature and stirred for 24 h. The residue was purified by preparative TLC (ethyl acetate/petroleum ether, 1:2) to give the desired product. White solid (100 mg, yield: 24%). ^{1}H NMR (400 MHz, DMSO-d_6) δ8.26 (t, J = 6.0 Hz, 2H), 7.59-7.51 (m, 5H), 7.39 (t, J = 8.0 Hz, 3H), 4.55 (s, 1H), 3.59 (s, 2H), 1.92-1.89 (m, 11H). LC-MS (ESI): *m/z* 417.5 $(M + H)^+$.

(*R*)-*N*-(3,4-dichlorobenzyl)-2-((4-methoxyphenyl)sulfonamido)-2-phenylacetamide (5.12).

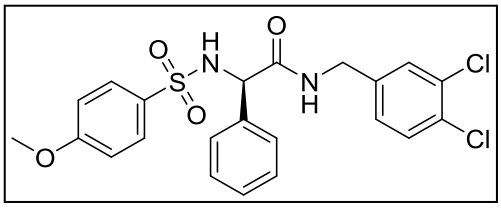

Yellow solid (120 mg, yield: 25%). ^{1}H NMR (400 MHz, DMSO-d_6) δ8.75 (t, J = 8.0 Hz, 1H), 7.64-7.57 (m, 1H), 7.49 (d, J = 8.4 Hz, 2H), 7.30-7.24 (m, 7H), 7.03-6.95 (m, 3H), 4.96 (s, 1H), 4.14 (t, J = 5.2 Hz, 2H), 3.79 (s, 3H). LC-MS (ESI): *m/z* 480.5 $(M + H)^+$. Enantiomeric excess (ee) = 98% (*R*).

(*R*)-*N*-(4-(diethylamino)benzyl)-2-((4-methoxyphenyl)sulfonamido)-2-phenylacetamide

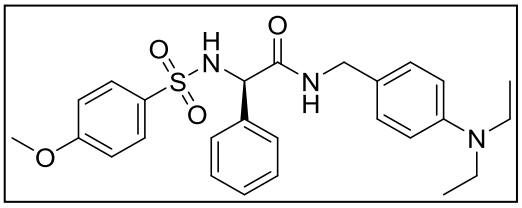

(5.13). Brown red solid (80 mg, 17%).^{1}H NMR (400 MHz, DMSO-d_6) δ8.42 (t, J = 8.2 Hz, 1H), 7.66 (d, J = 2.0 Hz, 2H), 7.33–7.31 (m, 1H), 7.42 (s, 1H), 7.26–7.21 (m, 2H), 6.98 (d, J = 9.2 Hz, 2H), 6.82 (d, J = 9.6 Hz, 2H), 6.54 (d, J = 8.4 Hz, 2H), 4.97 (s, 1H), 3.81 (s, 2H), 2.45–2.43 (m, 3H), 1.06 (t, J = 6.80 Hz, 6H), 0.94 (t, J = 7.2 Hz, 4H). LC-MS (ESI): *m/z* 482.0 $(M + H)^+$.

(*R*)-*N*-isobutyl-2-((4-methoxyphenyl)sulfonamido)-2-phenylacetamide (5.14).

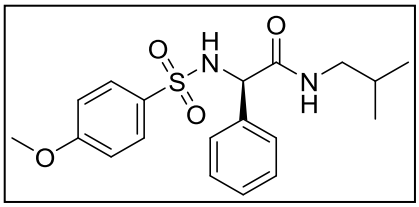

Yellow solid (10 mg, yield: 3%). ^{1}H NMR (400 MHz, DMSO-d_6) δ7.82 (d, J = 8.20 Hz, 1H), 7.67-7.38 (m, 7H), 6.85 (d, J = 8.0 Hz, 2H), 6.49 (s, 1H), 3.87 (s, 1H), 2.62 (s, 1H), 1.59 (t, J = 7.60 Hz, 2H), 1.34–1.30 (m, 1H), 1.24 (d, J = 7.2 Hz, 3H), 0.92 (t, J = 7.2 Hz, 6H). LC-MS (ESI): m/z 377.2 $(M + H)^+$.

(*R*)-2-((4-methoxyphenyl)sulfonamido)-*N*-pentyl-2-phenylacetamide (5.16).

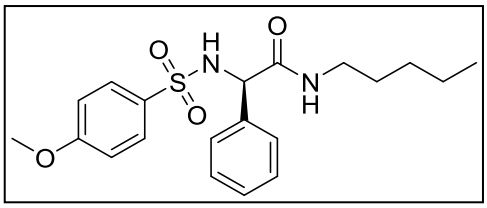

Yellow oil (30 mg, yield: 8%). ^{1}H NMR (400 MHz, DMSO-d_6) δ8.91 (s, 1H), 7.96 (t, J = 8.2 Hz, 1H), 7.86-7.52 (m, 9H), 3.81 (s, 1H), 3.47 (s, 3H), 1.53 (s, 3H), 1.32-1.24 (m, 5H), 0.91 (t, J = 7.2 Hz, 3H). LC-MS (ESI): m/z 391.8 $(M + H)^+$.

(*R*)-*N*-(4-(dimethylamino)phenyl)-2-((4-methoxyphenyl)sulfonamido)-2-phenylacetamide

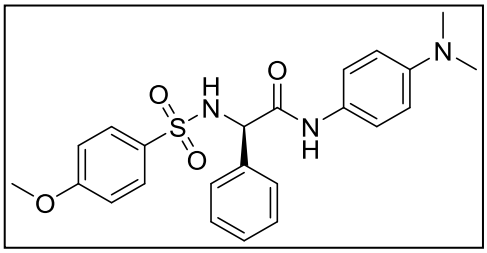

(5.23). Dark brown oil (102 mg, yield: 24%).^{1}H NMR (400 MHz, DMSO-d_6) δ8.12 (d, J = 7.2 Hz, 2H), 7.79–7.77 (m, 3H), 7.57–7.51 (m, 4H), 6.94 (d, J = 9.2 Hz, 3H), 6.75-6.73 (m, 3H), 3.96 (s, 1H), 3.78 (s, 3H), 1.24 (t, J = 8.2 Hz, 6H). LC-MS (ESI): m/z 440.6 $(M + H)^+$.

(*R*)-*N*-(cyclohexylmethyl)-2-(naphthalene-2-sulfonamido)-2-phenylacetamide (5.26).

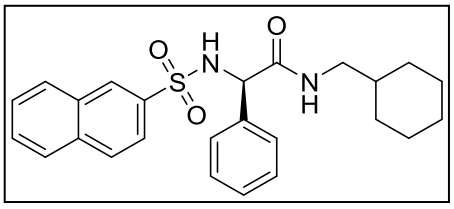

Yellow solid (60 mg, yield: 14%).^{1}H NMR (400 MHz, DMSO-d_6) δ8.10 (s, 1H), 7.69-7.56 (m, 3H), 7.45-7.39 (m, 5H), 7.16 (d, J = 7.2 Hz, 2H), 4.55 (s, 1H), 3.69 (s, 3H), 3.33 (d, J = 8.2 Hz, 2H), 1.61-1.55 (m, 11H). LC-MS (ESI): m/z 417.2 $(M + H)^+$.

(*R*)-*N*-(3,4-dichlorobenzyl)-2-(naphthalene-2-sulfonamido)-2-phenylacetamide (5.27).

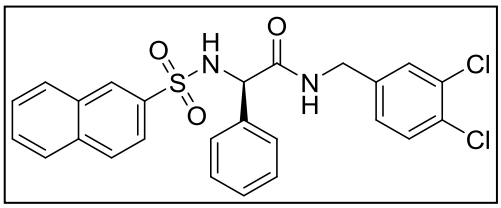

Yellow solid (30 mg, yield: 20%). ^{1}H NMR (400 MHz, DMSO-d_6) δ8.78–8.72 (m, 2H), 8.34 (s, 1H), 8.05–7.97 (m, 3H), 7.79 (t, J = 8.4 Hz, 1H), 7.70–7.65 (m, 2H), 7.32–7.27 (m, 4H), 7.22–7.16 (m, 4H), 6.85 (t, J = 6.4 Hz, 1H), 5.07 (d, J = 8.4 Hz, 1H), 1.25 (s, 2H). LC-MS (ESI): *m/z* 500.1 $(M + H)^+$.

Method 3:

General procedure for acid acylation and coupling [220]:

(*R*)-2-((4-methoxyphenyl)sulfonamido)-*N*,2-diphenylacetamide (5.15).

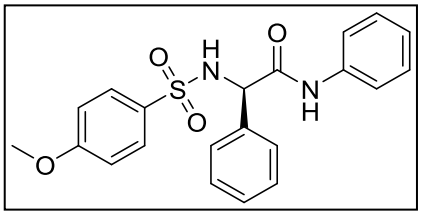

The ester hydrolyzed product **(5.7)** (321 mg, 1 mmol) was treated with thionyl chloride (238 mg, 2 mmol) in ethyl acetate. The mixture was refluxed for 2 h at 80 °C to give the corresponding acid chloride. The acid chloride intermediate (339 mg, 1 mmol) was dissolved in ethyl acetate. Aniline (97 mg, 1.05 mmol) was added to the mixture. Triethylamine (121 mg, 1.2 mmol) was added. The mixture was allowed to stir at room temperature for 12 h. The reaction solution was poured into water and extracted with EA. The combined organic layers were washed with water and brine and then dried over Na_2SO_4. The mixture was filtered and the solvent was evaporated in vacuum. The residue was purified by flash chromatography (ethyl acetate/petroleum ether, 1:2) on silica get to obtain the final product. Dark brown oil (144 mg, yield: 36%). ^{1}H NMR (400 MHz, DMSO-d_6) δ7.76 (d, J = 9.2 Hz, 1H), 7.68 (d, J = 9.2 Hz, 2H), 7.57 (d, J = 7.6 Hz, 1H), 7.41–7.36 (m, 4H), 7.28–7.26 (m, 6H), 6.90 (d, J = 8.8 Hz, 2H), 5.14 (s, 1H), 3.68 (s, 3H). LC-MS (ESI): *m/z* 397.1 $(M + H)^+$.

(*R*)-*N*-cycloheptyl-2-((4-methoxyphenyl)sulfonamido)-2-phenylacetamide (5.24).

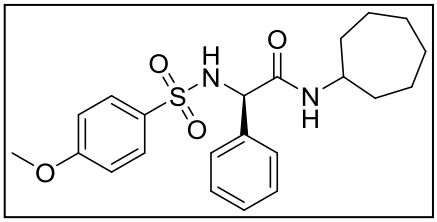

Yellow solid (65 mg, 16%). ^{1}H NMR (400 MHz, DMSO-d_6) δ8.36 (d, J = 7.0 Hz, 1H), 8.01 (d, J = 6.8 Hz, 1H), 7.66 (d, J = 8.8 Hz, 2H), 7.40-7.20 (m, 5H), 7.00-6.94 (m, 2H), 4.91 (d, J = 9.6 Hz, 1H), 3.80 (s, 3H), 3.18 (d, J = 4.8 Hz, 1H), 1.48-1.18 (m, 12H).). LC-MS (ESI): *m/z* 416.9 $(M + H)^+$.

(*R*)-2-(naphthalene-2-sulfonamido)-*N*,2-diphenylacetamide (5.29).

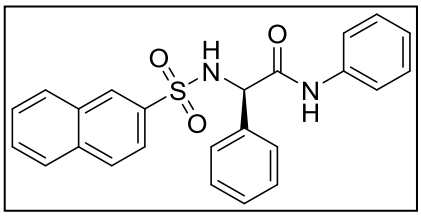

Brown oil (30 mg, 7%). ^{1}H NMR (400 MHz, DMSO-d_6) δ8.70–8.67 (m, 2H), 8.42 (s, 1H), 8.21-8.19 (m, 4H), 7.98 (t, J = 7.2 Hz, 1H), 7.77-7.68 (m, 4H), 7.62 (t, J = 8.2 Hz, 2H), 7.36-7.33 (m, 5H), 5.06 (s, 1H). LC-MS (ESI): *m/z* 417.2 $(M + H)^+$.

Method 4 [221]:

General procedure for coupling between amine and carbonyl:

(*R*)-*N*-((3S,5S,7S)-adamantan-1-yl)-2-((4-methoxyphenyl)sulfonamido)-2-phenylacetamide

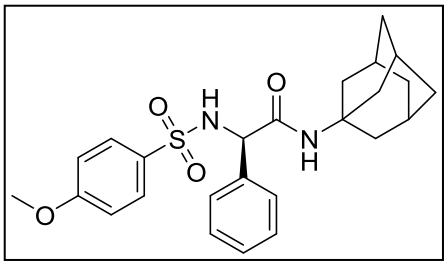

(5.17). The ester hydrolyzed product **(5.7)** (321 mg, 1 mmol) was dissolved in THF. 1-Hydroxybenzotriazole (HOBt) (162 mg, 1.2 mmol), 1-[3-(dimethylamino)propyl]-3-ethylcarbodiimide hydrochloride (EDCI, HCl) (310 mg, 2.0 mmol), and triethylamine (111 mg, 0.15 mL,1.1 mmol) were added. The mixture was stirred at room temperature for 2 h. Then adamantan-1-amine (181 mg, 1.2 mmol) was added. The mixture was stirred at room temperature for 24 h. The reaction solution was poured into water and extracted with EA. The combined organic layers were washed with water and brine and then dried over Na_2SO_4. The mixture was filtered and the solvent was evaporated in vacuum. The residue was

purified by flash chromatography (ethyl acetate/petroleum ether, 1:2) on silica get to obtain the final product. Yellow solid (50 mg, 11%). ^{1}H NMR (400 MHz, DMSO-d_6) δ8.16 (d, J = 9.20 Hz, 1H), 7.68 (d, J = 8.8 Hz, 2H), 7.54 (s, 1H), 7.33–7.21 (m, 5H), 7.02 (d, J = 9.2 Hz, 2H), 4.93 (d, J = 8.8 Hz, 1H), 3.81 (s, 3H), 1.92 (s, 3H), 1.65–1.60 (m, 6H), 1.58 – 1.50 (m, 6H). LC-MS (ESI): m/z 545.8 $(M + H)^+$.

(*R*)-2-((4-methoxyphenyl)sulfonamido)-2-phenyl-*N*-(thiophen-2-ylmethyl)acetamide (5.18).

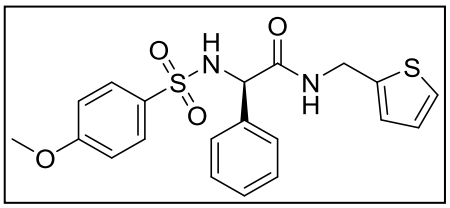

Yellow solid (110 mg, yield: 27%). ^{1}H NMR (400 MHz, DMSO-d_6) δ8.75 (t, J = 5.6 Hz, 1H), 8.41 (d, J = 9.60 Hz, 1H), 7.63 (d, J = 8.8 Hz, 2H), 7.37–7.21 (m, 6H), 6.97–6.89 (m, 2H), 6.94–6.79 (m, 1H), 6.80–6.79 (m, 1H), 4.96 (d, J = 9.6 Hz, 1H), 4.28–4.26 (m, 2H), 3.80 (s, 3H). LC-MS (ESI): m/z 416.9 $(M + H)^+$.

(*R*)-*N*-(furan-2-ylmethyl)-2-((4-methoxyphenyl)sulfonamido)-2-phenylacetamide (5.19).

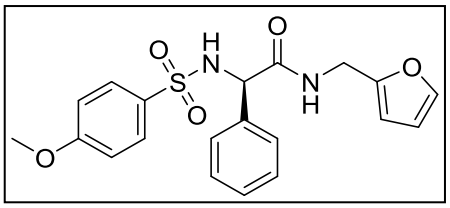

Yellow solid (151 mg, yield: 38%). ^{1}H NMR (400 MHz, DMSO-d_6) δ8.64 (t, J = 5.2 Hz, 1H), 8.40 (d, J = 9.6 Hz, 1H), 7.64–7.55 (m, 2H), 7.55 (d, J = 1.2 Hz, 1H), 7.31–7.21 (m, 5H), 6.95 (d, J = 8.8 Hz, 2H), 6.36–6.34 (m, 1H), 6.03–6.02 (m, 1H), 4.98 (d, J = 9.2 Hz, 1H), 4.11–4.08 (m, 2H), 3.80 (s, 3H). LC-MS (ESI): m/z 401.1 $(M + H)^+$.

(*2R*)-*N*-(bicyclo[2.2.1]heptan-2-yl)-2-((4-methoxyphenyl)sulfonamido)-2-phenylacetamide

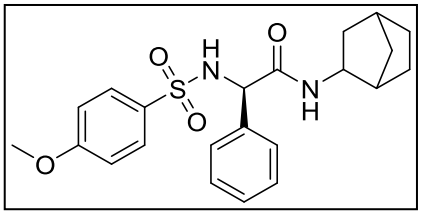

(5.20). Yellow solid (86 mg, yield: 21%). ^{1}H NMR (400 MHz, DMSO-d_6) δ8.32–8.27 (m, 1H), 7.92 (t, J = 11.6 Hz, 1H), 7.69–7.65 (m, 2H), 7.34–7.22 (m, 5H), 7.02–7.00 (m, 2H), 4.93-4.89 (m, 1H), 3.81 (s, 3H), 1.25–1.16 (m, 6H), 0.88–0.85 (m, 5H). LC-MS (ESI): m/z 414.9 $(M + H)^+$.

(*R*)-2-((4-methoxyphenyl)sulfonamido)-*N*-morpholino-2-phenylacetamide (5.21).

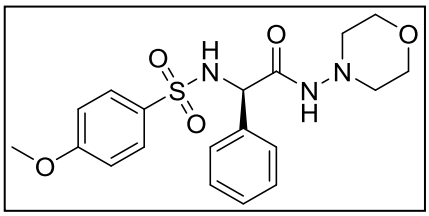

Yellow solid (65 mg, yield: 16%). ^{1}H NMR (400 MHz, DMSO-d_6) δ8.20 (d, J = 9.2 Hz, 1H), 7.67–7.65 (m, 2H), 7.28–7.25 (m, 5H), 7.01–6.99 (m, 2H), 5.34 (d, J = 9.20 Hz, 1H), 3.81 (s, 3H), 1.25 (s, 2H), 1.10 (t, J = 7.2 Hz, 2H), 1.00 (t, J = 6.8 Hz, 2H), 0.86–0.84 (m, 2H). LC-MS (ESI): m/z 406.3 $(M + H)^+$.

(*R*)-*N*-(4-hydroxyphenethyl)-2-((4-methoxyphenyl)sulfonamido)-2-phenylacetamide (5.22).

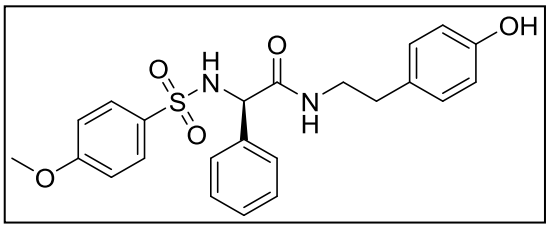

Yellow solid (20 mg, yield: 5%). ^{1}H NMR (400 MHz, DMSO-d_6) δ9.16 (s, 1H), 8.31 (d, J = 8.8 Hz, 8.17 (t, J = 5.6 Hz, 1H), 7.66–7.64 (m, 2H), 7.25–7.21 (m, 5H), 6.99–6.84 (m, 2H), 6.62–6.60 (m, 2H), 6.58 (s, 2H), 4.89 (d, J = 8.4 Hz, 1H), 3.78 (s, 3H), 2.99 (t, J = 4.0 Hz, 2H), 2.39 (t, J = 6.8 Hz, 2H). LC-MS (ESI): m/z 441.2 $(M + H)^+$.

(*2R*)-*N*-(bicyclo[3.1.1]heptan-6-yl)-2-(naphthalene-2-sulfonamido)-2-phenylacetamide

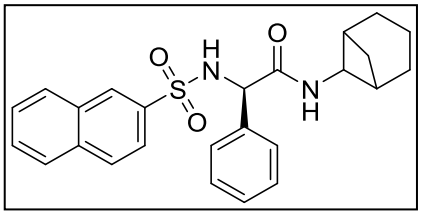

(5.28). Yellow solid (75 mg, yield: 18%). ^{1}H NMR (400 MHz, DMSO-d_6) δ8.33 (d, J = 10.8 Hz, 1H), 8.05–8.00 (m, 3H), 7.96-7.86 (m, 2H), 7.82-7.77 (m, 1H), 7.69–7.63 (m, 2H), 7.36–7.33 (m, 2H), 7.26–7.17 (m, 3H), 4.34 (s, 1H), 2.90 (s, 1H), 2.74 (s, 1H), 1.25 (s, 3H), 1.08–1.05 (m, 3H), 0.88–0.84 (m, 3H). LC-MS (ESI): m/z 435.1 $(M + H)^+$.

(*R*)-2-(naphthalene-2-sulfonamido)-2-phenyl-*N*-(3,4,5-trimethoxybenzyl)acetamide (5.30).

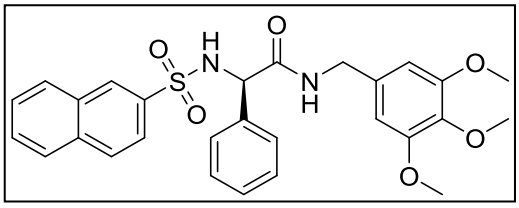

Yellow solid (60 mg, yield: 12%). ^{1}H NMR (400 MHz, DMSO-d_6) δ8.73–8.67 (m, 2H), 8.32 (s, 1H), 8.05–7.96 (m, 3H), 7.77 (t, J = 8.8 Hz, 1H), 7.70–7.62 (m, 3H),

7.34 (d, *J* = 7.2 Hz, 2H), 7.18–7.11 (m, 4H), 6.29 (s, 2H), 5.09 (d, *J* = 8.0 Hz, 1H), 3.89–3.83 (m, 2H), 3.56 (s, 9H). LC-MS (ESI): *m/z* 521.2 $(M + H)^+$.

(*2R*)-*N*-((1R,3R,5S)-adamantan-1-yl)-2-(naphthalene-2-sulfonamido)-2-phenylacetamide

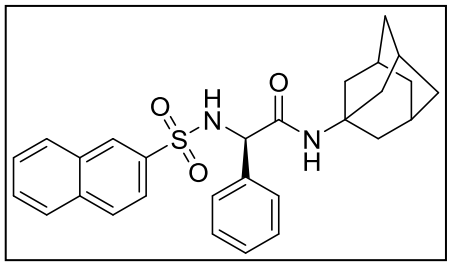

(5.31). Yellow solid (52 mg, 11%). ^{1}H NMR (400 MHz, DMSO-d_6) δ8.01 (s, 1H), 7.98–7.94 (m, 2H), 7.86–7.85 (m, 5H), 7.55–7.51 (m, 2H), 7.49–7.46 (m, 4H), 4.86 (s, 1H), 2.38–1.89 (m, 12H). LC-MS (ESI): *m/z* 474.9 $(M + H)^+$. Enantiomeric excess (ee) > 98% (*R*).

6.0 DESIGN, SYNTHESIS, AND BIOLOGICAL EVALUATION OF SUBSTITUTED 4-(AMINOMETHYL)-*N*,*N*-DIETHYLANILINE DERIVATIVS AS SELECTIVE CB2 LIGANDS

6.1 INTRODUCTION

The previous two series demonstrated novel CB2 chemical scaffolds with advantages and disadvantages for each. In order to overcome the limitations we faced in the previous two series, we aimed at designing and synthesizing selective and potent CB2 ligands by exploring different chemical scaffold. This was accomplished by performing structure-based drug design where we utilized molecular docking studies employing our CB2 homology model. Due to the lack of high-resolution 3D X-ray crystallographic co-crystal structure of the CB2 protein, our homology model developed in our lab served as a good starting point for our screening studies. We utilized the structure-based virtual screening protocol to screen known chemical databases based on docking and conformational analysis. The National Cancer Institute (NCI) 2010 chemical database was used to perform flexible molecular docking by the Surflex-Dock program in SYBYL X1.3 [207, 222]. Approximately 100 molecules with docking score greater than 7.0 were structurally inspected for binding mode conformation, chemical diversity and drug-like properties. Among the 100 molecules, 10 compounds were biologically evaluated for cannabinoid receptor binding activity using radio-ligand competitive binding assay (see appendix B, Table 7.1) [209].

As shown in Figure 6.1, the CB2 binding pocket is formed by helices III, V, VI, and VII. The important amino acids in this pocket are: Phe87$^{2.57}$, Phe91$^{2.61}$, Phe94$^{2.64}$, Asp101 (ECL1),

Phe106$^{3.25}$, Lys109$^{3.28}$, Ile110$^{3.29}$, Val113$^{3.32}$, Phe117$^{3.36}$, Glu181 (ECL2), Leu182 (ECL2), Phe183 (ECL2), Trp194$^{5.43}$, Phe197$^{5.46}$, Trp258$^{6.48}$, Val261$^{6.51}$, Met265$^{6.55}$, Phe281$^{7.35}$, and Ser285$^{7.39}$.

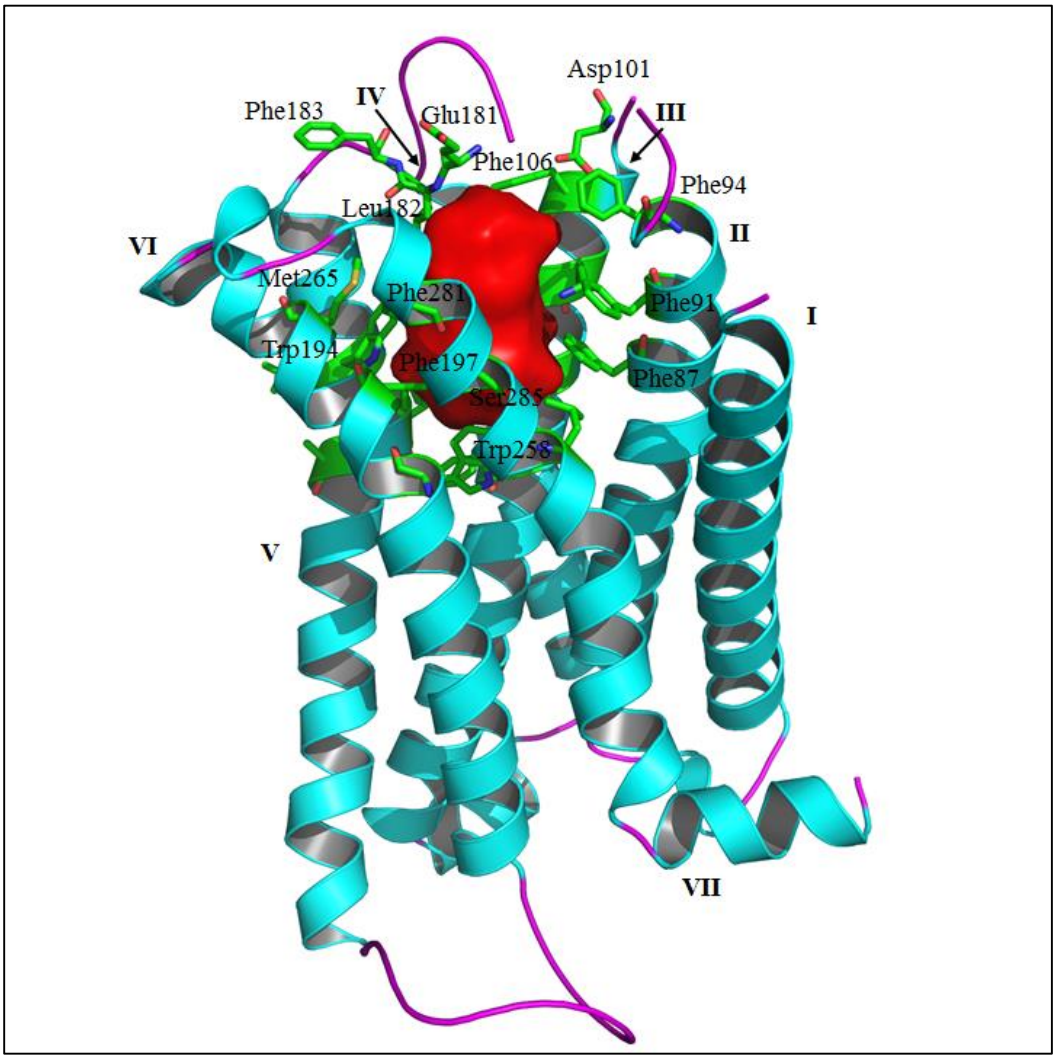

Figure 6.1. The CB2 homology model and the potential binding pocket.

The potential binding pocket is formed by helices III, V, VI, and VII. Important amino acids in the pocket are: Phe87$^{2.57}$, Phe91$^{2.61}$, Phe94$^{2.64}$, Asp101 (ECL1), Phe106$^{3.25}$, Lys109$^{3.28}$, Ile110$^{3.29}$, Val113$^{3.32}$, Phe117$^{3.36}$, Glu181 (ECL2), Leu182 (ECL2), Phe183 (ECL2), Trp194$^{5.43}$, Phe197$^{5.46}$, Trp258$^{6.48}$, Val261$^{6.51}$, Met265$^{6.55}$, Phe281$^{7.35}$, and Ser285$^{7.39}$.

Compound **6.1** (Figure 6.2) was chosen as a lead compound due to: a) docking score of 7.68, b) weak cannabinoid receptor affinity (CB2 K_i = 9 μM and CB1 K_i = 11 μM) which can be further optimized to generate selective CB2 ligands, further, c) this compound showed an interesting backbone as it has 3 phenyl rings connected to a chiral center in addition to the *para* nitro group that can be further modified. In addition, docking analysis showed multiple interactions with the amino acids in the binding pocket of the CB2 model. Hydrophobic interactions of ring A with Phe281 and Trp194 were observed. In addition, the sulphonyl group connected to ring A showed a hydrogen bonding interaction with Trp194. Rings B and C exhibited hydrophobic interactions with Phe91, Ph87, and Phe197, respectively. Another important interaction was observed between the *p*-NO_2 and Trp258. However, the sulphonyl group of ring B showed weak interactions with Ser285 and Lys109, suggesting that the hydrogen bond acceptor group at this position is not essential (Figure 6.3).

The modification strategy was to replace the central carbon with nitrogen, retain one of the sulfonyl groups and test different lengths, sizes and charges connected to the sulfonyl group, replacing the other sulfonyl group with different fragments varying at sizes, lengths and properties. In addition, the *para*-nitro group was replaced with *para*-diethylamine since this moiety had shown previously in Chapter 4, the di-amide scaffold, to improve the CB2 affinity; Figure 6.2 shows the new scaffold and modification points.

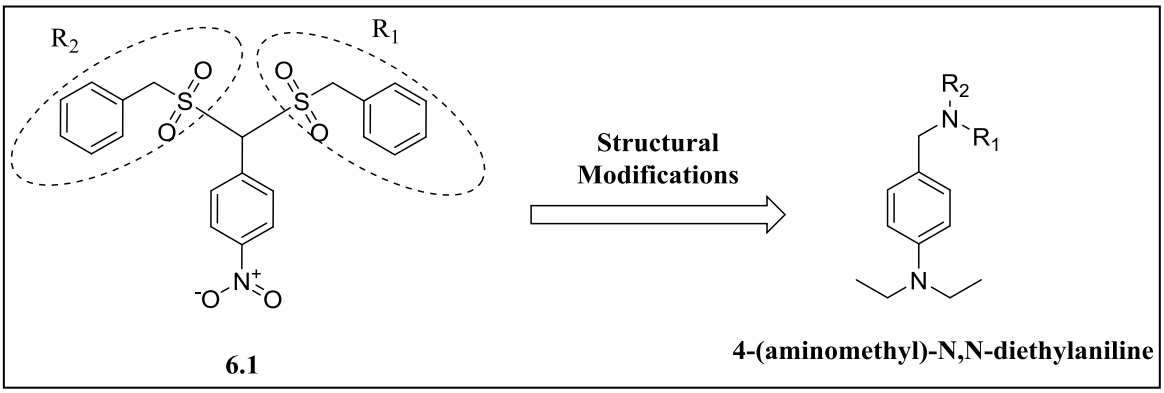

Figure 6.2. Chemical structure of the lead compound (6.1) and the lead optimization strategy.

Molecular docking screening studies were performed using Surflex-Dock software in SYBYL X1.3. NCI-2010 database was utilized for the screening studies with the following criteria: docking score > 7.0, and molecular weight between 200 – 500 Da. The lead optimization strategy was to connect different amine fragments at the R_1 position, connect different sulfonyl and aryl fragments at the R_2 position, to replace the carbon center nitrogen, and to replace the *para*-nitro group with diethylamine.

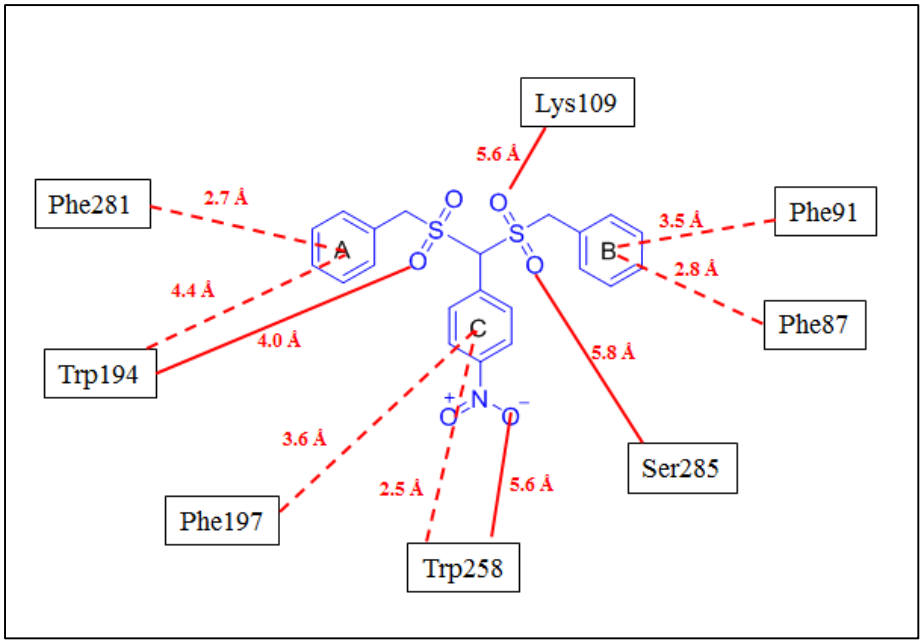

Figure 6.3 Molecular docking interactions of compound 6.1 with different amino acids in the CB2 binding pocket.

Molecular docking analysis was carried out using SYBYL X1.3 ® (Tripos Inc.) and refined using PyMol (Schrodinger). Red lines: hydrogen bonding, dashed lines: hydrophobic or pi-pi interactions. Compound **6.1 (NCI-294739)** showed pi-pi stacking interaction between ring A and Phe281. Hydrogen bonding between the sulfonyl moiety of ring A and Trp194. Pi-pi stacking interaction was also observed between ring C and Phe197 as well as Trp258. The nitro group on ring C showed a weak interaction with the Trp258. Pi-pi between ring B and Phe91 as well as Phe87. Weak interaction between the sulfonyl moiety of ring B and Lys109 as well as Ser285.

6.2 RESULTS AND DISCUSSION

6.2.1 Chemistry Synthesis

The synthetic routes to obtain the target substituted 4-(aminomethyl)-*N*,*N*-diethylaniline derivatives are depicted in Scheme 3. The commercially available 4-(diethylamino)benzaldehyde was reacted with 3,4,5-trimethoxybenzylamine to give **6.2**. Compound **6.2** was treated with $NaBH_4$ to give the secondary amine **6.3**. A coupling reaction was carried out between the intermediate **6.3** and sulfonyl chloride or acyl chloride yielded the corresponding compounds **6.4 - 6.18** (Table **6.1**). Similarly, reaction of 4-(diethylamino)benzaldehyde with 3-(aminomethyl)pyridine, piperonylamine, and pentanamine, then treated with $NaBH_4$ gave the intermediates **6.20**, **6.28** and **6.36**, respectively. Finally, coupling reaction of **6.20**, **6.28** and **6.36** with sulfonyl chloride and acyl chloride yielded the corresponding compounds **6.21 - 6.26** (Table **6.2**), **6.29 - 6.34** (Table **6.3**) and **6.37 - 6.42** (Table **6.4**), respectively. All final products were purified by flash column chromatography and verified by NMR (400 Hz or 600 Hz) and LC/MS.

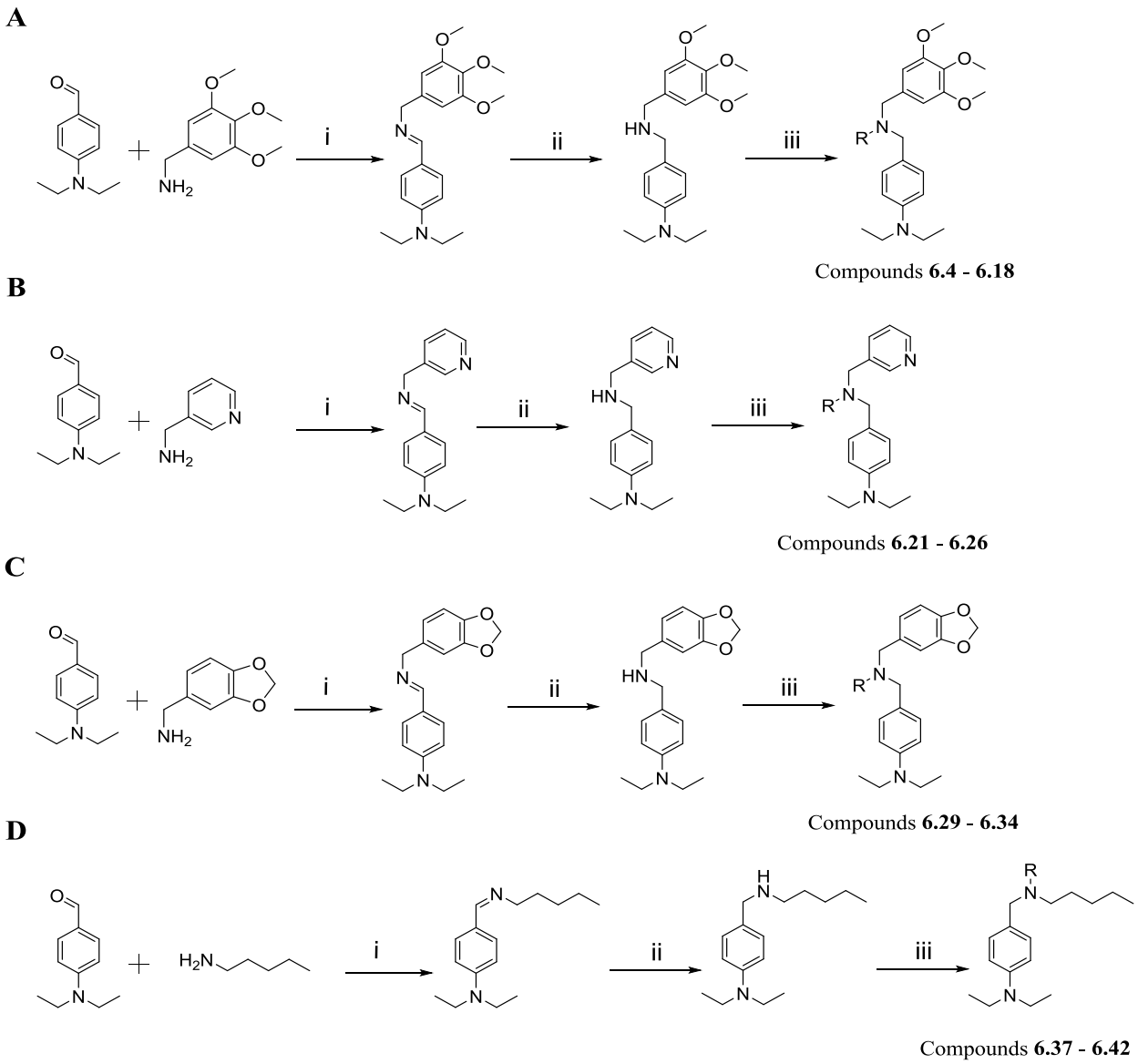

Scheme 3. Synthesis routes for 4-(aminomethyl)-*N*,*N*-diethylaniline derivatives.

Synthesis schemes of **(A)** *N*,*N*-diethyl-4-(((3,4,5-trimethoxybenzyl)amino)methyl)aniline derivatives; **(B)** *N*,*N*-diethyl-4-(((pyridin-3-ylmethyl)amino)methyl)aniline derivatives; **(C)** 4-(((benzo[*d*][1,3]dioxol-5-ylmethyl)amino)methyl)-*N*,*N*-diethylaniline derivatives, and **(D)** *N*,*N*-diethyl-4-((pentylamino)methyl)aniline. Reagents and conditions: (i) methanol, refluxed, 10 h; (ii) $NaBH_4$, methanol, rt, 12 h; (iii) sulfonyl chloride or acyl chloride, anhydrous dichloromethane, triethylamine, rt, 12 h.

6.2.2 Structure Activity Relationship Analysis

The structure activity relationship studies was carried out based on the CB2 binding affinity and selectivity. The binding affinities toward CB1 and CB2 were determined by performing [^{3}H]CP-55,940 radioligand competition binding assays using membrane protein preparations of CHO cells stably expressing human CB2 receptor. The CB1 binding affinity was conducted on derivatives exhibiting a CB2 K_i < 1000 nM by utilizing membrane protein preparations of CHO cells stably transfected with human CB1 receptor. SR144528 (CB2 inverse agonist) and SR141716 (CB1 inverse agonist) were used as CB2 and CB1 positive controls in bioassays experiments, respectively. The detailed radio-ligand competition binding assay was detailed in Chapter 3. Among the 41 analogues, ten compounds showed high CB2 affinity and selectivity with nanomolar K_i values (eight compounds exhibiting < 500 nM binding affinity). Table 6.1 - Table 6.4 summarize the chemical structure, physicochemical properties, binding affinities and selectivity indices.

For the SAR studies, several functional groups were introduced to the lead compound **6.1** aiming at obtaining high potency and selectivity toward the CB2 receptor. The strategies were to replace the *p*-nitrophenyl group with *p*-(diethylamino)benzyl group as previous studies (Chapter 4) have shown that this fragment played important roles to the selectivity towards the CB2 receptor. In addition, one of the sulfonyl groups was replaced with 3,4,5-trimethoxybenzylamine, 3-(aminomethyl)pyridine, piperonylamine, and pentanamine as these fragments varied in size, charge and properties. Further, the second sulfonyl group was either retained or replaced with a carbonyl group. Our studies have shown that the removal of one of the hydrophobic groups dramatically decreased the CB2 binding affinity (compounds **6.3**, **6.20**, **3.28**, and **6.36**, CB2 K_i =

42,350 nM, > 20,000 nM, > 20,000 nM and 40,170 nM, respectively) indicating the importance of having hydrophobic groups at the R_1 and R_2 positions to retain the binding activities.

The fragment (3,4,5-trimethoxyphenyl)methanamine was introduced at the R_1 position and synthesized 16 compounds (**6.3** – **6.18**, Table 6.1). These compounds differ at the R_2 position by replacing the phenylmethanesulfonyl fragment with different sulfonyl or carbonyl fragments varying in size and properties. Compared with compound **6.1**, reducing the distance between the benzene ring and the sulfonyl group by removing the methyl group and replacing the other phenylmethanesulfonyl with (3,4,5-trimethoxyphenyl)methanamine fragment dramatically increased the CB2 binding affinity with no affinity towards the CB1 receptor (compound **6.7**, CB2 K_i = 453 nM, CB1 K_i > 20,000 nM, selectivity index = 44). This indicates that the distance between the benzene ring and the sulfonyl group should be narrow and the other phenylmethanesulfonyl fragment is not necessary for selectivity and can be replaced with other fragments. To test the substitutions on the benzene ring of the benzene sulfonyl group at the R_2 position, we introduced different substituents at different positions on the ring. The introduction of *p*-methyl group retained the CB2 binding affinity but induced the CB1 binding affinity (compound **6.6**, CB2 K_i = 387 nM, CB1 K_i = 774 nM, selectivity index = 2). The introduction of *m*-methyl group improved the CB2 binding affinity yet retaining good CB1 binding affinity (compound **6.5**, CB2 K_i = 291 nM, CB1 K_i = 732 nM, selectivity index = 2.5). In addition, *o*-methyl substitution on the benzene ring increased the CB2 binding affinity as well as the CB1 binding affinity (compound **6.14**, CB2 K_i = 157 nM, CB1 K_i = 180 nM, selectivity index = 2). These results indicate that *para* substituents are more favorable than *meta*- and *ortho*- substitutions in increasing CB2 binding affinity, selectivity, and reducing CB1 affinity. Next, we explored different functional groups at the *para* position. The introduction of a methoxy group at the *para* position retained good CB2 binding affinity with no

CB1 affinity (compound **6.4**, CB2 K_i = 410 nM). However, introducing the *p*-isopropyl group improved the CB2 binding affinity but the CB1 binding affinity is much higher (compound **6.8**, CB2 K_i = 230 nM, CB1 K_i = 122 nM). Introducing trifluoromethoxy at the *para* position reduced the CB2 binding affinity and selectivity (compound **6.13**, CB2 K_i = 990 nM, CB1 K_i = 1240 nM, selectivity index = 2). Introduction of a *p*-formyl group improved CB2 binding affinity and selectivity (compound **6.18**, CB2 K_i = 242 nM, CB1 K_i = 2290, selectivity index = 9). Next, we explored different group sizes at the R_2 position. The introduction of naphthalene-2-sulfonyl at the R_2 position increased the CB1 binding affinity (compound **6.9**, CB2 K_i = 239 nM, CB1 K_i = 71 nM). Further, the introduction of [1,1'-biphenyl]-4-sulfonyl at the R_2 position abolished the CB1 binding affinity and improved the CB2 binding affinity (compound **6.10**, CB2 K_i = 322 nM).

Then we studied the effect of introducing heterocycle groups at the R_2 position. The introduction of a small heterocyclic group at the R_2 position (thiophene-2-sulfonyl) showed an increase in the CB2 binding affinity without CB1 binding affinity (compound **6.16**, CB2 K_i = 639 nM, CB1 K_i > 20000 nM). However, the introduction of a heterocyclic group with the replacement of the sulfonyl group with carbonyl group dramatically increased the CB2 binding affinity (compound **6.11**, CB2 K_i = 99 nM, CB1 K_i = 3282 nM, selectivity index = 33). In addition, we explored large heterocyclic groups at the R_2 position by introducing quinoxaline-2-carbonyl. The CB2 binding affinity and selectivity was greatly improved (compound **6.12**, CB2 K_i = 249 nM, CB1 K_i = 13020 nM, selectivity index = 52). These results indicated that introducing heterocyclic rings at the R_2 position will potentiate the affinity and selectivity towards the CB2 receptor. Finally, in order to improve the conjugation system between the two functional groups (sulfonyl and the benzyl ring) of the fragment at the R_2 position, we introduced a double bond between the

two functional groups. This modification improved dramatically the CB2 binding affinity and selectivity (compound **6.15**, CB2 K_i = 138 nM, CB1 K_i > 20000 nM).

Table 6.1. Chemical structures, physicochemical properties, radioligand competition binding affinity and selectivity index for intermediate 1 derivatives (Compounds 6.3 – 6.18)

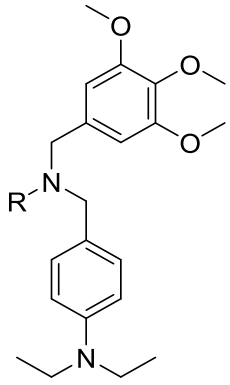

Entry	R	MW	cLogP	K_i (CB2), nM	K_i (CB1), nM	SI
6.3	H	358.48	3.19	42350	NT	-
6.4	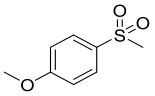	528.66	5.47	410	NB	50
6.5	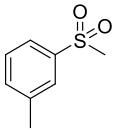	512.66	5.80	291	732	3
6.6	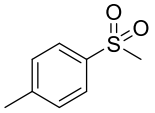	512.66	5.80	387	774	2
6.7	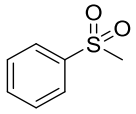	498.64	5.30	453	NB	44
6.8	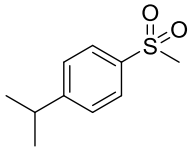	540.72	6.72	230	122	-
6.9	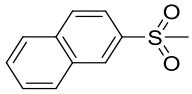	548.70	6.47	239	71	-
6.10	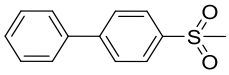	574.74	7.18	322	NB	62

6.11	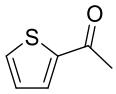	468.61	4.86	99	3282	33
6.12	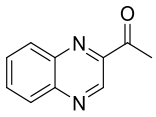	514.63	4.62	249	13020	52
6.13	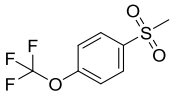	582.64	6.57	990	1240	2
6.14	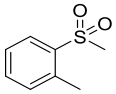	512.66	5.80	157	180	2
6.15	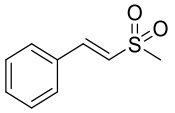	524.68	5.94	138	NB	145
6.16	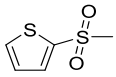	504.66	5.02	639	NB	32
6.17	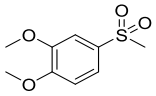	558.69	5.17	657	NT	-
6.18	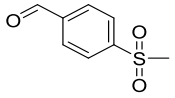	526.65	4.87	242	2290	9
SR144528				1.55	NT	-
SR141716				NT	1.2	-

Binding affinities for CB1 and CB2 receptor were evaluated using [^{3}H]CP-55,940 radioligand competition binding assay. NB: no binding, K_i > 20000 nM. NT: not tested. SI: selectivity index for CB2, calculated as K_i(CB1)/K_i(CB2) ratio. CB2 reference compound SR144528. CB1 reference compound SR141716.

To extend the SAR studies, we retained the 4-(diethylamino)benzyl group and replaced one of the phenylmethanesulfonyl with a heterocyclic group, 3-(aminomethyl)pyridine, and replaced the other phenylmethanesulfonyl with different sulfonyl and carbonyl groups to evaluate the effect on reducing the size of the fragment at the R_1 on the binding affinity and selectivity (compounds **6.20** – **6.26**, Table 6.2). Unfortunately, all of these compounds showed decreased CB2 binding activity (CB2 K_i > 1000 nM). However, introducing a bulky non-heterocyclic group at the R_2 position improved the CB2 binding affinity (compounds **6.24** and **6.25**, CB2 K_i < 1000 nM). In addition, introducing a double bond between the sulfonyl and the benzyl group slightly improved the CB2 binding affinity and selectivity (compound **6.23**, CB2 K_i = 899 nM, CB1 K_i = 5460 nM, selectivity index = 6).

Table 6.2. Chemical structures, physicochemical properties, radioligand competition binding affinity and selectivity index for intermediate 2 derivatives (Compounds 6.20 – 6.26)

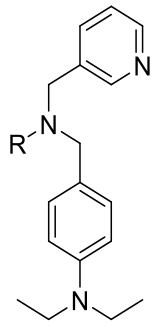

Entry	R	MW	cLogP	K_i (CB2), nM	K_i (CB1), nM	SI
6.20	H	269.39	2.39	NB	NT	-
6.21	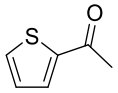	379.52	4.07	1020	NT	-
6.22	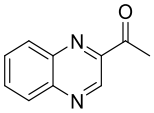	425.54	3.83	1205	NT	-
6.23	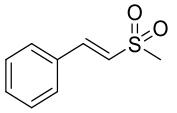	435.59	5.14	899	5460	6
6.24	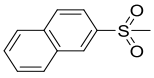	459.61	5.67	866	12040	14
6.25	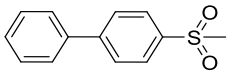	485.65	6.39	946	NB	21
SR144528				1.55	NT	-
SR141716				NT	1.2	-

Binding affinities for CB1 and CB2 receptor were evaluated using [^{3}H]CP-55,940 radioligand competition binding assay. NB: no binding, K_i > 20000 nM. NT: not tested. SI: selectivity index for CB2, calculated as K_i(CB1)/K_i(CB2) ratio. CB2 reference compound SR144528. CB1 reference compound SR141716.

We then replaced one of the phenylmethanesulfonyl with the fragment piperonylamine and the other phenylmethanesulfonyl with different sulfonyl and carbonyl groups (compounds **6.28** – **6.34**, Table 6.3). Replacing the phenylmethanesulfonyl at the R_2 position with a bulky heterocyclic group showed good CB2 binding affinity with weak CB1 binding affinity (compound **6.31**, CB2 K_i = 775 nM, CB1 K_i = 1267 nM, selectivity index = 2). On the other hand, smaller heterocyclic group abolished the CB2 selectivity (compound **6.32**, CB2 K_i = 574 nM, CB1 K_i = 727 nM, selectivity index = 2) indicating that the presence of two bulky heterocyclic groups at positions R_1 and R_2 improved the CB2 affinity and selectivity. This result is further confirmed by replacing phenylmethanesulfonyl at the R_2 position with 4-formylbenzenesulfonyl which showed a reduction in CB2 affinity and selectivity (compound **6.30**, CB2 K_i = 1872 nM, CB1 K_i = 2745 nM, selectivity index = 1). Similarly, the introduction of a double bond between the sulfonyl and the benzyl group showed good CB2 binding affinity as well as selectivity (compound **6.29**, CB2 K_i = 381 nM, CB1 K_i = 1159 nM, selectivity index = 3). Also, introducing bulky groups at the R_2 position such as naphthalene-2-sulfonyl and [1,1'-biphenyl]-4-sulfonyl reduced the CB2 binding affinity (compounds **6.33**, **6.34**, CB2 K_i = 882 nM, and 1995 nM, respectively).

Table 6.3. Chemical structures, physicochemical properties, radioligand competition binding affinity and selectivity index for intermediate 3 derivatives (Compounds 6.28 – 6.34)

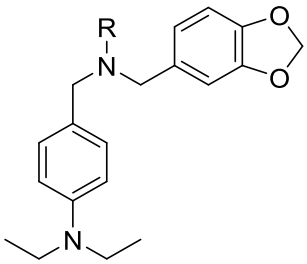

Entry	R	MW	cLogP	K_i (CB2), nM	K_i (CB1), nM	SI
6.28	H	312.41	3.86	NB	NT	NT
6.29	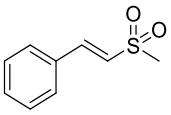	478.61	6.60	381	1159	3
6.30	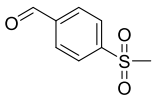	480.58	5.53	1872	2745	1
6.31	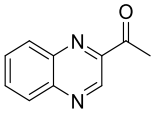	454.57	5.74	775	1267	2
6.32	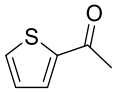	422.54	5.53	574	727	2
6.33	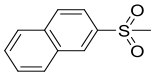	502.63	7.14	882	NT	-
6.34	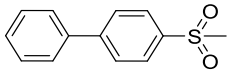	528.67	7.85	1995	NT	-
SR144528				1.55	NT	-
SR141716				NT	1.2	-

Binding affinities for CB1 and CB2 receptor were evaluated using [^{3}H]CP-55,940 radioligand competition binding assay. NB: no binding, K_i > 20000 nM. NT: not tested. SI: selectivity index for CB2, calculated as K_i(CB1)/K_i(CB2) ratio. CB2 reference compound SR144528. CB1 reference compound SR141716.

Finally, we replaced one of the phenylmethanesulfonyl with pentanamine to examine the effect of replacing aromatic groups with aliphatic groups (compounds **6.36** – **6.42**, Table 6.4). These compounds showed comparable results as previous series. Introducing a double bond between the sulfonyl and the benzyl group exhibited an increase in the CB2 affinity and selectivity (compound **6.37**, CB2 K_i = 1872 nM, CB1 K_i = 2745 nM, selectivity index = 10). In addition, small heterocyclic group showed good CB2 affinity and selectivity (compound **6.40**, CB2 K_i = 362 nM, CB1 K_i = 2437 nM, selectivity index = 7). However, bulky heterocyclic group showed an abolished CB2 selectivity (compound **6.39**, CB2 K_i = 1852 nM, CB1 K_i = 1863 nM). Also, introducing bulky groups at the R_2 position such as naphthalene-2-sulfonyl and [1,1'-biphenyl]-4-sulfonyl reduced the CB2 binding affinity (compounds **6.41**, and **6.42**, CB2 K_i = 1139 nM and 3147 nM, respectively). These results showed that it is not necessary to retain aromatic properties at all positions and the introduction of an aliphatic group will retain moderate CB2 binding affinity and selectivity but to a lesser extent than aromatic groups.

Table 6.4. Chemical structure, physicochemical properties, radioligand competition binding affinity and selectivity index for intermediate 4 derivatives (Compounds 6.36 – 6.42)

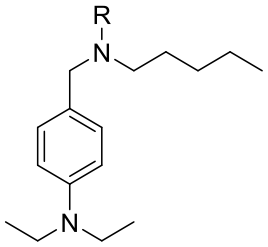

Entry	R	MW	cLogP	K_i (CB2), nM	K_i (CB1), nM	SI
6.36	H	248.41	4.85	40170	NT	NT
6.37	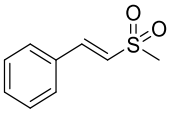	414.61	6.61	515	5242	10
6.38	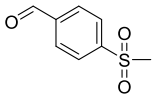	416.58	6.02	657	1786	3
6.39	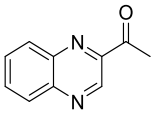	404.56	5.67	1852	1863	1
6.40	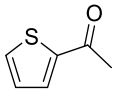	358.54	5.91	362	2437	7
6.41	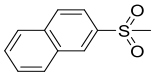	438.63	7.62	1139	NT	-
6.42	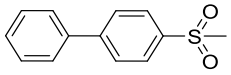	464.67	8.33	3147	NT	-
SR144528				1.55	NT	-
SR141716				NT	1.2	-

Binding affinities for CB1 and CB2 receptor were evaluated using [^{3}H]CP-55,940 radioligand competition binding assay. NB: no binding, K_i > 20000 nM. NT: not tested. SI: selectivity index for CB2, calculated as K_i(CB1)/K_i(CB2) ratio. CB2 reference compound SR144528. CB1 reference compound SR141716.

6.2.3 *In-Vitro* Functional Assay

The CB2 functional activities of the substituted 4-(aminomethyl)-*N*,*N*-diethylaniline derivatives were investigated by utilizing the cell-based LANCE cAMP assay. This assay distinguishes between agonists, inverse agonists and antagonists in GPCRs. The detailed experimental procedure was carried out as highlighted in Chapter 3. The cell-based LANCE cAMP assays were performed on 384-well plates using CHO cells stably expressing the CB2 receptors in the presence of phosphodiesterase inhibitor RO20-1724 and adenylate cyclase activator forskolin.

Three highly potent and selective compounds were selected; **6.11**, **6.15**, **6.18** as well as CB2 reference compounds SR144528 and CP55,940. As shown in Figure 6.4, reduction of the LANCE signal occurred with increasing concentrations of compounds **6.15, 6.18,** and SR-144,528. These ligands act as inverse agonists, indicated by increasing forskolin-induced cAMP production. On the other hand, compound **6.11** and the known CB2 agonist, CP55,940, inhibited cAMP production, which indicates that compound **6.11** is a CB2 selective agonist.

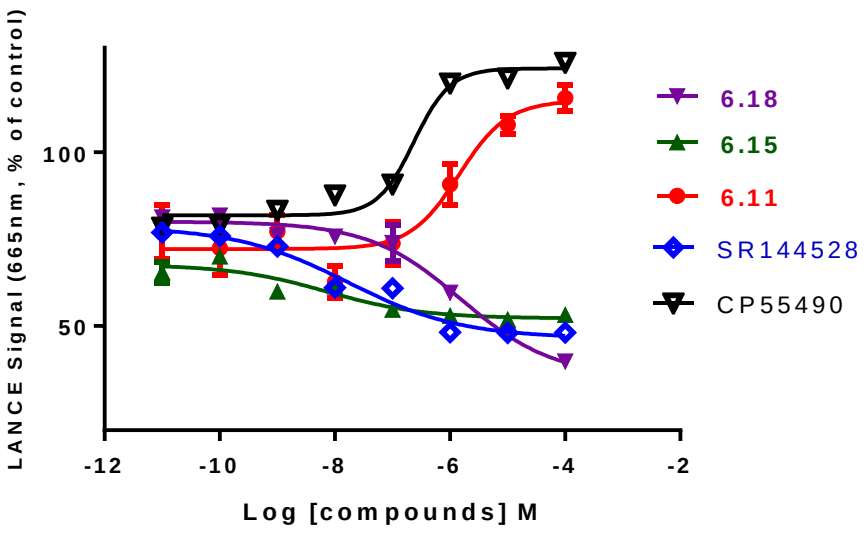

Figure 6.4. Functional activity of the 4-(aminomethyl)-*N*,*N*-diethylaniline derivatives.

Comparisons of LANCE signal of different CB2 receptor ligands in stably transfected CHO cells expressing human CB2 receptors in a concentration-dependent manner. Compounds CP55,940 as well as **6.11** behaved as agonists while compounds **6.15, 6.18** as well as SR-144,528 behaved as inverse agonists. Data represented as the mean ± SEM of one representative experiment of two or more carried out in triplicates.

6.2.4 Osteoclast Formation Assay

The osteoclast formation assay was carried out using mouse whole bone marrow cells obtained from 4- to 6-week old C57BL/6 mouse as described in Chapter 3. The three top compounds **6.11**, **6.15**, and **6.18** were chosen for the RANKL-induced osteoclast differentiation studies. In addition, we wanted to compare the different functionality the compounds (agonist **6.11** and inverse agonist **6.15** and **6.18**) on the osteoclast formation effects. As shown in Figure 6.5, compounds **6.15** and **6.18** induced a concentration-dependent inhibition of osteoclastogenesis, with > 95% inhibition rate at concentrations 5 μM and 10 μM. Good inhibitions was maintained even at lower doses (2.5 μM) for compounds **6.15** and **6.18**. These results indicated that the inhibition activities are consistent with the CB2 affinities. On the other hand, the agonist (compound **6.11**) showed an induction of osteoclast formation at higher doses (10 μM). These results showed that designing CB2 selective inverse agonist is more promising in the inhibition of OCL formation and the ultimate treatment of osteoporosis.

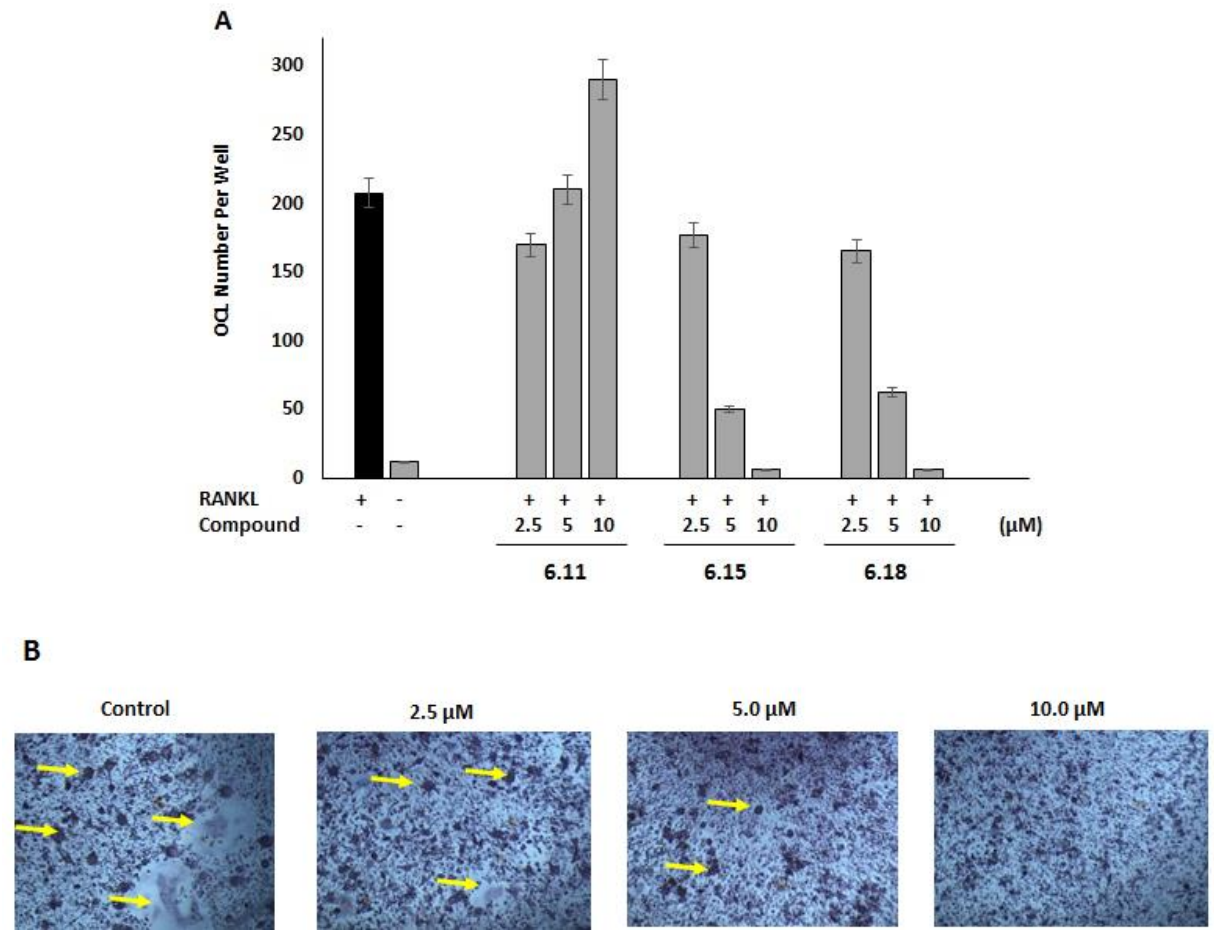

Figure 6.5. Anti-osteoclastogenesis activity of the potent 4-(Aminomethyl)-*N*,*N*-diethylaniline derivatives.

(A) Compounds **6.15** and **6.18** inhibited the RANKL-induced osteoclast differentiation in a dose-dependent manner. Compound **6.11** had low effect in inducing the osteoclast formation at higher doses. BM cells were seeded at a density of 2×10^5 cells/well in 96-well plates and treated with or without RANKL (100 ng/mL) and M-CSF (30 ng/mL). CB2 compounds were added at the indicated concentrations for 10 days and stained for TRAP expression. Data is the mean ± SD of three experiments carried out in triplicates. **(B)** Microscopic photographs of cells for compound **6.15** (magnification 100×). Statistical analysis: ***P<0.001, ****P<0.0001 compared to the control (RANKL+).

6.2.5 Multiple Myeloma Anti-proliferation Studies

To test the anti-proliferation effects of our synthesized CB2 ligands against multiple myeloma, MTT colorimetric assay was conducted. MTT assay was carried out using two multiple myeloma cell-lines; MM1.S and RPMI8226. The detailed experimental details were highlighted in Chapter 3.0 .The first run of the MTT assay was to screen the derivatives exhibiting high affinity and selectivity on the MM cell-lines using 10 µM constant concentrations for the compounds and utilizing nocodazole as a positive control and the negative control wells having < 0.1% concentration of DMSO. Eleven compounds with CB2 K_i < 500 nM were evaluated for their inhibition ability of MM cell-lines. As illustrated in Figure 6.6, compounds **6.11** and **6.15** exhibited an inhibitory effect of MM cell-lines (inhibition rate < 45%). Both were utilized to measure the IC_{50} effects using concentrations 100 µM to 6.25 µM. Compound **6.11** demonstrated an IC_{50} value of 5.1 µM and 6.0 µM for MM1.S and RPMI8226 cell-lines, respectively. In comparison, compound **6.15** exhibited an IC_{50} of 8.3 µM and 7.6 µM for MM1.S and RPMI8226, respectively. These results indicates that designing a CB2 agonist is promising in treating MM while inverse agonist may need higher concentrations.

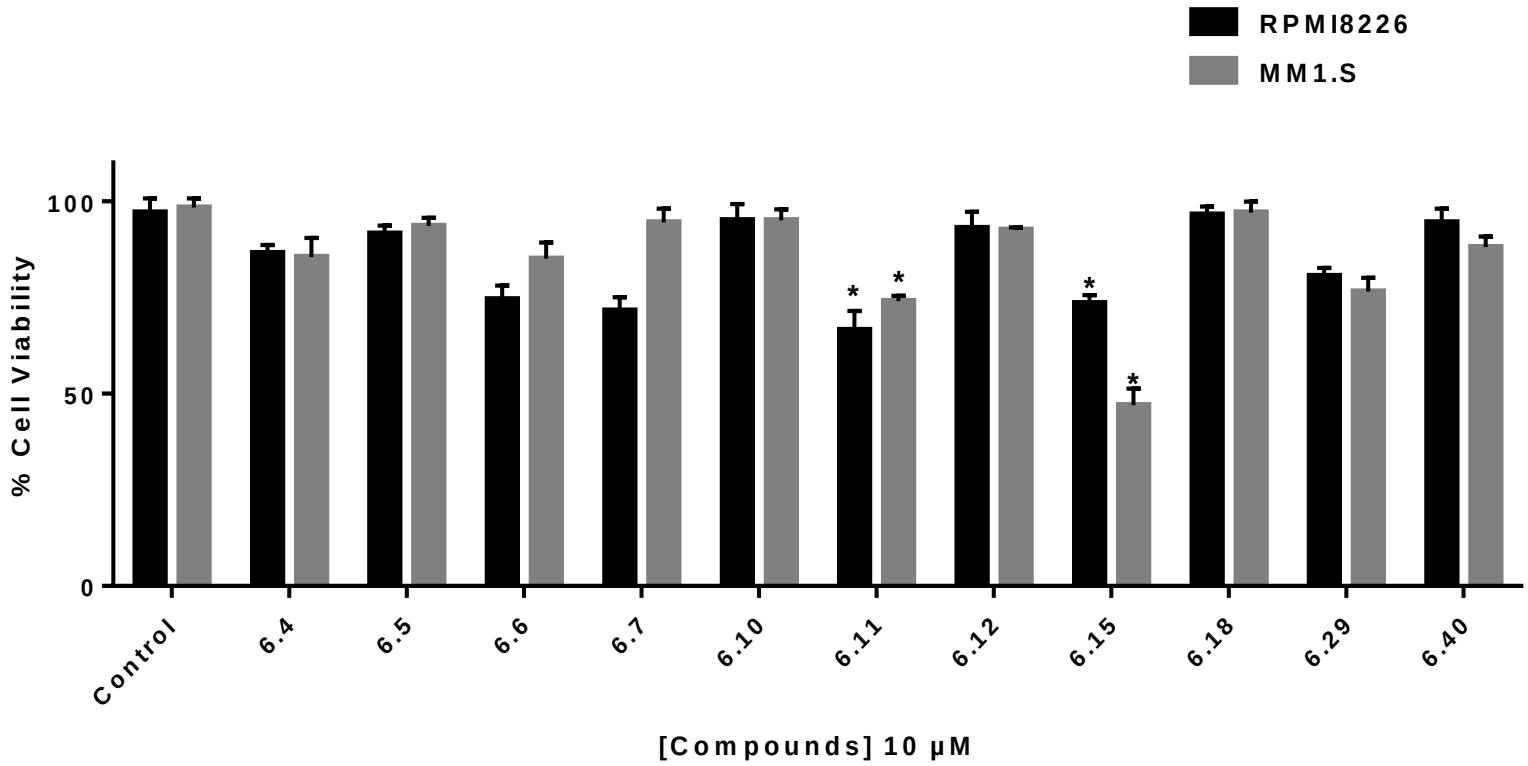

Figure 6.6. Anti-proliferation effects of the 4-(aminomethyl)-*N*,*N*-diethylaniline derivatives on MM cell-lines.

Two multiple myeloma cell-lines (MM1.S and RPMI8226) were utilized to study the anti-proliferation effects of the synthesized derivatives. Cells were plated at density of 3×10^3/well in 96-well plates. Cells were incubated with 10 µM concentration of the tested derivatives for 3 days. The cell viability was determined with the MTT assay. Compounds **6.11** and **6.15** exhibited cell viability of < 75% (inhibition rate > 45%). Data is the mean ± SD of three experiments carried out in triplicates. *P < 0.05 compared to the control.

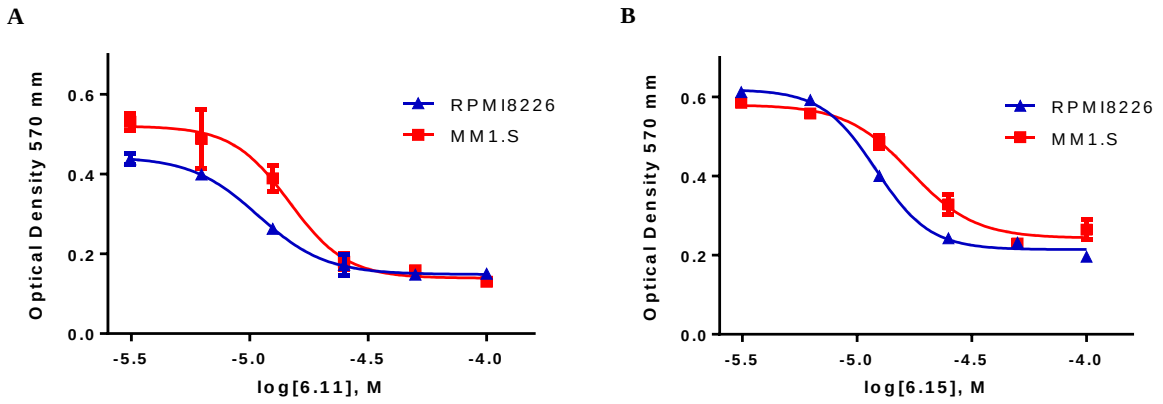

Figure 6.7. IC_{50} determination curve for the 4-(aminomethyl)-*N*,*N*-diethylaniline derivatives

50% inhibitory concentration of compounds **6.11**, and **6.15** were measured by utilizing the MTT colorimetric assay. Multiple myeloma cell-lines (MM1.S and RPMI8226) were utilized to study the anti-proliferation effects of the synthesized derivatives. Cells were plated at density of 3×10^3/well in 96-well plates. The cell viability was determined with the MTT assay. **(A)** IC_{50} of **6.11** = 5.1 µM and 6.0 µM for RPMI8226 and MM1.S cell-lines, respectively. **(B)** IC_{50} of **6.15** = 8.3 µM and 7.6 µM for RPMI8226 and MM1.S cell-lines, respectively. Data is the mean ± SD of three experiments carried out in triplicates

6.2.6 Cytotoxicity Studies of Compounds 6.15 and 6.18

Our newly discovered compounds **6.15** and **6.18** showed promising inhibition effects on osteoclastogenesis (osteoclast formation). To examine whether the impaired osteoclastogenesis effects of compounds **6.15** and **6.18** is due to decrease in the viability of the precursor cells not due to toxic effects, we investigated the cytotoxicity profile of these two compounds on osteoclast precursors RAW 264.7 and mouse bone marrow macrophages (BMM) by the MTT colorimetric cell viability assay. The assay was carried out as outlines in Chapter 3. First, RAW 264.7 cells and mouse BMM were plated on 96-well plates and incubated with compounds **6.15** and **6.18** for 3 days. The percentage of cell survival was determined with the MTT assay.

The results showed that cell viability was not significantly affected by the two compounds in comparison to the vehicle control group at 2.5 μM and 5 μM. Minor effects on cell viability were observed at higher concentrations 10 μM and 20 μM (Figure 6.8 and Figure 6.9). These results suggest that our newly discovered compounds have favorable therapeutic index and the effects on osteoclast differentiation were not derived from cytotoxicity effects.

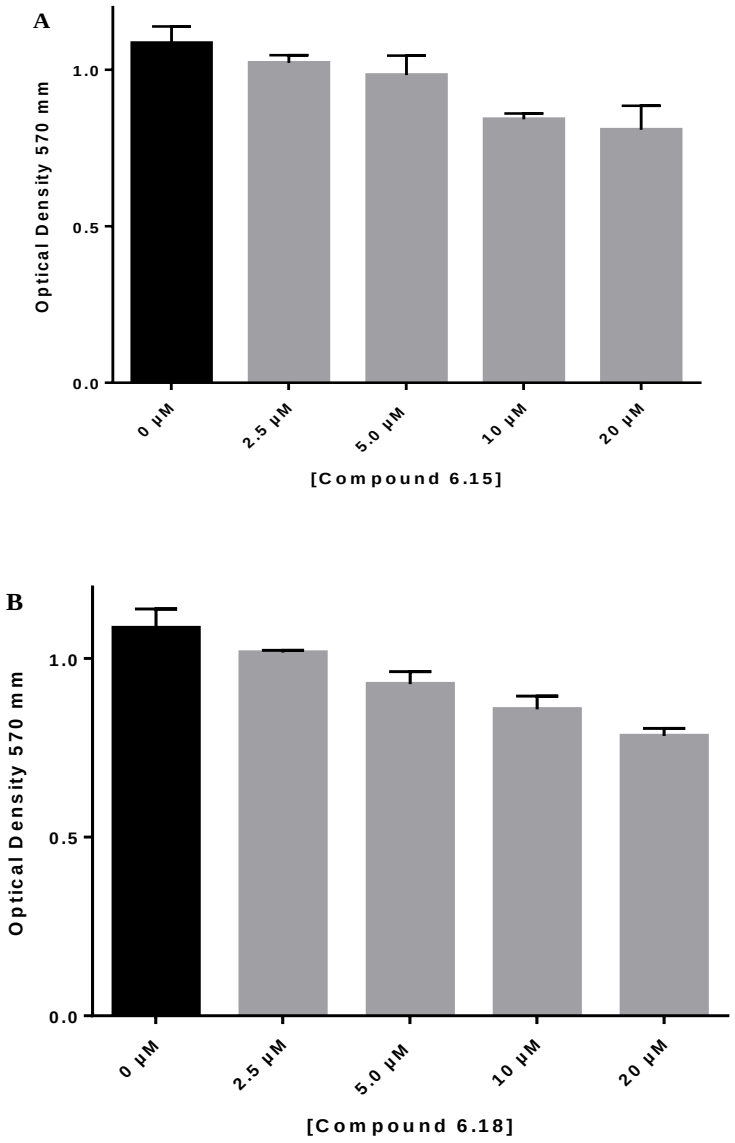

Figure 6.8. Cytotoxic effects of compounds 6.15 and 6.18 on RAW264.7 Cell-line.

Murine myeloid cell line (RAW264.7) cells were plated at density of 3×10^3/well on 96-well plates. Cells were incubated with the indicated doses of compounds **(A) 6.15** and **(B) 6.18** for 3 days. The cell viability was determined with the MTT assay. The data are the mean ± SD of two experiments carried out in triplicates. All test samples showed statistical non-significant (P>0.05) compared to control.

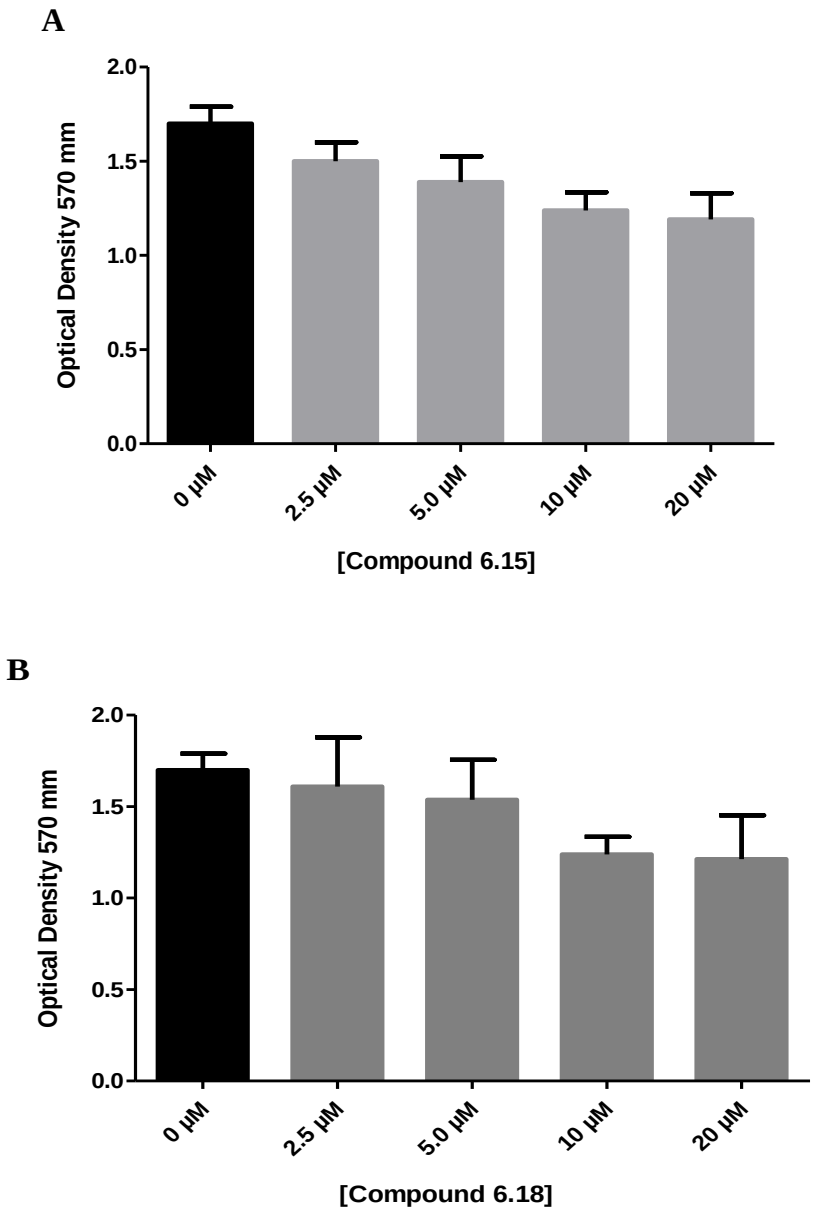

Figure 6.9. Cytotoxic effects of compounds 6.15 and 6.18 on BMM

Mouse BMM were plated at density of 3×10^3/well on 96-well plates. Cells were incubated with the indicated doses of compounds **(A) 6.15** and **(B) 6.18** for 3 days. The cell viability was determined with the MTT assay. The data are the mean ± SD of two experiments carried out in triplicates. All test samples showed statistical non-significant (P>0.05) compared to control.

6.2.7 Pharmacokinetic/Pharmacodynamic Studies of 6.11 and 6.15

The two highly potent and selective compounds **6.11** and **6.15** were evaluated for their pharmacokinetic properties. As demonstrated in Table 6.5, after oral administration, **6.11** exhibited an elimination half-life ($t_{1/2}$) of 1.646 hours and the maximum serum concentration was 87.03 µg/L in 0.19 hour and a clearance of 114.9 L/h/kg (Table 6.5). However, after iv administration, the elimination half-life was improved dramatically (14.79 h), maximum serum concentration was 422.10 µg/L in 0.08 h with a clearance of 4.56 L/h/kg (Table 6.5).

Table 6.5. Pharmacokinetic properties of 6.11

Parameter	Unit	Route of Administration	
		p.o.	i.v.
AUC	µg/L*h	160.3	336.30
$t_{1/2}$	h	1.65	14.79
T_{max}	h	0.19	0.08
Vd	L/kg	269.3	96.59
CL	L/h/kg	114.9	4.53
C_{max}	µg/L	87.03	422.10

Data is the mean of three rats.

Abbreviations: Cmax, peak plasma concentration of a drug after administration; Tmax, time to reach Cmax; $t_{1/2}$, elimination half-life; AUC, area under the concentration−time curve; CL, clearance; V, volume of distribution; p.o., per oral; i.v., intravenous.

Compound **6.15** exhibited an elimination half-life of 0.45 h after an oral administration. However, improved PK profiles was also observed after i.v. administration. The elimination half-life was 10.49 h, maximum serum concentration was 340.32 µg/L in 0.25 h, and the clearance was 3.56 L/h/kg after i.v. administration. (Table 6.6).

Table 6.6. Pharmacokinetic properties of 6.15

Parameter	Unit	Route of Administration	
		p.o.	i.v.
AUC	µg/L*h	11.50	298.52
$t_{1/2}$	h	0.45	10.49
T_{max}	h	0.50	0.25
Vd	L/kg	1.56	21.56
CL	L/h/kg	1649.10	3.56
C_{max}	µg/L	13.95	340.32

Data is the mean of three rats.

Abbreviations: Cmax, peak plasma concentration of a drug after administration; Tmax, time to reach Cmax; $t_{1/2}$, elimination half-life; AUC, area under the concentration−time curve; CL, clearance; V, volume of distribution; p.o., per oral; i.v., intravenous.

6.2.8 3D Quantitative Structure Activity Relationship (QSAR)

3D QSAR modeling studies were carried out on our synthesized derivatives in order to correlate the theoretical SAR model data and the experimental SAR data for further SAR studies. 3D QSAR CoMFA studies were carried out based on our published protocol [223, 224]. Compound **6.11** was chosen as a template compound in our CoMFA studies. Molecular dynamic simulations and molecular mechanics (MD/MM) were carried to search for the preferred conformation of compound **6.11**. The resulted conformations were compared with the docking pose conformation that resulted from molecular docking simulations using our in-house CB2 receptor homology model [225]. The closest conformation to the docking pose was chosen a template conformation. Compounds from training set (Table 6.7) and test set (Table 6.8) were subjected to molecular alignment to the preferred conformer of compound **6.11**. Figure 6.10 shows the final alignment of the training set and the test set.

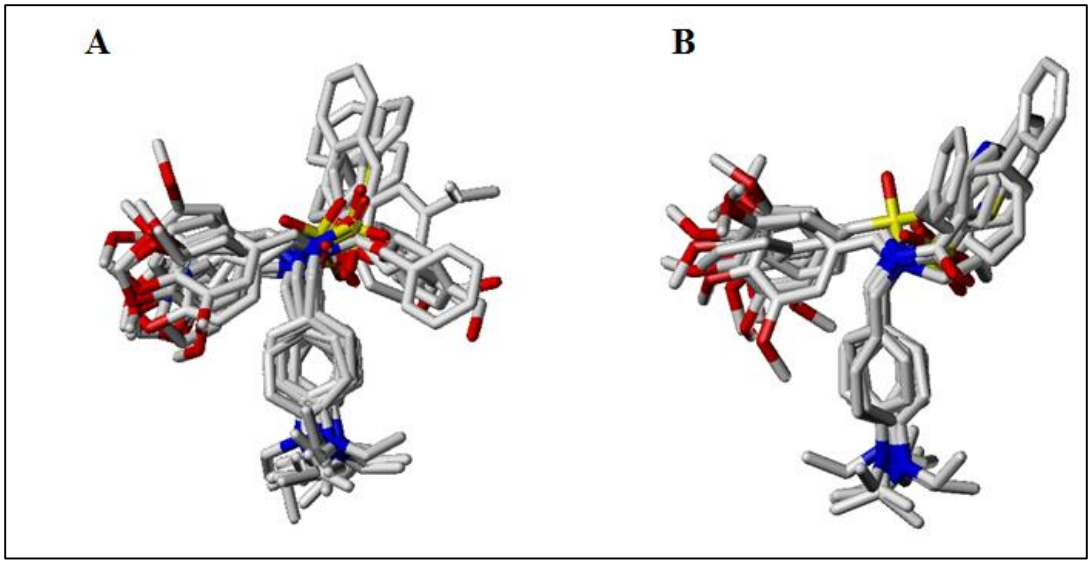

Figure 6.10. Database alignment to reference compound 6.11

Database alignment was achieved using the multi-fit module in SYBYL X 1.3 and manual alignment. **(A)** Training set database alignments to active molecule **6.11**. **(B)** Test set database alignments to the active molecule **6.11**

Partial least-square (PLS) analysis was performed using leave-one-out cross-validation (LOOCV). Leave-one-out cross-validation analysis is a method where each training sample is left out repeatedly and systemically in each training round to determine the optimal number of components. The predictive ability of each CoMFA model was determined by the cross-validated r^2: The r^2 is defined as $r_{cv}^2 = (SD - PRESS)/SD$, where SD is the sum of the squared deviations between the biological activity of the molecules. PRESS is the sum of all the squared deviations between the actual and predicted activity values.

The PLS analysis demonstrated that the optimal number of components was 6 and r_{cv}^2 was 0.503. The correlation coefficient (r^2) for the non-cross validated PLS analysis was 0.989 with a standard error of estimate (SEE) of 0.012. The field contribution of steric and electrostatic were 0.398 and 0.602, respectively. These results indicate that the trained CoMFA model correlates the structural information of the synthesized analogs to their CB2 receptor affinities. Further, the model was used to predict the binding affinities of test set compounds differing from those used before in the training set in order to evaluate our generated CoMFA model generalization ability. The correlation coefficient (r^2) for the test set was 0.956. Such results indicate that the CoMFA model had good generalization performance on the test set molecules. Figure 6.11 show the regression lines of the experimental and predicted activity of the training and test sets, respectively. The two regression lines display good linearity fit between the experimental pK_i and the predicted pK_i values indicating that the developed CoMFA model is able to predict CB2 receptor binding affinity (Figure 6.11).

Table 6.7. Experimental (expt.) and predicted (pred.) pK_i values of 4-(aminomethyl)-*N*,*N*-diethylaniline derivatives in the training set

Compd.	CB2 K_i (nM)	pK_i (expt.)	pK_i (pred.)	Residual
6.5	291	6.536107	6.537	-0.00089
6.8	230	6.638272	6.642	-0.00373
6.17	657	6.182435	6.18	0.002435
6.41	1139	5.943476	5.953	-0.00952
6.42	3147	5.502103	5.491	0.011103
6.11	99	6.970616	6.959	0.011616
6.24	866	6.062482	5.883	0.179482
6.13	990	6.004365	6.012	-0.00764
6.21	1020	5.9914	5.98	0.0114
6.18	242	6.616185	6.63	-0.01382
6.17	657	6.182435	6.167	0.015435
6.14	157	6.8041	6.795	0.0091
6.29	381	6.419075	6.074	0.345075
6.30	1872	5.727694	5.733	-0.00531
6.33	882	6.054531	6.045	0.009531
6.39	1852	5.732359	5.72	0.012359
6.31	775	6.110698	6.115	-0.0043
6.32	574	6.241088	6.254	-0.01291

pK_i calculated as –log K_i

Residual is the difference between pK_i (experimental) and pK_i (predicted).

Table 6.8. Experimental (expt.) and predicted (pred.) pKi values of 4-(aminomethyl)-*N*,*N*-diethylaniline derivatives in the test set

Compd.	CB2 K_i (nM)	pK_i (expt.)	pK_i (pred.)	Residual
6.4	410	6.387216	6.226	0.161216
6.40	362	6.441291	6.469	-0.02771
6.37	515	6.288193	6.21	0.078193
6.12	249	6.603801	6.689	-0.0852
6.23	899	6.04624	6.185	-0.13876
6.25	946	6.024109	6.195	-0.17089
6.15	138	6.860121	6.899	-0.03888
6.22	1205	5.919013	5.896	0.023013
6.16	639	6.194499	6.095	0.099499
6.6	387	6.412289	6.466	-0.05371
6.7	453	6.343902	6.469	-0.1251
6.11	99	6.970616	6.956	0.014616

pK_i calculated as –log K_i

Residual is the difference between pK_i (experimental) and pK_i (predicted).

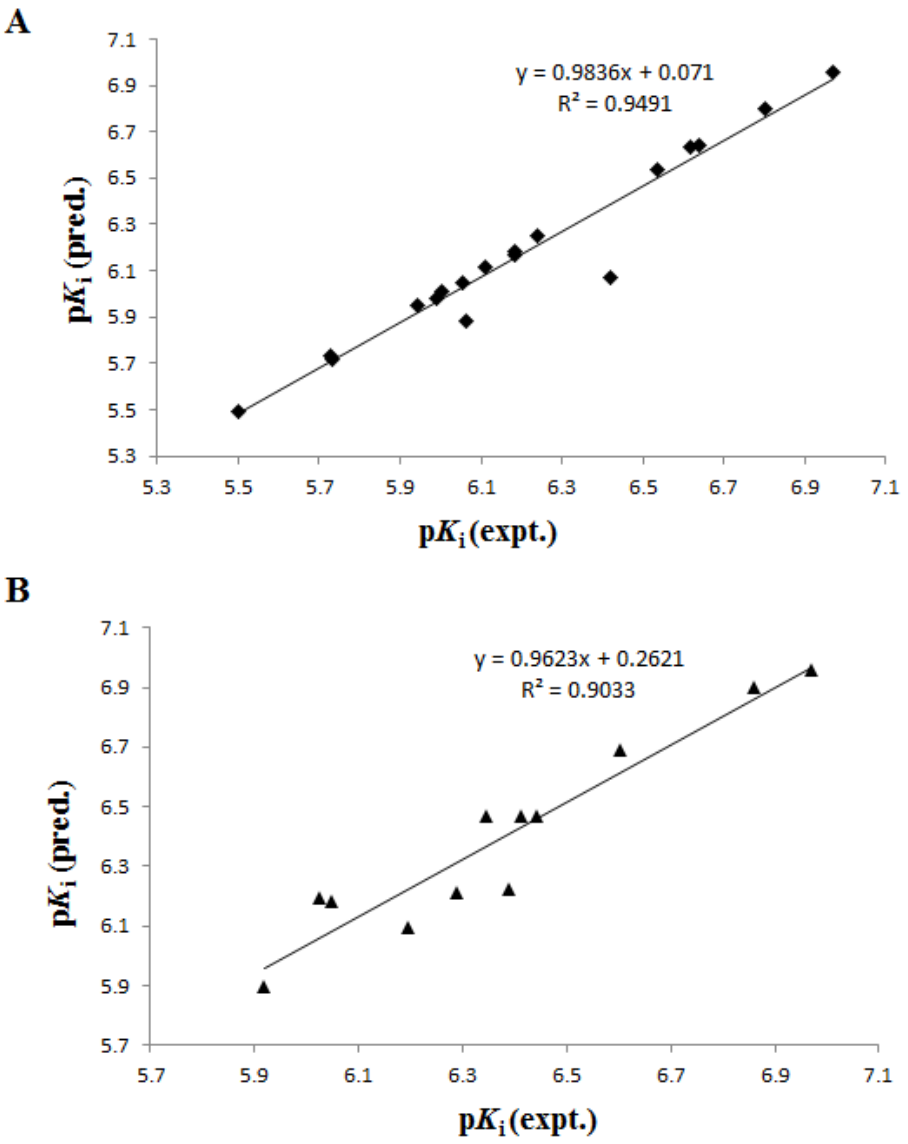

Figure 6.11. Plots of CoMFA-calculated and experimental binding affinity.

(A) CoMFA calculated and experimental binding affinity correlation for the training set. **(B)** CoMFA calculated and experimental binding affinity correlation for the test set.

CoMFA contour maps were then generated to predict the favorable and unfavorable regions of the new derivatives for CB2 binding affinity. The CoMFA contour maps display the color-coded steric and electrostatic regions around the molecules relating the ligands to their biological activities. Steric regions are displayed in green and yellow color-coding for sterically favored interactions and sterically unfavored interactions for the binding affinity, respectively. On the other hand, the electrostatic interactions are depicted in blue and red color-coding. The electropositive favored regions are displayed in blue contours while electronegative favored regions are displayed in red contours. As shown in Figure 6.12, a sterically favored region is present near the R1 position indicating that the introduction of bulky groups in this position will enhance the CB2 binding affinity. Also, at position R2, there is a large sterically unfavored region indicating that bulky groups at this position will negatively affect the binding affinity. In addition, electronegative interactions are preferred near the R1 position as highlighted by the blue region. Further, electropositive interactions are preferred near the R2 position as highlighted by the red region.

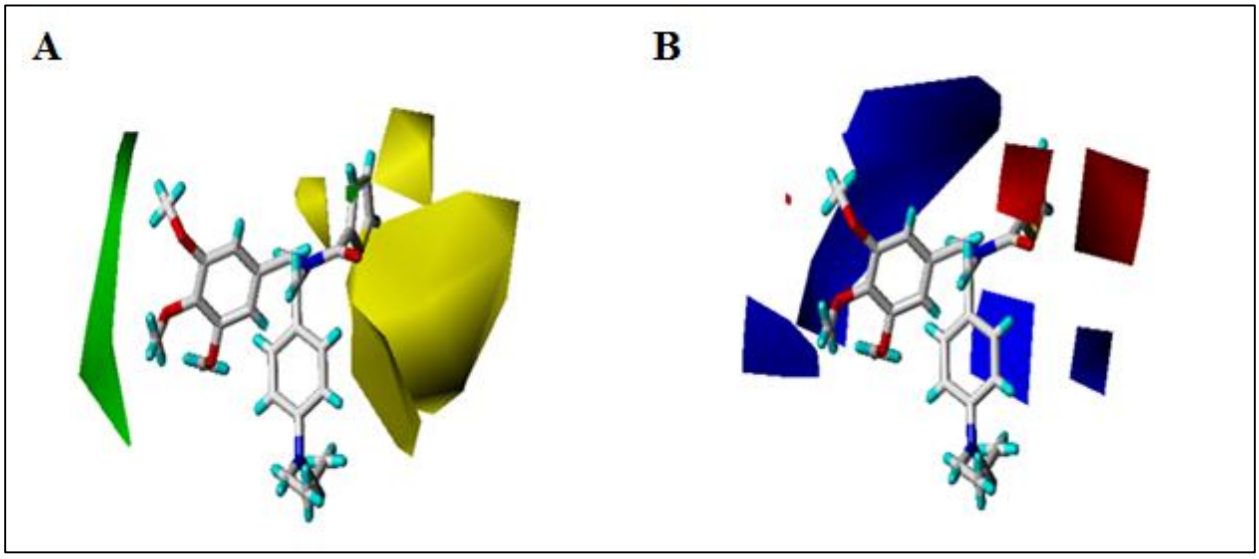

Figure 6.12. CoMFA contour maps of compound 6.11 showing steric and electrostatic interactions

Contour maps were generated using the QSAR module in SYBYL X1.3. Compound **6.11** was used as the reference molecule for QSAR model generation. **(A)** Sterically (bulk) favored areas are color-coded in green and sterically unfavored areas are in yellow. **(B)** The blue and red contours reflect whether electropositive or electronegative substituents, respectively, are favored at a particular position.

6.3 CONCLUSION

In this series, we have carried-out high throughput molecular docking screening of the NCI-2010 chemical database utilizing our 3D CB2 homology model in order to identify a novel chemical scaffold. As a result, the lead compound, (((4-nitrophenyl)methylenedisulfonyl)bis(methylene))dibenzene (compound **6.1**) was discovered. Compound **6.1** was subjected to medicinal chemistry structural modifications based on molecular docking studies aiming at increasing the CB2 affinity and potency synthesizing 42 analogs and evaluating their binding affinity and selectivity for the CB2/CB1 receptors in further SAR studies. Among the 42 analogs, nine compounds exhibited high binding affinity to the CB2 receptor (CB2 K_i < 500 nM) as well as optimal CB2 selectivity (CB1/CB2 of 7 to 145 fold). Top three compounds were measured in functional assays to evaluate their cellular properties. Compounds **6.15** and **6.18** behaved as inverse agonists, while compound **6.11** behaved as an agonist. Compound **6.11,** *N*-(4-(diethylamino)benzyl)-*N*-(3,4,5-trimethoxybenzyl)thiophene-2-carboxamide, represents a novel CB2 agonist. Consistent with previous results, the compounds behaving as inverse agonists (**6.15** and **6.18**) showed potent inhibitory activity on RANKL-induced osteoclast formation. While the agonist, **6.11**, stimulated the RANKL-induced osteoclast formation at high doses. The cytotoxicity studies of compounds **6.15** and **6.18** on RAW 264.7 and bone marrow macrophages (BMM) demonstrated low cytotoxicity effects as utilized by the MTT assay proving that the anti-OCL effects were not due to cytotoxicity. These results indicate that CB2 inverse agonists are potential agents for osteoporosis treatment.

The anti-proliferative effects on multiple myeloma of the top three compounds were evaluated by performing the MTT cell-viability assay utilizing two anti-MM cell-lines (RPMI 8226 and MM1.S). Compound **6.11** showed an inhibitory effect with IC_{50} of 5.1 μM and 6.0 on

RPMI 8226 and MM1.S, respectively. While compound **6.15** showed moderate inhibitory effects on these cell-lines (IC_{50} > 7 μM) suggesting that CB2 agonists holds promising effects as anti-MM agents. In addition, as the CB2 inverse agonist **6.15** showed high OCL inhibitory effects and good MM inhibition effects, this may be potential dual ligand treating MM while preventing bone lesions associated with MM disease.

In addition, we carried out pharmacokinetic studies in order to analyze the PK properties of our new scaffold. Compounds **6.11** and **6.15** were utilized in the *in-vivo* PK studies. The new scaffold showed improved PK profile as demonstrated with improved elimination half-life and clearance for both compounds especially after intravenous administration. These results indicate that our new scaffold is more stable than the di-amide scaffold.

Furthermore, 3D QSAR studies also confirmed our finding correlating experimental biological evaluations with mathematical calculations. The QSAR studies generated a CoMFA model that can be utilized for further design of CB2 ligands possessing high potency and selectivity.

6.4 EXPERIMENTAL

6.4.1 Chemistry

6.4.1.1 General Synthesis Procedure of Secondary Amine Building Blocks

(*E*)-*N*,*N*-diethyl-4-(((3,4,5-trimethoxybenzyl)imino)methyl)aniline (6.2).

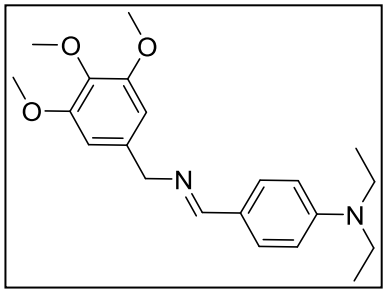

(3,4,5-trimethoxyphenyl)methanamine (1972 mg, 10 mmol) was added slowly to a solution of 4-(diethylamino)benzaldehyde (1770 mg, 10 mmol) and methanol (20 mL). The reaction mixture was stirred and refluxed for 12 h. The reaction mixture was cooled to room temperature, and the solvent was removed by evaporation in vacuum to give the crude compound **6.2**, which was used in the next step without further purification.

***N*,*N*-diethyl-4-(((3,4,5-trimethoxybenzyl)amino)methyl)aniline (6.3).**

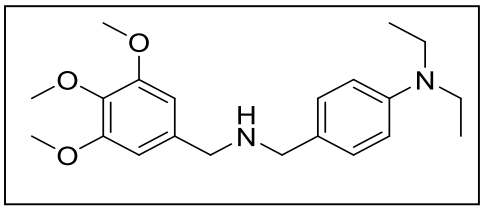

The crude compound (*E*)-*N*,*N*-diethyl-4-(((3,4,5-trimethoxybenzyl)imino)methyl)aniline **(6.2)** was dissolved in methanol (20 mL), and $NaBH_4$ (570 mg, 15 mmol) was added. Stirring of the mixture was continued for 12 h at room temperature. The reaction solution was poured into water and extracted with EA. The combined organic layers were washed with water and brine and then dried over Na_2SO_4. The residue was purified by flash chromatography (ethyl acetate/petroleum ether, 1:2) on silica get to obtain the final product **(6.3)**. Yellow oil (3350 mg, yield: 93%). ^{1}H NMR (400 MHz, DMSO-d_6) δ 7.12 (d, J = 8.4 Hz, 2H), 6.65 (s, 2H), 6.62 (d, J = 8.8 Hz, 2H), 3.76 (s, 6H), 3.64 (s, 3H), 3.60 (s, 2H), 3.54 (s, 2H), 1.07 (t, J = 7.2 Hz, 6H). LC-MS (ESI): *m/z* 359.0 $(M + H)^+$.

(*E*)-*N*,*N*-diethyl-4-(((pyridin-3-ylmethyl)imino)methyl)aniline (6.19).

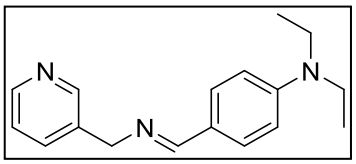

Compound **6.19** was prepared from pyridin-3-ylmethanamine (1081 mg, 10 mmol) and 4-(diethylamino)benzaldehyde (1770 mg, 10 mmol). The crude compound **6.19** was used in the next step without further purification.

***N*,*N*-diethyl-4-(((pyridin-3-ylmethyl)amino)methyl)aniline (6.20).**

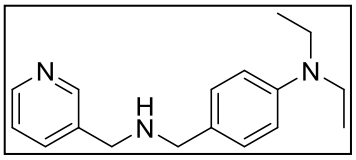

Compound **6.20** was prepared from the crude compound (*E*)-*N*,*N*-diethyl-4-(((pyridin-3-ylmethyl)imino)methyl)aniline **(6.19)** and $NaBH_4$ (570 mg, 15 mmol). The residue was purified by flash chromatography (methanol/DCM, 1:9) on silica get to obtain the final product **(6.20)**. Yellow oil (1140 mg, yield: 84%). ^{1}H NMR (400 MHz, DMSO-d_6) δ 8.52 (s, 1H), 8.51–8.43 (m, 1H), 7.76-7.32 (m, 1H), 7.36–7.32 (m, 1H), 7.11 (d, J = 8.4 Hz, 2H), 6.61 (d, J = 8.8 Hz, 2H), 3.68 (s, 2H), 3.54 (s, 2H), 3.31–3.28 (m, 4H), 2.85 (s, 1H), 1.07 (t, J = 6.8 Hz, 6H). LC-MS (ESI): *m/z* 270.2 $(M + H)^+$.

(*Z*)-4-(((benzo[*d*][1,3]dioxol-5-ylmethyl)imino)methyl)-*N*,*N*-diethylaniline (6.27).

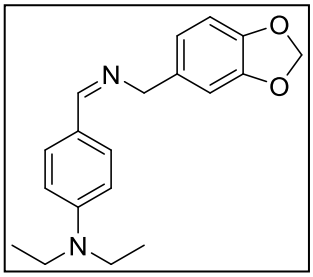

Compound **6.27** was prepared from benzo[*d*][1,3]dioxol-5-ylmethanamine (1511 mg, 10 mmol) and 4-(diethylamino)benzaldehyde (1770 mg, 10 mmol). The crude compound **6.27** was used in the next step without further purification.

4-(((benzo[*d*][1,3]dioxol-5-ylmethyl)amino)methyl)-*N*,*N*-diethylaniline (6.28). Compound

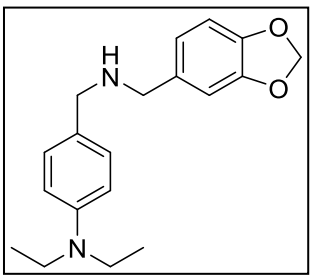

6.28 was prepared from the crude compound (*Z*)-4-(((benzo[*d*][1,3]dioxol-5-ylmethyl)imino)methyl)-*N*,*N*-diethylaniline **(6.27)** and NaBH4 (570 mg, 15 mmol). The residue was purified by flash chromatography (ethyl acetate/petroleum ether, 1:2) on silica get to

obtain the final product **(6.28)**. Yellow oil (2900 mg, yield: 92%). ^{1}H NMR (400 MHz, DMSO-d_6) δ7.09 (d, J = 8.4 Hz, 2H), 6.92 (s, 1H), 6.92–6.78 (m, 1H), 6.76 (d, J = 8.8 Hz, 2H), 5.98 (s, 2H), 3.57 (s, 2H), 3.50 (s, 2H), 3.31–3.27 (m, 4H), 1.07 (t, J = 7.2 Hz, 6H). LC-MS (ESI): *m/z* 313.3 $(M + H)^+$.

(*Z*)-*N*,*N*-diethyl-4-((pentylimino)methyl)aniline (6.35).

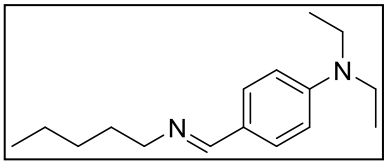

Compound **6.25** was prepared from pentan-1-amine (871 mg, 10 mmol) and 4-(diethylamino)benzaldehyde (1770 mg, 10 mmol). The crude compound **6.35** was used in the next step without further purification.

***N*,*N*-diethyl-4-((pentylamino)methyl)aniline (6.36).**

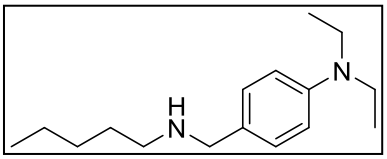

Compound **6.36** was prepared from the crude compound (*Z*)-*N*,*N*-diethyl-4-((pentylimino)methyl)aniline **(6.35)** and (570 mg, 15 mmol). The residue was purified by flash chromatography (ethyl acetate/petroleum ether, 2:1) on silica get to obtain the final product **(6.36)**. Yellow oil, (2450 mg, yield: 99%).^{1}H NMR (600 MHz, DMSO-d_6) δ7.08 (d, J = 13.2 Hz, 2H), 6.59 (d, J = 13.2 Hz, 2H), 3.52 (s, 2H), 3.31–3.27 (m, 4H), 2.47–2.43 (m, 2H), 1.42–1.39 (m, 2H0, 1.28–1.24 (m, 4H), 1.07 (t, J = 10.2 Hz, 6H), 0.85 (t, J = 7.80 Hz, 3H). LC-MS (ESI): *m/z* 249.4 $(M + H)^+$.

6.4.1.2 General Procedure for the Coupling Reaction Between Secondary Amine and Acyl Chloride or Sulfonic Chloride

***N*-(4-(diethylamino)benzyl)-4-methoxy-*N*-(3,4,5-trimethoxybenzyl)benzenesulfonamide**

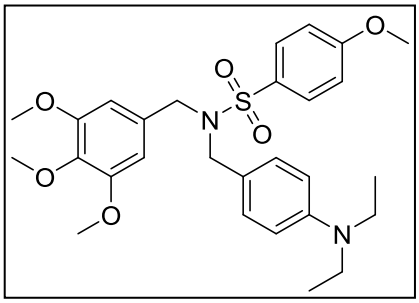

(6.4). The intermediate *N*,*N*-diethyl-4-(((3,4,5-trimethoxybenzyl)amino)methyl)aniline (compound **6.3**) (358 mg, 1.0 mmol) in dichloromethane (DCM, 10 mL) was chilled in ice bath with the exclusion of moisture, and then triethylamine (TEA, 121 mg, 1.2 mmol) was added to it. The resulting solution was treated dropwise under stirring with 4-methoxybenzenesulfonyl chloride (206 mg, 1.0 mmol), also dissolved in DCM, over 30 min at 0 ºC and then left overnight at room temperature. The reaction solution was poured into water and extracted with EA. The combined organic layers were washed with water and brine and then dried over Na_2SO_4. The mixture was filtered and the solvent was evaporated in vacuum. The residue was purified by flash chromatography (ethyl acetate/petroleum ether, 1:2) on silica gel to obtain *N*-(4-(diethylamino)benzyl)-4-methoxy-*N*-(3,4,5-trimethoxybenzyl)benzenesulfonamide **(6.4)**. Yellow solid (432 mg, yield: 82%). ^{1}H NMR (400 MHz, DMSO-d_6) δ 7.82 (d, J = 9.2 Hz, 2H), 7.14 (d, J = 8.8 Hz, 2H), 6.94 (d, J = 8.8 Hz, 2H), 6.54 (d, J = 8.8 Hz, 2H), 6.23 (s, 2H), 4.14 (d, J = 8.0 Hz, 4H), 3.86 (s, 3H), 3.59 (s, 3H), 3.58 (s, 6H), 3.31–3.28 (m, 5H), 1.05 (t, J = 6.8 Hz, 6H). LC-MS (ESI): *m/z* 529.1 $(M + H)^+$.

***N*-(4-(diethylamino)benzyl)-3-methyl-*N*-(3,4,5-trimethoxybenzyl)benzenesulfonamide (6.5).**

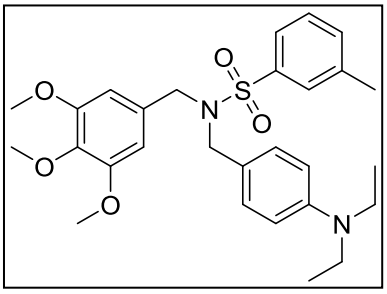

Compound **6.5** was prepared from the intermediate *N*,*N*-diethyl-4-(((3,4,5-trimethoxybenzyl)amino)methyl)aniline (compound **6.3**) (358 mg, 1.0 mmol) and 3-methylbenzenesulfonyl chloride (190 mg, 1.0 mmol). The residue was purified by flash chromatography (ethyl acetate/petroleum ether, 1:2) on silica gel to obtain *N*-(4-(diethylamino)benzyl)-3-methyl-*N*-(3,4,5-trimethoxybenzyl)benzenesulfonamide **(6.5)**. Yellow solid (331 mg, yield: 64%). ^{1}H NMR (400 MHz, DMSO-d_6) δ 7.68–7.64 (m, 2H), 7.50 (d, J = 5.6 Hz, 1H), 7.49 (s, 1H), 6.95 (d, J = 8.80 Hz, 2H), 6.55 (d, J = 8.8 Hz, 2H), 6.25 (s, 2H), 4.18 (d, J = 8.0 Hz, 4H), 3.59 (s, 9H), 3.31–3.27 (m, 4H), 2.39 (s, 3H), 1.06 (t, J = 7.2 Hz, 6H). LC-MS (ESI): *m/z* 513.3 $(M + H)^+$.

***N*-(4-(diethylamino)benzyl)-4-methyl-*N*-(3,4,5-trimethoxybenzyl)benzenesulfonamide (6.6).**

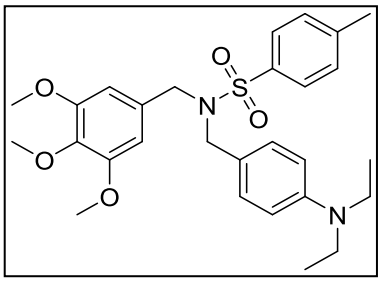

Compound **6.6** was prepared from the intermediate *N*,*N*-diethyl-4-(((3,4,5-trimethoxybenzyl)amino)methyl)aniline (compound **6.3**) (358 mg, 1.0 mmol) and 4-methylbenzenesulfonyl chloride (190 mg, 1.0 mmol). The residue was purified by flash chromatography (ethyl acetate/petroleum ether, 1:2) on silica gel to obtain *N*-(4-(diethylamino)benzyl)-4-methyl-*N*-(3,4,5-trimethoxybenzyl)benzenesulfonamide **(6.6).** Yellow solid (322 mg, yield: 62%). ^{1}H NMR (400 MHz, DMSO-d_6) δ 7.77 (d, J = 8.4 Hz, 2H), 7.43 (d, J = 8.0 Hz, 2H), 6.95 (d, J = 8.8 Hz, 2H), 6.54 (d, J = 8.8 Hz, 2H), 6.21 (s, 2H), 4.15 (d, J = 8.4 Hz, 4H), 3.59 (s, 3H), 3.58 (s, 6H), 3.30–3.26 (m, 4H), 2.42 (s, 3H), 1.06 (t, J = 7.20 Hz, 6H). LC-MS (ESI): *m/z* 513.3 $(M + H)^+$.

***N*-(4-(diethylamino)benzyl)-*N*-(3,4,5-trimethoxybenzyl)benzenesulfonamide (6.7).**

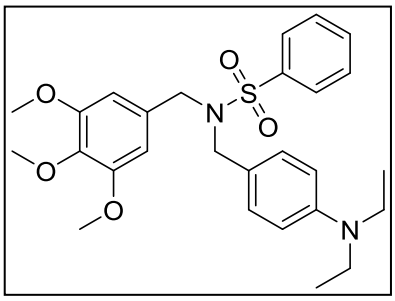

Compound **6.7** was prepared from the intermediate *N*,*N*-diethyl-4-(((3,4,5-trimethoxybenzyl)amino)methyl)aniline (compound **6.3**) (358 mg, 1.0 mmol) and benzenesulfonyl chloride (176 mg, 1.0 mmol). The residue was purified by flash chromatography (ethyl acetate/petroleum ether, 1:2) on silica gel to obtain *N*-(4-(diethylamino)benzyl)-*N*-(3,4,5-trimethoxybenzyl)benzenesulfonamide **(6.7)**. Brown solid (359 mg, yield: 72%). ^{1}H NMR (400 MHz, DMSO-d_6) δ 7.90 (d, J = 7.2 Hz, 2H), 7.71–7.63 (m, 3H), 6.93 (d, J = 8.8 Hz, 2H), 6.54 (d, J = 8.8 Hz, 2H), 6.23 (s, 2H), 4.18 (d, J = 6.8 Hz, 4H), 3.59 (s, 3H), 3.58 (s, 6H), 3.30–3.26 (m, 4H), 1.07 (t, J = 7.2 Hz, 6H). LC-MS (ESI): *m/z* 499.1 $(M + H)^+$.

***N*-(4-(diethylamino)benzyl)-4-isopropyl-*N*-(3,4,5-trimethoxybenzyl)benzenesulfonamide (6.8).**

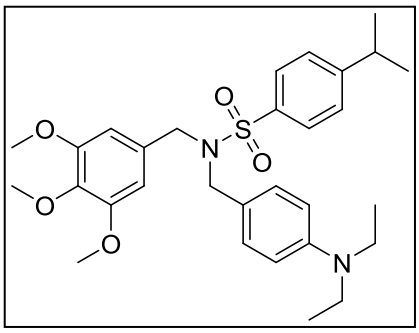

Compound **6.8** was prepared from the intermediate *N*,*N*-diethyl-4-(((3,4,5-trimethoxybenzyl)amino)methyl)aniline (compound **6.3**) (358 mg, 1.0 mmol) and 4-isopropylbenzenesulfonyl chloride (218 mg 1.0 mmol). The residue was purified by flash chromatography (ethyl acetate/petroleum ether, 1:2) on silica gel to obtain *N*-(4-(diethylamino)benzyl)-4-isopropyl-*N*-(3,4,5-trimethoxybenzyl)benzenesulfonamide **(6.8)**. Brown solid (229 mg, yield: 42%). ^{1}H NMR (400 MHz, DMSO-d_6) δ 7.80 (d, J = 8.40 Hz, 2H), 7.49 (d, J = 8.40 Hz, 2H), 6.93 (d, J = 8.40 Hz, 2H), 6.54 (d, J = 8.80 Hz, 2H), 6.23 (s, 2H), 4.18 (d, J = 7.20 Hz, 4H), 3.59 (s, 3H), 3.58 (s, 6H), 3.31–3.26 (m, 4H), 3.04–2.98 (m, 1H), 1.25 (d, J = 6.80 Hz, 6H), 1.06 (t, J = 6.80 Hz, 6H). LC-MS (ESI): *m/z* 541.20 $(M + H)^+$.

***N*-(4-(diethylamino)benzyl)-*N*-(3,4,5-trimethoxybenzyl)naphthalene-2-sulfonamide (6.9).**

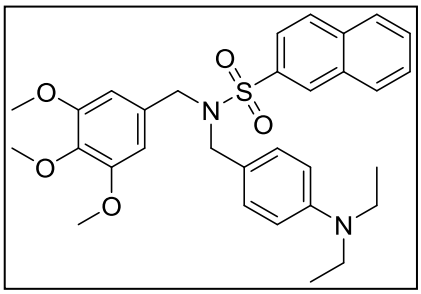

Compound **6.9** was prepared from the intermediate *N*,*N*-diethyl-4-(((3,4,5-trimethoxybenzyl)amino)methyl)aniline (compound **6.3**) (358 mg, 1.0 mmol) and 4-isopropylbenzenesulfonyl chloride (218 mg 1.0 mmol). The residue was purified by flash chromatography (ethyl acetate/petroleum ether, 1:2) on silica gel to obtain *N*-(4-(diethylamino)benzyl)-*N*-(3,4,5-trimethoxybenzyl)naphthalene-2-sulfonamide **(6.9)**. Yellow solid (454 mg, yield: 82%). ^{1}H NMR (400 MHz, DMSO-d_6) δ 8.52 (s, 1H), 8.16 (t, J = 8.4 Hz, 2H), 8.07, (d, J = 8.0 Hz, 1H), 7.91 (d, J = 1.6 Hz, 1H), 7.89–7.67 (m, 2H), 6.98 (d, J = 8.8 Hz, 2H), 6.53 (d, J = 8.8, 2H), 6.22 (s, 2H), 4.26 (s, 2H), 4.25 (s, 2H), 3.54 (s, 3H), 3.49 (s, 6H), 3.33–3.27 (m, 4H), 1.05 (t, J = 4.4 Hz, 6H). LC-MS (ESI): *m/z* 549.1(M + H)$^+$.

***N*-(4-(diethylamino)benzyl)-*N*-(3,4,5-trimethoxybenzyl)-[1,1'-biphenyl]-4-sulfonamide**

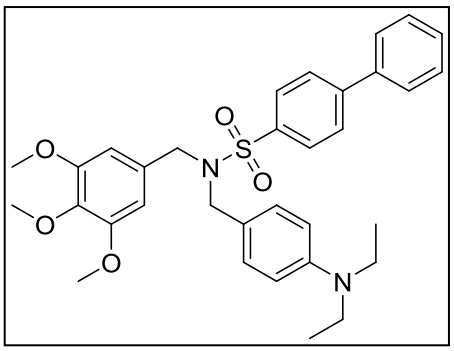

(6.10).

Compound **6.10** was prepared from the intermediate *N*,*N*-diethyl-4-(((3,4,5-trimethoxybenzyl)amino)methyl)aniline (compound **6.3**) (358 mg, 1.0 mmol) and 4-isopropylbenzenesulfonyl chloride (218 mg 1.0 mmol). The residue was purified by flash chromatography (ethyl acetate/petroleum ether, 1:2) on silica gel to obtain *N*-(4-(diethylamino)benzyl)-*N*-(3,4,5-trimethoxybenzyl)-[1,1'-biphenyl]-4-sulfonamide **(6.10)**. Yellow solid (365 mg, yield: 63%). ^{1}H NMR (400 MHz, DMSO-d_6) δ 7.97–7.89 (m, 4H), 7.75 (d, J = 7.2 Hz, 2H), 7.56–7.47 (m, 3H), 6.98 (d, J = 8.8 Hz, 2H), 6.55 (d, J = 8.8 Hz, 2H), 6.25 (s, 2H), 4.23 (d, J = 7.6 Hz, 4H), 3.57 (s, 9H), 3.27–3.26 (m, 4H), 1.05 (t, J = 6.8 Hz, 6H). LC-MS (ESI): *m/z* 575.1 (M + H)$^+$.

***N*-(4-(diethylamino)benzyl)-*N*-(3,4,5-trimethoxybenzyl)thiophene-2-carboxamide (6.11).**

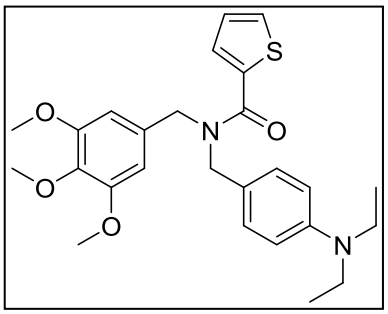

Compound **6.11** was prepared from the intermediate *N*,*N*-diethyl-4-(((3,4,5-trimethoxybenzyl)amino)methyl)aniline (compound **6.3**) (358 mg, 1.0 mmol) and thiophene-2-carbonyl chloride (146 mg 1.0 mmol). The residue was purified by flash chromatography (ethyl acetate/petroleum ether, 1:2) on silica gel to obtain *N*-(4-(diethylamino)benzyl)-*N*-(3,4,5-trimethoxybenzyl)thiophene-2-carboxamide **(6.11)**. Yellow oil (363 mg, yield: 77%). ^{1}H NMR (400 MHz, $CDCl_3$) δ 7.76 (s, 1H), 7.49 (t, J = 6.8 Hz, 2H), 7.35 (s, 1H), 7.15 (s, 1H), 7.015 (s. 1H), 6.70 (s, 1H), 6.49 (s, 2H), 4.67 (t, J = 9.6 Hz, 4H), 3.86 (s, 9H), 3.38 (d, J = 6.8 Hz, 3H), 3.15 (t, J = 5.2 Hz, 1H), 1.07 (d, J = 5.6 Hz, 6H). LC-MS (ESI): *m/z* 469.4 $(M + H)^+$.

***N*-(4-(diethylamino)benzyl)-*N*-(3,4,5-trimethoxybenzyl)quinoxaline-2-carboxamide (6.12).**

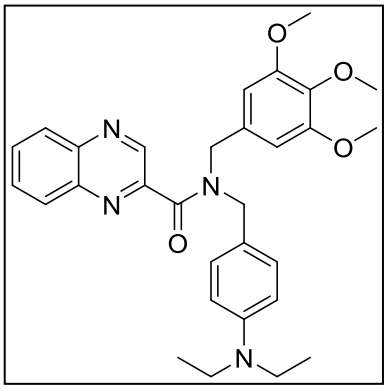

Compound **6.12** was prepared from the intermediate *N*,*N*-diethyl-4-(((3,4,5-trimethoxybenzyl)amino)methyl)aniline (compound **6.3**) (358 mg, 1.0 mmol) and quinoxaline-2-carbonyl chloride (192 mg 1.0 mmol). The residue was purified by flash chromatography (ethyl acetate/petroleum ether, 1:2) on silica gel to obtain *N*-(4-(diethylamino)benzyl)-*N*-(3,4,5-trimethoxybenzyl)quinoxaline-2-carboxamide **(6.12)**. Yellowish oil (400 mg, yield: 77%). ^{1}H NMR (400 MHz, DMSO-d_6) δ 8.92 (s, 1H), 8.16–8.09 (m, 2H), 7.98–7.93 (m, 2H), 7.27 (d, J = 8.8 Hz, 1H), 7.10 (d, J = 8.8 Hz, 1H), 6.70–6.58 (m, 3H), 6.25 (s, 1H), 4.62–4.49 (m, 4H), 1.052 (t, J = 3.6 Hz, 6H). LC-MS (ESI): *m/z* 515.2 $(M + H)^+$.

***N*-(4-(diethylamino)benzyl)-4-(trifluoromethoxy)-*N*-(3,4,5-trimethoxybenzyl)benzenesulfonamide (6.13).**

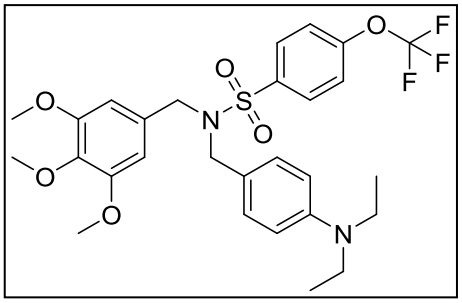

Compound **6.13** was prepared from the intermediate *N*,*N*-diethyl-4-(((3,4,5-trimethoxybenzyl)amino)methyl)aniline (compound **6.3**) (358 mg, 1.0 mmol) and 4-(trifluoromethoxy)benzenesulfonyl chloride (260 mg, 1.0 mmol. The residue was purified by flash chromatography (ethyl acetate/petroleum ether, 1:2) on silica gel to obtain *N*-(4-(diethylamino)benzyl)-4-(trifluoromethoxy)-*N*-(3,4,5-trimethoxybenzyl)benzenesulfonamide **(6.13)**. Yellow solid (455 mg, yield: 78 %). ^{1}H NMR (400 MHz, DMSO-d_6) δ 8.0 (d, J = 8.80 Hz, 2H), 7.59 (d, J = 8.0 Hz, 2H), 6.94 (d, J = 8.8 Hz, 2H), 6.54 (d, J = 8.8 Hz, 2H), 6.27 (s, 2H), 4.23 (d, J = 7.6 Hz, 4H), 3.60 (s, 6H), 3.59 (s, 3H), 3.30–3.25 (m, 4H), 1.06 (t, J = 7.2 Hz, 6H). LC-MS (ESI): *m/z* 583.1 $(M + H)^+$.

***N*-(4-(diethylamino)benzyl)-2-methyl-*N*-(3,4,5-trimethoxybenzyl)benzenesulfonamide**

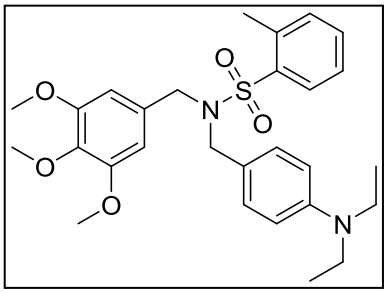

(3.14). Compound **6.14** was prepared from the intermediate *N*,*N*-diethyl-4-(((3,4,5-trimethoxybenzyl)amino)methyl)aniline (compound **6.3**) (358 mg, 1.0 mmol) and 2-methylbenzenesulfonyl chloride (190 mg, 1.0 mmol). The residue was purified by flash chromatography (ethyl acetate/petroleum ether, 1:2) on silica gel to obtain *N*-(4-(diethylamino)benzyl)-2-methyl-*N*-(3,4,5-trimethoxybenzyl)benzenesulfonamide **(6.14)**. Yellow solid (216 mg, yield: 42%). ^{1}H NMR (400 MHz, DMSO-d_6) δ 7.90 (d, J = 6.8 Hz, 1H), 7.59 (t, J = 6.4 Hz, 1H), 7.49–7.40 (m, 2H), 6.94 (d, J = 8.8 Hz, 2H), 6.54 (d, J = 8.8 Hz, 2H), 6.27 (s, 2H), 4.22 (s, 2H), 4.19 (s, 2H), 3.62 (s, 6H), 3.61 (3H), 3.30–3.28 (m, 4H), 2.56 (s, 3H), 1.07 (t, J = 6.8 Hz, 6H). LC-MS (ESI): *m/z* 513.1 $(M + H)^+$.

(*E*)-*N*-(4-(diethylamino)benzyl)-2-phenyl-*N*-(3,4,5-trimethoxybenzyl)ethene-1-sulfonamide

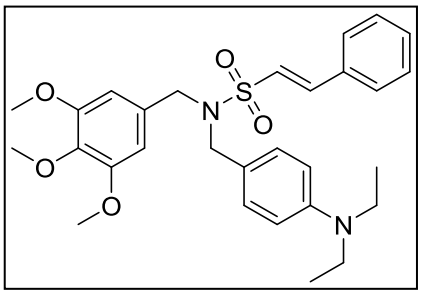

(6.15). Compound **6.15** was prepared from the intermediate *N*,*N*-diethyl-4-(((3,4,5-trimethoxybenzyl)amino)methyl)aniline (compound **6.3**) (358 mg, 1.0 mmol) and (*E*)-2-phenylethene-1-sulfonyl chloride (202 mg, 1.0 mmol). The residue was purified by flash chromatography (ethyl acetate/petroleum ether, 1:2) on silica gel to obtain (*E*)-*N*-(4-(diethylamino)benzyl)-2-phenyl-*N*-(3,4,5-trimethoxybenzyl)ethene-1-sulfonamidebenzenesulfonamide **(6.15)**. White solid (278 mg, yield: 53%). ^{1}H NMR (400 MHz, DMSO-d_6) δ7.65 (t, J = 2.4 Hz, 2H), 7.44–7.42 (m, 3H), 7.38 (s, 1H), 7.26 (s, 1H), 7.09 (d, J = 8.80 Hz, 2H), 6.59 (d, J = 8.40 Hz, 2H), 6.47 (s, 2H), 4.22 (s, 2H), 4.19 (s, 2H), 3.65 (s, 6H), 3.59 (s, 3H), 3.30–3.25 (m, 4H), 1.06 (t, J = 7.20 Hz, 6H). ^{1}H NMR (400 MHz, $CDCl_3$) δ7.44 – 7.37 (m, 6H), 6.64 (d, J = 8.80 Hz, 2H), 6.56–6.502 (m, 3H), 4.28 (s, 4H), 3.85 (s, 3H), 3.82 (s, 6H), 1.18 (t, J = 6.80 Hz, 6H). LC-MS (ESI): *m/z* 525.2 $(M + H)^+$.

***N*-(4-(diethylamino)benzyl)-*N*-(3,4,5-trimethoxybenzyl)thiophene-2-sulfonamide (6.16).**

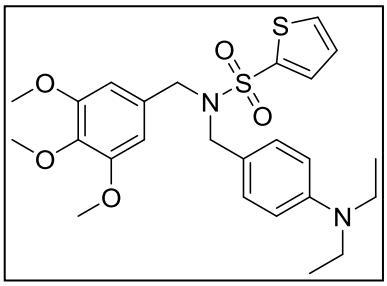

Compound **6.16** was prepared from the intermediate *N*,*N*-diethyl-4-(((3,4,5-trimethoxybenzyl)amino)methyl)aniline (compound **6.3**) (358 mg, 1.0 mmol) and thiophene-2-sulfonyl chloride (182 mg, 1.0 mmol). The residue was purified by flash chromatography (ethyl acetate/petroleum ether, 1:2) on silica gel to obtain *N*-(4-(diethylamino)benzyl)-*N*-(3,4,5-trimethoxybenzyl)thiophene-2-sulfonamide **(6.16)**. Yellow solid (270 mg, yield: 54%). ^{1}H NMR (400 MHz, DMSO-d_6) δ 8.03–8.02 (m, 1H), 7.76–7.75 (m, 1H), 7.28–7.25 (m, 1H), 6.96 (d, J = 8.40 Hz, 2H), 6.55 (d, J = 8.80 Hz, 2H), 6.28 (s, 2H), 4.20 (s, 2H), 4.17 (s, 2H), 3.61 (s, 6H), 3.60 (s, 3H), 3.30–3.26 (m, 4H), 1.06 (t, J = 11.20 Hz, 6H). LC-MS (ESI): *m/z* 505.5 $(M + H)^+$.

***N*-(4-(diethylamino)benzyl)-3,4-dimethoxy-*N*-(3,4,5-trimethoxybenzyl)benzenesulfonamide**

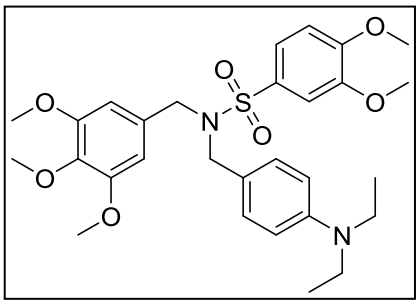

(6.17). Compound **6.17** was prepared from the intermediate *N*,*N*-diethyl-4-(((3,4,5-trimethoxybenzyl)amino)methyl)aniline (compound **6.3**) (358 mg, 1.0 mmol) 3,4-dimethoxybenzenesulfonyl chloride (236 mg, 1.0 mmol. The residue was purified by flash chromatography (ethyl acetate/petroleum ether, 1:2) on silica gel to obtain *N*-(4-(diethylamino)benzyl)-3,4-dimethoxy-*N*-(3,4,5-trimethoxybenzyl)benzenesulfonamide **(6.17)**. Brown oil (436 mg, yield: 78%). ^{1}H NMR (400 MHz, DMSO-d_6) δ 7.49 (d, J = 2.4 Hz, 1H), 7.47 (s, 1H), 7.46–7.223 (m, 1H), 7.15 (d, J = 8.80 Hz, 2H), 6.55 (d, J = 8.80 Hz, 2H), 6.25 (s, 2H), 4.18 (s, 2H), 4.17 (s, 2H), 3.86 (s, 3H), 3.79 (s, 3H), 3.79 (s, 6H), 3.59 (s, 3h), 3.31–3.28 (m, 4H), 1.06 (t, J = 7.20 Hz, 6H). LC-MS (ESI): *m/z* 559.4 $(M + H)^+$.

***N*-(4-(diethylamino)benzyl)-4-formyl-*N*-(3,4,5-trimethoxybenzyl)benzenesulfonamide**

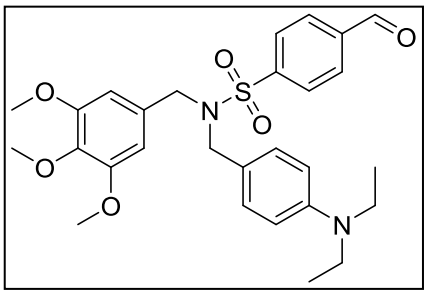

(6.18). Compound **6.**18 was prepared from the intermediate *N*,*N*-diethyl-4-(((3,4,5-trimethoxybenzyl)amino)methyl)aniline (compound **6.3**) (358 mg, 1.0 mmol) and 4-formylbenzenesulfonyl chloride (204 mg, 1.0 mmol). The residue was purified by flash chromatography (ethyl acetate/petroleum ether, 1:2) on silica gel to obtain *N*-(4-(diethylamino)benzyl)-4-formyl-*N*-(3,4,5-trimethoxybenzyl)benzenesulfonamide **(6.18)**. Yellow solid (374 mg, yield: 71%). ^{1}H NMR (400 MHz, DMSO-d_6) δ10.13 (s, 1H), 8.11–8.06 (m, 4H), 6.95 (d, J = 8.80 Hz, 2H), 6.53 (d, J = 8.40 Hz, 2H), 6.26 (s, 2H), 4.24 (d, J = 7.20 Hz, 4H), 3.59 (s, 9H), 3.30 – 3.26 (m, 4H), 1.05 (t, J = 6.80 Hz, 6H). ^{1}H NMR (600 MHz, $CDCl_3$) δ7.99 (d, J = 1.80 Hz, 4H), 6.86 (d, J = 9.0 Hz, 2H), 6.49

(d, *J* = 8.40 Hz, 2H), 6.30 (s, 2H), 4.30 (s, 2H), 4.27 (s, 2H), 3.81 (s, 3H), 3.72 (s, 6H), 1.13 (t, *J* = 7.20 Hz, 6H). LC-MS (ESI): *m/z* 527.4 $(M + H)^+$.

***N*-(4-(diethylamino)benzyl)-N-(pyridin-3-ylmethyl)thiophene-2-carboxamide (6.21).**

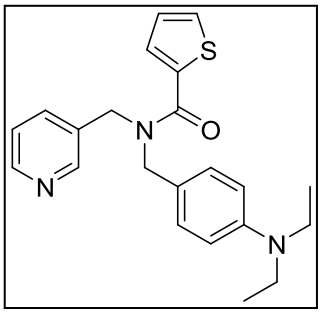

Compound **6.21** was prepared from the intermediate *N*,*N*-diethyl-4-(((pyridin-3-ylmethyl)amino)methyl)aniline (compound **6.20**) (269 mg, 1.0 mmol) and thiophene-2-carbonyl chloride (156 mg, 1.0 mmol). The residue was purified by flash chromatography (ethyl acetate/petroleum ether, 1:2) on silica gel to obtain *N*-(4-(diethylamino)benzyl)-*N*-(pyridin-3-ylmethyl)thiophene-2-carboxamide **(6.21)**. Dark brown oil (342 mg, yield: 90%). ^{1}H NMR (400 MHz, DMSO-d_6) δ8.50–8.47 (m, 2H), 7.78 (d, *J* = 4.40 Hz, 1H), 7.77–7.66 (m, 1H), 7.39–7.36 (m, 2H), 7.11–7.04 (m, 3H), 6.65 (d, *J* = 8.40 Hz, 2H), 4.62 (d, *J* = 12.40 Hz, 4H), 3.31–3.28 (m, 4H), 1.08 (t, *J* = 6.80 Hz, 6H). LC-MS (ESI): *m/z* 380.0 $(M + H)^+$.

***N*-(4-(diethylamino)benzyl)-*N*-(pyridin-3-ylmethyl)quinoxaline-2-carboxamide (6.22).**

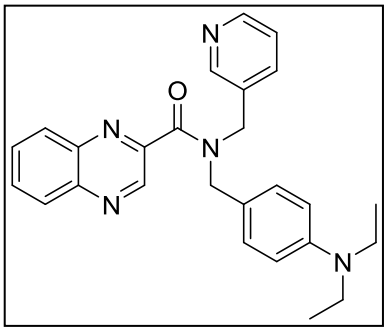

Compound **6.22** was prepared from **t**he intermediate *N*,*N*-diethyl-4-(((pyridin-3-ylmethyl)amino)methyl)aniline (compound **6.20**) (269 mg, 1.0 mmol) and quinoxaline-2-carbonyl chloride (192 mg, 1.0 mmol. The residue was purified by flash chromatography (ethyl acetate/petroleum ether, 1:2) on silica gel to obtain *N*-(4-(diethylamino)benzyl)-*N*-(pyridin-3-ylmethyl)quinoxaline-2-carboxamide **(6.22)**. Yellow solid (305 mg, yield: 72%). ^{1}H NMR (400 MHz, DMSO-d_6) δ9.17 (s, 1H), 8.57 (d, *J* = 1.60 Hz, 1H), 8.52–8.51 (m, 1H), 8.48–8.43 (m, 1H), 8.18–8.14 (m, 1H), 7.99–7.91 (m, 2H), 7.80–7.76 (m, 1H), 4.68 (s, 2H), 4.57 (s, 1H), 4.53 (s, 1H), 3.37–3.28 (m, 4H), 1.06 (t, *J* = 7.20 Hz, 6H). LC-MS (ESI): *m/z* 426.1 $(M + H)^+$.

(*E*)-N-(4-(diethylamino)benzyl)-2-phenyl-*N*-(pyridin-3-ylmethyl)ethene-1-sulfonamide

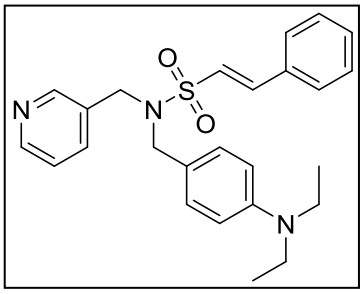

(6.23). Compound **6.23** was prepared from the intermediate *N*,*N*-diethyl-4-(((pyridin-3-ylmethyl)amino)methyl)aniline (compound **3.20**) (269 mg, 1.0 mmol) and (*E*)-2-phenylethene-1-sulfonyl chloride (202 mg, 1.0 mmol). The residue was purified by flash chromatography (ethyl acetate/petroleum ether, 1:2) on silica gel to obtain (*E*)-*N*-(4-(diethylamino)benzyl)-2-phenyl-*N*-(pyridin-3-ylmethyl)ethene-1-sulfonamide **(6.23)**. Brown solid (270 mg, yield: 62%). ^{1}H NMR (400 MHz, DMSO-d_6) δ8.43–8.41 (m, 2H), 7.66–7.61 (m, 3H), 7.454–7.43 (m, 3H), 7.42 (s, 1H), 7.31–7.27 (m, 1H), 7.28 (s, 1H), 7.07 (d, J = 8.80 Hz, 2H), 4.31 (s, 2H), 4.20 (s, 2H), 3.31–3.26 (m, 4H), 1.05 (t, J = 6.80 Hz, 6H). LC-MS (ESI): *m/z* 436.2 $(M + H)^+$.

***N*-(4-(diethylamino)benzyl)-*N*-(pyridin-3-ylmethyl)naphthalene-2-sulfonamide (6.24).**

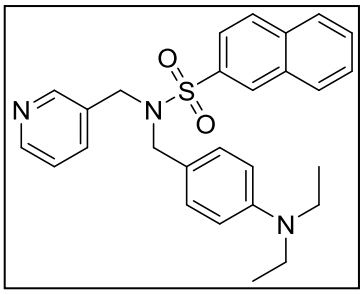

Compound **6.24** was prepared from the intermediate *N*,*N*-diethyl-4-(((pyridin-3-ylmethyl)amino)methyl)aniline (compound **6.20**) (269 mg, 1.0 mmol) and naphthalene-2-sulfonyl chloride (226 mg, 1.0 mmol). The residue was purified by flash chromatography (ethyl acetate/petroleum ether, 1:2) on silica gel to obtain *N*-(4-(diethylamino)benzyl)-*N*-(pyridin-3-ylmethyl)naphthalene-2-sulfonamide **(6.24)**. Brown solid (285 mg, yield: 62%). ^{1}H NMR (400 MHz, DMSO-d_6) δ8.51 (s, 1H), 8.36 (d, J = 1.60 Hz, 1H), 8.28 (s, 1H), 8.18–8.14 (m, 2H), 8.09 (d, J = 7.60 Hz, 1H), 7.88 (dd, J_1 = 2.0 Hz, J_2 = 8.80 Hz, 2H), 7.76–7.70 (m, 3H), 7.22–7.18 (m, 1H), 6.91 (d, J = 8.80 Hz, 2H), 6.45 (d, J = 8.80 Hz, 2H), 4.35 (s, 2H), 4.24 (s, 2H), 3.27–3.24 (m, 4H), 1.02 (t, J = 7.20 Hz, 6H). LC-MS (ESI): *m/z* 460.3 $(M + H)^+$.

***N*-(4-(diethylamino)benzyl)-*N*-(pyridin-3-ylmethyl)-[1,1'-biphenyl]-4-sulfonamide (6.25).**

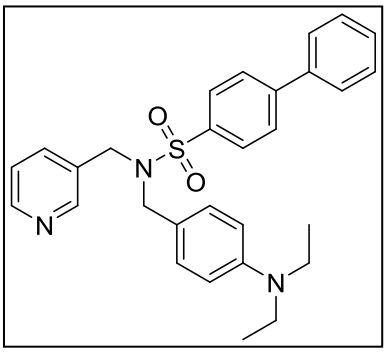

Compound **6.25** was prepared from the intermediate *N*,*N*-diethyl-4-(((pyridin-3-ylmethyl)amino)methyl)aniline (compound **6.20**) (269 mg, 1.0 mmol) and [1,1'-biphenyl]-4-sulfonyl chloride (252 mg, 1.0 mmol. The residue was purified by flash chromatography (ethyl acetate/petroleum ether, 1:2) on silica gel to obtain *N*-(4-(diethylamino)benzyl)-*N*-(pyridin-3-ylmethyl)-[1,1'-biphenyl]-4-sulfonamide **(6.25)**. Yellow solid (273 mg, yield: 56%). ^{1}H NMR (400 MHz, DMSO-d_6) δ8.38–8.37 (m, 1H), 8.28 (d, J = 1.60 Hz, 1H), 7.96–7.90 (m, 4H), 7.79–7.77 (m, 2H), 7.57–7.53 (m, 2H), 7.49–7.45 (m, 2H), 7.23–7.19 (m, 1H), 6.91 (d, J = 8.80 Hz, 2H), 6.48 (d, J = 8.80 Hz, 2H), 4.32 (s, 2H), 4.22 (s, 2H), 3.29–3.25 (m, 4H), 1.03 (t, J = 6.80 Hz, 6H). LC-MS (ESI): *m/z* 486.2 $(M + H)^+$.

(*E*)-*N*-(benzo[*d*][1,3]dioxol-5-ylmethyl)-*N*-(4-(diethylamino)benzyl)-2-phenylethene-1-

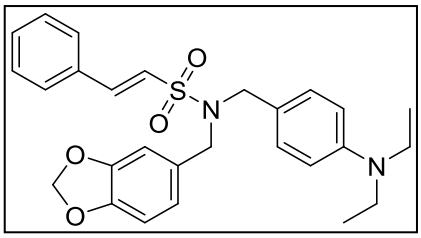

sulfonamide (6.29). Compound **6.29** was prepared from the intermediate 4-(((benzo[*d*][1,3]dioxol-5-ylmethyl)amino)methyl)-*N*,*N*-diethylaniline (compound **6.28**) (312 mg, 1.0 mmol) and (*E*)-2-phenylethene-1-sulfonyl chloride (202 mg, 1.0 mmol. The residue was purified by flash chromatography (ethyl acetate/petroleum ether, 1:2) on silica gel to obtain (*E*)-*N*-(benzo[*d*][1,3]dioxol-5-ylmethyl)-*N*-(4-(diethylamino)benzyl)-2-phenylethene-1-sulfonamide **(6.29)**. White solid (100 mg, yield: 20%). ^{1}H NMR (400 MHz, DMSO-d_6) δ7.61–7.59 (m, 2H), 7.43 (s, 2H), 7.42 (s, 1H), 7.31 (s, 1H), 7.11 (s, 1H), 7.07 (t, J = 4.80 Hz, 2H), 6.84 (d, J = 7.60 Hz, 1H), 6.81 (s, 1H), 6.76 (d, J = 7.60 Hz, 1H), 6.58 (d, J = 8.80 Hz, 2H), 5.96 (s, 2H), 4.15 (d, J = 6.40 Hz, 4H), 3.31–3.27 (m, 4H), 1.05 (t, J = 7.20 Hz, 6H). LC-MS (ESI): 479.4 $(M + H)^+$.

***N*-(benzo[*d*][1,3]dioxol-5-ylmethyl)-*N*-(4-(diethylamino)benzyl)-4-formylbenzenesulfonamide (6.30).**

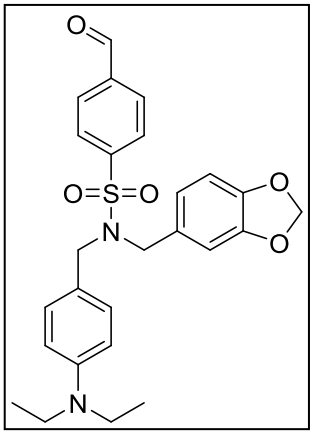

Compound **6.30** was prepared from the intermediate 4-(((benzo[*d*][1,3]dioxol-5-ylmethyl)amino)methyl)-*N*,*N*-diethylaniline (compound **6.28**) (312 mg, 1.0 mmol) and 4-formylbenzenesulfonyl chloride (204 mg, 1.0 mmol). The residue was purified by flash chromatography (ethyl acetate/petroleum ether, 1:2) on silica gel to obtain *N*-(benzo[*d*][1,3]dioxol-5-ylmethyl)-*N*-(4-(diethylamino)benzyl)-4-formylbenzenesulfonamide **(6.30)**. Yellow solid (410 mg, yield: 85%).^{1}H NMR (400 MHz, DMSO-d_6) δ10.13 (s, 1H), 8.07 (d, J = 8.40 Hz, 2H), 8.01 (d, J = 8.40 Hz, 2H), 6.86 (d, J = 8.80 Hz, 2H), 6.78 (d, J = 8.0 Hz, 1H), 6.62–6.57 (m, 1H), 6.57 (s, 1H), 6.49 (d, J = 8.80 Hz, 2H), 5.95 (s, 2H), 4.23 (s, 2H), 4.19 (s, 2H), 3.30–3.25 (m, 4H), 1.04 (t, J = 7.20 Hz, 6H), LC-MS (ESI): *m/z* 480.2 $(M + H)^+$.

4-(((benzo[*d*][1,3]dioxol-5-ylmethyl)(quinoxalin-2-ylmethyl)amino)methyl)-*N*,*N*-diethylaniline (6.31).

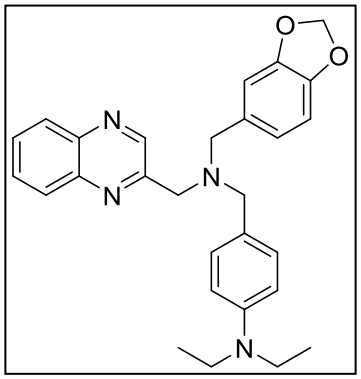

Compound **6.31** was prepared from the intermediate 4-(((benzo[*d*][1,3]dioxol-5-ylmethyl)amino)methyl)-*N*,*N*-diethylaniline (compound **6.28**) (312 mg, 1.0 mmol and quinoxaline-2-carbonyl chloride (192 mg, 1.0 mmol). The residue was purified by flash chromatography (ethyl acetate/petroleum ether, 1:2) on silica gel to obtain 4-(((benzo[*d*][1,3]dioxol-5-ylmethyl)(quinoxalin-2-ylmethyl)amino)methyl)-*N*,*N*-diethylaniline **(6.31)**. Brown oil (418 mg, yield: 89%).^{1}H NMR (600 MHz, DMSO-d_6) δ9.13 (s, 1H), 8.16–8.13 (m, 2H), 7.96–7.93 (m, 2H), 6.40–6.91 (m, 2H), 6.87–

6.83 (m, 1H), 6.67 (d, *J* = 8.40 Hz, 2H), 6.57 (d, *J* = 8.40 Hz, 2H), 5.99 (s, 2H), 4.50 (s, 2H), 4.40 (s, 2H), 3.30–3.27 (m, 4H), 1.05 (t, *J* = 7.20 Hz, 6H). LC-MS (ESI): *m/z* 469.1 $(M + H)^+$.

***N*-(benzo[*d*][1,3]dioxol-5-ylmethyl)-*N*-(4-(diethylamino)benzyl)thiophene-2-carboxamide (6.32).**

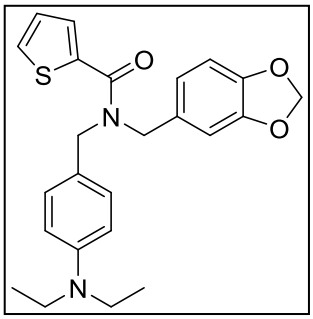

Compound **6.32** was prepared from the intermediate 4-(((benzo[*d*][1,3]dioxol-5-ylmethyl)amino)methyl)-*N*,*N*-diethylaniline (compound **6.28**) (312 mg, 1.0 mmol) and thiophene-2-carbonyl chloride (146 mg, 1.0 mmol). The residue was purified by flash chromatography (ethyl acetate/petroleum ether, 1:2) on silica gel to obtain *N*-(benzo[*d*][1,3]dioxol-5-ylmethyl)-*N*-(4-(diethylamino)benzyl)thiophene-2-carboxamide **(6.32)**. Dark brown oil (290 mg, yield: 69%).^{1}H NMR (400 MHz, DMSO-d_6) δ7.78–7.76 (m, 1H), 7.33 (s, 1H), 7.09–7.07 (m, 1H), 7.04 (d, *J* = 8.0 Hz, 2H), 6.90 (d, *J* = 8.0 Hz, 1H), 6.82 (s, 1H), 6.73 (d, *J* = 7.20 Hz, 1H), 6.65 (d, *J* = 8.80 Hz, 2H), 6.02 (s, 2H), 4.52 (s, 4H), 3.36–3.02 (m, 4H), 1.08 (t, *J* = 7.20 Hz, 6H). LC-MS (ESI): *m/z* 423.2 $(M + H)^+$.

***N*-(benzo[*d*][1,3]dioxol-5-ylmethyl)-*N*-(4-(diethylamino)benzyl)naphthalene-2-sulfonamide (6.33).**

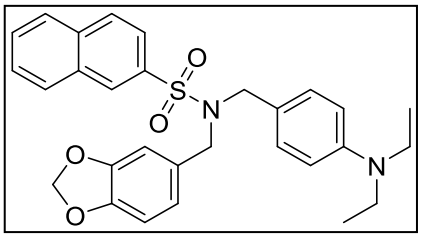

Compound **6.33** was prepared from the intermediate 4-(((benzo[*d*][1,3]dioxol-5-ylmethyl)amino)methyl)-*N*,*N*-diethylaniline (compound **6.28**) (312 mg, 1.0 mmol) and naphthalene-2-sulfonyl chloride (226 mg, 1.0 mmol). The residue was purified by flash chromatography (ethyl acetate/petroleum ether, 1:2) on silica gel to obtain *N*-(benzo[*d*][1,3]dioxol-5-ylmethyl)-*N*-(4-(diethylamino)benzyl)naphthalene-2-sulfonamide **(6.33)**. Yellow oil (76 mg, yield: 15%).^{1}H NMR (400 MHz, DMSO-d_6) δ8.42 (d, *J* = 1.6 Hz, 1H), 8.14–

8.11 (m, 12H), 8.07 (d, *J* = 8.0 Hz, 1H), 7.84–7.82 (m, 1H), 7.73–7.68 (m, 2H), 6.88 (d, *J* = 8.8 Hz, 2H), 6.75 (d, *J* = 8.0 Hz, 1H), 6.64–6.61 (m, 1H), 6.57 (d, *J* = 1.6 Hz, 1H), 6.47 (d, *J* = 8.8 Hz, 2H), 5.91 (s, 2H), 4.22 (d, *J* = 6.8 Hz, 4H), 3.29–3.23 (m, 4H), 1.02 (t, *J* = 6.8 Hz, 6H). LC-MS (ESI): *m/z* 503.6 $(M + H)^+$.

***N*-(benzo[*d*][1,3]dioxol-5-ylmethyl)-*N*-(4-(diethylamino)benzyl)-[1,1'-biphenyl]-4-sulfonamide (6.34).**

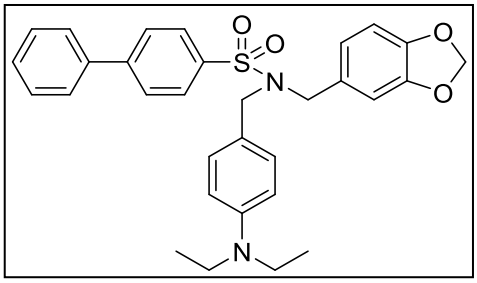

Compound **6.34** was prepared from the intermediate 4-(((benzo[*d*][1,3]dioxol-5-ylmethyl)amino)methyl)-*N*,*N*-diethylaniline (compound **6.28**) (312 mg, 1.0 mmol) and [1,1'-biphenyl]-4-sulfonyl chloride (252 mg, 1.0 mmol). The residue was purified by flash chromatography (ethyl acetate/petroleum ether, 1:2) on silica gel to obtain *N*-(benzo[*d*][1,3]dioxol-5-ylmethyl)-*N*-(4-(diethylamino)benzyl)-[1,1'-biphenyl]-4-sulfonamide **(6.34)**. Yellow oil (363 mg, yield: 69%).^{1}H NMR (400 MHz, DMSO-d_6) δ7.88 (d, *J* = 2.0 Hz, 4H), 7.77–7.75 (m, 2H), 7.56–7.52 (m, 2H), 7.49–7.45 (m, 1H), 6.88 (d, *J* = 8.4 Hz, 2H), 6.77 (d, *J* = 8.0 Hz, 1H), 6.62–6.60 (m, 1H), 6.57 (d, *J* = 1.6 Hz, 1H), 6.50 (d, *J* = 8.8 Hz, 2H), 4.19 (d, *J* = 9.6 Hz, 4H), 3.28–3.24 (m, 4H), 1.03 (t, *J* = 7.2 Hz, 6H). LC-MS (ESI): *m/z* 529.1 $(M + H)^+$.

(*E*)-*N*-(4-(diethylamino)benzyl)-*N*-pentyl-2-phenylethene-1-sulfonamide (6.37).

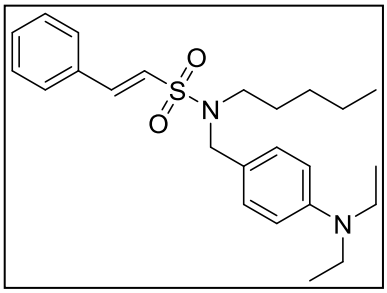

Compound **6.37** was prepared from the intermediate *N*,*N*-diethyl-4-((pentylamino)methyl)aniline (compound **6.36**) (248 mg, 1.0 mmol) and (*E*)-2-phenylethene-1-sulfonyl chloride (202 mg, 1.0 mmol). The residue was purified by flash chromatography (ethyl acetate/petroleum ether, 1:2) on silica gel to obtain (*E*)-*N*-(4-(diethylamino)benzyl)-*N*-pentyl-2-

phenylethene-1-sulfonamide **(6.37)**. Dark brown oil (285 mg, yield: 69%).^{1}H NMR (600 MHz, DMSO-d_6) δ7.67 (t, J = 3.60 Hz, 2H), 7.43 (s, 3H), 7.34 (d, J = 15.60 Hz, 1H), 7.18–7.13 (m, 2H), 6.62 (d, J = 8.40 Hz, 2H), 4.18 (a, 2H), 3.29–3.05 (m, 4H), 3.03–3.02 (m, 2H), 1.41 (t, J = 7.20 Hz, 2H), 1.89–1.16 (m, 4H), 1.05 (t, J = 6.60 Hz, 6H), 0.76 (t, J = 7.20 Hz, 3H). LC-MS (ESI): m/z 415.2 $(M + H)^+$.

***N*-(4-(diethylamino)benzyl)-4-formyl-*N*-pentylbenzenesulfonamide (6.38).**

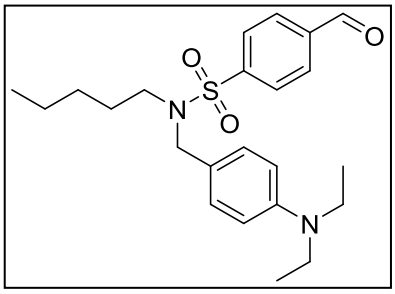

Compound **6.38** was prepared from the intermediate *N*,*N*-diethyl-4-((pentylamino)methyl)aniline (compound **6.36**) (248 mg, 1.0 mmol) and 4-formylbenzenesulfonyl chloride (204 mg, 1.0 mmol). The residue was purified by flash chromatography (ethyl acetate/petroleum ether, 1:2) on silica gel to obtain *N*-(4-(diethylamino)benzyl)-4-formyl-*N*-pentylbenzenesulfonamide **(6.38)**. Yellow solid (259 mg, yield: 62%).^{1}H NMR (600 MHz, DMSO-d_6) δ8.10 (d, J = 8.40 Hz, 2H), 8.03 (d, J = 7.80 Hz, 2H), 7.04 (d, J = 8.40 Hz, 2H), 6.58 (d, J = 9.0 Hz, 2H), 4.19 (s, 2H), 3.32–3.28 (m, 4H), 3.04 (t, J = 7.80 Hz, 2H), 1.26 (t, J = 7.20 Hz, 2H), 1.08 (t, J = 6.40 Hz, 4H), 1.02 (t, J = 7.20 Hz, 6H), 0.707 (t, J = 7.80 Hz, 3H). LC-MS (ESI): m/z 417.7 $(M + H)^+$.

***N*-(4-(diethylamino)benzyl)-*N*-pentylquinoxaline-2-carboxamide (6.39).**

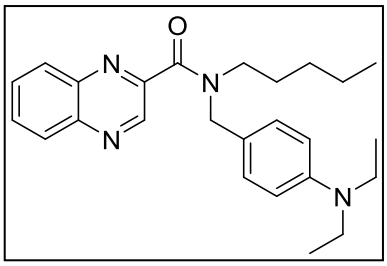

Compound **6.39** was prepared from the intermediate *N*,*N*-diethyl-4-((pentylamino)methyl)aniline (compound **6.35**) (248 mg, 1.0 mmol) and quinoxaline-2-carbonyl chloride (192 mg, 1.0 mmol). The residue was purified by flash chromatography (ethyl acetate/petroleum ether, 1:2) on silica gel to obtain *N*-(4-(diethylamino)benzyl)-*N*-pentylquinoxaline-2-carboxamide **(6.39)**. Yellow solid (364 mg, yield: 90%).^{1}H NMR (600 MHz,

DMSO-d_6) δ9.06 (s, 1H), 7.22 (d, J = 9.0 Hz, 2H), 7.09 (d, J = 9.0 Hz, 2H), 6.67 (d, J = 8.40 Hz, 2H), 6.58 (d, J = 8.40 Hz, 2H), 4.49 (s, 2H), 3.29 – 3.27 (m, 4H), 1.62–1.58 (m, 2H), 1.32–1.24 (m, 4H), 1.08 (t, J = 7.20 Hz, 6H), 0.87 (t, J = 6.60 Hz, 3H). LC-MS (ESI): *m/z* 405.5 $(M + H)^+$.

***N*-(4-(diethylamino)benzyl)-*N*-pentylthiophene-2-carboxamide (6.40).**

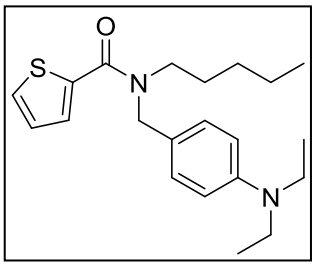

Compound **6.40** was prepared from the intermediate *N*,*N*-diethyl-4-((pentylamino)methyl)aniline (compound **6.35**) (248 mg, 1.0 mmol) and thiophene-2-carbonyl chloride (146 mg, 1.0 mmol). The residue was purified by flash chromatography (ethyl acetate/petroleum ether, 1:2) on silica gel to obtain *N*-(4-(diethylamino)benzyl)-*N*-pentylthiophene-2-carboxamide **(6.40)**. Dark brown solid (230 mg, yield: 69%).^{1}H NMR (600 MHz, DMSO-d_6) δ7.74 (d, J = 4.80 Hz, 1H), 7.35 (s, 1H), 7.08 (d, J = 6.0 Hz, 3H), 6.65 (s, 2H), 4.58 (s, 2H), 3.34–3.31 (m, 4H), 1.98 (t, J = 6.40 Hz, 2H), 1.56 (s, 2H), 1.17 (t, J = 7.20 Hz, 4H), 1.07 (t, J = 4.80 Hz, 6H), 0.83 (d, J = 5.40 Hz, 3H). LC-MS (ESI): *m/z* 359.6 $(M + H)^+$.

***N*-(4-(diethylamino)benzyl)-*N*-pentylnaphthalene-1-sulfonamide (6.41).**

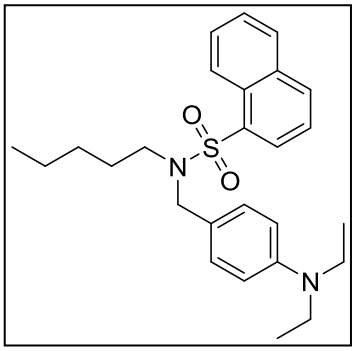

Compound **6.41** was prepared from the intermediate *N*,*N*-diethyl-4-((pentylamino)methyl)aniline (compound **6.35**) (248 mg, 1.0 mmol) and naphthalene-2-sulfonyl chloride (226 mg, 1.0 mmol). The residue was purified by flash chromatography (ethyl acetate/petroleum ether, 1:2) on silica gel to obtain *N*-(4-(diethylamino)benzyl)-*N*-pentylnaphthalene-1-sulfonamide **(6.41)**. Yellow solid (308 mg, yield: 70%).^{1}H NMR (600 MHz, DMSO-d_6) δ8.47 (s, 1H), 8.19–8.17 (m, 1H), 8.14–8.12 (m, 1H), 8.07–8.05 (m, 1H), 7.84–7.82 (m, 1H), 7.73–7.69 (m, 2H), 7.07–7.05 (m, 2H), 6.58–6.56 (m, 2H), 4.22

(d, *J* = 3.0 Hz, 2H), 3.30–3.27 (m, 4H), 3.06–3.03 (m, 2H), 1.33–1.23 (m, 2H), 1.05–1.04 (m, 4H), 1.02 (t, *J* = 5.40 Hz, 6H), 0.65 (t, *J* = 3.60 Hz, 3H). LC-MS (ESI): *m/z* 439.4 $(M + H)^+$.

***N*-(4-(diethylamino)benzyl)-*N*-pentyl-[1,1'-biphenyl]-4-sulfonamide (6.42).**

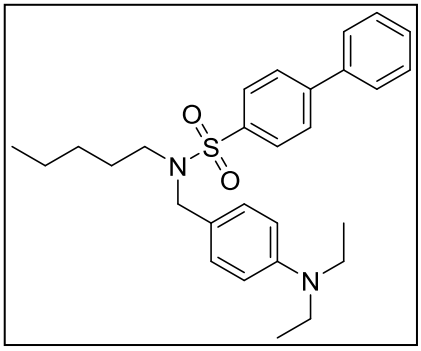

Compound **6.42** was prepared from the intermediate *N*,*N*-diethyl-4-((pentylamino)methyl)aniline (compound **6.35**) (248 mg, 1.0 mmol) and [1,1'-biphenyl]-4-sulfonyl chloride (252 mg, 1.0 mmol). The residue was purified by flash chromatography (ethyl acetate/petroleum ether, 1:2) on silica gel to obtain *N*-(4-(diethylamino)benzyl)-*N*-pentyl-[1,1'-biphenyl]-4-sulfonamide **(6.42)**. Yellow solid (272 mg, yield: 59%).^{1}H NMR (400 MHz, DMSO-d_6) δ7.90 (s, 4H), 7.77–7.75 (m, 2H), 7.56–7.52 (m, 2H), 7.48–7.44 (m, 1H), 7.08 (d, *J* = 8.8 Hz, 2H), 6.61 (d, *J* = 8.8 Hz, 2H), 4.20 (s, 2H), 3.32–3.28 (m, 4H), 3.04 (t, *J* = 7.6, 2H), 1.30–1.27 (m, 2H), 1.6 (t, *J* = 7.2, 6H), 0.71 (t, *J* = 7.20 Hz, 3H). LC-MS (ESI): *m/z* 464.1 $(M + H)^+$.

6.4.2 3D QSAR/CoMFA Studies

Out of the 41 compounds from Table 6.1 - Table 6.4, 32 compounds were used in the 3D QSAR CoMFA studies. Compounds that showed no binding were ignored in the study. The compounds were randomly divided into training (20 compounds) and test (12 compounds) sets. SYBYL X1.3 was used for the CoMFA studies. The best compound, **6.11**, was selected to perform the molecular dynamic simulations. As previously described, dynamic simulations were simulated at 300 K with a time of steps of 1 fs for a total duration of 300 ps, and sampling of the conformations were collected at every 1 ps resulting in 300 conformers of the compound **6.11**. The conformers are then minimized and converged into five families. The five families were compared to the docking pose to generate the most preferable conformation. The docking was performed using the Surflex-Dock module from the Tripos modeling software. Finally, the conformer with maximum agreement from these experiments was further used for CoMFA studies. The structures were built and energy minimized using Tripos force field with 0.05 kcal/ (mol Å). Charges were calculated using the Gasteiger-Huckel method. Powell method was used for energy minimization with 2000 iterations. Alignments of the structures to the preferred conformer of compound **6.11** were performed using the MultiFit program in Sybyl X 1.3. The CoMFA study was then carried out using the SYBYL/CoMFA module. Leave one-out cross-validation (LOOCV) partial least-squares (PLS) analysis was performed with a minimum σ (column filter) value of 5.0 kcal·mol−1 to improve the signal-to-noise ratio by omitting those lattice points with an energy variation below this threshold. The final model (non-cross-validated analysis) was developed from the LOOCV model with the highest cross-validated r^2, using the optimal number of components determined by the LOOCV model.

7.0 SUMMARY AND CONCLUSION

The cannabinoid system emerged as a major therapeutic target in recent years. Several research groups have represented the potential of cannabinoid ligands for treating several disease, such as pain, multiple sclerosis, bone diseases as well as cancer attenuation. With the recent withdrawal of the CB1 inverse agonist, Rimonabant, research groups are focusing on targeting the CB2 receptor to avoid serious psychoactive side effects. However, designing novel CB2 ligands remains challenging due to the lack of high-resolution X-ray crystal structure. Several chemical design approaches were employed in the designing of some of the known CB2 ligands, such as molecular docking, pharmacophore modeling, high-throughput screening methods as well as mutational studies.

The main objective of this dissertation is to discover novel CB2 ligands with therapeutic potentials on MM and on bone diseases. This was accomplished by: 1) employing chemistry design and discovery tools, such as pharmacophore, molecular docking and interaction studies as well as high-throughput screening, in order to identify novel chemical structures (scaffolds) with optimal CB2 potency, 2) to carry out medicinal chemistry design and chemistry synthesis in order to perform SAR studies utilizing the newly discovered scaffolds aiming at identifying chemical derivatives with high CB2 receptor affinity and selectivity, 3) addressing the functionality of the newly discovered compounds, and 4) to validate the therapeutic efficacy of the these derivatives.

In our first series of compounds, we developed a pharmacophore model based on known CB2 inverse agonists along with our novel compound **XIE-35**. The pharmacophore model was utilized in the high-throughput screening module UNITY which aided in the discovery of the di-

amide scaffold (lead compound **4.1**). The di-amide scaffold represented a novel CB2 chemotype and was subjected to chemical modifications in order to generate derivatives with high CB2 receptor affinity and selectivity. The highly potent and selective derivatives were then further validated for their *in-vitro* functionality as well as their therapeutic potentials. As a result, several derivatives with high potency and selectivity were identified ((compounds **4.9**, **4.12**, and **4.17**; CB2 K_i < 100 nM, CB1 K_i > 20000). The new di-amide derivatives were identified as novel CB2 inverse agonists by cAMP assay. Furthermore, OCL formation assay showed that these new CB2 inverse agonists were potent OCL inhibitors. However, anti-proliferations studies demonstrated low inhibition rates of these CB2 inverse agonists on MM cell-lines. Nevertheless, PK studies illustrated stability limitations of the di-amide scaffold which resulted in poor PK profile.

In the second series, we performed scaffold-hopping and replaced the di-amide scaffold with an amide-sulfonamide scaffold (the substituted 2-(sulfonylamino)-2-phenylacetamide scaffold). Chemistry modifications and SAR studies were carried out and generated several derivatives. However, nearly all the derivatives exhibited weak-to-no binding to the CB2 receptor (CB2 K_i > 1860 nM, except compound **5.13** CB2 K_i = 586 nM). Anti-proliferation studies, on the other hand, demonstrated two compounds (compounds **5.12** and **5.31**) with high inhibition rates. As a result, we employed our developed HTD tool to identify the potential targets of the two ligands. Both compounds showed high docking score and excellent fit to the MAPK-14 protein with strong interactions to important amino acids identified in the binding pocket. This new discovery will be further investigated in order to study the *in-vitro* biochemical mechanisms.

As the previous two series demonstrated some limitations, we performed high-throughput screening utilizing NCI-2010 database in order to identify new CB2 scaffolds. A new lead compound (lead compound **6.1**) was identified and its scaffold was subjected to medicinal

chemistry modifications and SAR studies. As a result, several compounds with the 4-(aminomethyl)-*N*,*N*-diethylaniline scaffold demonstrated high CB2 affinity (CB2 K_i < 500 nM). Further studies of these new derivatives demonstrated the discovery of a novel CB2 agonist (compound **6.11**) and novel CB2 inverse agonists (compounds **6.15** and **6.18**) with unique scaffold. OCL formation assay demonstrated high inhibition rates of the inverse agonists; however, the agonist stimulated the OCL formation at high doses. In addition, anti-proliferation studies demonstrated that the new CB2 agonist has anti-MM properties and the CB2 inverse agonists demonstrated moderate anti-MM properties. Furthermore, PK studies showed that the 4-(aminomethyl)-*N*,*N*-diethylaniline scaffold is much more stable than the di-amide scaffold.

In conclusion, developing CB2 inverse agonists is a promising approach for developing novel osteoporosis agents as CB2 inverse agonists are potent inhibitors of OCL formation. Also, to develop anti-MM agents, CB2 agonists showed the most promising approach as anti-cancer agents, although, the CB2 inverse agonists demonstrated moderate MM growth inhibition. As the major complications of MM disease is bone lesions and osteoporosis, another advantage of developing inverse agonists is that these ligands will act as dual inhibitors of OCL and MM growth, eradicating the disease and preventing serious side effects.

In this dissertation, we opened up new avenues in the structure-based and ligand-based drug design. We were able to identify novel scaffolds as well as novel functional groups. The first identification of the diethylamine group in Chapter 4.0 aided in further design of novel CB2 ligands. This group can be introduced in different scaffold that may potentiate the CB2 receptor affinity. In addition, we concluded that designing CB2 inverse agonists are more promising as anti-OCL agents and for the ultimate treatment of osteoporosis. However, CB2 agonists is more promising as anti-MM agents Furthermore. The newly discovered CB2 inverse agonists and

agonist can serve as chemical probes in different biochemical and computational experiments. Molecular signaling mechanism studies are needed in order to study the signaling cascades of both diseases. Nevertheless, chemistry modifications should focus on optimizing the PK profiles and obtain further insights into the metabolism of these ligands. Importantly, *in-vivo* studies utilizing MM diseases animal models as well as osteoporotic animal models are needed in order to develop these newly discovered ligands to reach the clinic.

APPENDIX A

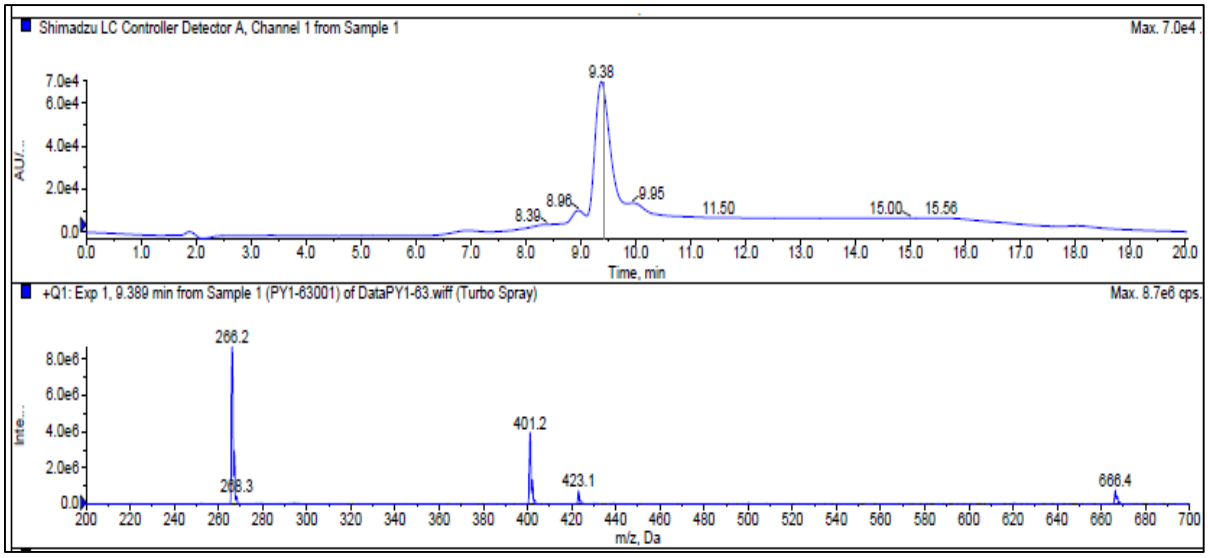

Figure 7.1. HPLC-LC/MS chromatogram for compound 4.9

Upper panel: UV absorption spectrum using UV detection at 254 and 214 nm, lower panel MS. Column: Hamilton reverse phase column (HxSil, C18, 3µm, 2.1 mm × 50 mm (H2)). Flow rate: 0.2 mL/min. Mobile phase: eluent A consists of 5% CH_3CN in H_2O; eluent B consists of 90% CH_3CN in H_2O. *N*,*N*′-((4-isopropylphenyl)methylene)bis(2-phenylacetamide), calculated molecular weight: 400.52 Da. LC-MS (ESI): *m/z* 401.2 $(M + H)^+$.

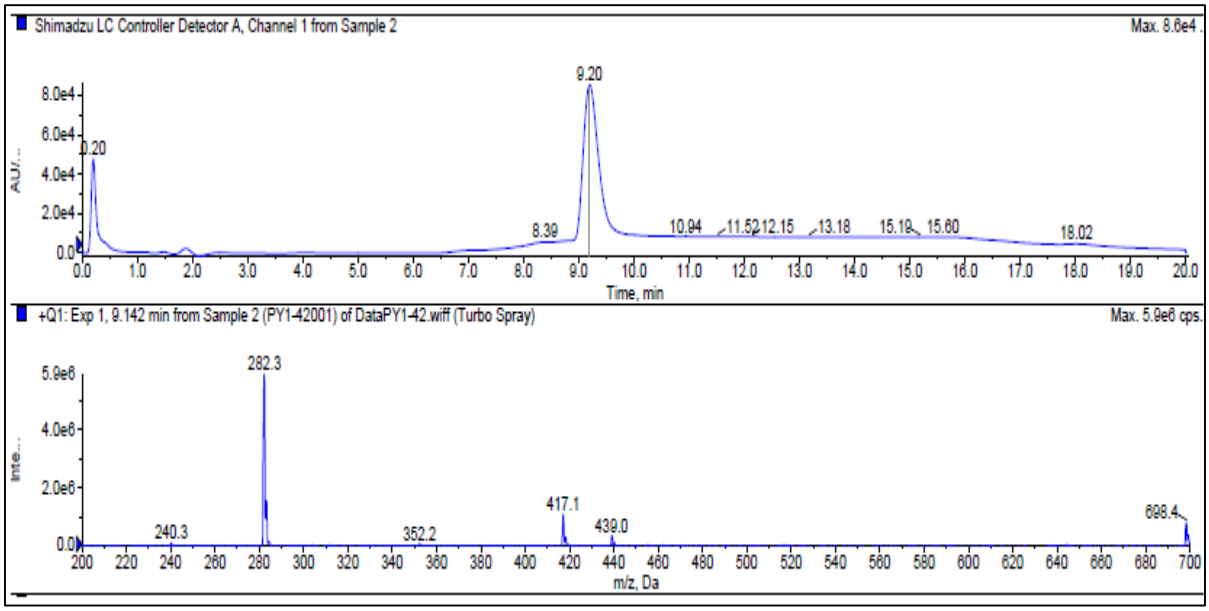

Figure 7.2. HPLC-LC/MS chromatogram for compound 4.12

Upper panel: UV absorption spectrum using UV detection at 254 and 214 nm, lower panel MS. Column: Hamilton reverse phase column (HxSil, C18, 3µm, 2.1 mm × 50 mm (H2)). Flow rate: 0.2 mL/min. Mobile phase: eluent A consists of 5% CH_3CN in H_2O; eluent B consists of 90% CH_3CN in H_2O. *N*,*N*′-((4-isopropoxyphenyl)methylene)bis(2-phenylacetamide), calculated molecular weight: 416.52 Da. LC-MS (ESI): *m/z* 417.2 $(M + H)^+$.

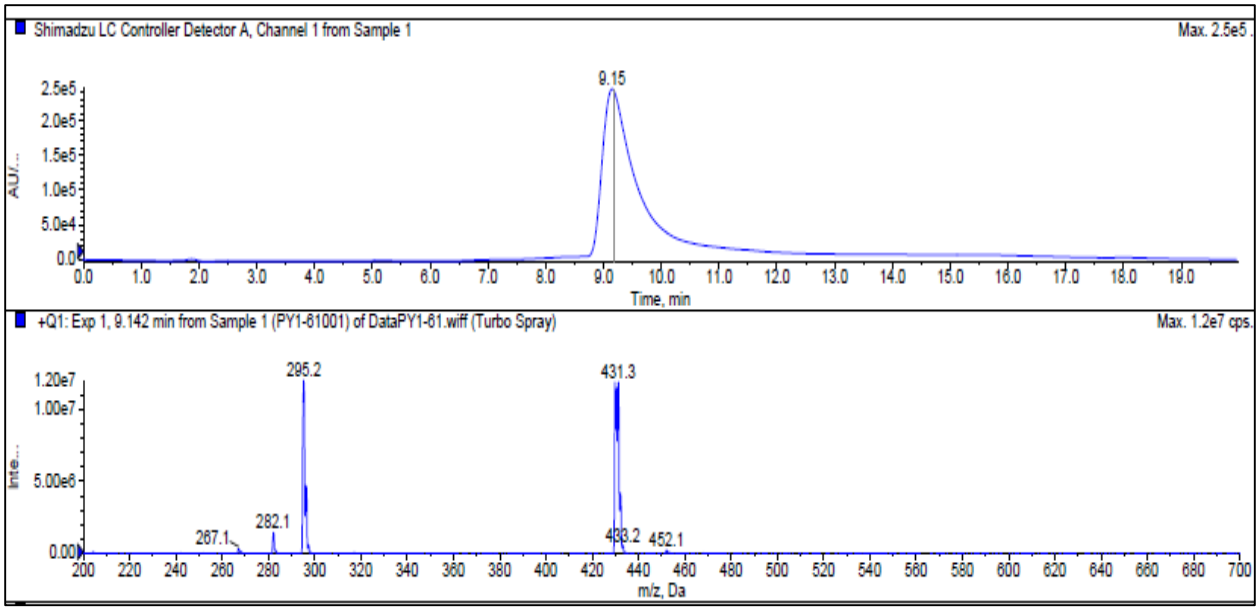

Figure 7.3. HPLC-LC/MS chromatogram for compound 4.17

Upper panel: UV absorption spectrum using UV detection at 254 and 214 nm, lower panel MS. Column: Hamilton reverse phase column (HxSil, C18, 3µm, 2.1 mm × 50 mm (H2)). Flow rate: 0.2 mL/min. Mobile phase: eluent A consists of 5% CH_3CN in H_2O; eluent B consists of 90% CH_3CN in H_2O. *N*,*N*′-((4-(diethylamino)phenyl)methylene)bis(2-phenylacetamide), calculated molecular weight: 430.56 Da. LC-MS: *m*/z 431.3 $(M + H)^+$.

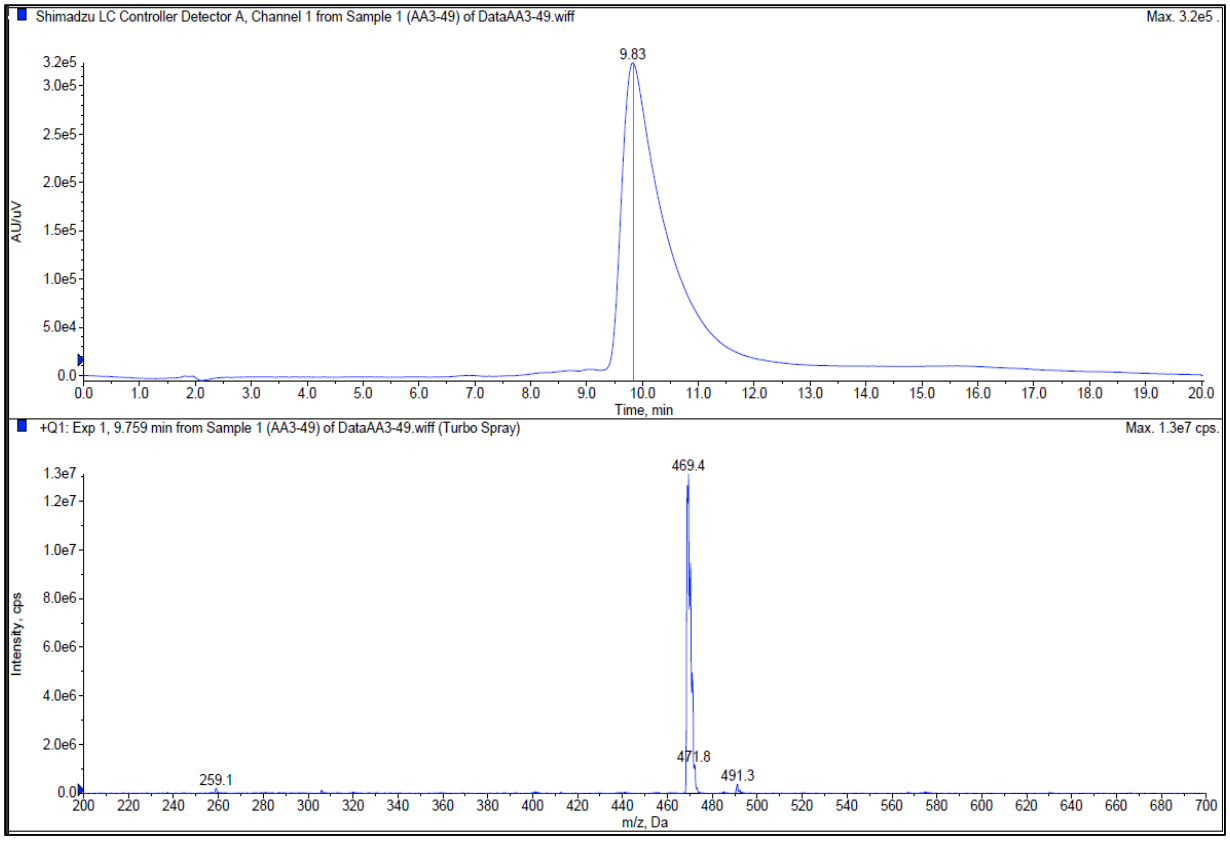

Figure 7.4. HPLC-LC/MS chromatogram for compound 6.11

Upper panel: UV absorption spectrum using UV detection at 254 and 214 nm, lower panel MS. Column: Hamilton reverse phase column (HxSil, C18, 3µm, 2.1 mm × 50 mm (H2)). Flow rate: 0.2 mL/min. Mobile phase: eluent A consists of 5% CH_3CN in H_2O; eluent B consists of 90% CH_3CN in H_2O. *N*-(4-(diethylamino)benzyl)-*N*-(3,4,5-trimethoxybenzyl)thiophene-2-carboxamide, calculated molecular weight: 468.61 Da. LC-MS: *m/*z 469.4 $(M + H)^+$.

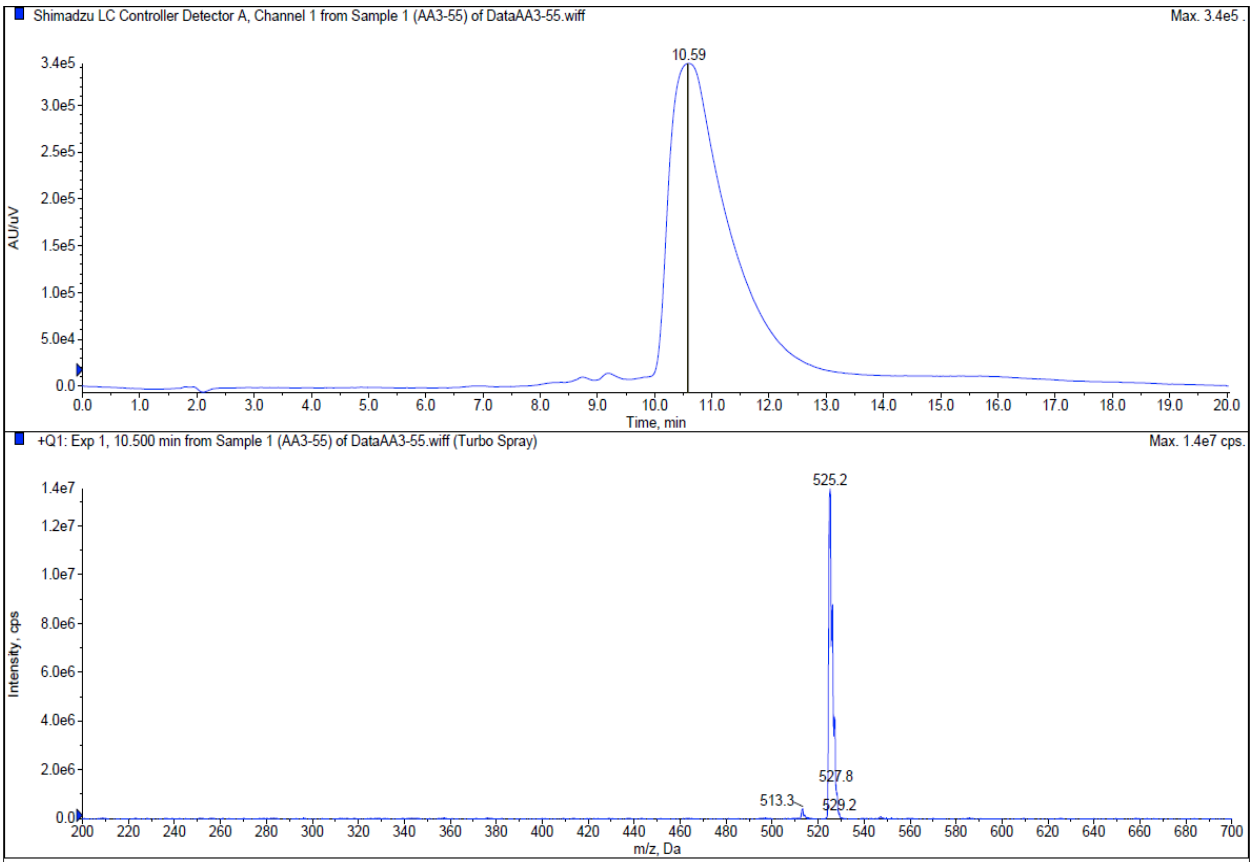

Figure 7.5. HPLC-LC/MS chromatogram for compound 6.15

Upper panel: UV absorption spectrum using UV detection at 254 and 214 nm, lower panel MS. Column: Hamilton reverse phase column (HxSil, C18, 3µm, 2.1 mm × 50 mm (H2)). Flow rate: 0.2 mL/min. Mobile phase: eluent A consists of 5% CH_3CN in H_2O; eluent B consists of 90% CH_3CN in H_2O. (*E*)-*N*-(4-(diethylamino)benzyl)-2-phenyl-*N*-(3,4,5-trimethoxybenzyl)ethene-1-sulfonamide, calculated molecular weight: 424.68 Da. LC-MS: *m/*z 425.2 $(M + H)^+$.

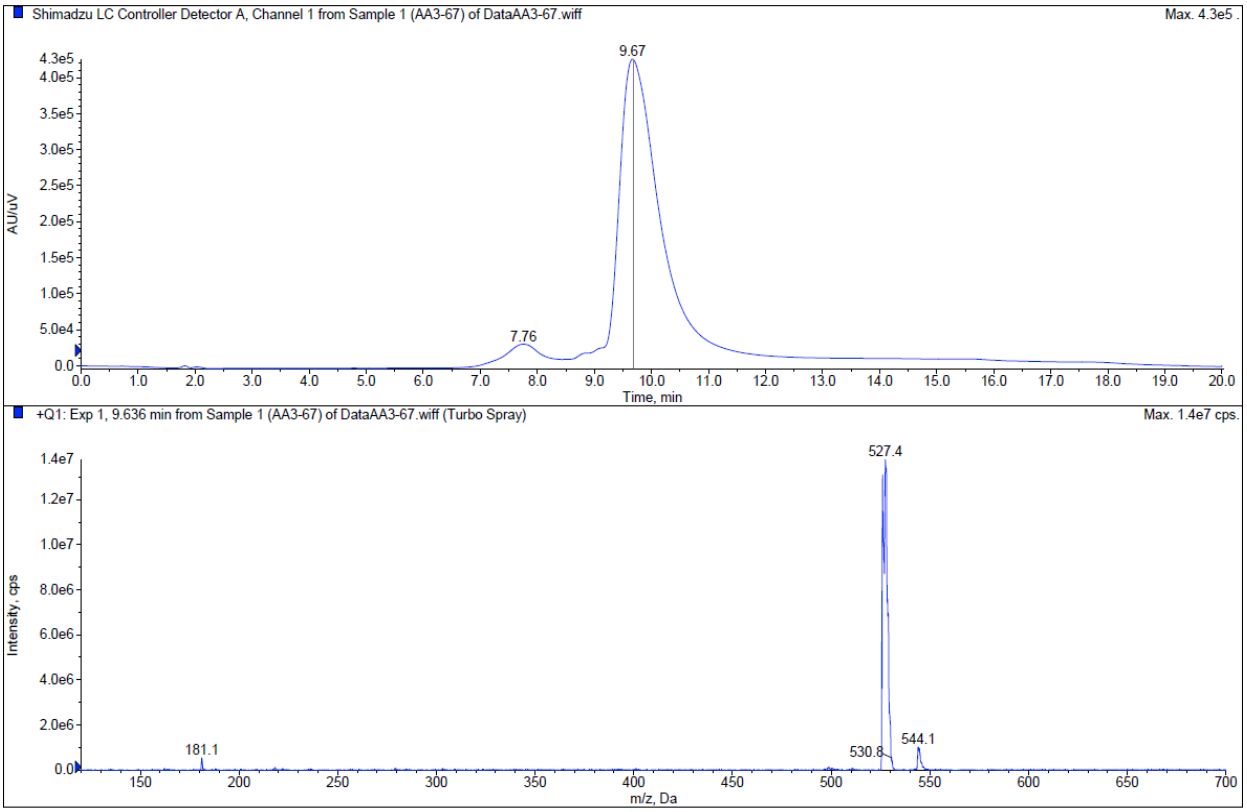

Figure 7.6. HPLC-LC/MS chromatogram for compound 6.18

Upper panel: UV absorption spectrum using UV detection at 254 and 214 nm, lower panel MS. Column: Hamilton reverse phase column (HxSil, C18, 3µm, 2.1 mm × 50 mm (H2)). Flow rate: 0.2 mL/min. Mobile phase: eluent A consists of 5% CH_3CN in H_2O; eluent B consists of 90% CH_3CN in H_2O. *N*-(4-(diethylamino)benzyl)-4-formyl-*N*-(3,4,5-trimethoxybenzyl)benzenesulfonamide, calculated molecular weight: 426.65 Da. LC-MS: *m/*z 427.4 $(M + H)^+$.

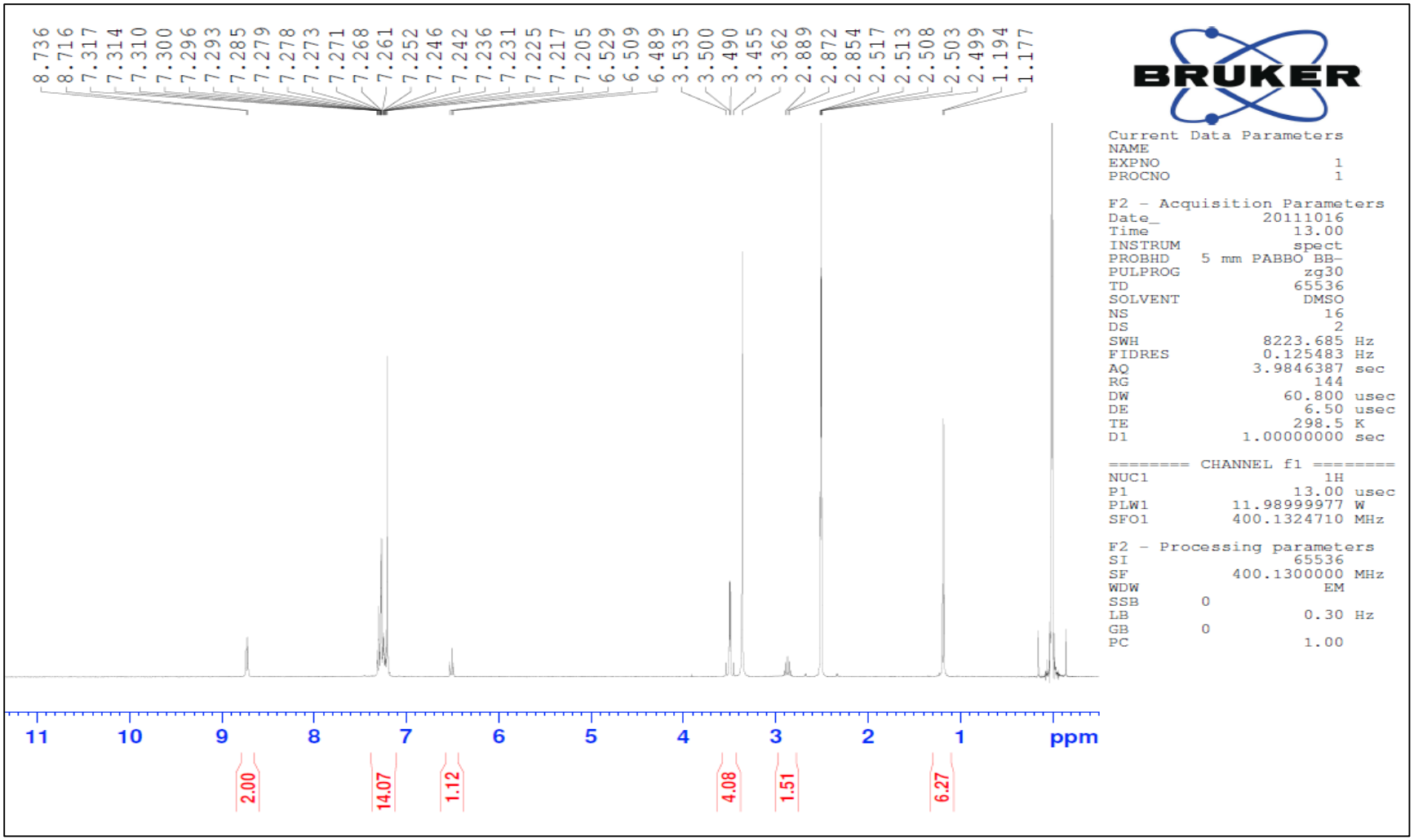

Figure 7.7. ^{1}H NMR Spectrum for 4.9 using DMSO-d_6 solvent

BRUKER 400 MHz NMR machine using deuterated dimethyl sulfoxide ($(CD_3)_2S=O$)) solvent with TMS internal standard

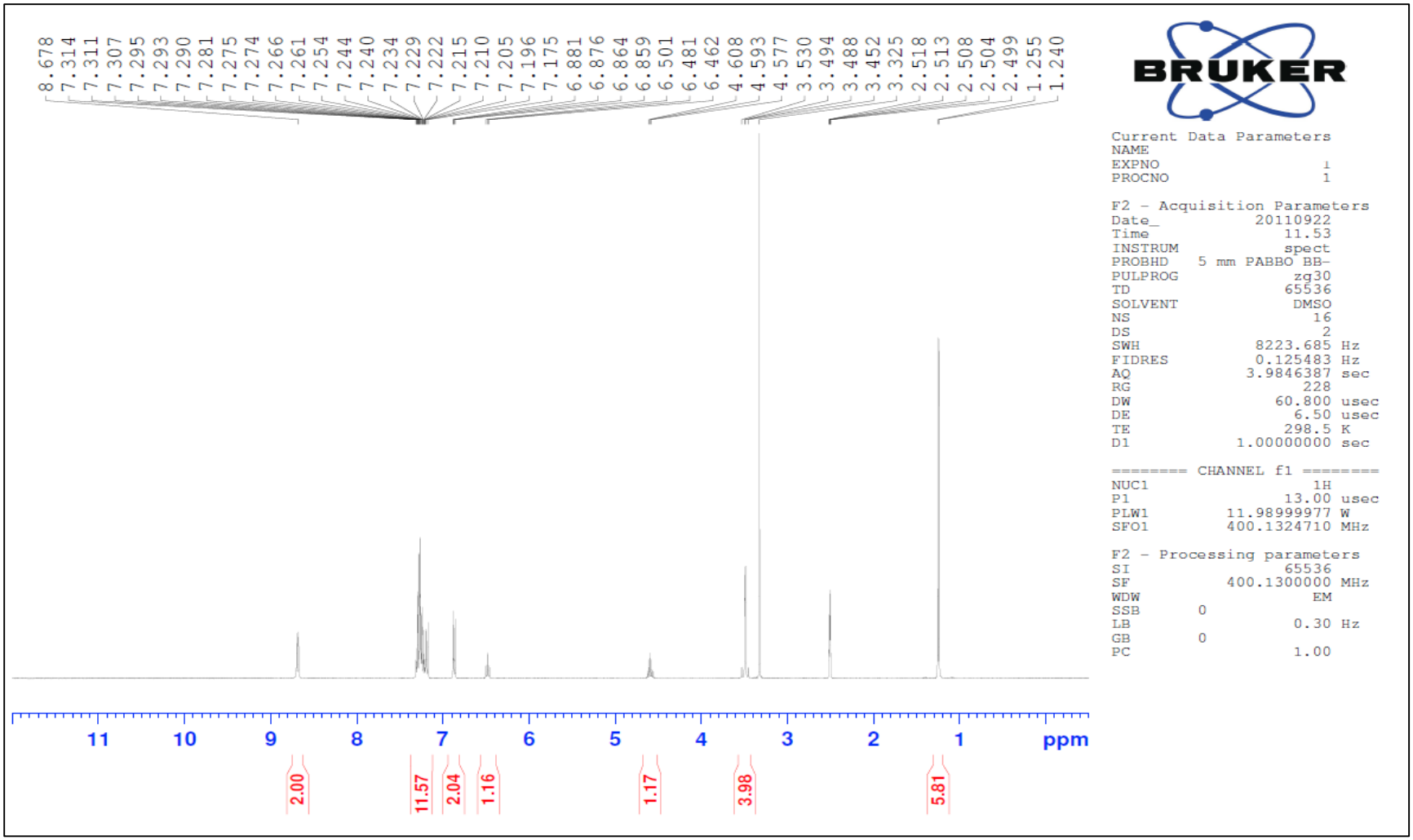

Figure 7.8. ^{1}H NMR Spectrum for 4.12 using DMSO-d_6 solvent

BRUKER 400 MHz NMR machine using deuterated dimethyl sulfoxide ($(CD_3)_2S=O$)) solvent with TMS internal standard

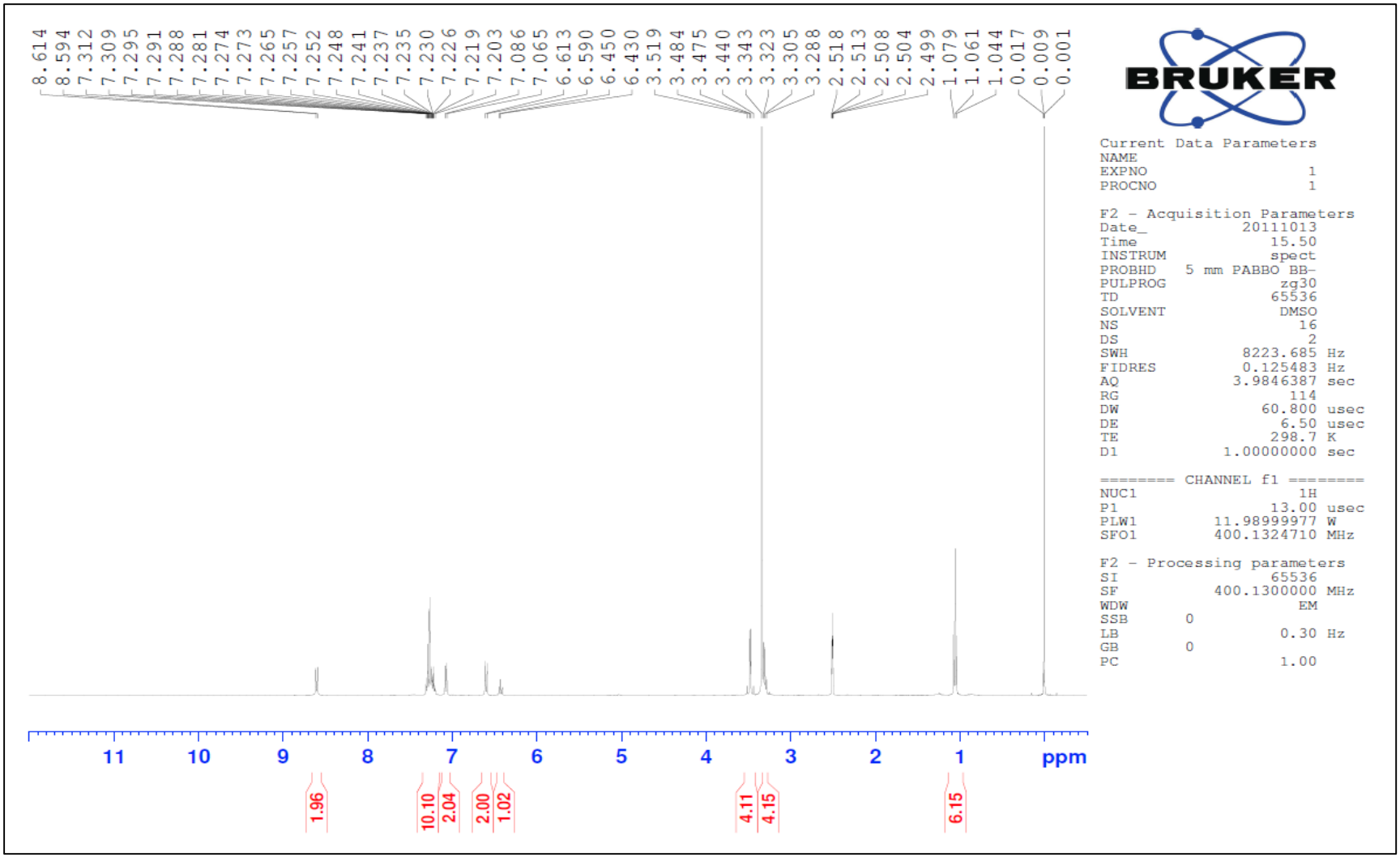

Figure 7.9. ^{1}H NMR Spectrum for 4.17 using DMSO-d_6 solvent

BRUKER 400 MHz NMR machine using deuterated dimethyl sulfoxide ($(CD_3)_2S=O$)) solvent with TMS internal standard

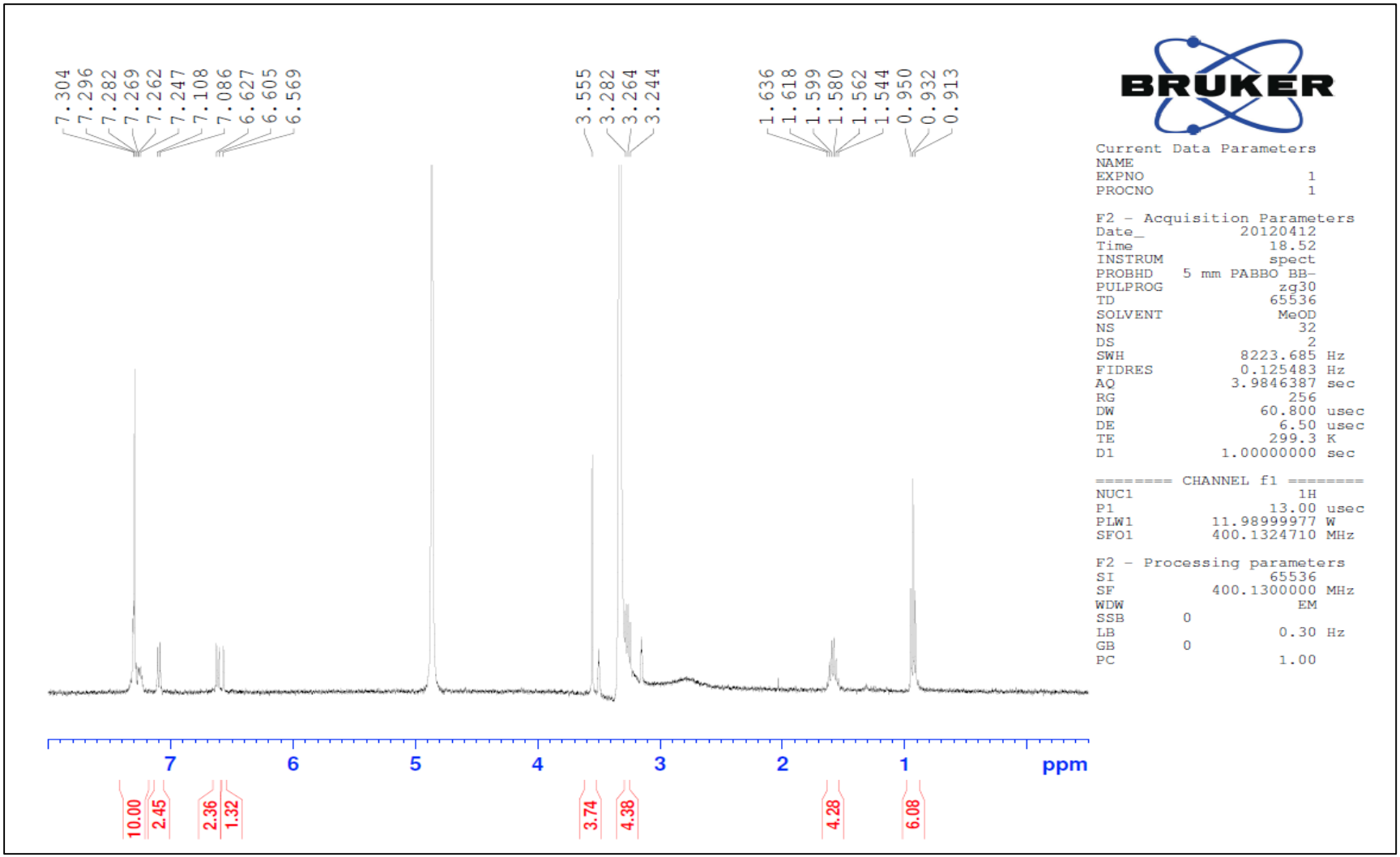

Figure 7.10. ^{1}H NMR Spectrum for 4.18 using CD_3OD solvent

BRUKER 400 MHz NMR machine using deuterated methanol (CD_3OD) solvent with TMS internal standard

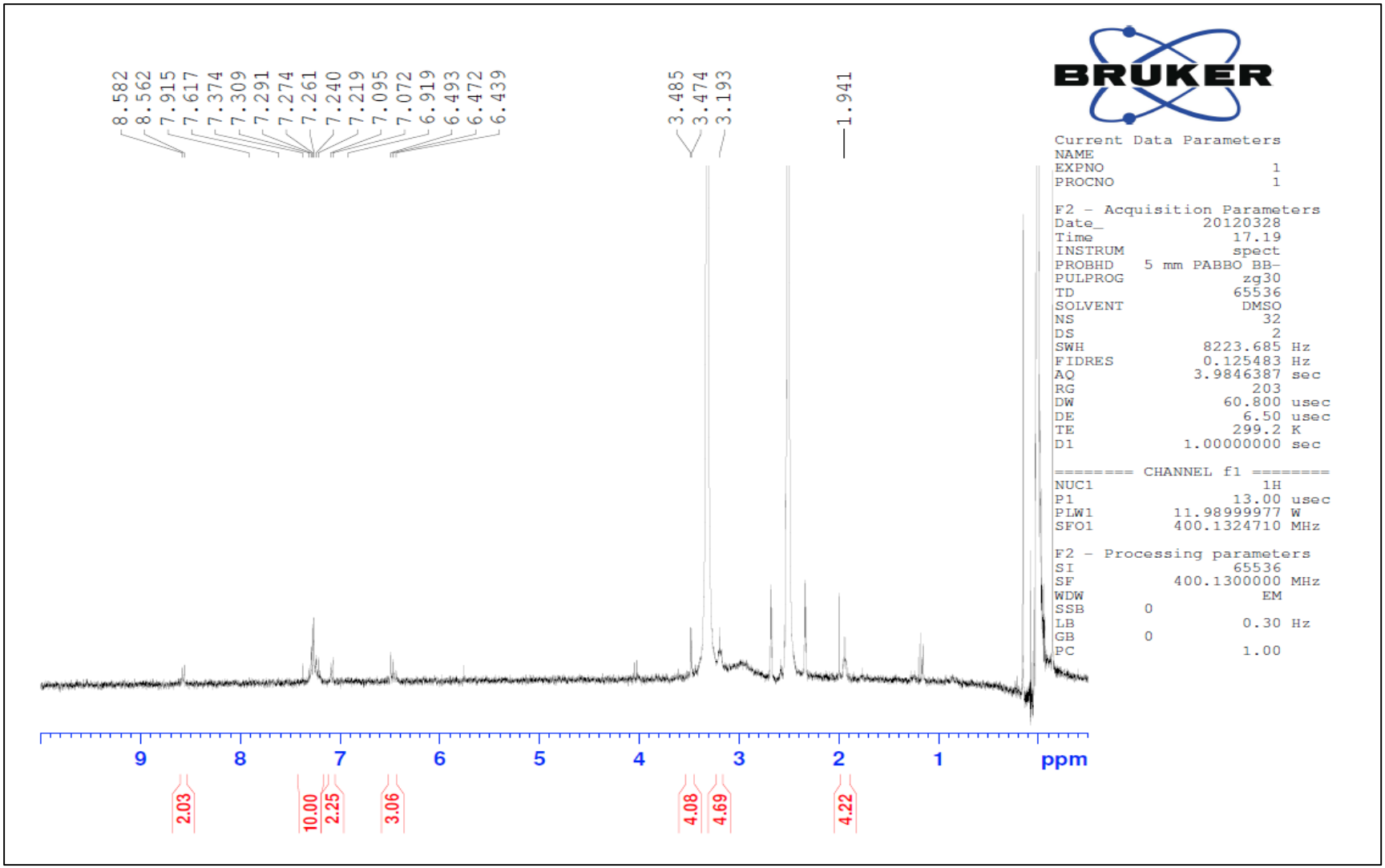

Figure 7.11. ^{1}H NMR Spectrum for 4.21 using DMSO-d_6 solvent

BRUKER 400 MHz NMR machine using deuterated dimethyl sulfoxide ($(CD_3)_2S=O$)) solvent with TMS internal standard

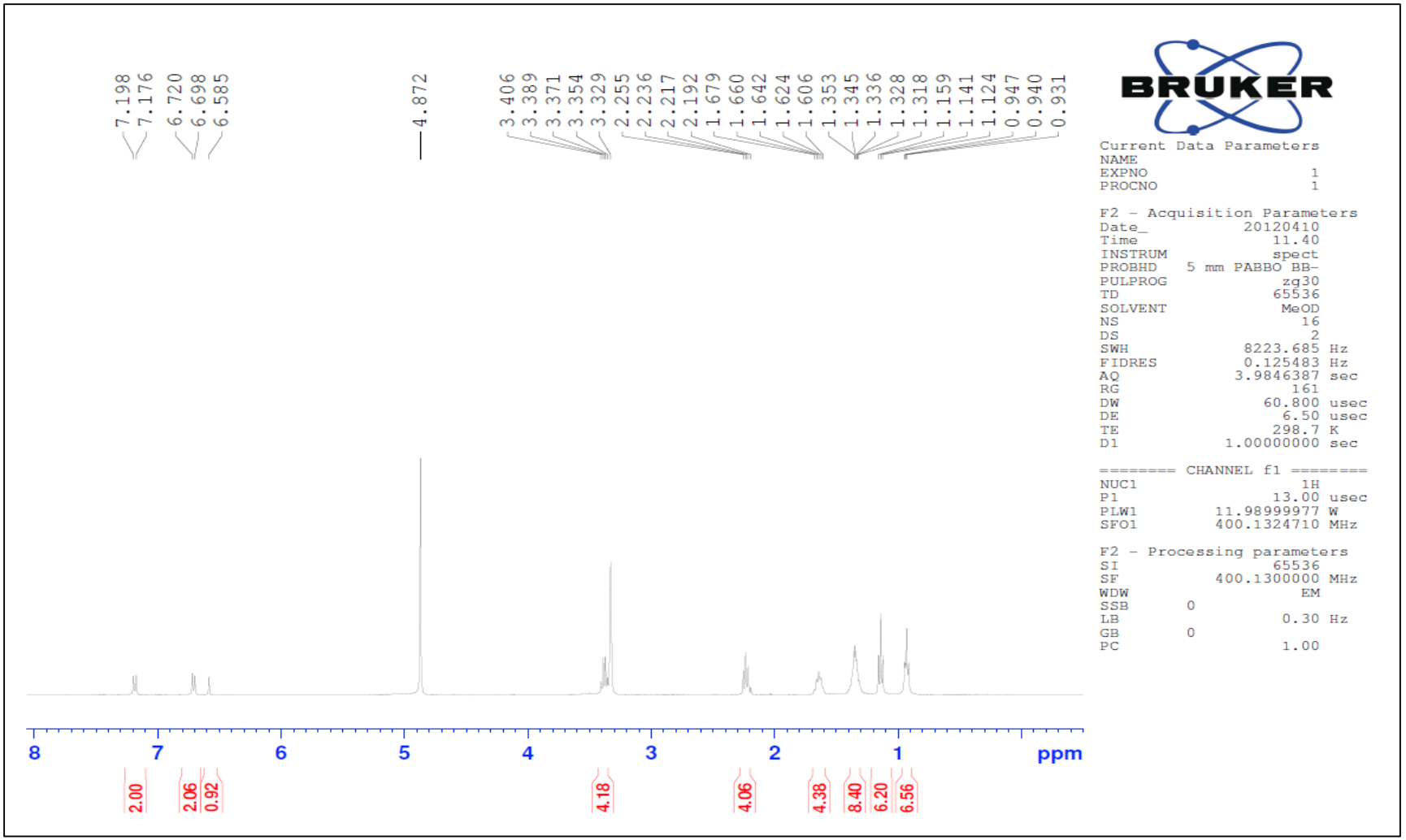

Figure 7.12. 1H NMR Spectrum for 4.47 using CD_3OD solvent

BRUKER 400 MHz NMR machine using deuterated methanol (CD_3OD) solvent with TMS internal standard

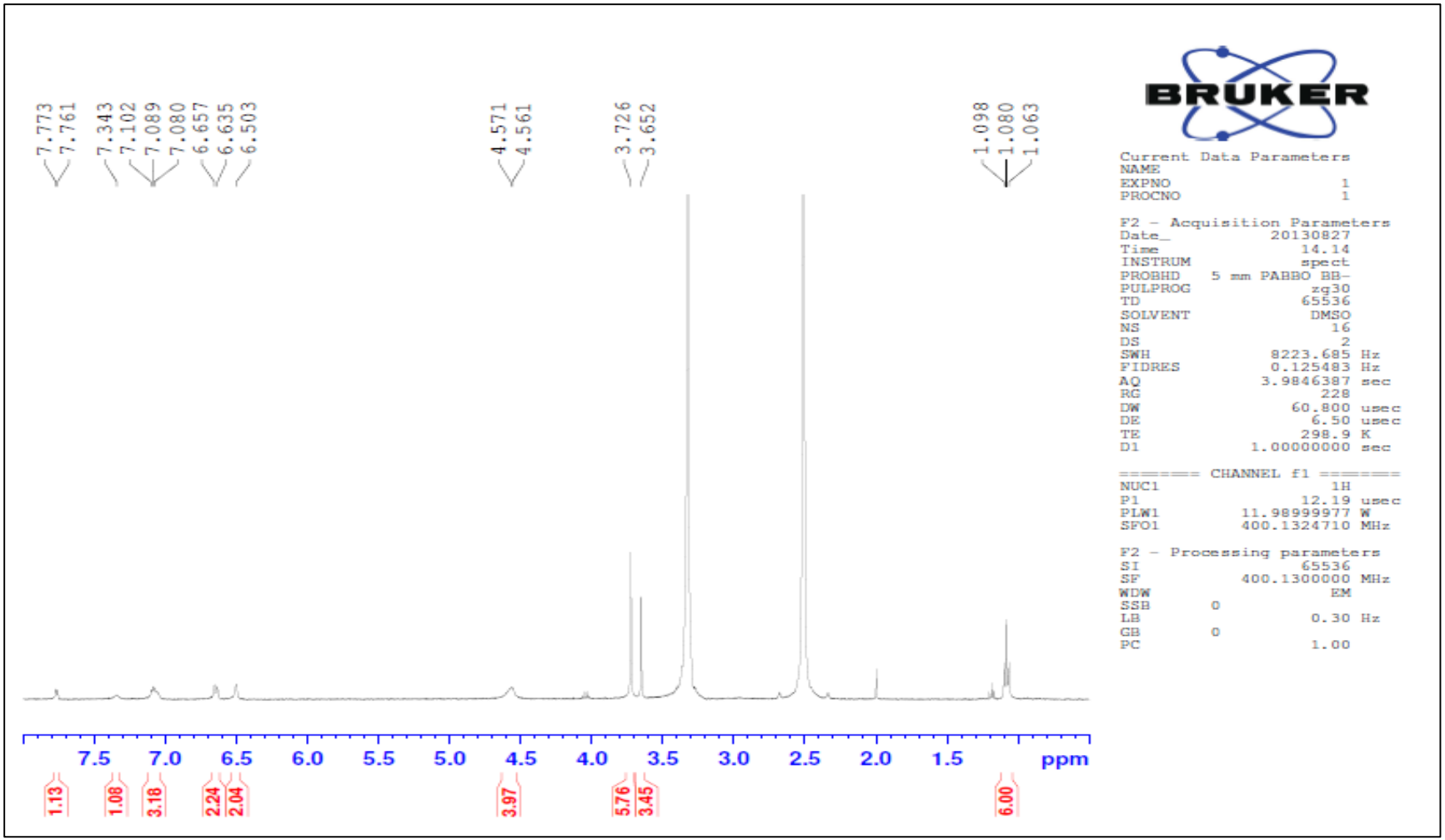

Figure 7.13. ^{1}H NMR Spectrum for 6.11 using DMSO-d_6 solvent

BRUKER 400 MHz NMR machine using deuterated dimethyl sulfoxide ($(CD_3)_2S=O$)) solvent with TMS internal standard.

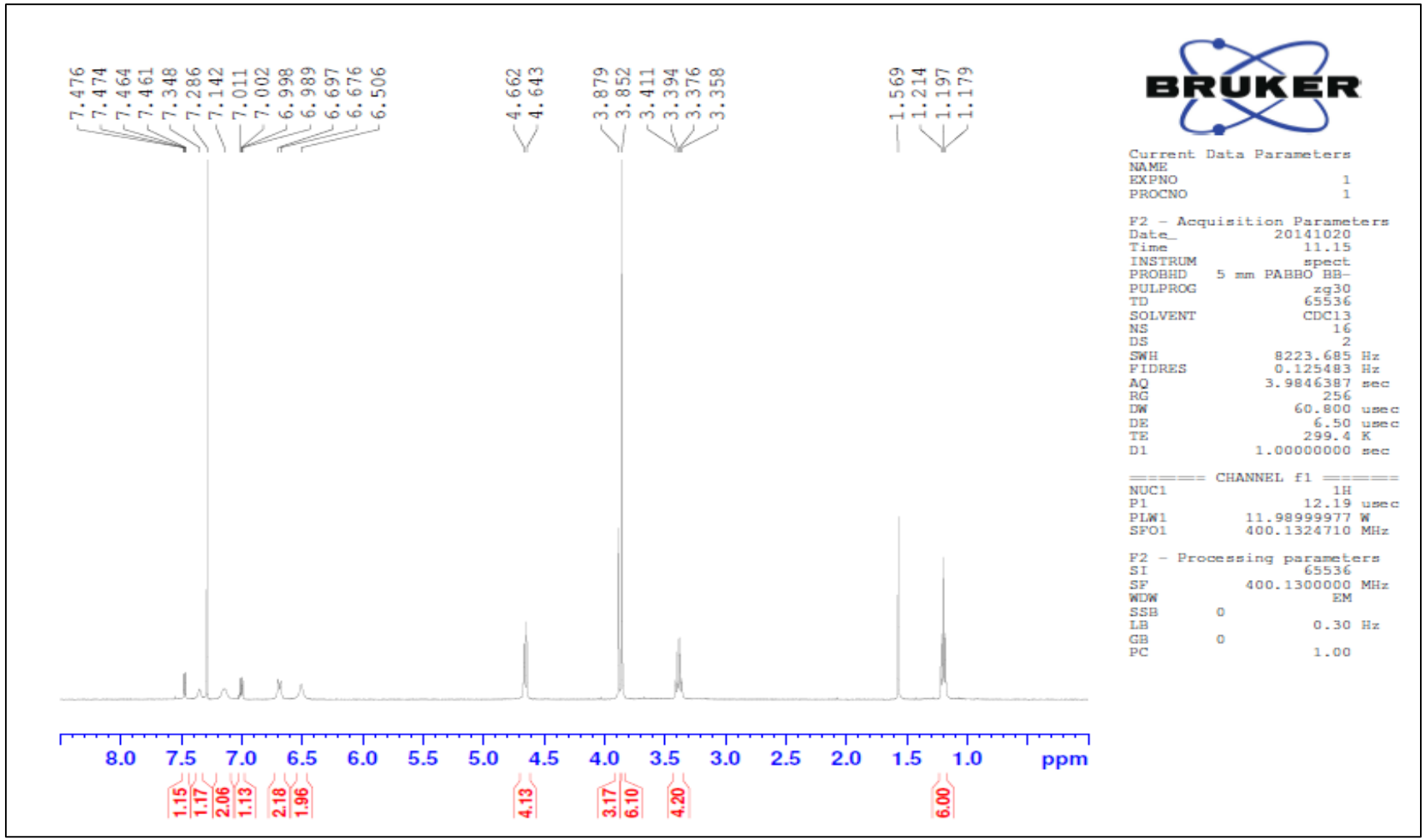

Figure 7.14. 1H NMR Spectrum for 6.11 using $CDCl_3$ solvent

BRUKER 600 MHz NMR machine using deuterated chloroform ($CDCl_3$) solvent with TMS internal standard.

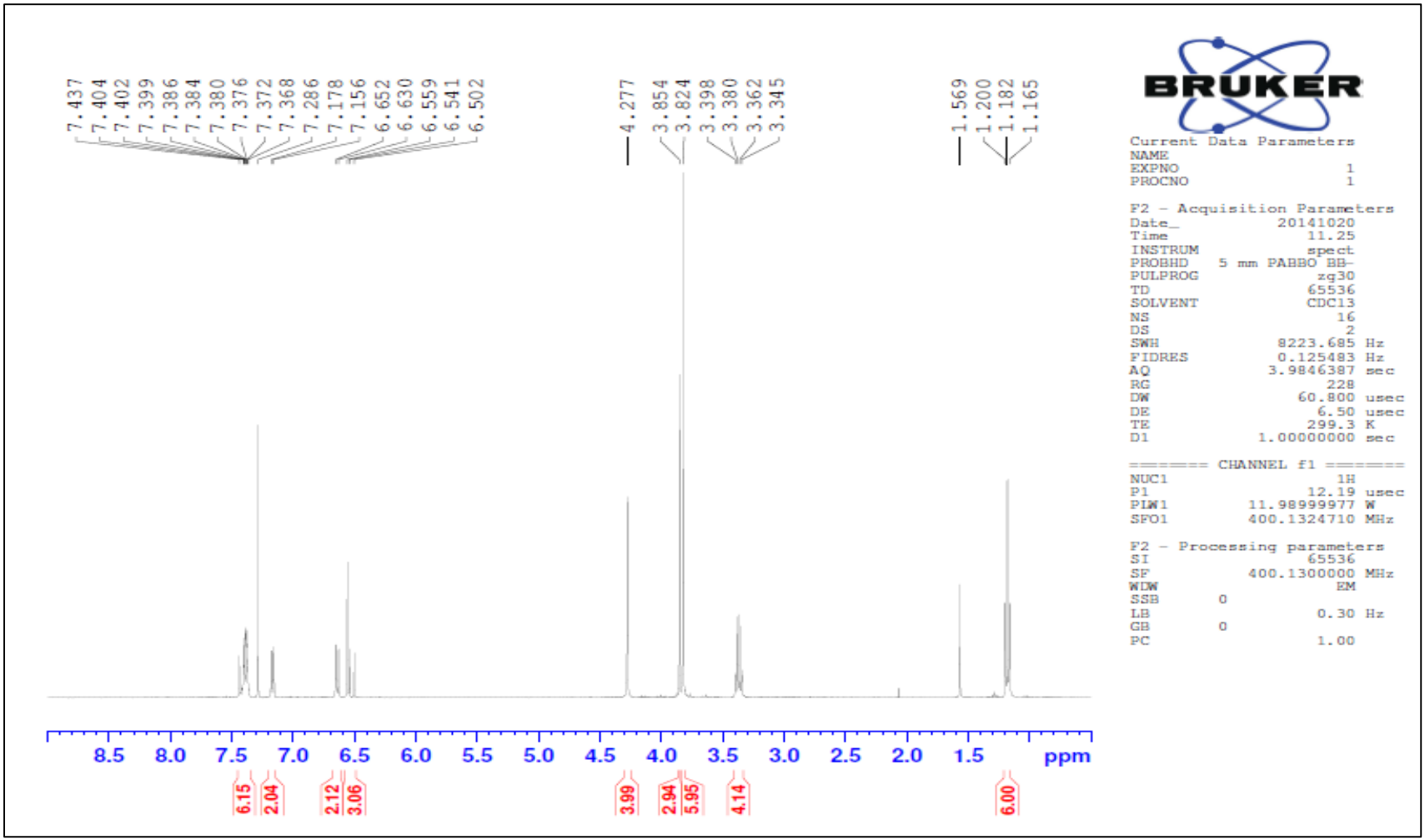

Figure 7.15. 1H NMR Spectrum for 6.15 using $CDCl_3$ solvent

BRUKER 400 MHz NMR machine using deuterated chloroform ($CDCl_3$) solvent with TMS internal standard.

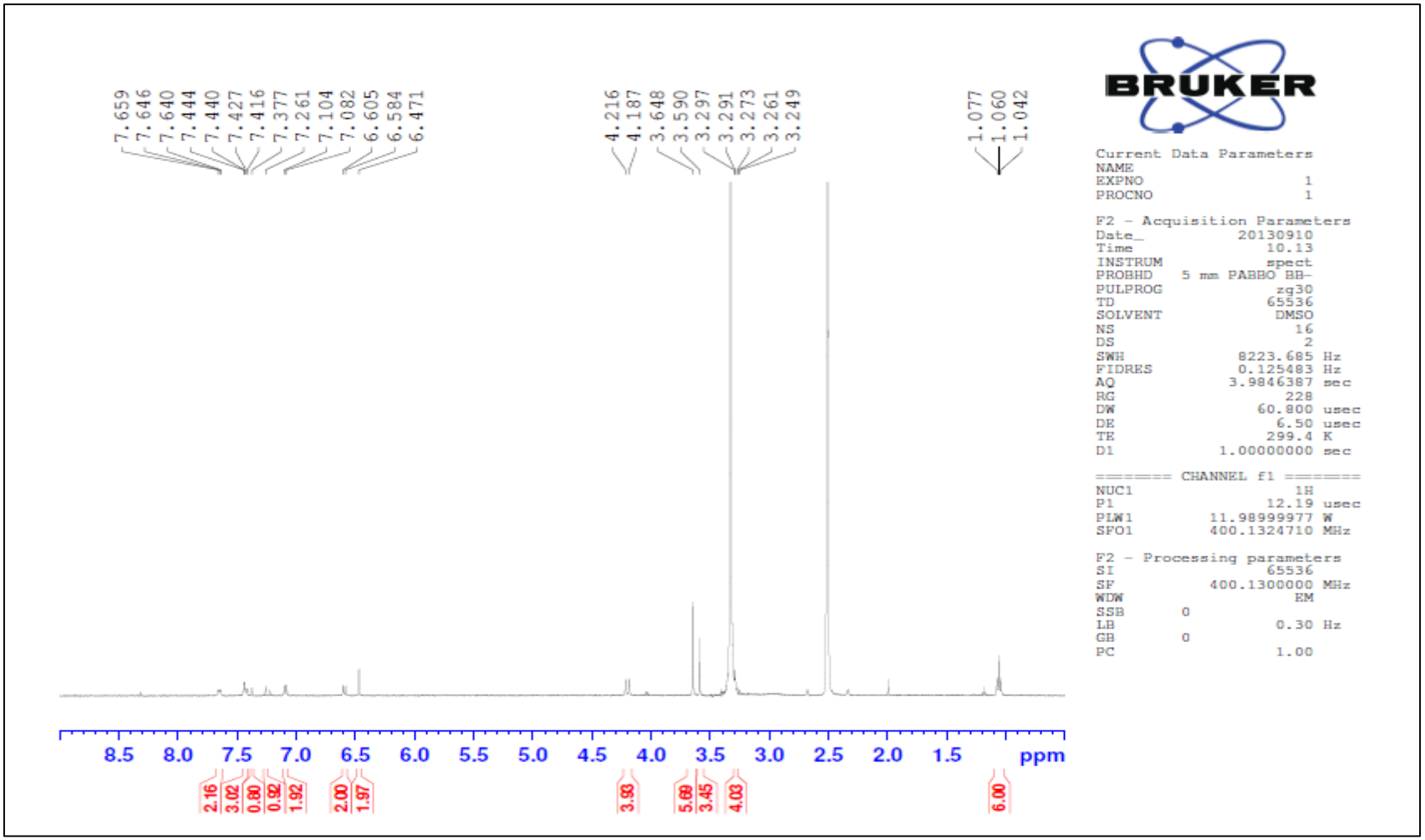

Figure 7.16. ^{1}H NMR Spectrum for 6.15 using DMSO-d_6 solvent

BRUKER 600 MHz NMR machine using deuterated dimethyl sulfoxide ((CD3)2S=O)) solvent with TMS internal standard.

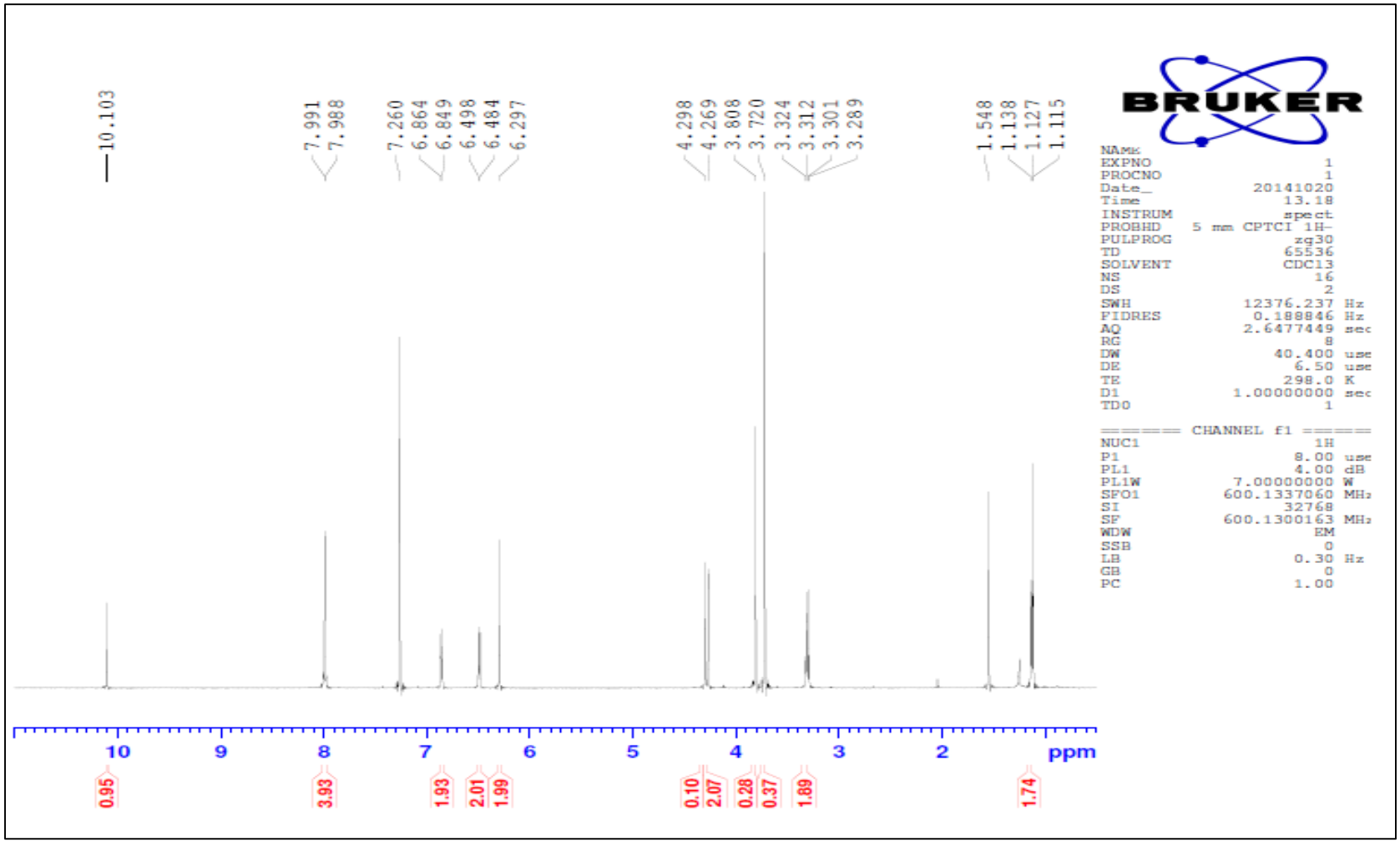

Figure 7.17. ^{1}H NMR Spectrum for 6.18 using $CDCl_3$ solvent

BRUKER 400 MHz NMR machine using deuterated chloroform ($CDCl_3$) solvent with TMS internal standard

APPENDIX B

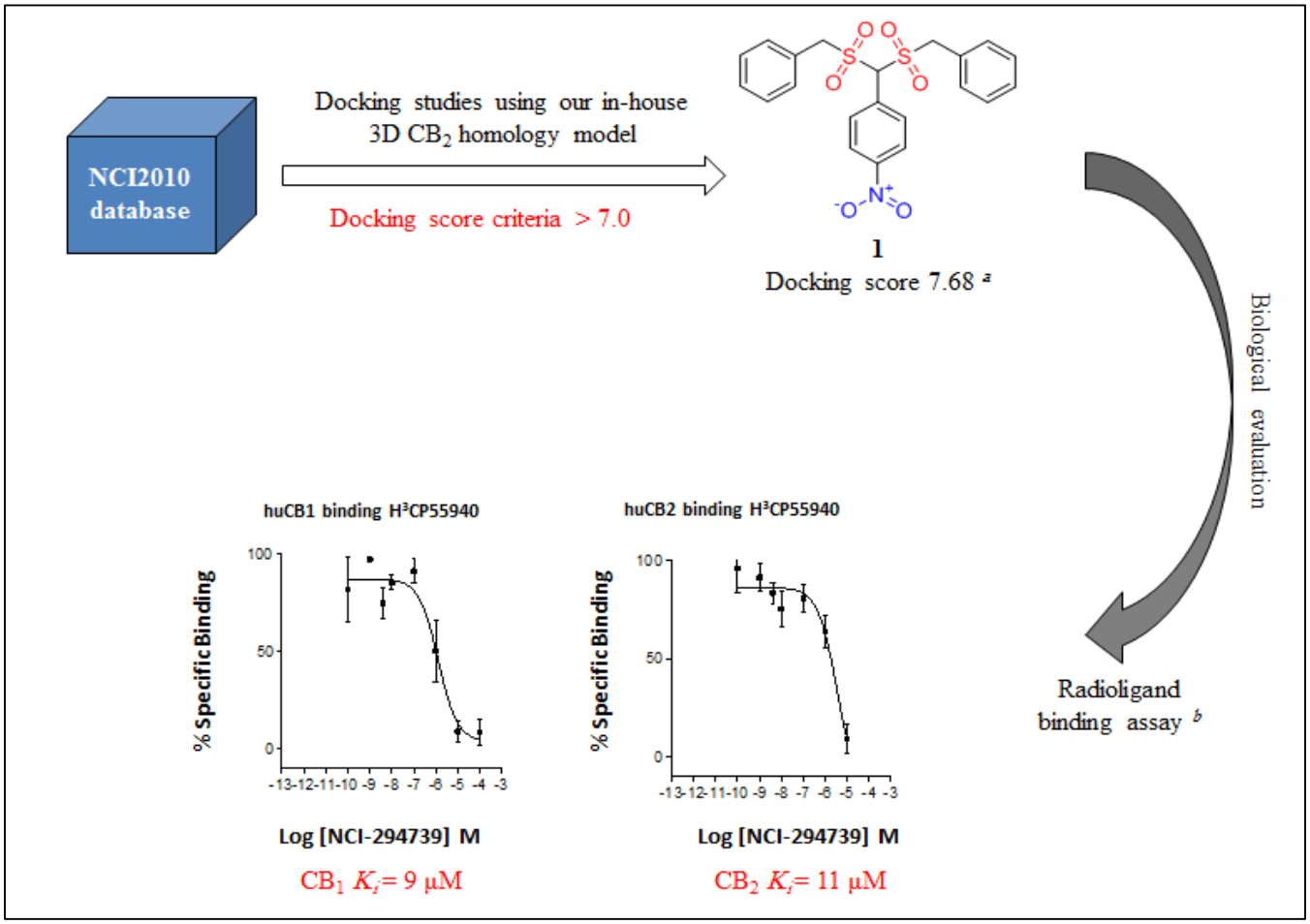

Figure 7.18. High-throughput molecular screening of NCI database.

The hit compound (**6.1**) was subjected to radio-ligand competition binding assay to confirm its CB affinity. [a] NCI compound screening was performed using Surflex-Dock program in SYBYL-X1.3. [b] Binding affinities for CB1 and CB2 receptors were evaluated using [^{3}H]CP-55,940 radioligand competition binding assay.

The National Cancer Institute (NCI) 2010 database contains more than 265,000 compounds that were subjected to refinements based on the Lipinski rule of five; molecular weight < 500, calculated logarithmic partition coefficient (cLog *P*) value of < 5, number of hydrogen bond donors (the sum of OHs and NHs) ≤ 5, and the number of hydrogen bond acceptors (the sum of Ns and Os) ≤ 10 [226]. The resulted new refined database (i.e. NCI2010_refined) was subjected the computational molecular docking studies using the Surflex-Dock module in the SYBYL X 1.3 software (Tripos Inc.). We utilized our published 3D CB2 homology receptor [207, 208, 222]. The docking interactions were analyzed based on the FlexX-Pharm Docking/CScore method to rank the hits with a better value of interactions. The docking criteria cutoff was 7.0 which was utilized as to filter the docking results. Ten compounds (listed in Table 7.1) showed a docking score of > 7.0 that were subjected to radio-ligand displacement assay. Compound **6.1** (NCI-294739) exhibited a docking score of 7.68, molecular weight of 445.50 (< 500), cLogP of 2.40 (< 5), number of hydrogen bond donors of 0 (< 5), number of hydrogen bond acceptors 7 (< 10), and with a CB2 K_i = 9236 nM, CB1 K_i = 11023 nM. This compound was chosen as a lead compound for further modifications.

Table 7.1. NCI database screening results

No.	Chemical Structure	NCI name[a]	CB2 Docking Score[b]	MW[c]	cLog P[d]	HBD[e]	HBA[f]	CB2 K_i (nM)[g]	CB1 K_i (nM)[h]
1	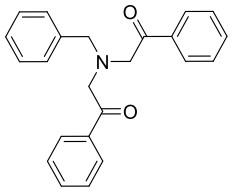	NCI-85077	7.74	343.43	4.66	0	3	8530	NT
2	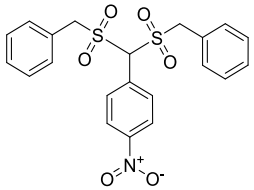	NCI-294739	7.68	445.50	2.40	0	7	9236	11023
3	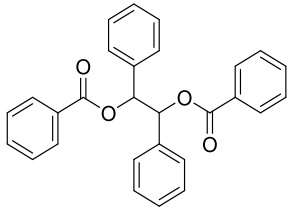	NCI-46432	9.13	422.48	7.14	0	4	NB	NT
4	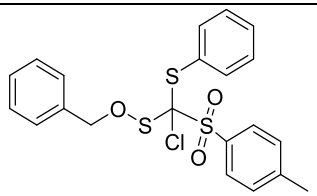	NCI-313383	7.74	451.01	6.79	0	3	7018	NT

5	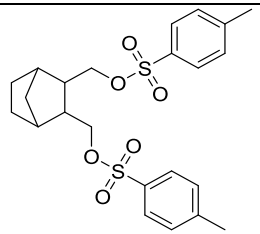	NCI-173740	10.31	464.60	5.01	0	6	NB	NT
6	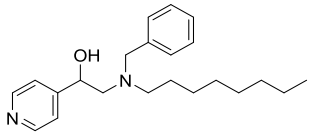	NCI-39810	8.23	340.51	5.23	1	3	NB	NT
7	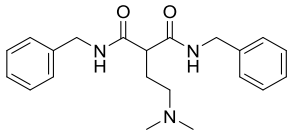	NCI-25896	7.27	353.47	1.75	2	5	NB	NT
8	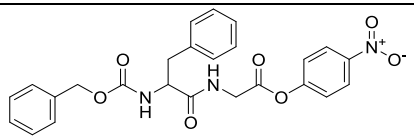	NCI-118451	8.92	477.47	3.97	2	10	16850	NT
9	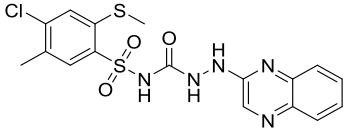	NCI-681179	6.11	437.92	2.53	3	8	NB	NT
10	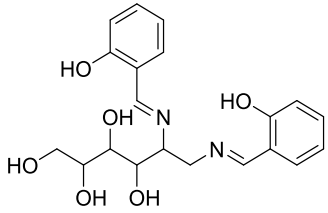	NCI-21559	8.26	388.42	0.21	6	8	NB	NT

[a] National Cancer Institute chemical structure name, [b] CB2 molecular docking score by the Surflex-Dock module in SYBYL X1.3 (Tripos Inc.), [c] Molecular weight (Da), [d] calculated logarithmic partition coefficient using ChemDraw (Perkin Elmer), [e] hydrogen bond

donor, [f] hydrogen bond acceptor, [g] CB2 binding affinity utilizing [^{3}H]CP-55,940 radioligand competition binding assay, [h] CB1 binding affinity utilizing [^{3}H]CP-55,940 radioligand competition binding assay (NB = no binding K_i >20000 nM, NT = not determined

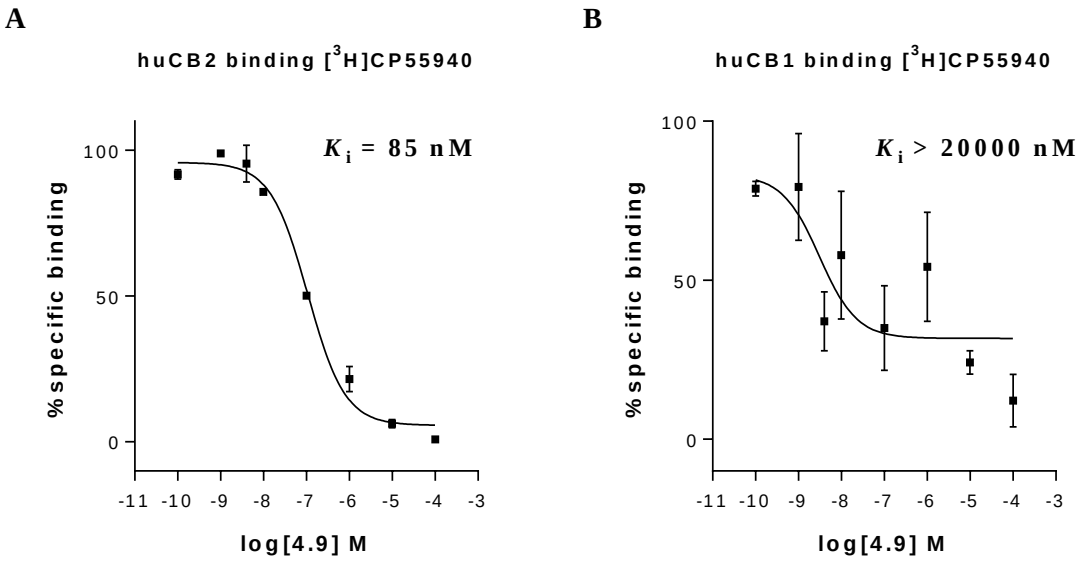

Figure 7.19 Binding profile of 4.9

Competition displacement of the [^{3}H]-CP55,940 was obtained by using an increased amount of the cold ligand **4.9** utilizing **(A)** human CB2 membrane (K_i = 85 nM), and **(B)** human CB1 membrane (K_i > 20000 nM). Assay was performed in triplicate (n = 3). Data represented as mean ± SEM.

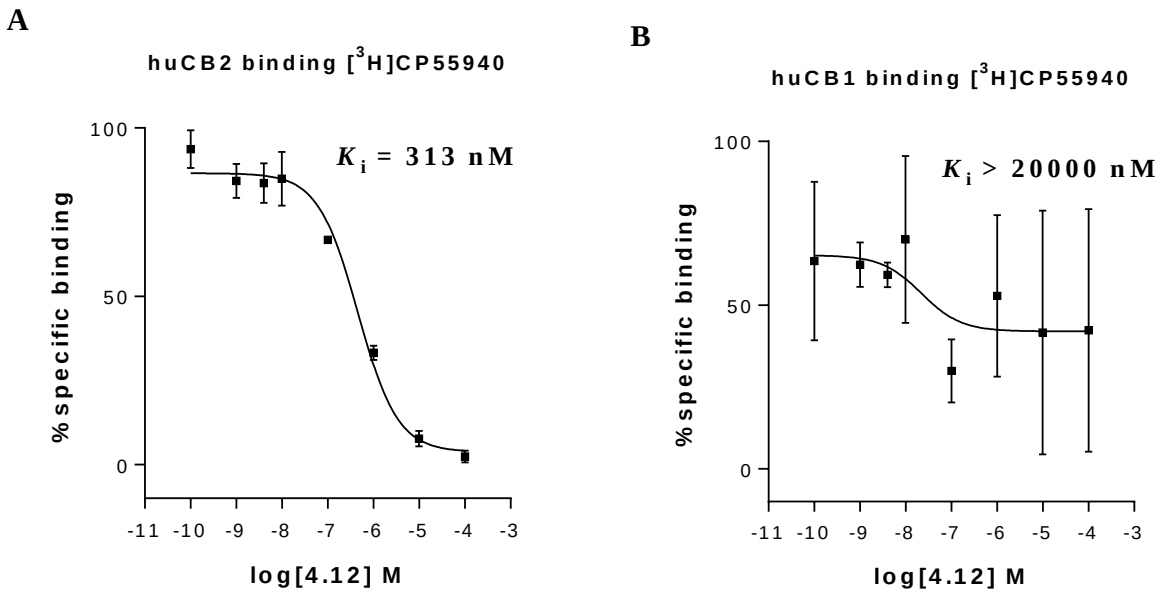

Figure 7.20. Binding profile of 4.12

Competition displacement of the [^{3}H]-CP55,940 was obtained by using an increased amount of the cold ligand **4.12** utilizing **(A)** human CB2 membrane (K_i = 313 nM), and **(B)** human CB1 membrane (K_i > 20000 nM). Assay was performed in triplicate (n = 3). Data represented as mean ± SEM.

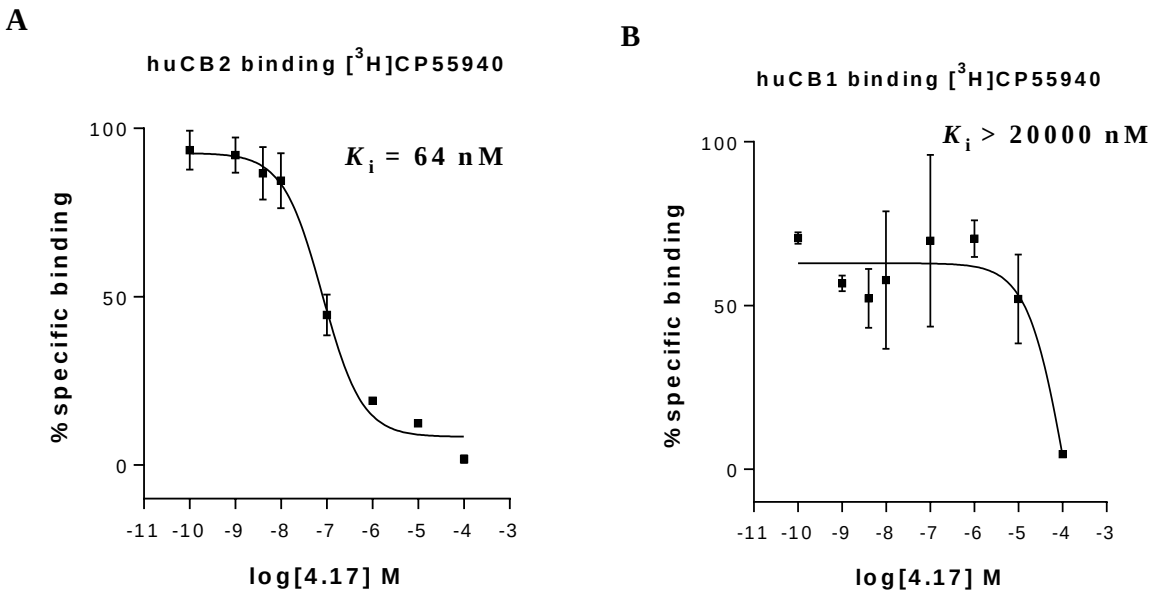

Figure 7.21. Binding profile of 4.17

Competition displacement of the [^{3}H]-CP55,940 was obtained by using an increased amount of the cold ligand **4.17** utilizing **(A)** human CB2 membrane (K_i = 64 nM), and **(B)** human CB1 membrane (K_i > 20000 nM). Assay was performed in triplicate (n = 3). Data represented as mean ± SEM.

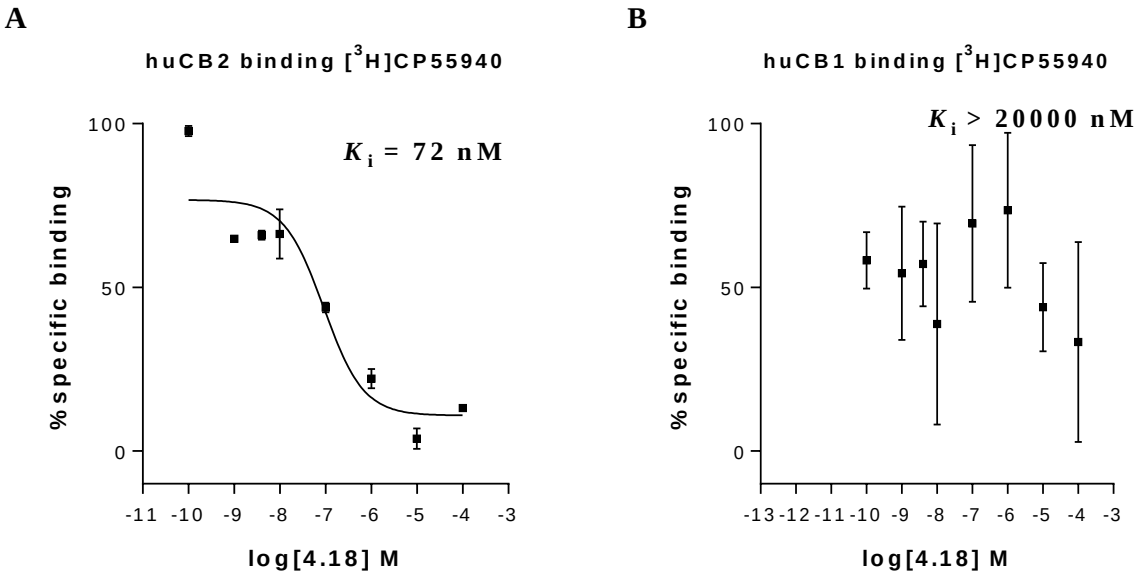

Figure 7.22. Binding profile of 4.18

Competition displacement of the [^{3}H]-CP55,940 was obtained by using an increased amount of the cold ligand **4.18** utilizing **(A)** human CB2 membrane (K_i = 72 nM), and **(B)** human CB1 membrane (K_i > 20000 nM). Assay was performed in triplicate (n = 3). Data represented as mean ± SEM.

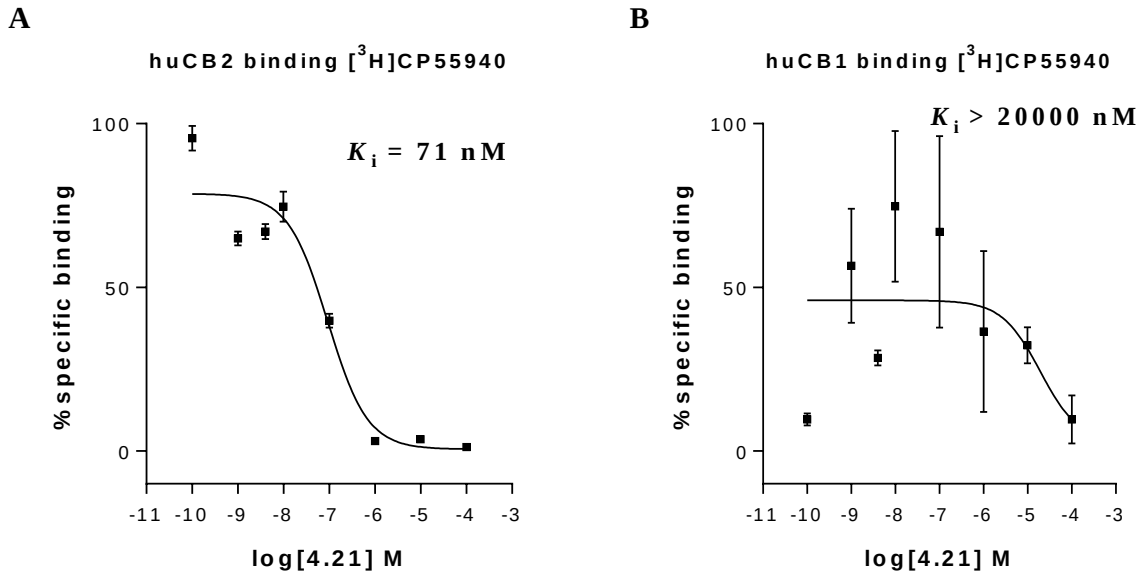

Figure 7.23. Binding profile of 4.21

Competition displacement of the [^{3}H]-CP55,940 was obtained by using an increased amount of the cold ligand **4.21** utilizing **(A)** human CB2 membrane (K_i = 71 nM), and **(B)** human CB1 membrane (K_i > 20000 nM). Assay was performed in triplicate (n = 3). Data represented as mean ± SEM.

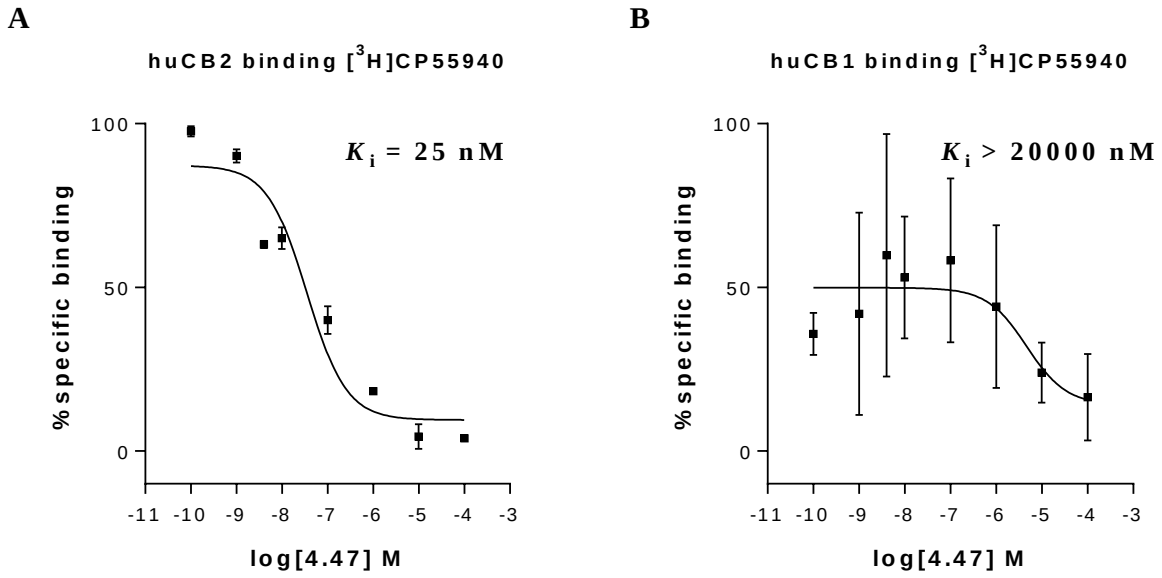

Figure 7.24. Binding profile of 4.47

Competition displacement of the [^{3}H]-CP55,940 was obtained by using an increased amount of the cold ligand **4.47** utilizing **(A)** human CB2 membrane (K_i = 25 nM), and **(B)** human CB1 membrane (K_i > 20000 nM). Assay was performed in triplicate (n = 3). Data represented as mean ± SEM.

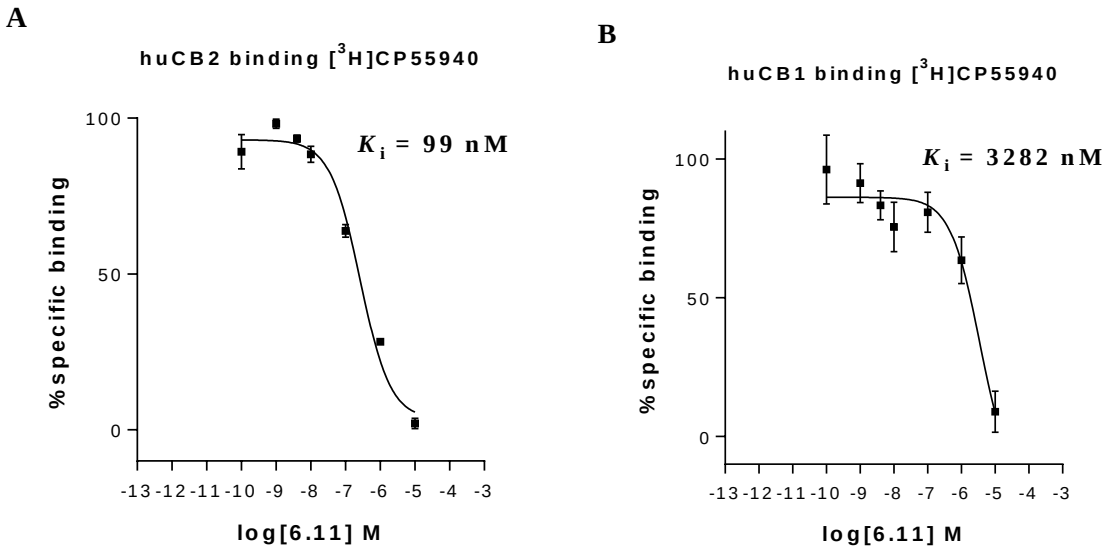

Figure 7.25 Binding profile of 6.11

Competition displacement of the [^{3}H]-CP55,940 was obtained by using an increased amount of the cold ligand **6.11** utilizing **(A)** human CB2 membrane (K_i = 99 nM), and **(B)** human CB1 membrane (K_i = 2382 nM). Assay was performed in triplicate (n = 3). Data represented as mean ± SEM.

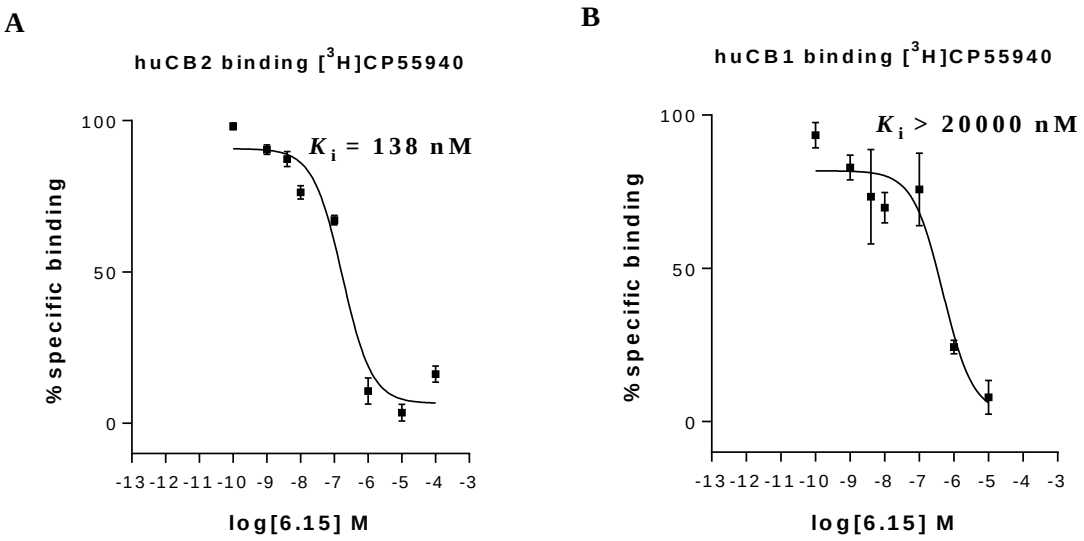

Figure 7.26. Binding profile of 6.15.

Competition displacement of the [^{3}H]-CP55,940 was obtained by using an increased amount of the cold ligand **6.15** utilizing **(A)** human CB2 membrane (K_i = 138 nM), and **(B)** human CB1 membrane (K_i = 20000 nM). Assay was performed in triplicate (n = 3). Data represented as mean ± SEM.

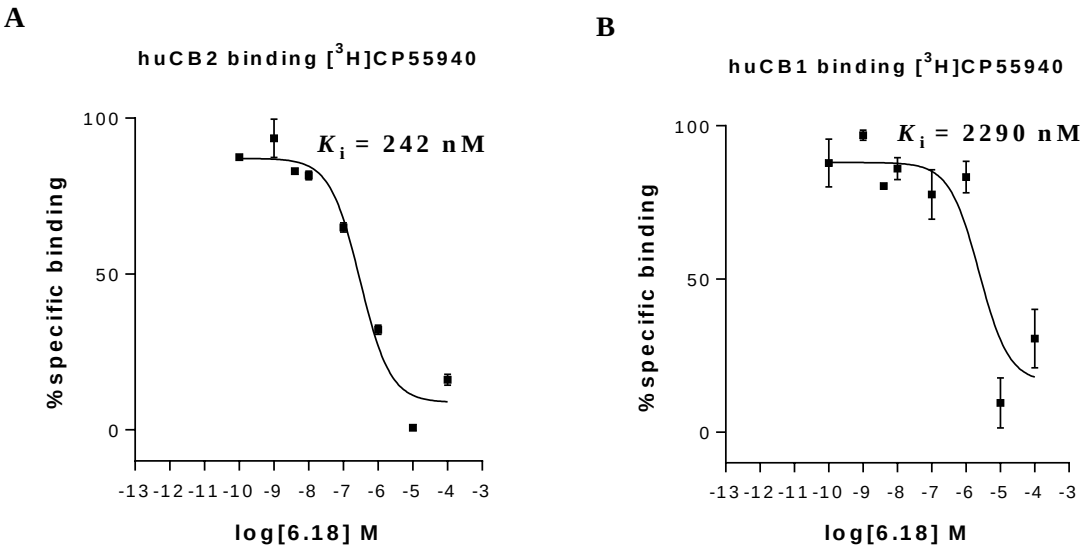

Figure 7.27. Binding profile of 6.18.

Competition displacement of the [^{3}H]-CP55,940 was obtained by using an increased amount of the cold ligand **6.18** utilizing **(A)** human CB2 membrane (K_i = 242 nM), and **(B)** human CB1 membrane (K_i = 2290 nM). Assay was performed in triplicate (n = 3). Data represented as mean ± SEM.

APPENDIX C

Pharmacokinetic/Pharmacodynamic Studies

A. Pharmacokinetic Studies of 4.17

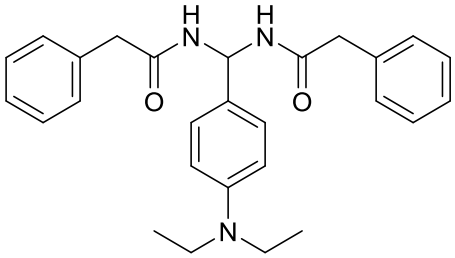

4.17

***N*,*N*'-((4-(diethylamino)phenyl)methylene)bis(2-phenylacetamide)**

Chemical Formula: $C_{27}H_{31}N_3O_2$

Molecular Weight: 429.56

CLogP: 4.96

Table 7.2. Oral plasma concentration for 4.17

T(h)	Conc. (ng/mL)	SD
0	0	0
0.08	5.851	2.205
0.17	7.240	4.106
0.25	6.279	2.936
0.5	3.232	1.292
0.75	3.828	1.411
1	3.895	0.8213
2	2.760	0.5935
4	1.294	0.2148
6	1.695	0.3184
8	0.8374	0.3342
12	0.6186	0.1067
24	0.4740	0.0148

Concentration mean of three rats (n = 3) measured in ng/mL

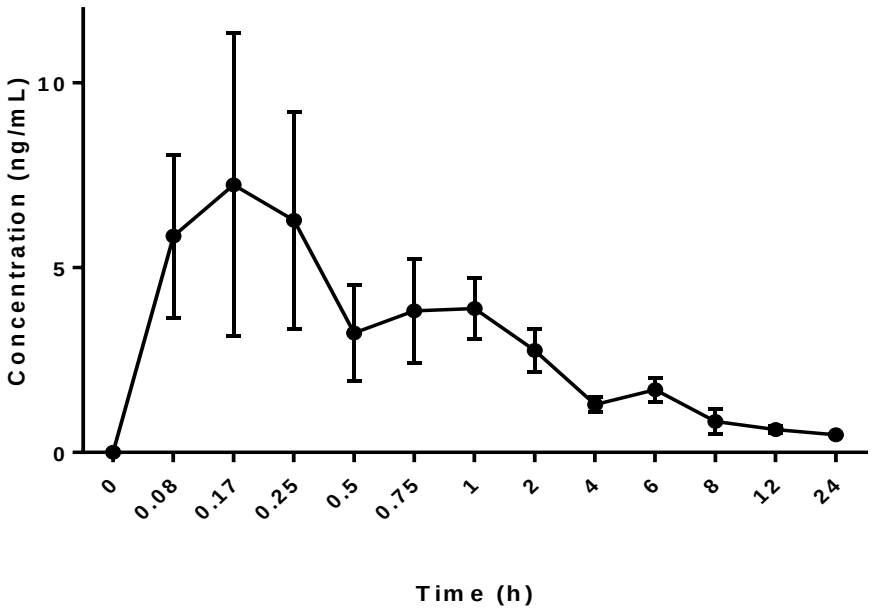

Figure 7.28. Plasma concentration after oral administration of 4.17

Plots of the plasma concentration after oral administration of **4.17**. Data are mean ± SD of three rats.

Table 7.3. Oral pharmacokinetic parameters of 4.17

Parameter	Unit	No.1	No.2	No.3	Mean
$AUC_{(0-t)}$	μg/L*h	14.20	28.08	28.10	23.46
$AUC_{(0-\infty)}$	μg/L*h	16.47	28.10	28.19	24.25
λ	1/h	0.23	0.32	0.24	0.26
C_{last}	μg/L	0.52	0.01	0.023	0.18
$t_{1/2}$	h	3.04	2.20	2.84	2.69
T_{max}	h	0.17	0.17	1.00	0.44
Vd	L/kg	5326	2260	2908	3498
CL	L/h/kg	1214	712	709	879
C_{max}	μg/L	8	11	4	8

B. Pharmacokinetic Studies of 6.11

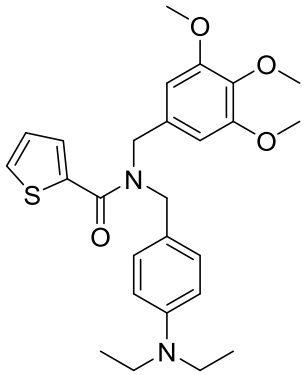

6.11
***N*-(4-(diethylamino)benzyl)-*N*-(3,4,5-trimethoxybenzyl)thiophene-2-carboxamide**
Chemical Formula: $C_{26}H_{32}N_2O_4S$
Molecular Weight: 468.61
CLogP: 4.8626

Table 7.4. Oral plasma concentration for 6.11

Time (h)	Conc. (ng/mL)	SD
0	0	0
0.08	76.09	11.91
0.17	81.82	12.47
0.25	85.54	14.31
0.5	71.34	17.21
0.75	43.20	6.52
1	39.28	1.12
2	32.78	4.58
4	14.79	6.72
6	5.709	0.68
8	-	-
10	-	-
24	-	-

Concentration mean of three rats (n = 3) measured in ng/mL.

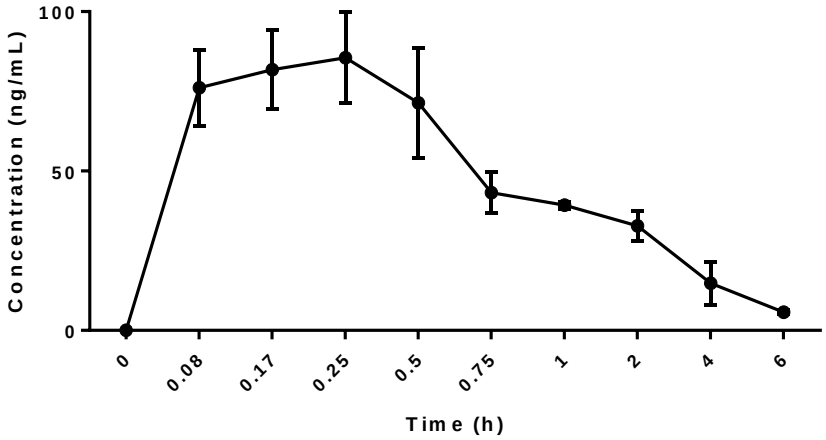

Figure 7.29. Plasma concentration after oral administration of 6.11

Plots of the plasma concentration after oral administration of **6.11**. Data are mean ± SD of three rats.

Table 7.5. Oral pharmacokinetic properties of 6.11

Parameter	Unit	No.1	No.2	No.3	Mean
$AUC_{(0-t)}$	μg/L*h	181.5	136.1	163.2	160.3
$AUC_{(0-\infty)}$	μg/L*h	198.6	153.0	176.3	176.0
λ	1/h	0.37	0.51	0.41	0.43
C_{last}	μg/L	6.34	8.61	5.32	6.75
$t_{1/2}$	h	1.87	1.37	1.70	1.65
T_{max}	h	0.25	0.25	0.08	0.19
Vd	L/kg	271.6	257.6	278.7	269.3
CL	L/h/kg	100.7	130.7	113.5	114.9
C_{max}	μg/L	96.73	90.47	73.88	87.03

Table 7.6. Intravenous plasma concentration of 6.11

Time (h)	Conc. (ng/mL)	SD
0	0	0
0.08	422.1	86.33
0.17	246.9	43.16
0.25	141.2	32.25
0.5	56.80	11.25
0.75	32.09	5.41
1	22.32	2.10
2	16.37	1.41
4	13.35	0.57
6	11.51	0.77
8	10.70	1.07
10	7.52	1.28
24	4.99	0.26

Concentration mean of three rats (n = 3) measured in ng/mL.

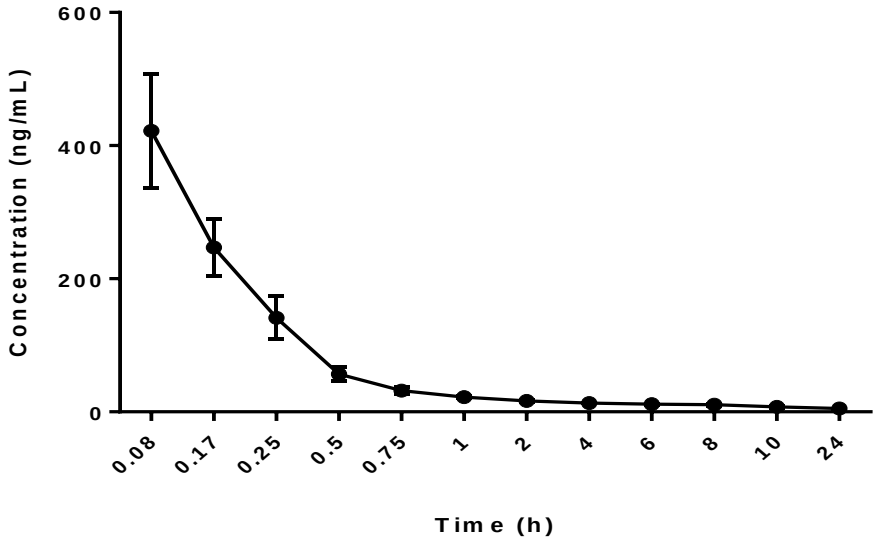

Figure 7.30. Plasma concentration after intravenous administration of 6.11

Plots of the plasma concentration after intravenous administration of **6.11**. Data are mean ± SD of three rats.

Table 7.7. Intravenous pharmacokinetic properties of 6.11

Parameter	Unit	No.1	No.2	No.3	Mean
$AUC_{(0-t)}$	μg/L*h	363.4	331.6	313.9	336.3
$AUC_{(0-\infty)}$	μg/L*h	475.5	431.2	421.9	442.9
λ	1/h	0.05	0.05	0.05	0.05
C_{last}	μg/L	5.16	4.67	5.15	4.99
$t_{1/2}$	h	15.05	14.79	14.54	14.79
T_{max}	h	0.08	0.08	0.08	0.08
Vd	L/kg	91.33	98.98	99.46	96.59
CL	L/h/kg	4.21	4.64	4.74	4.53
C_{max}	μg/L	499.5	437.8	329.0	422.1

C. Pharmacokinetic Studies of 6.15

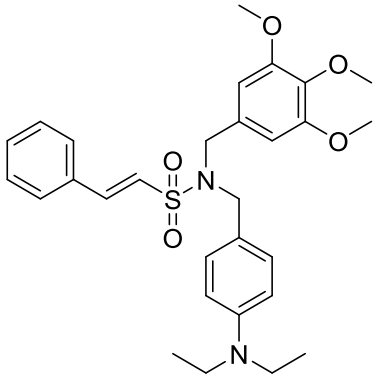

6.15
(*E*)-*N*-(4-(diethylamino)benzyl)-2-phenyl-*N*-(3,4,5-trimethoxybenzyl)ethene-1-sulfonamide
Chemical Formula: $C_{29}H_{36}N_2O_5S$
Molecular Weight: 524.68
CLogP: 5.9371

Table 7.8. Oral plasma concentration for 6.15

T (h)	Average conc. (ng/mL)	SD
0	0	0
0.08	4.52	1.86
0.17	9.01	3.54
0.25	12.38	2.02
0.5	13.05	5.59
0.75	7.86	3.52
1	4.47	2.44
2	4.52	3.05
4	-	-
6	-	-
8	-	-
12	-	-
24	-	-

Concentration mean of three rats (n = 3) measured in ng/mL

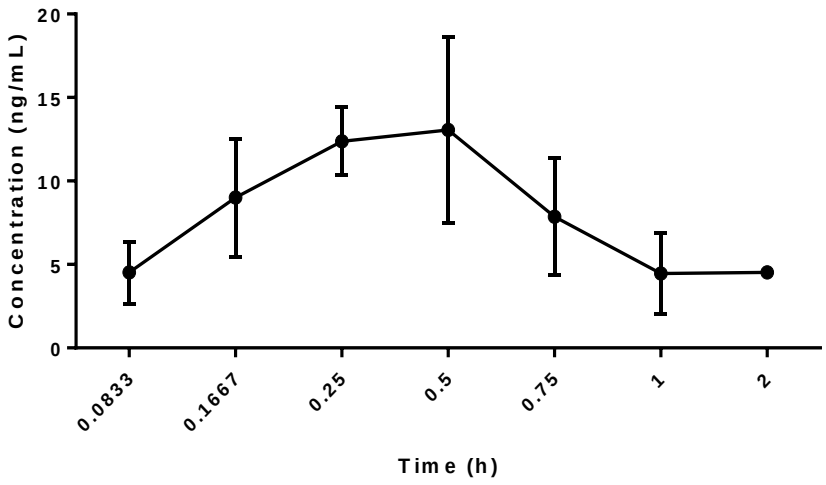

Figure 7.31. Plasma concentration after oral administration of 6.15

Plots of the plasma concentration after oral administration of **6.15**. Data are mean ± SD of three rats.

Table 7.9. Oral pharmacokinetic parameters of 6.15

Parameter	Unit	No.1	No.2	No.3	Mean
$AUC_{(0-t)}$	μg/L*h	6.24	8.80	19.46	11.50
$AUC_{(0-\infty)}$	μg/L*h	8.48	12.35	20.61	13.82
λ	1/h	1.50	1.63	1.55	1.56
C	μg/L	3.361	5.78	1.78	3.64
$t_{1/2}$	h	0.463	0.43	0.45	0.45
T_{max}	h	0.25	0.5	0.5	0.42
Vd	L/kg	1573.7	992.9	628.1	1064.9
CL	L/h/kg	2357.3	1619.9	970.3	1649.1
C_{max}	μg/L	10.32	13.23	18.3	13.95

BIBLIOGRAPHY

1. Fredriksson, R., M.C. Lagerstrom, L.G. Lundin, and H.B. Schioth, *The G-protein-coupled receptors in the human genome form five main families. Phylogenetic analysis, paralogon groups, and fingerprints.* Mol Pharmacol, 2003. **63**(6): p. 1256-72.
2. Venkatakrishnan, A.J., X. Deupi, G. Lebon, C.G. Tate, G.F. Schertler, and M.M. Babu, *Molecular signatures of G-protein-coupled receptors.* Nature, 2013. **494**(7436): p. 185-94.
3. Dorsam, R.T. and J.S. Gutkind, *G-protein-coupled receptors and cancer.* Nat Rev Cancer, 2007. **7**(2): p. 79-94.
4. Neves, S.R., P.T. Ram, and R. Iyengar, *G protein pathways.* Science, 2002. **296**(5573): p. 1636-9.
5. Wettschureck, N. and S. Offermanns, *Mammalian G proteins and their cell type specific functions.* Physiol Rev, 2005. **85**(4): p. 1159-204.
6. Devane, W.A., L. Hanus, A. Breuer, R.G. Pertwee, L.A. Stevenson, G. Griffin, D. Gibson, A. Mandelbaum, A. Etinger, and R. Mechoulam, *Isolation and structure of a brain constituent that binds to the cannabinoid receptor.* Science, 1992. **258**(5090): p. 1946-9.
7. Mechoulam, R., S. Ben-Shabat, L. Hanus, M. Ligumsky, N.E. Kaminski, A.R. Schatz, A. Gopher, S. Almog, B.R. Martin, D.R. Compton, and et al., *Identification of an endogenous 2-monoglyceride, present in canine gut, that binds to cannabinoid receptors.* Biochem Pharmacol, 1995. **50**(1): p. 83-90.
8. Howlett, A.C., F. Barth, T.I. Bonner, G. Cabral, P. Casellas, W.A. Devane, C.C. Felder, M. Herkenham, K. Mackie, B.R. Martin, R. Mechoulam, and R.G. Pertwee, *International Union of Pharmacology. XXVII. Classification of cannabinoid receptors.* Pharmacol Rev, 2002. **54**(2): p. 161-202.
9. Bisogno, T., A. Ligresti, and V. Di Marzo, *The endocannabinoid signalling system: biochemical aspects.* Pharmacol Biochem Behav, 2005. **81**(2): p. 224-38.
10. Cravatt, B.F., D.K. Giang, S.P. Mayfield, D.L. Boger, R.A. Lerner, and N.B. Gilula, *Molecular characterization of an enzyme that degrades neuromodulatory fatty-acid amides.* Nature, 1996. **384**(6604): p. 83-7.
11. Dinh, T.P., D. Carpenter, F.M. Leslie, T.F. Freund, I. Katona, S.L. Sensi, S. Kathuria, and D. Piomelli, *Brain monoglyceride lipase participating in endocannabinoid inactivation.* Proc Natl Acad Sci U S A, 2002. **99**(16): p. 10819-24.
12. Piomelli, D., *The molecular logic of endocannabinoid signalling.* Nat Rev Neurosci, 2003. **4**(11): p. 873-84.
13. De Petrocellis, L., M.G. Cascio, and V. Di Marzo, *The endocannabinoid system: a general view and latest additions.* Br J Pharmacol, 2004. **141**(5): p. 765-74.

14. Gerdeman, G.L., J.G. Partridge, C.R. Lupica, and D.M. Lovinger, *It could be habit forming: drugs of abuse and striatal synaptic plasticity.* Trends Neurosci, 2003. **26**(4): p. 184-92.
15. van der Stelt, M. and V. Di Marzo, *The endocannabinoid system in the basal ganglia and in the mesolimbic reward system: implications for neurological and psychiatric disorders.* Eur J Pharmacol, 2003. **480**(1-3): p. 133-50.
16. Iversen, L. and V. Chapman, *Cannabinoids: a real prospect for pain relief?* Curr Opin Pharmacol, 2002. **2**(1): p. 50-5.
17. Randall, M.D., D. Harris, D.A. Kendall, and V. Ralevic, *Cardiovascular effects of cannabinoids.* Pharmacol Ther, 2002. **95**(2): p. 191-202.
18. Di Carlo, G. and A.A. Izzo, *Cannabinoids for gastrointestinal diseases: potential therapeutic applications.* Expert Opin Investig Drugs, 2003. **12**(1): p. 39-49.
19. Maccarrone, M. and T. Wenger, *Effects of cannabinoids on hypothalamic and reproductive function.* Handb Exp Pharmacol, 2005(168): p. 555-71.
20. Di Marzo, V. and S. Petrosino, *Endocannabinoids and the regulation of their levels in health and disease.* Curr Opin Lipidol, 2007. **18**(2): p. 129-40.
21. Ligresti, A., T. Bisogno, I. Matias, L. De Petrocellis, M.G. Cascio, V. Cosenza, G. D'Argenio, G. Scaglione, M. Bifulco, I. Sorrentini, and V. Di Marzo, *Possible endocannabinoid control of colorectal cancer growth.* Gastroenterology, 2003. **125**(3): p. 677-87.
22. Petersen, G., B. Moesgaard, P.C. Schmid, H.H. Schmid, H. Broholm, M. Kosteljanetz, and H.S. Hansen, *Endocannabinoid metabolism in human glioblastomas and meningiomas compared to human non-tumour brain tissue.* J Neurochem, 2005. **93**(2): p. 299-309.
23. Schmid, P.C., L.E. Wold, R.J. Krebsbach, E.V. Berdyshev, and H.H. Schmid, *Anandamide and other N-acylethanolamines in human tumors.* Lipids, 2002. **37**(9): p. 907-12.
24. Pagotto, U., G. Marsicano, F. Fezza, M. Theodoropoulou, Y. Grubler, J. Stalla, T. Arzberger, A. Milone, M. Losa, V. Di Marzo, B. Lutz, and G.K. Stalla, *Normal human pituitary gland and pituitary adenomas express cannabinoid receptor type 1 and synthesize endogenous cannabinoids: first evidence for a direct role of cannabinoids on hormone modulation at the human pituitary level.* J Clin Endocrinol Metab, 2001. **86**(6): p. 2687-96.
25. Guzman, M., C. Sanchez, and I. Galve-Roperh, *Cannabinoids and cell fate.* Pharmacol Ther, 2002. **95**(2): p. 175-84.
26. Matsuda, L.A., S.J. Lolait, M.J. Brownstein, A.C. Young, and T.I. Bonner, *Structure of a cannabinoid receptor and functional expression of the cloned cDNA.* Nature, 1990. **346**(6284): p. 561-4.
27. Gerard, C.M., C. Mollereau, G. Vassart, and M. Parmentier, *Molecular cloning of a human cannabinoid receptor which is also expressed in testis.* Biochem J, 1991. **279 (Pt 1)**: p. 129-34.
28. Galiegue, S., S. Mary, J. Marchand, D. Dussossoy, D. Carriere, P. Carayon, M. Bouaboula, D. Shire, G. Le Fur, and P. Casellas, *Expression of central and peripheral cannabinoid receptors in human immune tissues and leukocyte subpopulations.* Eur J Biochem, 1995. **232**(1): p. 54-61.
29. Moreira, F.A. and J.A. Crippa, *The psychiatric side-effects of rimonabant.* Rev Bras Psiquiatr, 2009. **31**(2): p. 145-53.

30. Sam, A.H., V. Salem, and M.A. Ghatei, *Rimonabant: From RIO to Ban.* J Obes, 2011. **2011**: p. 432607.
31. Munro, S., K.L. Thomas, and M. Abu-Shaar, *Molecular characterization of a peripheral receptor for cannabinoids.* Nature, 1993. **365**(6441): p. 61-5.
32. Schatz, A.R., M. Lee, R.B. Condie, J.T. Pulaski, and N.E. Kaminski, *Cannabinoid receptors CB1 and CB2: a characterization of expression and adenylate cyclase modulation within the immune system.* Toxicol Appl Pharmacol, 1997. **142**(2): p. 278-87.
33. Pettit, D.A., D.L. Anders, M.P. Harrison, and G.A. Cabral, *Cannabinoid receptor expression in immune cells.* Adv Exp Med Biol, 1996. **402**: p. 119-29.
34. Sawzdargo, M., T. Nguyen, D.K. Lee, K.R. Lynch, R. Cheng, H.H. Heng, S.R. George, and B.F. O'Dowd, *Identification and cloning of three novel human G protein-coupled receptor genes GPR52, PsiGPR53 and GPR55: GPR55 is extensively expressed in human brain.* Brain Res Mol Brain Res, 1999. **64**(2): p. 193-8.
35. Ryberg, E., N. Larsson, S. Sjogren, S. Hjorth, N.O. Hermansson, J. Leonova, T. Elebring, K. Nilsson, T. Drmota, and P.J. Greasley, *The orphan receptor GPR55 is a novel cannabinoid receptor.* Br J Pharmacol, 2007. **152**(7): p. 1092-101.
36. Whyte, L.S., E. Ryberg, N.A. Sims, S.A. Ridge, K. Mackie, P.J. Greasley, R.A. Ross, and M.J. Rogers, *The putative cannabinoid receptor GPR55 affects osteoclast function in vitro and bone mass in vivo.* Proc Natl Acad Sci U S A, 2009. **106**(38): p. 16511-6.
37. Lauckner, J.E., J.B. Jensen, H.Y. Chen, H.C. Lu, B. Hille, and K. Mackie, *GPR55 is a cannabinoid receptor that increases intracellular calcium and inhibits M current.* Proc Natl Acad Sci U S A, 2008. **105**(7): p. 2699-704.
38. Henstridge, C.M., N.A. Balenga, L.A. Ford, R.A. Ross, M. Waldhoer, and A.J. Irving, *The GPR55 ligand L-alpha-lysophosphatidylinositol promotes RhoA-dependent Ca2+ signaling and NFAT activation.* FASEB J, 2009. **23**(1): p. 183-93.
39. Pertwee, R.G., A.C. Howlett, M.E. Abood, S.P. Alexander, V. Di Marzo, M.R. Elphick, P.J. Greasley, H.S. Hansen, G. Kunos, K. Mackie, R. Mechoulam, and R.A. Ross, *International Union of Basic and Clinical Pharmacology. LXXIX. Cannabinoid receptors and their ligands: beyond CB and CB.* Pharmacol Rev. **62**(4): p. 588-631.
40. Glass, M. and C.C. Felder, *Concurrent stimulation of cannabinoid CB1 and dopamine D2 receptors augments cAMP accumulation in striatal neurons: evidence for a Gs linkage to the CB1 receptor.* J Neurosci, 1997. **17**(14): p. 5327-33.
41. Sanchez, C., D. Rueda, B. Segui, I. Galve-Roperh, T. Levade, and M. Guzman, *The CB(1) cannabinoid receptor of astrocytes is coupled to sphingomyelin hydrolysis through the adaptor protein fan.* Mol Pharmacol, 2001. **59**(5): p. 955-9.
42. Sanchez, C., M.L. de Ceballos, T. Gomez del Pulgar, D. Rueda, C. Corbacho, G. Velasco, I. Galve-Roperh, J.W. Huffman, S. Ramon y Cajal, and M. Guzman, *Inhibition of glioma growth in vivo by selective activation of the CB(2) cannabinoid receptor.* Cancer Res, 2001. **61**(15): p. 5784-9.
43. Galve-Roperh, I., C. Sanchez, M.L. Cortes, T. Gomez del Pulgar, M. Izquierdo, and M. Guzman, *Anti-tumoral action of cannabinoids: involvement of sustained ceramide accumulation and extracellular signal-regulated kinase activation.* Nat Med, 2000. **6**(3): p. 313-9.
44. Davis, M.I., J. Ronesi, and D.M. Lovinger, *A predominant role for inhibition of the adenylate cyclase/protein kinase A pathway in ERK activation by cannabinoid receptor 1 in N1E-115 neuroblastoma cells.* J Biol Chem, 2003. **278**(49): p. 48973-80.

45. Derkinderen, P., E. Valjent, M. Toutant, J.C. Corvol, H. Enslen, C. Ledent, J. Trzaskos, J. Caboche, and J.A. Girault, *Regulation of extracellular signal-regulated kinase by cannabinoids in hippocampus.* J Neurosci, 2003. **23**(6): p. 2371-82.
46. Carrier, E.J., C.S. Kearn, A.J. Barkmeier, N.M. Breese, W. Yang, K. Nithipatikom, S.L. Pfister, W.B. Campbell, and C.J. Hillard, *Cultured rat microglial cells synthesize the endocannabinoid 2-arachidonylglycerol, which increases proliferation via a CB2 receptor-dependent mechanism.* Mol Pharmacol, 2004. **65**(4): p. 999-1007.
47. Sanchez, M.G., L. Ruiz-Llorente, A.M. Sanchez, and I. Diaz-Laviada, *Activation of phosphoinositide 3-kinase/PKB pathway by CB(1) and CB(2) cannabinoid receptors expressed in prostate PC-3 cells. Involvement in Raf-1 stimulation and NGF induction.* Cell Signal, 2003. **15**(9): p. 851-9.
48. Bouaboula, M., B. Bourrie, M. Rinaldi-Carmona, D. Shire, G. Le Fur, and P. Casellas, *Stimulation of cannabinoid receptor CB1 induces krox-24 expression in human astrocytoma cells.* J Biol Chem, 1995. **270**(23): p. 13973-80.
49. Bouaboula, M., C. Poinot-Chazel, J. Marchand, X. Canat, B. Bourrie, M. Rinaldi-Carmona, B. Calandra, G. Le Fur, and P. Casellas, *Signaling pathway associated with stimulation of CB2 peripheral cannabinoid receptor. Involvement of both mitogen-activated protein kinase and induction of Krox-24 expression.* Eur J Biochem, 1996. **237**(3): p. 704-11.
50. Nackley, A.G., A. Makriyannis, and A.G. Hohmann, *Selective activation of cannabinoid CB(2) receptors suppresses spinal fos protein expression and pain behavior in a rat model of inflammation.* Neuroscience, 2003. **119**(3): p. 747-57.
51. Rueda, D., I. Galve-Roperh, A. Haro, and M. Guzman, *The CB(1) cannabinoid receptor is coupled to the activation of c-Jun N-terminal kinase.* Mol Pharmacol, 2000. **58**(4): p. 814-20.
52. Mackie, K., W.A. Devane, and B. Hille, *Anandamide, an endogenous cannabinoid, inhibits calcium currents as a partial agonist in N18 neuroblastoma cells.* Mol Pharmacol, 1993. **44**(3): p. 498-503.
53. Sugiura, T., T. Kodaka, S. Kondo, T. Tonegawa, S. Nakane, S. Kishimoto, A. Yamashita, and K. Waku, *Inhibition by 2-arachidonoylglycerol, a novel type of possible neuromodulator, of the depolarization-induced increase in intracellular free calcium in neuroblastoma x glioma hybrid NG108-15 cells.* Biochem Biophys Res Commun, 1997. **233**(1): p. 207-10.
54. Caulfield, M.P. and D.A. Brown, *Cannabinoid receptor agonists inhibit Ca current in NG108-15 neuroblastoma cells via a pertussis toxin-sensitive mechanism.* Br J Pharmacol, 1992. **106**(2): p. 231-2.
55. Pan, X., S.R. Ikeda, and D.L. Lewis, *Rat brain cannabinoid receptor modulates N-type Ca2+ channels in a neuronal expression system.* Mol Pharmacol, 1996. **49**(4): p. 707-14.
56. Huang, C.C., S.W. Lo, and K.S. Hsu, *Presynaptic mechanisms underlying cannabinoid inhibition of excitatory synaptic transmission in rat striatal neurons.* J Physiol, 2001. **532**(Pt 3): p. 731-48.
57. Mackie, K., Y. Lai, R. Westenbroek, and R. Mitchell, *Cannabinoids activate an inwardly rectifying potassium conductance and inhibit Q-type calcium currents in AtT20 cells transfected with rat brain cannabinoid receptor.* J Neurosci, 1995. **15**(10): p. 6552-61.
58. Hampson, A.J., L.M. Bornheim, M. Scanziani, C.S. Yost, A.T. Gray, B.M. Hansen, D.J. Leonoudakis, and P.E. Bickler, *Dual effects of anandamide on NMDA receptor-mediated responses and neurotransmission.* J Neurochem, 1998. **70**(2): p. 671-6.

59. Gebremedhin, D., A.R. Lange, W.B. Campbell, C.J. Hillard, and D.R. Harder, *Cannabinoid CB1 receptor of cat cerebral arterial muscle functions to inhibit L-type Ca2+ channel current.* Am J Physiol, 1999. **276**(6 Pt 2): p. H2085-93.
60. Sugiura, T., T. Kodaka, S. Kondo, T. Tonegawa, S. Nakane, S. Kishimoto, A. Yamashita, and K. Waku, *2-Arachidonoylglycerol, a putative endogenous cannabinoid receptor ligand, induces rapid, transient elevation of intracellular free Ca2+ in neuroblastoma x glioma hybrid NG108-15 cells.* Biochem Biophys Res Commun, 1996. **229**(1): p. 58-64.
61. Bash, R., V. Rubovitch, M. Gafni, and Y. Sarne, *The stimulatory effect of cannabinoids on calcium uptake is mediated by Gs GTP-binding proteins and cAMP formation.* Neurosignals, 2003. **12**(1): p. 39-44.
62. Rubovitch, V., M. Gafni, and Y. Sarne, *The involvement of VEGF receptors and MAPK in the cannabinoid potentiation of Ca2+ flux into N18TG2 neuroblastoma cells.* Brain Res Mol Brain Res, 2004. **120**(2): p. 138-44.
63. Zoratti, C., D. Kipmen-Korgun, K. Osibow, R. Malli, and W.F. Graier, *Anandamide initiates Ca(2+) signaling via CB2 receptor linked to phospholipase C in calf pulmonary endothelial cells.* Br J Pharmacol, 2003. **140**(8): p. 1351-62.
64. Vasquez, C., R.A. Navarro-Polanco, M. Huerta, X. Trujillo, F. Andrade, B. Trujillo-Hernandez, and L. Hernandez, *Effects of cannabinoids on endogenous K+ and Ca2+ currents in HEK293 cells.* Can J Physiol Pharmacol, 2003. **81**(5): p. 436-42.
65. Pertwee, R.G., *Cannabinoid pharmacology: the first 66 years.* Br J Pharmacol, 2006. **147 Suppl 1**: p. S163-71.
66. Mechoulam, R., L. Hanus, and E. Fride, *Towards cannabinoid drugs--revisited.* Prog Med Chem, 1998. **35**: p. 199-243.
67. Walker, J.M., A.G. Hohmann, W.J. Martin, N.M. Strangman, S.M. Huang, and K. Tsou, *The neurobiology of cannabinoid analgesia.* Life Sci, 1999. **65**(6-7): p. 665-73.
68. Kumar, R.N., W.A. Chambers, and R.G. Pertwee, *Pharmacological actions and therapeutic uses of cannabis and cannabinoids.* Anaesthesia, 2001. **56**(11): p. 1059-68.
69. Croxford, J.L. and T. Yamamura, *Cannabinoids and the immune system: potential for the treatment of inflammatory diseases?* J Neuroimmunol, 2005. **166**(1-2): p. 3-18.
70. Izzo, A.A. and A.A. Coutts, *Cannabinoids and the digestive tract.* Handb Exp Pharmacol, 2005(168): p. 573-98.
71. Adams, R., B.R. Baker, and R.B. Wearn, *Structure of Cannabinol. III. Synthesis of Cannabinol, 1-Hydroxy-3-n-amyl-6,6,9-trimethyl-6-dibenzopyran1*. Journal of the American Chemical Society, 1940. **62**(8): p. 2204-2207.
72. Adams, R., M. Harfenist, and S. Loewe, *New Analogs of Tetrahydrocannabinol. XIX*. Journal of the American Chemical Society, 1949. **71**(5): p. 1624-1628.
73. Mechoulam, R., A. Shani, H. Edery, and Y. Grunfeld, *Chemical basis of hashish activity.* Science, 1970. **169**(3945): p. 611-2.
74. Grunfeld, Y. and H. Edery, *Psychopharmacological activity of the active constituents of hashish and some related cannabinoids.* Psychopharmacologia, 1969. **14**(3): p. 200-10.
75. Kozlowski, J.A., N.-Y. Shih, B.J. Lavey, R.K. Rizvi, B.B. Shankar, J.M. Spitler, L. Tong, R.L. Wolin, and M.K. Wong, *Preparation of N-(α-methylbenzyl) sulfonamides as cannabinoid receptor ligands*, 2003, Schering Corporation, USA . p. 68 pp., Cont.-in-part of U.S. Ser. No. 72,354.

76. Huffman, J.W. and L.W. Padgett, *Recent developments in the medicinal chemistry of cannabimimetic indoles, pyrroles and indenes.* Curr Med Chem, 2005. **12**(12): p. 1395-411.
77. Sugiura, T., S. Kondo, A. Sukagawa, S. Nakane, A. Shinoda, K. Itoh, A. Yamashita, and K. Waku, *2-Arachidonoylglycerol: a possible endogenous cannabinoid receptor ligand in brain.* Biochem Biophys Res Commun, 1995. **215**(1): p. 89-97.
78. Compton, D.R., K.C. Rice, B.R. De Costa, R.K. Razdan, L.S. Melvin, M.R. Johnson, and B.R. Martin, *Cannabinoid structure-activity relationships: correlation of receptor binding and in vivo activities.* J Pharmacol Exp Ther, 1993. **265**(1): p. 218-26.
79. Steffens, M., J. Zentner, J. Honegger, and T.J. Feuerstein, *Binding affinity and agonist activity of putative endogenous cannabinoids at the human neocortical CB1 receptor.* Biochem Pharmacol, 2005. **69**(1): p. 169-78.
80. Shoemaker, J.L., B.K. Joseph, M.B. Ruckle, P.R. Mayeux, and P.L. Prather, *The endocannabinoid noladin ether acts as a full agonist at human CB2 cannabinoid receptors.* J Pharmacol Exp Ther, 2005. **314**(2): p. 868-75.
81. Huffman, J.W., G. Zengin, M.J. Wu, J. Lu, G. Hynd, K. Bushell, A.L. Thompson, S. Bushell, C. Tartal, D.P. Hurst, P.H. Reggio, D.E. Selley, M.P. Cassidy, J.L. Wiley, and B.R. Martin, *Structure-activity relationships for 1-alkyl-3-(1-naphthoyl)indoles at the cannabinoid CB(1) and CB(2) receptors: steric and electronic effects of naphthoyl substituents. New highly selective CB(2) receptor agonists.* Bioorg Med Chem, 2005. **13**(1): p. 89-112.
82. Hanus, L., A. Breuer, S. Tchilibon, S. Shiloah, D. Goldenberg, M. Horowitz, R.G. Pertwee, R.A. Ross, R. Mechoulam, and E. Fride, *HU-308: a specific agonist for CB(2), a peripheral cannabinoid receptor.* Proc Natl Acad Sci U S A, 1999. **96**(25): p. 14228-33.
83. Ibrahim, M.M., H. Deng, A. Zvonok, D.A. Cockayne, J. Kwan, H.P. Mata, T.W. Vanderah, J. Lai, F. Porreca, A. Makriyannis, and T.P. Malan, Jr., *Activation of CB2 cannabinoid receptors by AM1241 inhibits experimental neuropathic pain: pain inhibition by receptors not present in the CNS.* Proc Natl Acad Sci U S A, 2003. **100**(18): p. 10529-33.
84. Thomas, B.F., M.E. Francisco, H.H. Seltzman, J.B. Thomas, S.E. Fix, A.K. Schulz, A.F. Gilliam, R.G. Pertwee, and L.A. Stevenson, *Synthesis of long-chain amide analogs of the cannabinoid CB1 receptor antagonist N-(piperidinyl)-5-(4-chlorophenyl)-1-(2,4-dichlorophenyl)-4-methyl-1H-pyrazole-3- carboxamide (SR141716) with unique binding selectivities and pharmacological activities.* Bioorg Med Chem, 2005. **13**(18): p. 5463-74.
85. Lan, R., Q. Liu, P. Fan, S. Lin, S.R. Fernando, D. McCallion, R. Pertwee, and A. Makriyannis, *Structure-activity relationships of pyrazole derivatives as cannabinoid receptor antagonists.* J Med Chem, 1999. **42**(4): p. 769-76.
86. Lan, R., J. Gatley, Q. Lu, P. Fan, S.R. Fernando, N.D. Volkow, R. Pertwee, and A. Makriyannis, *Design and synthesis of the CB1 selective cannabinoid antagonist AM281: a potential human SPECT ligand.* AAPS PharmSci, 1999. **1**(2): p. E4.
87. Kim, M.-a., H. Yun, H. Kwak, J. Kim, and J. Lee, *Design, chemical synthesis, and biological evaluation of novel triazolyl analogues of taranabant (MK-0364), a cannabinoid-1 receptor inverse agonist.* Tetrahedron, 2008. **64**(48): p. 10802-10809.
88. Fong, T.M., X.M. Guan, D.J. Marsh, C.P. Shen, D.S. Stribling, K.M. Rosko, J. Lao, H. Yu, Y. Feng, J.C. Xiao, L.H. Van der Ploeg, M.T. Goulet, W.K. Hagmann, L.S. Lin, T.J. Lanza, Jr., J.P. Jewell, P. Liu, S.K. Shah, H. Qi, X. Tong, J. Wang, S.S. Xu, B. Francis, A.M. Strack, D.E. MacIntyre, and L.P. Shearman, *Antiobesity efficacy of a novel cannabinoid-1*

receptor inverse agonist, N-[(1S,2S)-3-(4-chlorophenyl)-2-(3-cyanophenyl)-1-methylpropyl]-2-methyl-2-[[5-(t rifluoromethyl)pyridin-2-yl]oxy]propanamide (MK-0364), in rodents. J Pharmacol Exp Ther, 2007. **321**(3): p. 1013-22.

89. Ruiu, S., G.A. Pinna, G. Marchese, J.M. Mussinu, P. Saba, S. Tambaro, P. Casti, R. Vargiu, and L. Pani, *Synthesis and characterization of NESS 0327: a novel putative antagonist of the CB1 cannabinoid receptor.* J Pharmacol Exp Ther, 2003. **306**(1): p. 363-70.
90. Rinaldi-Carmona, M., F. Barth, J. Millan, J.M. Derocq, P. Casellas, C. Congy, D. Oustric, M. Sarran, M. Bouaboula, B. Calandra, M. Portier, D. Shire, J.C. Breliere, and G.L. Le Fur, *SR 144528, the first potent and selective antagonist of the CB2 cannabinoid receptor.* J Pharmacol Exp Ther, 1998. **284**(2): p. 644-50.
91. Ross, R.A., H.C. Brockie, L.A. Stevenson, V.L. Murphy, F. Templeton, A. Makriyannis, and R.G. Pertwee, *Agonist-inverse agonist characterization at CB1 and CB2 cannabinoid receptors of L759633, L759656, and AM630.* Br J Pharmacol, 1999. **126**(3): p. 665-72.
92. Turkman, N., A. Shavrin, R.A. Ivanov, B. Rabinovich, A. Volgin, J.G. Gelovani, and M.M. Alauddin, *Fluorinated cannabinoid CB2 receptor ligands: synthesis and in vitro binding characteristics of 2-oxoquinoline derivatives.* Bioorg Med Chem, 2011. **19**(18): p. 5698-707.
93. Iwamura, H., H. Suzuki, Y. Ueda, T. Kaya, and T. Inaba, *In vitro and in vivo pharmacological characterization of JTE-907, a novel selective ligand for cannabinoid CB2 receptor.* J Pharmacol Exp Ther, 2001. **296**(2): p. 420-5.
94. Pacher, P., S. Batkai, and G. Kunos, *The endocannabinoid system as an emerging target of pharmacotherapy.* Pharmacol Rev, 2006. **58**(3): p. 389-462.
95. Todaro, B., *Cannabinoids in the treatment of chemotherapy-induced nausea and vomiting.* J Natl Compr Canc Netw, 2012. **10**(4): p. 487-92.
96. Pertwee, R.G., *Emerging strategies for exploiting cannabinoid receptor agonists as medicines.* Br J Pharmacol, 2009. **156**(3): p. 397-411.
97. *Cannabis-based medicines--GW pharmaceuticals: high CBD, high THC, medicinal cannabis--GW pharmaceuticals, THC:CBD.* Drugs R D, 2003. **4**(5): p. 306-9.
98. Oreja-Guevara, C., *Clinical efficacy and effectiveness of Sativex, a combined cannabinoid medicine, in multiple sclerosis-related spasticity.* Expert Rev Neurother, 2012. **12**(4 Suppl): p. 3-8.
99. Vermersch, P., *Sativex((R)) (tetrahydrocannabinol + cannabidiol), an endocannabinoid system modulator: basic features and main clinical data.* Expert Rev Neurother, 2011. **11**(4 Suppl): p. 15-9.
100. Velasco, G., C. Sanchez, and M. Guzman, *Towards the use of cannabinoids as antitumour agents.* Nat Rev Cancer, 2012. **12**(6): p. 436-44.
101. Di Marzo, V., M. Bifulco, and L. De Petrocellis, *The endocannabinoid system and its therapeutic exploitation.* Nat Rev Drug Discov, 2004. **3**(9): p. 771-84.
102. Pagotto, U. and R. Pasquali, *Fighting obesity and associated risk factors by antagonising cannabinoid type 1 receptors.* Lancet, 2005. **365**(9468): p. 1363-4.
103. Cota, D., G. Marsicano, M. Tschop, Y. Grubler, C. Flachskamm, M. Schubert, D. Auer, A. Yassouridis, C. Thone-Reineke, S. Ortmann, F. Tomassoni, C. Cervino, E. Nisoli, A.C. Linthorst, R. Pasquali, B. Lutz, G.K. Stalla, and U. Pagotto, *The endogenous cannabinoid system affects energy balance via central orexigenic drive and peripheral lipogenesis.* J Clin Invest, 2003. **112**(3): p. 423-31.

104. Christensen, R., P.K. Kristensen, E.M. Bartels, H. Bliddal, and A. Astrup, *Efficacy and safety of the weight-loss drug rimonabant: a meta-analysis of randomised trials.* Lancet, 2007. **370**(9600): p. 1706-13.
105. Despres, J.P., I. Lemieux, and N. Almeras, *Contribution of CB1 blockade to the management of high-risk abdominal obesity.* Int J Obes (Lond), 2006. **30 Suppl 1**: p. S44-52.
106. Siegel, R., J. Ma, Z. Zou, and A. Jemal, *Cancer statistics, 2014.* CA Cancer J Clin, 2014. **64**(1): p. 9-29.
107. Guindon, J. and A.G. Hohmann, *The endocannabinoid system and cancer: therapeutic implication.* Br J Pharmacol. **163**(7): p. 1447-63.
108. Nomura, D.K., J.Z. Long, S. Niessen, H.S. Hoover, S.W. Ng, and B.F. Cravatt, *Monoacylglycerol lipase regulates a fatty acid network that promotes cancer pathogenesis.* Cell, 2010. **140**(1): p. 49-61.
109. Thors, L., A. Bergh, E. Persson, P. Hammarsten, P. Stattin, L. Egevad, T. Granfors, and C.J. Fowler, *Fatty acid amide hydrolase in prostate cancer: association with disease severity and outcome, CB1 receptor expression and regulation by IL-4.* PLoS One, 2010. **5**(8): p. e12275.
110. Munson, A.E., L.S. Harris, M.A. Friedman, W.L. Dewey, and R.A. Carchman, *Antineoplastic activity of cannabinoids.* J Natl Cancer Inst, 1975. **55**(3): p. 597-602.
111. Oesch, S. and J. Gertsch, *Cannabinoid receptor ligands as potential anticancer agents--high hopes for new therapies?* J Pharm Pharmacol, 2009. **61**(7): p. 839-53.
112. Sarfaraz, S., V.M. Adhami, D.N. Syed, F. Afaq, and H. Mukhtar, *Cannabinoids for cancer treatment: progress and promise.* Cancer Res, 2008. **68**(2): p. 339-42.
113. Ramer, R. and B. Hinz, *Inhibition of cancer cell invasion by cannabinoids via increased expression of tissue inhibitor of matrix metalloproteinases-1.* J Natl Cancer Inst, 2008. **100**(1): p. 59-69.
114. Qamri, Z., A. Preet, M.W. Nasser, C.E. Bass, G. Leone, S.H. Barsky, and R.K. Ganju, *Synthetic cannabinoid receptor agonists inhibit tumor growth and metastasis of breast cancer.* Mol Cancer Ther, 2009. **8**(11): p. 3117-29.
115. Caffarel, M.M., C. Andradas, E. Mira, E. Perez-Gomez, C. Cerutti, G. Moreno-Bueno, J.M. Flores, I. Garcia-Real, J. Palacios, S. Manes, M. Guzman, and C. Sanchez, *Cannabinoids reduce ErbB2-driven breast cancer progression through Akt inhibition.* Mol Cancer, 2010. **9**: p. 196.
116. Ligresti, A., A.S. Moriello, K. Starowicz, I. Matias, S. Pisanti, L. De Petrocellis, C. Laezza, G. Portella, M. Bifulco, and V. Di Marzo, *Antitumor activity of plant cannabinoids with emphasis on the effect of cannabidiol on human breast carcinoma.* J Pharmacol Exp Ther, 2006. **318**(3): p. 1375-87.
117. Bray, F., J. Lortet-Tieulent, J. Ferlay, D. Forman, and A. Auvinen, *Prostate cancer incidence and mortality trends in 37 European countries: an overview.* Eur J Cancer, 2010. **46**(17): p. 3040-52.
118. Datta, K., M. Muders, H. Zhang, and D.J. Tindall, *Mechanism of lymph node metastasis in prostate cancer.* Future Oncol, 2010. **6**(5): p. 823-36.
119. Bubendorf, L., A. Schopfer, U. Wagner, G. Sauter, H. Moch, N. Willi, T.C. Gasser, and M.J. Mihatsch, *Metastatic patterns of prostate cancer: an autopsy study of 1,589 patients.* Hum Pathol, 2000. **31**(5): p. 578-83.

120. Melck, D., L. De Petrocellis, P. Orlando, T. Bisogno, C. Laezza, M. Bifulco, and V. Di Marzo, *Suppression of nerve growth factor Trk receptors and prolactin receptors by endocannabinoids leads to inhibition of human breast and prostate cancer cell proliferation.* Endocrinology, 2000. **141**(1): p. 118-26.
121. Nithipatikom, K., M.P. Endsley, M.A. Isbell, J.R. Falck, Y. Iwamoto, C.J. Hillard, and W.B. Campbell, *2-arachidonoylglycerol: a novel inhibitor of androgen-independent prostate cancer cell invasion.* Cancer Res, 2004. **64**(24): p. 8826-30.
122. Sarfaraz, S., F. Afaq, V.M. Adhami, and H. Mukhtar, *Cannabinoid Receptor as a Novel Target for the Treatment of Prostate Cancer.* Cancer Research, 2005. **65**(5).
123. Velasco, L., L. Ruiz, M.G. Sanchez, and I. Diaz-Laviada, *delta(9)-Tetrahydrocannabinol increases nerve growth factor production by prostate PC-3 cells. Involvement of CB1 cannabinoid receptor and Raf-1.* Eur J Biochem, 2001. **268**(3): p. 531-5.
124. Ruiz, L., A. Miguel, and I. Diaz-Laviada, *Delta9-tetrahydrocannabinol induces apoptosis in human prostate PC-3 cells via a receptor-independent mechanism.* FEBS Lett, 1999. **458**(3): p. 400-4.
125. Olea-Herrero, N., D. Vara, S. Malagarie-Cazenave, and I. Diaz-Laviada, *Inhibition of human tumour prostate PC-3 cell growth by cannabinoids R(+)-Methanandamide and JWH-015: involvement of CB2.* Br J Cancer, 2009. **101**(6): p. 940-50.
126. Bovee, J.V., P.C. Hogendoorn, J.S. Wunder, and B.A. Alman, *Cartilage tumours and bone development: molecular pathology and possible therapeutic targets.* Nat Rev Cancer, 2010. **10**(7): p. 481-8.
127. Khasabova, I.A., S.G. Khasabov, C. Harding-Rose, L.G. Coicou, B.A. Seybold, A.E. Lindberg, C.D. Steevens, D.A. Simone, and V.S. Seybold, *A decrease in anandamide signaling contributes to the maintenance of cutaneous mechanical hyperalgesia in a model of bone cancer pain.* J Neurosci, 2008. **28**(44): p. 11141-52.
128. Hald, A., M. Ding, K. Egerod, R.R. Hansen, D. Konradsen, S.G. Jorgensen, B. Atalay, A. Nasser, O.J. Bjerrum, and A.M. Heegaard, *Differential effects of repeated low dose treatment with the cannabinoid agonist WIN 55,212-2 in experimental models of bone cancer pain and neuropathic pain.* Pharmacol Biochem Behav, 2008. **91**(1): p. 38-46.
129. Lozano-Ondoua, A.N., C. Wright, A. Vardanyan, T. King, T.M. Largent-Milnes, M. Nelson, J.M. Jimenez-Andrade, P.W. Mantyh, and T.W. Vanderah, *A cannabinoid 2 receptor agonist attenuates bone cancer-induced pain and bone loss.* Life Sci, 2010. **86**(17-18): p. 646-53.
130. Hamamoto, D.T., S. Giridharagopalan, and D.A. Simone, *Acute and chronic administration of the cannabinoid receptor agonist CP 55,940 attenuates tumor-evoked hyperalgesia.* Eur J Pharmacol, 2007. **558**(1-3): p. 73-87.
131. Curto-Reyes, V., S. Llames, A. Hidalgo, L. Menendez, and A. Baamonde, *Spinal and peripheral analgesic effects of the CB2 cannabinoid receptor agonist AM1241 in two models of bone cancer-induced pain.* Br J Pharmacol, 2010. **160**(3): p. 561-73.
132. McKallip, R.J., C. Lombard, M. Fisher, B.R. Martin, S. Ryu, S. Grant, P.S. Nagarkatti, and M. Nagarkatti, *Targeting CB2 cannabinoid receptors as a novel therapy to treat malignant lymphoblastic disease*. Vol. 100. 2002. 627-634.
133. Gustafsson, K., B. Christensson, B. Sander, and J. Flygare, *Cannabinoid receptor-mediated apoptosis induced by R(+)-methanandamide and Win55,212-2 is associated with ceramide accumulation and p38 activation in mantle cell lymphoma.* Mol Pharmacol, 2006. **70**(5): p. 1612-20.

134. Hideshima, T., C. Mitsiades, G. Tonon, P.G. Richardson, and K.C. Anderson, *Understanding multiple myeloma pathogenesis in the bone marrow to identify new therapeutic targets.* Nat Rev Cancer, 2007. **7**(8): p. 585-98.
135. Hideshima, T. and K.C. Anderson, *Molecular mechanisms of novel therapeutic approaches for multiple myeloma.* Nat Rev Cancer, 2002. **2**(12): p. 927-37.
136. Siegel, R., D. Naishadham, and A. Jemal, *Cancer statistics, 2013.* CA Cancer J Clin, 2013. **63**(1): p. 11-30.
137. Blade, J., M.T. Cibeira, C. Fernandez de Larrea, and L. Rosinol, *Multiple myeloma.* Ann Oncol, 2010. **21 Suppl 7**: p. vii313-9.
138. Caers, J., I. Vande broek, H. De Raeve, L. Michaux, F. Trullemans, R. Schots, B. Van Camp, and K. Vanderkerken, *Multiple myeloma--an update on diagnosis and treatment.* Eur J Haematol, 2008. **81**(5): p. 329-43.
139. Laubach, J., P. Richardson, and K. Anderson, *Multiple myeloma.* Annu Rev Med, 2011. **62**: p. 249-64.
140. Oyajobi, B.O., *Multiple myeloma/hypercalcemia.* Arthritis Res Ther, 2007. **9 Suppl 1**: p. S4.
141. Lacy, M.Q. and A.R. McCurdy, *Pomalidomide.* Blood, 2013. **122**(14): p. 2305-9.
142. Kumar, S.K., S.V. Rajkumar, A. Dispenzieri, M.Q. Lacy, S.R. Hayman, F.K. Buadi, S.R. Zeldenrust, D. Dingli, S.J. Russell, J.A. Lust, P.R. Greipp, R.A. Kyle, and M.A. Gertz, *Improved survival in multiple myeloma and the impact of novel therapies.* Blood, 2008. **111**(5): p. 2516-20.
143. Almehizia, A.A., P. Yang, L. Wang, and X.Q. Xie, *Latest advances in the multiple myeloma drug research: from molecular signaling pathways to small molecules development.* Current Trends in Medicinal Chemistry, 2013. **7**: p. 105-133.
144. Roodman, G.D., *Cell biology of the osteoclast.* Exp Hematol, 1999. **27**(8): p. 1229-41.
145. Yasuda, H., N. Shima, N. Nakagawa, K. Yamaguchi, M. Kinosaki, S. Mochizuki, A. Tomoyasu, K. Yano, M. Goto, A. Murakami, E. Tsuda, T. Morinaga, K. Higashio, N. Udagawa, N. Takahashi, and T. Suda, *Osteoclast differentiation factor is a ligand for osteoprotegerin/osteoclastogenesis-inhibitory factor and is identical to TRANCE/RANKL.* Proc Natl Acad Sci U S A, 1998. **95**(7): p. 3597-602.
146. Lacey, D.L., E. Timms, H.L. Tan, M.J. Kelley, C.R. Dunstan, T. Burgess, R. Elliott, A. Colombero, G. Elliott, S. Scully, H. Hsu, J. Sullivan, N. Hawkins, E. Davy, C. Capparelli, A. Eli, Y.X. Qian, S. Kaufman, I. Sarosi, V. Shalhoub, G. Senaldi, J. Guo, J. Delaney, and W.J. Boyle, *Osteoprotegerin ligand is a cytokine that regulates osteoclast differentiation and activation.* Cell, 1998. **93**(2): p. 165-76.
147. Sarma, U. and A.M. Flanagan, *Macrophage colony-stimulating factor induces substantial osteoclast generation and bone resorption in human bone marrow cultures.* Blood, 1996. **88**(7): p. 2531-40.
148. Weinstein, R.S. and S.C. Manolagas, *Apoptosis and osteoporosis.* Am J Med, 2000. **108**(2): p. 153-64.
149. Bab, I., B.A. Ashton, D. Gazit, G. Marx, M.C. Williamson, and M.E. Owen, *Kinetics and differentiation of marrow stromal cells in diffusion chambers in vivo.* J Cell Sci, 1986. **84**: p. 139-51.
150. Ducy, P., T. Schinke, and G. Karsenty, *The osteoblast: a sophisticated fibroblast under central surveillance.* Science, 2000. **289**(5484): p. 1501-4.

151. Nefussi, J.R., J.M. Sautier, V. Nicolas, and N. Forest, *How osteoblasts become osteocytes: a decreasing matrix forming process.* J Biol Buccale, 1991. **19**(1): p. 75-82.
152. Raisz, L.G., *Pathogenesis of osteoporosis: concepts, conflicts, and prospects.* J Clin Invest, 2005. **115**(12): p. 3318-25.
153. Johnell, O. and J.A. Kanis, *An estimate of the worldwide prevalence and disability associated with osteoporotic fractures.* Osteoporos Int, 2006. **17**(12): p. 1726-33.
154. Gullberg, B., O. Johnell, and J.A. Kanis, *World-wide projections for hip fracture.* Osteoporos Int, 1997. **7**(5): p. 407-13.
155. Jilka, R.L., *Cytokines, bone remodeling, and estrogen deficiency: a 1998 update.* Bone, 1998. **23**(2): p. 75-81.
156. Bord, S., D.C. Ireland, S.R. Beavan, and J.E. Compston, *The effects of estrogen on osteoprotegerin, RANKL, and estrogen receptor expression in human osteoblasts.* Bone, 2003. **32**(2): p. 136-41.
157. Patschan, D., K. Loddenkemper, and F. Buttgereit, *Molecular mechanisms of glucocorticoid-induced osteoporosis.* Bone, 2001. **29**(6): p. 498-505.
158. Idris, A.I., A. Sophocleous, E. Landao-Bassonga, R.J. van't Hof, and S.H. Ralston, *Regulation of bone mass, osteoclast function, and ovariectomy-induced bone loss by the type 2 cannabinoid receptor.* Endocrinology, 2008. **149**(11): p. 5619-26.
159. Idris, A.I., R.J. van 't Hof, I.R. Greig, S.A. Ridge, D. Baker, R.A. Ross, and S.H. Ralston, *Regulation of bone mass, bone loss and osteoclast activity by cannabinoid receptors.* Nat Med, 2005. **11**(7): p. 774-9.
160. Ofek, O., M. Karsak, N. Leclerc, M. Fogel, B. Frenkel, K. Wright, J. Tam, M. Attar-Namdar, V. Kram, E. Shohami, R. Mechoulam, A. Zimmer, and I. Bab, *Peripheral cannabinoid receptor, CB2, regulates bone mass.* Proc Natl Acad Sci U S A, 2006. **103**(3): p. 696-701.
161. Abe, M., *Targeting the interplay between myeloma cells and the bone marrow microenvironment in myeloma.* Int J Hematol, 2011. **94**(4): p. 334-43.
162. Burdick, D., R. DeOrazio, P. Guzzo, A. Habershaw, M. Helle, B. Paul, and M. Wolf, *Synthesis and structure-activity relationship of substitutions at the C-1 position of Delta9-tetrahydrocannabinol.* Bioorg Med Chem Lett, 2010. **20**(4): p. 1424-6.
163. Hollinshead, S.P., P.C. Astles, M.G. Chambers, M.P. Johnson, J. Palmer, and M.W. Tidwell, *Discovery and optimization of novel purines as potent and selective CB2 agonists.* Bioorg Med Chem Lett, 2012. **22**(15): p. 4962-6.
164. Gleave, R.J., P.J. Beswick, A.J. Brown, G.M. Giblin, C.P. Haslam, D. Livermore, A. Moses, N.H. Nicholson, L.W. Page, B. Slingsby, and M.E. Swarbrick, *2-Amino-5-aryl-pyridines as selective CB2 agonists: synthesis and investigation of structure-activity relationships.* Bioorg Med Chem Lett, 2009. **19**(23): p. 6578-81.
165. Gleave, R.J., P.J. Beswick, A.J. Brown, G.M. Giblin, P. Goldsmith, C.P. Haslam, W.L. Mitchell, N.H. Nicholson, L.W. Page, S. Patel, S. Roomans, B.P. Slingsby, and M.E. Swarbrick, *Synthesis and evaluation of 3-amino-6-aryl-pyridazines as selective CB(2) agonists for the treatment of inflammatory pain.* Bioorg Med Chem Lett, 2010. **20**(2): p. 465-8.
166. Bartolozzi, A., A. Berry, P.F. Cirillo, E.R. Hickey, D. Riether, L. Wu, and R.M. Zindell, *Preparation of pyridine-based compounds as therapeutic modulators of CB2 receptor*, 2010, Boehringer Ingelheim International GmbH, Germany . p. 208pp.

167. Chu, G.H., C.T. Saeui, K. Worm, D.G. Weaver, A.J. Goodman, R.L. Broadrup, J.A. Cassel, R.N. DeHaven, C.J. LaBuda, M. Koblish, B. Brogdon, S. Smith, B. Le Bourdonnec, and R.E. Dolle, *Novel pyridine derivatives as potent and selective CB2 cannabinoid receptor agonists.* Bioorg Med Chem Lett, 2009. **19**(20): p. 5931-5.
168. van der Stelt, M., J. Cals, S. Broeders-Josten, J. Cottney, A.A. van der Doelen, M. Hermkens, V. de Kimpe, A. King, J. Klomp, J. Oosterom, I. Pols-de Rooij, J. de Roos, M. van Tilborg, S. Boyce, and J. Baker, *Discovery and optimization of 1-(4-(pyridin-2-yl)benzyl)imidazolidine-2,4-dione derivatives as a novel class of selective cannabinoid CB2 receptor agonists.* J Med Chem, 2011. **54**(20): p. 7350-62.
169. Clayton, N., F.H. Marshall, C. Bountra, and C.T. O'Shaughnessy, *CB1 and CB2 cannabinoid receptors are implicated in inflammatory pain.* Pain, 2002. **96**(3): p. 253-60.
170. Giblin, G.M., C.T. O'Shaughnessy, A. Naylor, W.L. Mitchell, A.J. Eatherton, B.P. Slingsby, D.A. Rawlings, P. Goldsmith, A.J. Brown, C.P. Haslam, N.M. Clayton, A.W. Wilson, I.P. Chessell, A.R. Wittington, and R. Green, *Discovery of 2-[(2,4-dichlorophenyl)amino]-N-[(tetrahydro- 2H-pyran-4-yl)methyl]-4-(trifluoromethyl)- 5-pyrimidinecarboxamide, a selective CB2 receptor agonist for the treatment of inflammatory pain.* J Med Chem, 2007. **50**(11): p. 2597-600.
171. Belvisi, M.G., H.J. Patel, V. Freund-Michel, D.J. Hele, N. Crispino, and M.A. Birrell, *Inhibitory activity of the novel CB2 receptor agonist, GW833972A, on guinea-pig and human sensory nerve function in the airways.* Br J Pharmacol, 2008. **155**(4): p. 547-57.
172. Stern, E., G.G. Muccioli, R. Millet, J.F. Goossens, A. Farce, P. Chavatte, J.H. Poupaert, D.M. Lambert, P. Depreux, and J.P. Henichart, *Novel 4-oxo-1,4-dihydroquinoline-3-carboxamide derivatives as new CB2 cannabinoid receptors agonists: synthesis, pharmacological properties and molecular modeling.* J Med Chem, 2006. **49**(1): p. 70-9.
173. Stern, E., G.G. Muccioli, B. Bosier, L. Hamtiaux, R. Millet, J.H. Poupaert, J.P. Henichart, P. Depreux, J.F. Goossens, and D.M. Lambert, *Pharmacomodulations around the 4-oxo-1,4-dihydroquinoline-3-carboxamides, a class of potent CB2-selective cannabinoid receptor ligands: consequences in receptor affinity and functionality.* J Med Chem, 2007. **50**(22): p. 5471-84.
174. Manera, C., V. Benetti, M.P. Castelli, T. Cavallini, S. Lazzarotti, F. Pibiri, G. Saccomanni, T. Tuccinardi, A. Vannacci, A. Martinelli, and P.L. Ferrarini, *Design, synthesis, and biological evaluation of new 1,8-naphthyridin-4(1H)-on-3-carboxamide and quinolin-4(1H)-on-3-carboxamide derivatives as CB2 selective agonists.* J Med Chem, 2006. **49**(20): p. 5947-57.
175. Cianchi, F., L. Papucci, N. Schiavone, M. Lulli, L. Magnelli, M.C. Vinci, L. Messerini, C. Manera, E. Ronconi, P. Romagnani, M. Donnini, G. Perigli, G. Trallori, E. Tanganelli, S. Capaccioli, and E. Masini, *Cannabinoid receptor activation induces apoptosis through tumor necrosis factor alpha-mediated ceramide de novo synthesis in colon cancer cells.* Clin Cancer Res, 2008. **14**(23): p. 7691-700.
176. Manera, C., G. Saccomanni, B. Adinolfi, V. Benetti, A. Ligresti, M.G. Cascio, T. Tuccinardi, V. Lucchesi, A. Martinelli, P. Nieri, E. Masini, V. Di Marzo, and P.L. Ferrarini, *Rational design, synthesis, and pharmacological properties of new 1,8-naphthyridin-2(1H)-on-3-carboxamide derivatives as highly selective cannabinoid-2 receptor agonists.* J Med Chem, 2009. **52**(12): p. 3644-51.
177. Pasquini, S., L. Botta, T. Semeraro, C. Mugnaini, A. Ligresti, E. Palazzo, S. Maione, V. Di Marzo, and F. Corelli, *Investigations on the 4-quinolone-3-carboxylic acid motif. 2.*

Synthesis and structure-activity relationship of potent and selective cannabinoid-2 receptor agonists endowed with analgesic activity in vivo. J Med Chem, 2008. **51**(16): p. 5075-84.

178. Cascio, M.G., D. Bolognini, R.G. Pertwee, E. Palazzo, F. Corelli, S. Pasquini, V. Di Marzo, and S. Maione, *In vitro and in vivo pharmacological characterization of two novel selective cannabinoid CB(2) receptor inverse agonists.* Pharmacol Res, 2010. **61**(4): p. 349-54.
179. El Bakali, J., G.G. Muccioli, N. Renault, D. Pradal, M. Body-Malapel, M. Djouina, L. Hamtiaux, V. Andrzejak, P. Desreumaux, P. Chavatte, D.M. Lambert, and R. Millet, *4-Oxo-1,4-dihydropyridines as selective CB2 cannabinoid receptor ligands: structural insights into the design of a novel inverse agonist series.* J Med Chem, 2010. **53**(22): p. 7918-31.
180. Brogi, S., F. Corelli, V. Di Marzo, A. Ligresti, C. Mugnaini, S. Pasquini, and A. Tafi, *Three-dimensional quantitative structure-selectivity relationships analysis guided rational design of a highly selective ligand for the cannabinoid receptor 2.* Eur J Med Chem, 2011. **46**(2): p. 547-55.
181. Pasquini, S., M. De Rosa, V. Pedani, C. Mugnaini, F. Guida, L. Luongo, M. De Chiaro, S. Maione, S. Dragoni, M. Frosini, A. Ligresti, V. Di Marzo, and F. Corelli, *Investigations on the 4-quinolone-3-carboxylic acid motif. 4. Identification of new potent and selective ligands for the cannabinoid type 2 receptor with diverse substitution patterns and antihyperalgesic effects in mice.* J Med Chem, 2011. **54**(15): p. 5444-53.
182. Mugnaini, C., S. Nocerino, V. Pedani, S. Pasquini, A. Tafi, M. De Chiaro, L. Bellucci, M. Valoti, F. Guida, L. Luongo, S. Dragoni, A. Ligresti, A. Rosenberg, D. Bolognini, M.G. Cascio, R.G. Pertwee, R. Moaddel, S. Maione, V. Di Marzo, and F. Corelli, *Investigations on the 4-quinolone-3-carboxylic acid motif part 5: modulation of the physicochemical profile of a set of potent and selective cannabinoid-2 receptor ligands through a bioisosteric approach.* ChemMedChem, 2012. **7**(5): p. 920-34.
183. Pasquini, S., M. De Rosa, A. Ligresti, C. Mugnaini, A. Brizzi, N.P. Caradonna, M.G. Cascio, D. Bolognini, R.G. Pertwee, V. Di Marzo, and F. Corelli, *Investigations on the 4-quinolone-3-carboxylic acid motif. 6. Synthesis and pharmacological evaluation of 7-substituted quinolone-3-carboxamide derivatives as high affinity ligands for cannabinoid receptors.* Eur J Med Chem, 2012. **58**: p. 30-43.
184. Manera, C., G. Saccomanni, A.M. Malfitano, S. Bertini, F. Castelli, C. Laezza, A. Ligresti, V. Lucchesi, T. Tuccinardi, F. Rizzolio, M. Bifulco, V. Di Marzo, A. Giordano, M. Macchia, and A. Martinelli, *Rational design, synthesis and anti-proliferative properties of new CB2 selective cannabinoid receptor ligands: an investigation of the 1,8-naphthyridin-2(1H)-one scaffold.* Eur J Med Chem, 2012. **52**: p. 284-94.
185. Baraldi, P.G., G. Saponaro, A.R. Moorman, R. Romagnoli, D. Preti, S. Baraldi, E. Ruggiero, K. Varani, M. Targa, F. Vincenzi, P.A. Borea, and M. Aghazadeh Tabrizi, *7-Oxo-[1,4]oxazino[2,3,4-ij]quinoline-6-carboxamides as selective CB(2) cannabinoid receptor ligands: structural investigations around a novel class of full agonists.* J Med Chem, 2012. **55**(14): p. 6608-23.
186. Aghazadeh Tabrizi, M., P.G. Baraldi, G. Saponaro, A.R. Moorman, R. Romagnoli, D. Preti, S. Baraldi, C. Corciulo, F. Vincenzi, P.A. Borea, and K. Varani, *Design, synthesis, and pharmacological properties of new heteroarylpyridine/heteroarylpyrimidine derivatives as CB(2) cannabinoid receptor partial agonists.* J Med Chem, 2013. **56**(3): p. 1098-112.

187. Trotter, B.W., K.K. Nanda, C.S. Burgey, C.M. Potteiger, J.Z. Deng, A.I. Green, J.C. Hartnett, N.R. Kett, Z. Wu, D.A. Henze, K. Della Penna, R. Desai, M.D. Leitl, W. Lemaire, R.B. White, S. Yeh, M.O. Urban, S.A. Kane, G.D. Hartman, and M.T. Bilodeau, *Imidazopyridine CB2 agonists: optimization of CB2/CB1 selectivity and implications for in vivo analgesic efficacy.* Bioorg Med Chem Lett, 2011. **21**(8): p. 2354-8.
188. Verbist, B.M., M.A. De Cleyn, M. Surkyn, E. Fraiponts, J. Aerssens, M.J. Nijsen, and H.J. Gijsen, *5-Sulfonyl-benzimidazoles as selective CB2 agonists.* Bioorg Med Chem Lett, 2008. **18**(8): p. 2574-9.
189. Gijsen, H.J., M.A. De Cleyn, M. Surkyn, G.R. Van Lommen, B.M. Verbist, M.J. Nijsen, T. Meert, J.V. Wauwe, and J. Aerssens, *5-sulfonyl-benzimidazoles as selective CB2 agonists-part 2.* Bioorg Med Chem Lett, 2012. **22**(1): p. 547-52.
190. Yu, X.H., C.Q. Cao, G. Martino, C. Puma, A. Morinville, S. St-Onge, E. Lessard, M.N. Perkins, and J.M. Laird, *A peripherally restricted cannabinoid receptor agonist produces robust anti-nociceptive effects in rodent models of inflammatory and neuropathic pain.* Pain, 2010. **151**(2): p. 337-44.
191. Watson, C., D.R. Owen, D. Harding, I.K. Kon, M.L. Lewis, H.J. Mason, M. Matsumizu, T. Mukaiyama, M. Rodriguez-Lens, A. Shima, M. Takeuchi, I. Tran, and T. Young, *Optimisation of a novel series of selective CNS penetrant CB(2) agonists.* Bioorg Med Chem Lett, 2011. **21**(14): p. 4284-7.
192. Beckett, R.P., R. Foster, C. Henault, J.L. Ralbovsky, C.M. Gauss, G.R. Gustafson, Z. Luo, A.-M. Campbell, and T.E. Shelekhin, *Preparation of substituted imidazoheterocycles, particularly 5,6,7,8-tetrahydroimidazo[1,5-a]pyrazines and 6,7,8,9-tetrahydroimidazo[1,5-a][1,4]diazepines, as cannabinoid receptor modulators*, 2008, Cara Therapeutics, Inc., USA . p. 239pp.
193. Lange, J.H., M.A. van der Neut, H.C. Wals, G.D. Kuil, A.J. Borst, A. Mulder, A.P. den Hartog, H. Zilaout, W. Goutier, H.H. van Stuivenberg, and B.J. van Vliet, *Synthesis and SAR of novel imidazoles as potent and selective cannabinoid CB2 receptor antagonists with high binding efficiencies.* Bioorg Med Chem Lett, 2010. **20**(3): p. 1084-9.
194. Yang, S.W., J. Smotryski, J. Matasi, G. Ho, D. Tulshian, W.J. Greenlee, R. Brusa, M. Beltramo, and K. Cox, *Structure-activity relationships of 2,4-diphenyl-1H-imidazole analogs as CB2 receptor agonists for the treatment of chronic pain.* Bioorg Med Chem Lett, 2011. **21**(1): p. 182-5.
195. Nelson, D.W., J.M. Frost, K.R. Tietje, A.S. Florjancic, K. Ryther, W.A. Carroll, M.J. Dart, A.V. Daza, B.A. Hooker, G.K. Grayson, Y. Fan, T.R. Garrison, O.F. El-Kouhen, B. Yao, M. Pai, P. Chandran, C. Zhu, G.C. Hsieh, and M.D. Meyer, *Synthesis and evaluation of 2-amido-3-carboxamide thiophene CB(2) receptor agonists for pain management.* Bioorg Med Chem Lett, 2012. **22**(7): p. 2604-8.
196. Thur, Y., A. Bhalerao, Z. Munshi, N. Pansare, K. Mann, G. Hanauer, H.P. Kley, S. Nappe, C. Weiss-Haljiti, C. Ostermann, C. Zitt, M. Schaefer, D. Mondal, A. Ali Siddiki, V. Armugam, V. Gudaghe, M. Gupta, P. Rayudu, F.M. Dautzenberg, and K. Das Sarma, *Structure-activity relationships of 2-arylamido-5,7-dihydro-4H-thieno[2,3-c]pyran-3-carboxamide derivatives as cannabinoid receptor agonists and their analgesic action.* Bioorg Med Chem Lett, 2012. **22**(24): p. 7314-21.
197. Berry, A., P.F. Cirillo, E.R. Hickey, D. Riether, D. Thomson, R.M. Zindell, M. Ermann, J.E. Jenkins, I. Mushi, M. Taylor, C. Chowdhury, C.F. Palmer, and N. Blumire, *2-Sulfonyl carboxamide compounds which modulate the CB2 receptor and their preparation,*

pharmaceutical compositions and use in the treatment of diseases, 2008, Boehringer Ingelheim International G.m.b.H., Germany; Boehringer Ingelheim Pharma G.m.b.H. & Co. K.-G. . p. 143 pp.
198. Regan, J. and D. Riether, *Preparation of heterocyclic sulfone compounds as modulators of the CB2 receptor for treating inflammation, pain, and other diseases*, 2010, Boehringer Ingelheim International G.m.b.H., Germany; Boehringer Ingelheim Pharma G.m.b.H. & Co. K.-G. . p. 63 pp.
199. Shankar, B.B., B.J. Lavey, G. Zhou, J.A. Spitler, L. Tong, R. Rizvi, D.Y. Yang, R. Wolin, J.A. Kozlowski, N.Y. Shih, J. Wu, R.W. Hipkin, W. Gonsiorek, and C.A. Lunn, *Triaryl bis-sulfones as cannabinoid-2 receptor ligands: SAR studies.* Bioorg Med Chem Lett, 2005. **15**(20): p. 4417-20.
200. Gilbert, E.J., G. Zhou, M.K. Wong, L. Tong, B.B. Shankar, C. Huang, J. Kelly, B.J. Lavey, S.W. McCombie, L. Chen, R. Rizvi, Y. Dong, Y. Shu, J.A. Kozlowski, N.Y. Shih, R.W. Hipkin, W. Gonsiorek, A. Malikzay, C.A. Lunn, L. Favreau, and D.J. Lundell, *Non-aromatic A-ring replacement in the triaryl bis-sulfone CB2 receptor inhibitors.* Bioorg Med Chem Lett, 2010. **20**(2): p. 608-11.
201. Lavey, B.J., J.A. Kozlowski, B.B. Shankar, J.M. Spitler, G. Zhou, D.Y. Yang, Y. Shu, M.K. Wong, S.C. Wong, N.Y. Shih, J. Wu, S.W. McCombie, R. Rizvi, R.L. Wolin, and C.A. Lunn, *Optimization of triaryl bis-sulfones as cannabinoid-2 receptor ligands.* Bioorg Med Chem Lett, 2007. **17**(13): p. 3760-4.
202. Tong, L., B.B. Shankar, L. Chen, R. Rizvi, J. Kelly, E. Gilbert, C. Huang, D.Y. Yang, J.A. Kozlowski, N.Y. Shih, W. Gonsiorek, R.W. Hipkin, A. Malikzay, C.A. Lunn, and D.J. Lundell, *Expansion of SAR studies on triaryl bis sulfone cannabinoid CB2 receptor ligands.* Bioorg Med Chem Lett, 2010. **20**(22): p. 6785-9.
203. EvaluatePharma. *Glenmark's Molecule for Neuropathic Pain, Osteoarthritis - GRC 10693, Successfully Completes Phase I Trials*. 2009 [cited 2015 February 2]; Available from: http://www.evaluategroup.com/Universal/View.aspx?type=Story&id=183092.
204. Kyowa Hakko Kirin Co., L.A.R. *Development summary*. 2011 [cited 2015 February 2]; Available from: http://www.kyowa-kirin.com/investors/annual_report/.
205. Odan, M., N. Ishizuka, Y. Hiramatsu, M. Inagaki, H. Hashizume, Y. Fujii, S. Mitsumori, Y. Morioka, M. Soga, M. Deguchi, K. Yasui, and A. Arimura, *Discovery of S-777469: an orally available CB2 agonist as an antipruritic agent.* Bioorg Med Chem Lett, 2012. **22**(8): p. 2803-6.
206. ClinicalTrials. *A Randomized, Double-Blind Study to Evaluate the Safety and Efficacy of 2 Doses of S-777469 in Patients With Atopic Dermatitis*. 2011 [cited 2015 February 2]; Available from: https://clinicaltrials.gov/show/NCT00703573.
207. Chen, J.Z., J. Wang, and X.Q. Xie, *GPCR structure-based virtual screening approach for CB2 antagonist search.* J Chem Inf Model, 2007. **47**(4): p. 1626-37.
208. Feng, Z., M.H. Alqarni, P. Yang, Q. Tong, A. Chowdhury, L. Wang, and X.Q. Xie, *Modeling, Molecular Dynamics Simulation, and Mutation Validation for Structure of Cannabinoid Receptor 2 Based on Known Crystal Structures of GPCRs.* J Chem Inf Model, 2014. **54**(9): p. 2483-99.
209. Leifert, W.R., O. Bucco, M.Y. Abeywardena, and G.S. Patten, *Radioligand binding assays: application of [(125)I]angiotensin II receptor binding.* Methods Mol Biol, 2009. **552**: p. 131-41.

210. Zhang, Y., Z. Xie, L. Wang, B. Schreiter, J.S. Lazo, J. Gertsch, and X.Q. Xie, *Mutagenesis and computer modeling studies of a GPCR conserved residue W5.43(194) in ligand recognition and signal transduction for CB2 receptor.* Int Immunopharmacol, 2011. **11**(9): p. 1303-10.
211. van Meerloo, J., G.J. Kaspers, and J. Cloos, *Cell sensitivity assays: the MTT assay.* Methods Mol Biol, 2011. **731**: p. 237-45.
212. Yu, M., X. Chen, C. Lv, X. Yi, Y. Zhang, M. Xue, S. He, G. Zhu, and H. Wang, *Curcumol suppresses RANKL-induced osteoclast formation by attenuating the JNK signaling pathway.* Biochem Biophys Res Commun, 2014. **447**(2): p. 364-70.
213. Feng, R., G. Anderson, G. Xiao, G. Elliott, L. Leoni, M.Y. Mapara, G.D. Roodman, and S. Lentzsch, *SDX-308, a nonsteroidal anti-inflammatory agent, inhibits NF-kappaB activity, resulting in strong inhibition of osteoclast formation/activity and multiple myeloma cell growth.* Blood, 2007. **109**(5): p. 2130-8.
214. Xie XQ, C.J.-Z., Zhang Y-X, *Ligands Specific for Cannabinoid Receptor Subtype 2*, in *(University of Pittsburgh of the Commonwealth System of Higher Education, USA)*, I. WO, Editor 2009, 2008-US12395, WO 2009058377, 2009058339pp: USA.
215. Wan, J.-P., Y.-F. Chai, J.-M. Wu, and Y.-J. Pan, *N,N′-(Phenylmethylene)diacetamide Analogues as Economical and Efficient Ligands in Copper-Catalyzed Arylation of Aromatic Nitrogen-Containing Heterocycles.* Synlett, 2008. **2008**(19): p. 3068-3072.
216. Bayer, A. and M.E. Maier, *Synthesis of enamides from aldehydes and amides.* Tetrahedron, 2004. **60**(31): p. 6665-6677.
217. Nelson, F.C., E. Delos Santos, J.I. Levin, J.M. Chen, J.S. Skotnicki, J.F. DiJoseph, M.A. Sharr, A. Sung, L.M. Killar, R. Cowling, G. Jin, C.E. Roth, and J.D. Albright, *Benzodiazepine inhibitors of the MMPs and TACE.* Bioorg Med Chem Lett, 2002. **12**(20): p. 2867-70.
218. Iwaszkiewicz-Grzes, D., G. Cholewinski, A. Kot-Wasik, P. Trzonkowski, and K. Dzierzbicka, *Synthesis and biological activity of mycophenolic acid-amino acid derivatives.* Eur J Med Chem, 2013. **69**: p. 863-71.
219. Conley, J.D. and H. Kohn, *Functionalized DL-amino acid derivatives. Potent new agents for the treatment of epilepsy.* J Med Chem, 1987. **30**(3): p. 567-74.
220. Singh, M., S. Kumar, A. Kumar, P. Kumar, and B. Narasimhan, *Synthesis, antimicrobial evaluation, and QSAR analysis of 2-isopropyl-5-methylcyclohexanol derivatives.* Medicinal Chemistry Research, 2012. **21**(4): p. 511-522.
221. Wei, L., J. Babich, W.C. Eckelman, and J. Zubieta, *Rhenium tricarbonyl core complexes of thymidine and uridine derivatives.* Inorg Chem, 2005. **44**(7): p. 2198-209.
222. Xie, X.Q., J.Z. Chen, and E.M. Billings, *3D structural model of the G-protein-coupled cannabinoid CB2 receptor.* Proteins, 2003. **53**(2): p. 307-19.
223. Myint, K.Z. and X.Q. Xie, *Recent advances in fragment-based QSAR and multi-dimensional QSAR methods.* Int J Mol Sci, 2010. **11**(10): p. 3846-66.
224. Chen, J.Z., X.W. Han, Q. Liu, A. Makriyannis, J. Wang, and X.Q. Xie, *3D-QSAR studies of arylpyrazole antagonists of cannabinoid receptor subtypes CB1 and CB2. A combined NMR and CoMFA approach.* J Med Chem, 2006. **49**(2): p. 625-36.
225. Xie, X.Q., L.S. Melvin, and A. Makriyannis, *The conformational properties of the highly selective cannabinoid receptor ligand CP-55,940.* J Biol Chem, 1996. **271**(18): p. 10640-7.

226. Lipinski, C.A., F. Lombardo, B.W. Dominy, and P.J. Feeney, *Experimental and computational approaches to estimate solubility and permeability in drug discovery and development settings.* Adv Drug Deliv Rev, 2001. **46**(1-3): p. 3-26.